AN ABSTRACT OF THE THESIS OF

Scott B. Katz for the degree of Master of Science in Water Resources Engineering presented on June 6th. 2016.

Title: Sediment Transport Modeling and Implications for Benthic Primary Producers in Oak Creek, OR.

Abstract approved:

_____

Catalina Segura

The spatial and temporal variability of sediment transport processes in Oak Creek, OR was investigated and used to explore two study questions: 1) How do sediment transport processes influence benthic algal communities?, and 2) Can fluvial-hydraulic models make accurate predictions of bed load transport rates? Our study was conducted in a 96 m reach of Oak Creek, OR – a small gravel bed stream in the Oregon Coast range. The study site is located in the same reach that was used to collect the historic Oak Creek bed load dataset of Milhous [1973].

To answer study question 1 we characterized the variability in sediment transport for a series of eight high flow events ranging from 0.64-3.4 m^3/s using modeled shear stress (τ) from a field calibrated, high resolution (<0.1 m^2) 2-dimensional hydrodynamic model (FaSTMECH) coupled with detailed measurements of the channel substrate. The stream bed was then categorized into regions of high and low disturbance based on potential mobility of the median grain size using a Shield's stress approach. High resolution (<0.25m^2), in-situ measurements benthic Chlorophyll-*a* (used as a metric of benthic algal production) were taken before and after high flow events in regions of contrasting disturbance to understand how benthic algal communities respond to sediment transport disturbance through both space and

time. Growth factors including temperature, light, and nutrients were also measured. There was high spatial and temporal variability in both sediment transport and benthic Chl-*a* throughout the study period. We found significant differences ($p<0.05$) in benthic Chl-*a* concentrations between regions of high and low disturbance in half of the sampling events. The influence of sediment transport on benthic Chl-*a* was dependent on both the bed mobility and pre-disturbance Chl-*a* concentrations. There were also differences in benthic algal recovery rates in regions of contrasting disturbance following high flow events. The relationship between τ and Chl-*a* was highly variable, however the 95th percentile quantile regression of Chl-*a* was consistent with the bell-curve shape of the intermediate disturbance hypothesis for 10/18 sampling events. This study shows that sediment transport processes do influence benthic algal growth dynamics however the magnitude of that influence is also dependent on pre-disturbance productivity.

To answer study question 2 we made contemporary bed load measurements during 5 flow events ranging from 0.24 bankfull (Q_{bf}) to 0.52 Q_{bf} using a Helly-Smith bed load sampler in order to confirm the stability of sediment transport dynamics in Oak Creek. The contemporary measurements were consistent with the historical dataset for total load however, they had a finer grain size distribution (GSD). A 2-dimensional (2-D) hydrodynamic model (FaSTMECH) was used to calculate spatial distributions of τ for 5 flow levels ranging from 0.2 Q_{bf} to Q_{bf} (0.64-3.4 m^3/s). Results indicate that τ is highly variable within the study reach and that mean normalized τ distributions are remarkably similar between flow levels. The τ distributions were then discretized and used to calculate bed load using surface and subsurface transport equations, and compared against the historical dataset for accuracy. Modeled bed load was consistently larger and coarser than the historical samples. Areas of τ greater than 2 times the mean comprised <2.5% of the bed and were responsible for transporting >32% of the bed load. We hypothesize that the inconsistency in our estimates may be due to combining 2-D τ with a reach averaged reference shields stress (τ_r^*) value which may have caused such high transport rates from a small portion of the bed.

Scaling τ_r^* with τ throughout a reach may provide the basis for future work to incorporate spatially variable τ into commonly used bed load transport functions.

Sediment Transport Modeling and Implications for Benthic Primary Producers in Oak Creek, OR.

by
Scott B. Katz

A THESIS

submitted to

Oregon State University

in partial fulfillment of
the requirements for the
degree of

Master of Science

Presented June 6th, 2016
Commencement June 2017

Master of Science thesis of Scott B. Katz presented on June 6th, 2016

APPROVED:

Major Professor, representing Water Resources Engineering

Director of the Water Resources Graduate Program

Dean of the Graduate School

I understand that my thesis will become part of the permanent collection of Oregon State University libraries. My signature below authorizes release of my thesis to any reader upon request.

Scott B. Katz, Author

ACKNOWLEDGEMENTS

I give my sincerest appreciation for the guidance that I received from my adviser, Dr. Catalina Segura, who helped me transform from an eager environmental chemist into a fluvial geomorphologist. She allowed me the space to explore my own research questions while also keeping me focused and on track. Her infectious energy, creativity, curiosity, and most importantly patience, were inspiring throughout the duration of this project – thank you. I also am grateful for the support of my other committee members, Drs. Dana Warren, Gordon Grant, who contributed greatly to the completion of this work. Their intellectual, logistical, and personal support were essential. I would also like to thank my graduate council representative, Dr. Woodam Chung, for agreeing to join the team at the last minute. Finally I would like to thank Drs. Desirée Tullos and Pete Klingeman and for their guidance and encouragement.

I am appreciative for the support of Stephen Fitzgerald and the rest of the College of Forestry Research Forests staff for their unwavering support in helping to establish our study reach as a place of research within the MacDonald-Dunn forest. Although the dogs may have ignored the signs, you tried your best to maintain as natural conditions as possible within my study site and for this I am grateful. I hope that Oak Creek remains a place of research for many years to come.

I thank Dr. Mary Santelmann and the rest of the faculty in the OSU WRGP for providing such a strong academic community for me to flourish in. I also thank my office mates, specifically Russell Bair, Kira Puntenney, and Lydia Nickolas, for their friendship, intellectual/silly conversations, open-minds and late-night popcorn eating. The office became my second home during this experience not because of the décor or fantastic view, but because you all were there – you will be missed. A big thanks to the rest of the Hydrophiles for being such a supportive community throughout my graduate studies and whom there are too many amazing people to name individually.

I would like to thank the entirety of the entirety of the Warren lab (Matt Kaylor, Brian VerWey and Emily Heaston) for all of their field, lab, and conceptual help during this project – it was a blast to collaborate with you all. A big thanks to my amazing undergraduate field crew including Joey Tinker, Olivia Cantwell, and Catalina Seufert, who were always willing to help rain or shine. Thank you to the College of Forestry administrative staff including Madison Miller, Erica Hanna, and Chelsey Durling for making everything else run smoothly even if my thesis project wasn't. I recognize the financial support provided by the Forest Engineering, Resources and Management (FERM) department and the College of Forestry and appreciate this generosity during my 2 years at OSU. Finally, I am thankful to my family and friends for always believing in me not only in graduate school, but in any new adventure that I embark on.

TABLE OF CONTENTS

TABLE OF CONTENTS

TABLE OF CONTENTS

LIST OF FIGURES

LIST OF TABLES

1. INTRODUCTION

The transport of sediment along a rivers flow path is a defining feature of natural alluvial river systems. Sediment transport is the result of complex interactions between the flow and sediment regimes which create spatially and temporally heterogeneous patterns of transport within a river system [*Pitlick*, 1988; *Lisle et al.*, 2000; *Clayton and Pitlick*, 2007; *McDonald et al.*, 2010; *Segura et al.*, 2011; *Recking*, 2013a; *Segura and Pitlick*, 2015]. The variability of these processes is expressed through adjustments in channel form and flow hydraulics and can be complicated by a myriad of additional processes such as changes in sediment supply [*Schumm*, 1960; *Beechie and Bolton*, 1999; *Buffington et al.*, 2003] and influences from the surrounding riparian vegetation [*Yager and Schmeeckle*, 2013; *Bywater-Reyes et al.*, 2015] , hillslope [*Grant et al.*, 1990; *Faustini and Jones*, 2003; *Yager et al.*, 2007], as well as the lithology of the watershed itself [*Mueller and Pitlick*, 2014; *O'Connor et al.*, 2014]. The complex interaction of these processes generate non-linear relationships between flow and sediment; thus it is important to incorporate variability when quantifying sediment transport to avoid significant uncertainties in calculations [*Recking*, 2013a]. In this thesis, I seek to incorporate the spatial and temporal variability of sediment transport processes in investigations of disturbance in stream ecosystems and to improve the accuracy of sediment transport estimates.

Characterizing variability in sediment transport is important to understand how fluvial disturbance influences stream ecosystems. Benthic algae are ideal organisms to investigate these interactions. Their habitat is comprised of the stream substrate and thus the movement of sediment particles during a high flow event directly impacts their growing conditions [e.g., *Biggs et al.*, 1999; *Segura et al.*, 2011]. Spatial variability in sediment transport processes during high flows create variable responses in benthic algal communities [*Luce et al.*, 2010, 2013; *Segura et al.*, 2011]. During a high flow event, the spatial heterogeneity of flow and resisting forces act to simultaneously create mobile and stable areas in the channel [*Lisle et al.*, 2000; *May et al.*, 2009; *Segura et al.*, 2011; *Segura and Pitlick*, 2015]. This creates contrasting regions of high and low disturbance

for benthic communities, including algae [*Luce et al.*, 2010, 2013; *Segura et al.*, 2011]. However, studies typically quantify the magnitude of a high flow disturbance on benthic algal communities based on discharge [e.g. *Fisher et al.*, 1982; *Biggs and Close*, 1989; *Townsend and Douglas*, 2014] and one dimensional estimates of sediment transport [*Uehlinger et al.*, 1996; *Biggs et al.*, 1999] and do not account for spatial changes in transport intensity during an individual event [*Lisle et al.*, 2000; *Stewart et al.*, 2005; *May et al.*, 2009; *McDonald et al.*, 2010; *Legleiter et al.*, 2011; *Segura et al.*, 2011; *Segura and Pitlick*, 2015]. By oversimplifying the sediment transport processes to a single flow dependent metric, the underlying disturbance processes cannot be fully identified and thus variable responses of benthic algae to increasing discharge have been reported [e.g. *Stevenson*, 1990; *Jowett and Biggs*, 1997; *Biggs et al.*, 1999; *Francoeur and Biggs*, 2006; *Townsend and Douglas*, 2014]. Characterizing sediment transport through flow dependent metrics also creates uncertainty in transport relationships used to estimate bed load transport rates.

Empirical sediment transport functions have been developed by many researchers in order to estimate bed load transport rates in lieu of making costly, dangerous, and uncertain field measurements [*Parker and Klingeman*, 1982; *Parker et al.*, 1982; *Parker*, 1990; *Wilcock and Crowe*, 2003; *Barry et al.*, 2004; *Recking*, 2013b]. Although these transport relations have been successfully applied to many types of river systems, recent work by Recking [2013a] highlights the variability that can be incorporated into calculation results due to uncertainty in input shear stress (τ) values. The high spatial variability in τ throughout a river reach has been well documented [*Lisle et al.*, 2000; *Clayton and Pitlick*, 2007; *May et al.*, 2009; *McDonald et al.*, 2010; *Segura et al.*, 2011; *Recking*, 2013a; *Segura and Pitlick*, 2015; *Monsalve et al.*, 2016]. Most transport functions however, utilize width and reach averaged estimates of τ in their calculations and are highly sensitive to uncertainties in these values due to the non-linear exponents on each function [*Recking*, 2013a]. Significant differences in bed load estimates computed using both 1-D and 2-D approximations of τ have been found to be caused because of the spatial variability of τ [*Gomez and Church*, 1989; *Ferguson*, 2003; *Recking*, 2013a]. Thus, the oversimplification of τ to a 1-D variable may not capture

spatial changes in sediment transport associated with localized values of high τ [*Segura and Pitlick*, 2015].

The objective of this thesis is to incorporate the known spatial and temporal variability of sediment transport processes in investigations of stream processes. Specifically, the objectives are:

- To understand how spatial and temporal variability in sediment transport processes influence the response and recovery of benthic algal communities to multiple high flow events
- To test the applicability of using spatially variable estimates of τ and commonly used transport equations to make accurate estimates of bed load transport rates

Objective 1 will be addressed in Chapter 2 entitled "The influence of sediment transport processes on benthic algae in mountain headwater streams." Objective 2 will be addressed in Chapter 3 entitled "Can fluvial-hydraulic models be used to accurately predict bed load transport rates?" Data pertaining to quantifying spatially variable τ is utilized in both Chapters. To avoid redundancy, these methods and most data are discussed in detail in Chapter 2, and only mentioned briefly in Chapter 3.

2. THE INFLUENCE OF SEDIMENT TRANSPORT PROCESSES ON BENTHIC ALGAE IN MOUNTAIN HEADWATER STREAMS

2.1 Abstract

This study explores how the spatial and temporal variability of stream flow and sediment transport influence the growth dynamics of benthic algae in a rainfall dominated mountain stream. Benthic algae sustain higher trophic levels in stream ecosystems and thus understanding how disturbance by sediment transport processes affect their productivity can provide insight into broader ecosystem processes. Our study was conducted in a 96 m reach of Oak Creek, OR, a small, forested gravel-bed stream in the Oregon Coast range with a bankfull width of 5.6 m and a bankfull discharge (Q_{bf}) of 3.4 m^3/s. We characterized the variability in sediment transport for a series of 8 high flow events ranging from 0.64-3.4 m^3/s using shear stress (τ) calculated using a field calibrated, high resolution (<0.1 m^2) 2-dimensional hydrodynamic model (FaSTMECH) coupled with detailed measurements of the channel substrate. The stream bed was then categorized into regions of high and low disturbance based on potential mobility of the median grain size using a Shield's stress approach. High resolution (<0.25m^2), in-situ measurements of benthic Chlorophyll-*a* (used as a metric of benthic algal production) were taken before and after high flow events in regions of contrasting disturbance to understand how benthic algal communities respond to sediment transport disturbance through both space and time. Growth factors including temperature, light, and nutrients were also measured. There was high spatial and temporal variability in both sediment transport and benthic Chl-*a* throughout the study period. We found significant differences in benthic Chl-*a* concentrations between regions of high and low disturbance in 9/18 sampling events. The influence of sediment transport on benthic Chl-*a* was dependent on both the bed mobility and pre-disturbance Chl-*a* concentrations. There were also differences in benthic algal recovery rates in regions of contrasting disturbance following high flow events. Our results indicate that 2-D estimates of bed mobility are a better predictor of sediment transport disturbance to benthic algae than 1-dimensional metrics such as discharge. The relationship between τ and Chl-*a* was highly variable, however the 95th percentile quantile regression of Chl-*a* was consistent with the bell-curve shape of

the intermediate disturbance hypothesis for 10/18 sampling events. This study shows that sediment transport processes influence benthic algal growth dynamics however the magnitude of that influence is also dependent on pre-disturbance productivity.

2.2 Introduction

Fluvial systems are characterized by the ability of water to transport sediment along a river's flow path. The process of sediment transport expresses the physical form and function of a river and along with the flow regime, provides a physical habitat template for aquatic ecosystems. In natural systems, the interaction between water and sediment is complicated by processes including the flow regime [*Leopold and Maddock Jr.*, 1953; *Ferguson*, 1986; *Knighton*, 1998], sediment supply [*Schumm*, 1960; *Beechie and Bolton*, 1999; *Buffington et al.*, 2003], channel geometry [*Leopold and Maddock Jr.*, 1953; *Parker*, 1979; *Mueller et al.*, 2005], and surrounding riparian conditions such as vegetation [*Yager and Schmeeckle*, 2013; *Bywater-Reyes et al.*, 2015], hillslope geomorphic processes [*Grant et al.*, 1990; *Faustini and Jones*, 2003; *Yager et al.*, 2007], and watershed lithology [*Mueller and Pitlick*, 2014; *O'Connor et al.*, 2014]. The complex interaction of these processes generate non-linear relationships between water and sediment which in turn result in spatial and temporal heterogeneity of sediment transport within a river system [*Parker*, 1979, 1990; *Wilcock and Crowe*, 2003; *Mueller et al.*, 2005; *Pitlick et al.*, 2008; *Segura and Pitlick*, 2015]. In terms of aquatic ecosystems, this heterogeneity is expressed as spatial differences in features of plan-form habitat (i.e. pools, riffles, runs, steps) and flow hydraulics (e.g. fast vs slow velocity) as well as temporal differences in discharge (i.e. floods, base-flow, droughts) and climatic conditions. The interaction between both the spatial and temporal components of aquatic habitat provides the basis for the physical disturbance regime, where pulse disturbances caused by high flow are followed by periods of organism and habitat recovery [*Resh et al.*, 1988; *Poff et al.*, 1997; *Lake*, 2000; *Allan and Castillo*, 2007]. Quantifying how these processes interact in both space and time is essential for understanding how disturbance influences aquatic ecosystem's ability to support life.

Benthic algae are ideal organisms to investigate how sediment transport processes influence stream ecosystems. Their habitat is comprised of the stream substrate and thus the movement of sediment particles during a high flow event directly impacts their growing conditions [e.g., *Biggs et al.*, 1999; *Segura et al.*, 2011]. Benthic algae are also fundamental to stream ecosystems as they are the main autotrophic primary producers in

headwater streams and act as high quality food sources for higher trophic levels [*McCutchan and Lewis*, 2002; *Power and Dietrich*, 2002; *Larned*, 2010]. Changes to benthic algal communities from high flows can thus cascade up the food-web and influence the rest of the ecosystem [*Rosemond et al.*, 1993; *Woodward and Hildrew*, 2002]. Understanding how high flow disturbances influence these communities (and thus the ecosystem as a whole) is important for a wide range of environmental management applications including setting meaningful environmental flow targets [*Biggs*, 2000; *Osmundson et al.*, 2002; *Davie and Mitrovic*, 2014], restoring natural processes through river rehabilitation projects [*Murdock et al.*, 2004; *Lake et al.*, 2007; *Stanley et al.*, 2010], and providing insight into how ecosystems will respond to increased variability in precipitation regimes as a result of climate change [*IPCC*, 2014].

The growth dynamics of benthic algae across a variety of stream ecosystems are highly dependent on high flow disturbance [*Rounick and Gregory*, 1981; *Fisher et al.*, 1982; *Power and Stewart*, 1987; *Biggs and Close*, 1989; *Biggs and Gerbeaux*, 1993; *Uehlinger et al.*, 1996; *Biggs et al.*, 1999; *Townsend and Padovan*, 2005; *Francoeur and Biggs*, 2006; *Luce et al.*, 2010, 2013; *Hart et al.*, 2013; *Davie and Mitrovic*, 2014]. High flows reduce benthic algal biomass through disturbance from the flow hydraulics (i.e. shear stress and velocity) [e.g. *Biggs and Close*, 1989; *Biggs et al.*, 1999] abrasion from suspended sediment [e.g. *Francoeur and Biggs*, 2006; *Luce et al.*, 2010, 2013], and bed load transport directly [e.g. *Fisher et al.*, 1982; *Biggs et al.*, 1999; *Segura et al.*, 2011; *Davie et al.*, 2012]. Both the magnitude of the disturbance [*Fisher et al.*, 1982; *Power and Stewart*, 1987; *Biggs and Close*, 1989; *Uehlinger et al.*, 1996; *Biggs et al.*, 1999; *Segura et al.*, 2011; *Stanish et al.*, 2011; *Luce et al.*, 2013; *Townsend and Douglas*, 2014] and the taxonomy of the algal community [*Peterson and Stevenson*, 1992; *Biggs and Thomsen*, 1995; *Johnson et al.*, 1997; *Snell et al.*, 2014] control how benthic algal communities respond to high flows. The amount of biomass reduction and change in species composition caused by an individual high flow in turn influences how the community will recover after the disturbance has occurred [*Biggs and Close*, 1989; *Peterson et al.*, 1994; *Johnson et al.*, 1997; *Biggs et al.*, 1998; *Gustina and Hoffmann*, 2000; *Stanish et al.*, 2011; *Davie et al.*, 2012; *Snell et al.*, 2014; *Coundoul et al.*, 2015].

Thus, any variability in disturbance processes will influence both the response and recovery of the benthic algal community from that particular event, and change how the community will respond to high flows in the future. In order to understand these complex interactions, both the spatial and temporal variability of sediment transport processes needs to be considered.

Spatial variability in sediment transport processes during high flows create variable responses in benthic algal communities [*Luce et al.*, 2010, 2013; *Segura et al.*, 2011]. During a high flow event, the spatial heterogeneity of flow and resisting forces act to simultaneously create mobile and stable areas in the channel [*Lisle et al.*, 2000; *May et al.*, 2009; *Segura et al.*, 2011; *Segura and Pitlick*, 2015]. This creates contrasting regions of high and low disturbance for benthic communities, including algae [*Luce et al.*, 2010, 2013; *Segura et al.*, 2011]. However, studies typically quantify the magnitude of a high flow disturbance on benthic algal communities based on discharge [e.g. *Fisher et al.*, 1982; *Biggs and Close*, 1989; *Townsend and Douglas*, 2014] and one dimensional estimates of sediment transport [*Uehlinger et al.*, 1996; *Biggs et al.*, 1999] and do not account for spatial changes in transport intensity during an individual event. [*Lisle et al.*, 2000; *Stewart et al.*, 2005; *May et al.*, 2009; *McDonald et al.*, 2010; *Legleiter et al.*, 2011; *Segura et al.*, 2011; *Segura and Pitlick*, 2015]. By oversimplifying the sediment transport processes to a single flow dependent metric, the underlying disturbance processes cannot be fully identified and thus variable responses of benthic algae to increasing discharge have been reported [e.g. *Stevenson*, 1990; *Jowett and Biggs*, 1997; *Biggs et al.*, 1999; *Francoeur and Biggs*, 2006; *Townsend and Douglas*, 2014]. In the few studies to date where spatial variability in sediment transport disturbance to benthic algae has been investigated [*Luce et al.*, 2010, 2013; *Segura et al.*, 2011], the experiments were conducted in streams with stable snow-melt flow regimes and thus temporal changes to the response and recovery of benthic algae to multiple disturbance events were not considered.

Another factor complicating the investigation of the influence of disturbance on benthic algae is the amount of spatial variability within algal communities themselves.

The abundance of benthic algae varies in multiple scales of inference throughout a stream system including on an individual sediment particle [*Sekar et al.*, 1998; *Kanavillil et al.*, 2014], between particles of different sizes [*Cattaneo et al.*, 1997], and in portions of the stream bed with different morphologies such as riffles and pools [*Cardinale et al.*, 2002; *Segura et al.*, 2011; *Luce et al.*, 2013]. This heterogeneity is not however, captured by common sampling protocols where few (i.e. <30) sediment particles are sampled for benthic algae in either random [*Biggs and Close*, 1989; *Davie and Mitrovic*, 2014; *Townsend and Douglas*, 2014], transect [*Biggs et al.*, 1999; *Townsend and Padovan*, 2005], or patch [*Segura et al.*, 2011] sampling schemes. By not sampling within the scales of spatial variability of both benthic algae and flow forces, additional uncertainty can be introduced into cause and effect relationships of sediment transport processes and benthic algal communities. For example, while Segura et al. [2011] considered spatial variations in bed mobility on a <1 m scale, benthic algae was characterized based on 2-4 samples from 9 patches throughout the stream reach which could not fully account for the natural variability in benthic algal communities throughout the stream bed. Thus, much could be learned about the influence of disturbance on algal communities from characterizing benthic algae on similar scales as sediment transport processes.

The objective of this study is to understand how spatial and temporal variability in sediment transport processes influence the response and recovery of benthic algal communities to multiple high flow disturbances. We use a two-dimensional (2-D) hydraulic model coupled with detailed measurements of the channel substrate to quantify locations in the bed in which sediment mobilization is possible for multiple storm events during the study period. In addition we make high resolution (0.25 m^2) measurements of benthic Chlorophyll-*a* (which is used as a metric of benthic algal production) and track the concentrations through both space and time. These data are used to investigate the relation between benthic Chlorophyll-*a* and shear stress at high resolution (<0.25m^2) and to understand how benthic algal communities respond to contrasting disturbance metrics defined based on a sediment transport criteria. The results are contextualized in a framework of ecological resistance and resilience as well as the intermediate disturbance

hypothesis [*Connell*, 1978] in order to understand how high flow events influence the ecosystem as a whole.

2.3 Study Site

This study was conducted in a 96 m reach of Oak Creek, Corvallis, OR. Oak Creek drains 7 km^2 of steep forested terrain, underlain by basaltic lithology [*Milhous*, 1973; *O'Connor et al.*, 2014] (Figure 2.1, Table 2.1). The climate is Mediterranean with wet winter and dry summer seasons. The riparian vegetation is primarily deciduous with Alder (*Alnus sp*), Black Cottonwood (*Papulus trichocarpa*), Big Leaf Maple (*Acer macrophyllus*) dominating the upper canopy and Salmonberry (*Rubus spectabilis*), Blackberry (*Rubus armeniacus*), Willow (*Salix sp*) populating the understory. The reach has a pool-riffle / plain bed morphology [*Montgomery and Buffington*, 1997] with 1 pool-riffle sequence comprising the upstream portion of the reach and a straight plain bed section comprising the downstream portion. The reach is located directly upstream from a historic sediment transport sampling facility where bed-load samples were collected between 1969-1973 [*Milhous*, 1973]. Although the vortex sampler has since been dismantled, a hardened broadside weir 3.65 m wide, 8 m long, and 0.9 m high still remains at the downstream end of the study reach (Figure 2.1).

Table 2.1 - Study Site Characteristics: Characteristics of the study reach in Oak Creek, OR (± are standard errors)

Slope (m/m)	0.014
Bankfull width (m)	6
Bankfull depth (m)	0.46
Bankfull hydraulic radius (m)	0.44
Bankfull discharge (m^3/s)	3.4
D_{16} ± standard error (mm)	19.0 ± 1.1
D_{50} ± standard error (mm)	45.1 ± 2.5
D_{84} ± standard error (mm)	83.2 ± 3.5

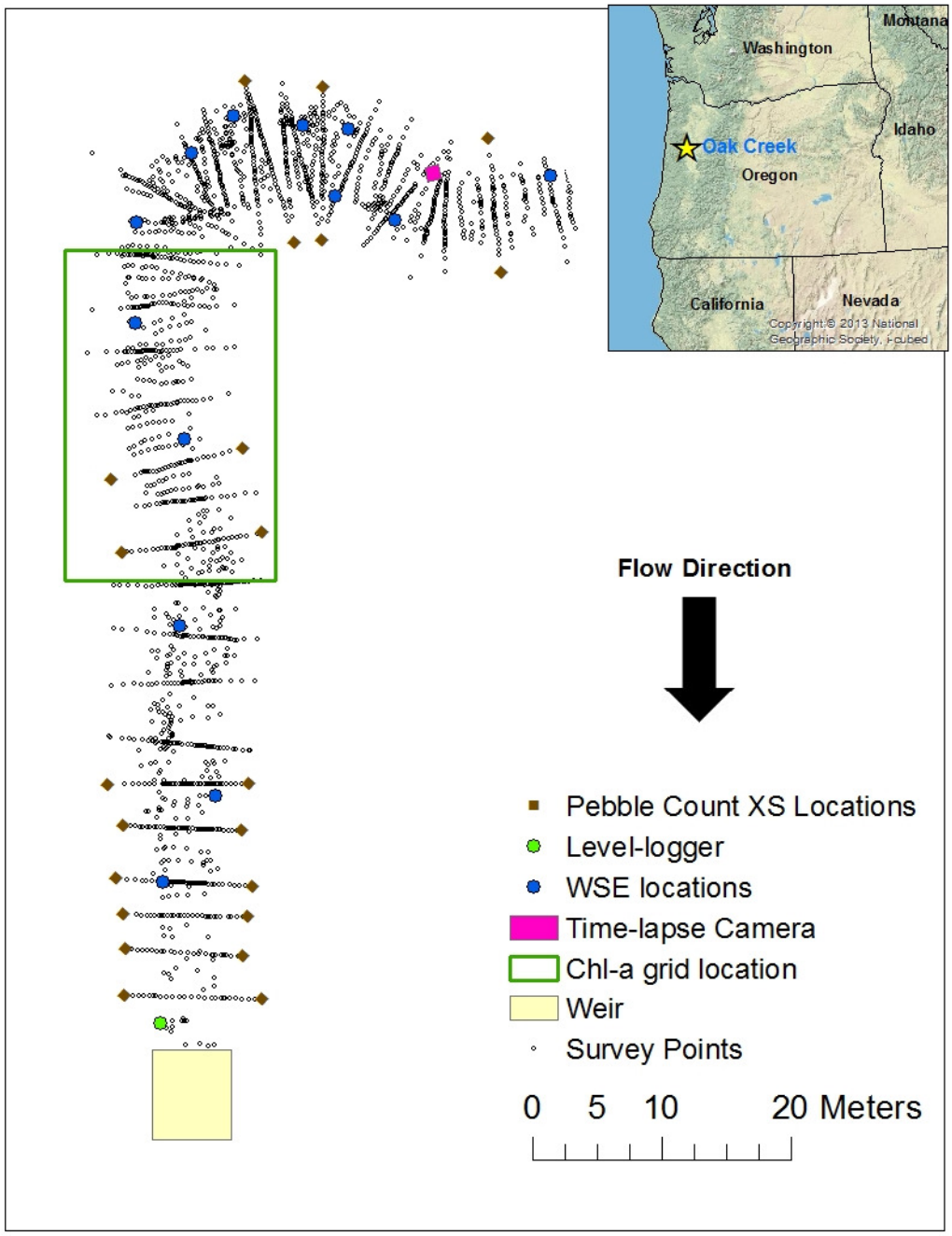

Figure 2.1 - Map of Study Site: Study reach in Oak Creek, OR. Topographic surveying points and cross section pebble count locations are indicated. A water level logger is located at the downstream end of the reach. Water surface elevation (WSE) monitoring locations used during calibration along the reach are also depicted in addition to a time lapse camera in the upstream end. The location of the grid used to monitor Chl *a* is also included.

2.4 Methods

2.4.1 Characterization of Sediment Transport

2.4.1.1 Field Data

Detailed topography of the study site was surveyed using a Nikon total station during the summer of 2015 (Figure 2.1). A total of 32 cross sections (XS) were surveyed (Appendix B). The average distance between XS was 0.5 bankfull widths. XS endpoints were placed at least 2 meters beyond the field identified bankfull elevation to ensure capturing the topography within the region of the active channel at high flows. Additional points were surveyed between cross sections in order to characterize longitudinal changes of bed topography and improve the interpolation of the topography within the hydraulic model FaSTMECH (Figure 2.2). A total of 2121 points were surveyed yielding an average resolution of 1.9 points/m^2 for the whole reach and 3.27 points/m^2 for the active channel. This bed elevation information was imported into ARCGIS to develop a topographic map which was used as input of the flow model. The input topographic surface was generated using the Natural Neighbor interpolation algorithim within the 3D analyst toolbox embedded in ARCGIS which minimized cusping and produced a smooth topographic surface [*Merwade et al.*, 2006, 2008; *Merwade*, 2009]. The bed surface grain size distribution (GSD) was characterized based on point pebble counts along 23 cross sections totaling 2347 particles [*Wolman*, 1954]. Individual point counts were then combined to obtain a reach averaged GSD (Figure 2.3) that was summarized in terms of the grain sizes representing the 16^{th}, 50^{th}, and 84^{th} percentiles of the distribution (D_{16}, D_{50}, D_{84}, Table 2.1 - Study Site Characteristics). The calculated D_{50} was 45.1 ± 2.5 mm which is finer than the previously reported value for Oak Creek of 54 mm [*Milhous*, 1973].

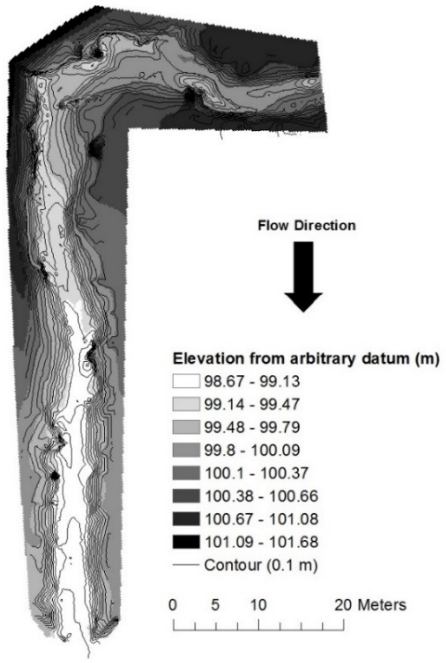

Figure 2.2 - Interpolated Topography: Interpolated topography used to model flow hydraulics. The interpolation was based on the natural neighbor algorithm within ArcGIS. Elevation from an arbitrary datum is showed for the raster surface. Contour lines with a 0.1 m resolution created from the same topographic dataset are also included.

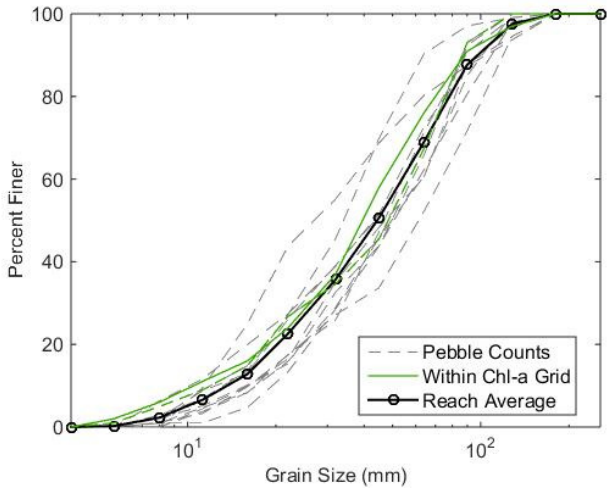

Figure 2.3 - Surface Grain Size Distribution: Grain Size Distribution (GSD) of the surface substrate of Oak Creek. Individual pebble counts are shown in grey and green, with the green lines depicting locations within the Chl-*a* sampling grid. The bolded line is the reach average used to calculate the D_{16}, D_{50}, and D_{84}.

2.4.1.2 Discharge measurements and rating curve development

A total of 12 discharge (Q) measurements between 0.043-1.94 m^3/s were taken within the hardened broadside weir at the downstream end of the reach. In all instances we used a Hach FH950 portable velocity meter to take measurements every 0.4 m, which are used to develop a water stage-Q relationship (Figure 2.4). This relationship enables Q estimates based on 10-minute stage observations taken using a Hobo U20 Water Level logger with a precision of +/- 0.03 m (Figure 2.5). The logger is located 1 m upstream from the broadside weir (Figure 2.1). Discharge outside of the measured range was estimated within the hardened cross section at the downstream end of the reach using a resistance equation. First, a relationship was found between the recorded depth in the level logger and the depth in the weir, measured during each flow measurement off of a staff gauge attached to the weir (Figure 2.4a). Hypothetical depths up to the top of the weir (i.e. up to 0.9m) were then estimated using this relationship (Figure 2.4b). The hydraulic radius (R) of each hypothetical flow was then calculated based on the weir geometry and used together with the channel slope (S) to estimate the shear velocity (u^*):

$$u^* = \sqrt{gSR} \tag{2-1}$$

where g is gravitational acceleration, S is the channel slope, and R is the hydraulic radius within the broadside weir. Velocity (u) within the weir was then calculated based on the D_{84} (Table 2.1) and the flow resistance equation of Ferguson [2007]:

$$u = u^* * a_1 a_2 (\frac{d}{D_{84}}) / [a_1^2 + a_2^2 \left(\frac{d}{D_{84}}\right)^{\frac{5}{3}}]^{\frac{1}{2}} \tag{2-2}$$

where a_1 and a_2 are optimized fitting coefficients presented in Ferguson [2007] (6.5 and 2.5 respectively) and d is the depth inside of the weir.

Discharge was calculated based on continuity. The results of these calculations produced stage-discharge relationships for all possible flow values where the water remained within the weir which included flows ranging from 0.043 m^3/s to 6.65 m^3/s. However, we will only use calculated Q based on this relationship to Q_{bf} because once the

Q increases outside of the banks, the flow becomes dissipated by the floodplain and it is uncertain if it remains entirely inside of the weir. Thus, our rating curve includes values from 0.043m^3/s to 3.4 m^3/s, which is the previously estimated bankfull flow for Oak Creek [*Milhous*, 1973] (Figure 2.4).

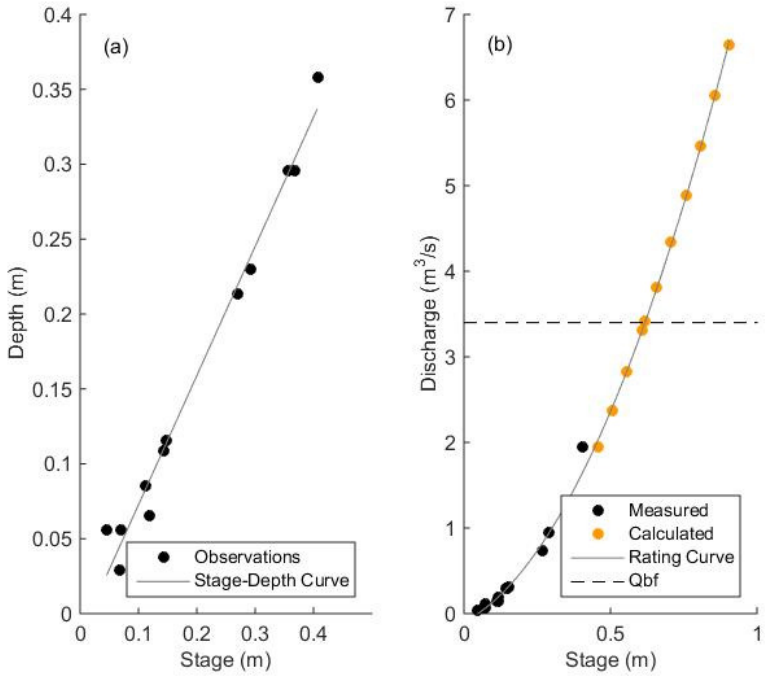

Figure 2.4 - Site Rating Curve: a) Weir depth versus logger stage relationship for the 12 instances at which discharge was measured (the total weir depth is 0.9 m). The line represents the linear regression equation (y = 0.8628x – 0.0137, R^2=0.984) used to estimate depth in the weir. b) Stage-discharge relationship using both measured (n = 12) and estimated (n = 12) values of depth (with the relation in panel a). The line represents the best fit 2nd order polynomial equation (y= 6.364x^2 + 1.7304x – 0.0962 R^2=0.999) used as the rating curve. The dashed line represents bankfull discharge (3.4 m^3/s).

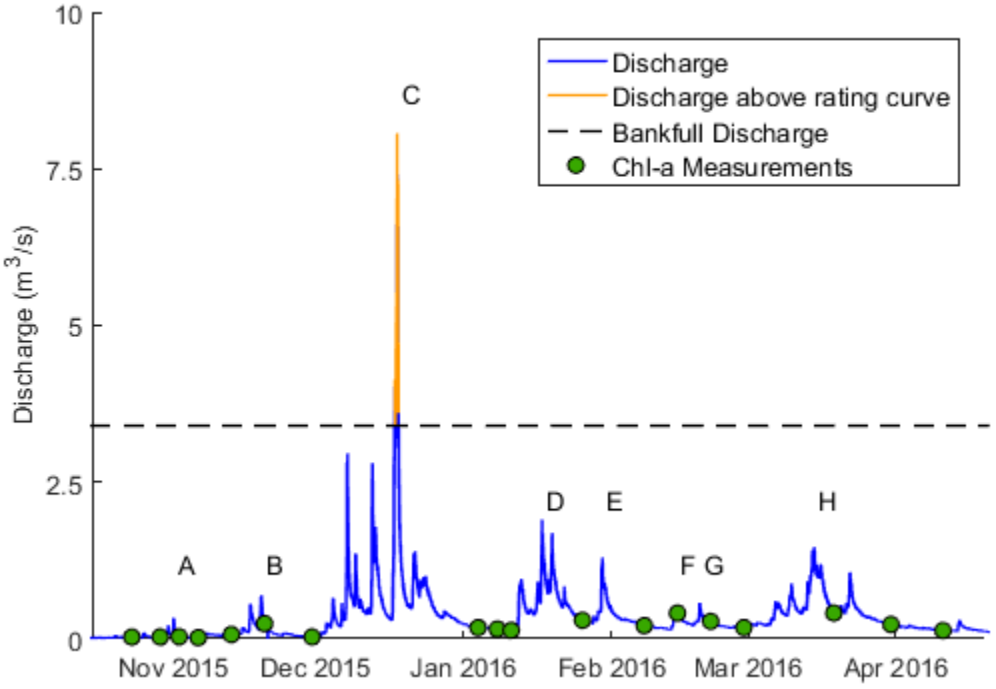

Figure 2.5 - Hydrograph during Study Period: Hydrograph of Oak Creek, OR during study period. Discharge values are calculated based on measurements taken at 10-minute intervals and the site rating curve (Figure 2.4). Discharge estimates for stage measurements taken outside of the bounds of the rating-curve are denoted in orange. The bankfull discharge (Q_{bf}, 3.4 m^3/s) is denoted by the dashed line. Chlorophyll-*a* (Chl-*a*) sampling events are marked in green. High flow event classifications are denoted as letters above the peak discharge of each high flow event.

2.4.1.3 *Two dimensional Hydrodynamic model*

We made 2-D estimates of velocity (*u)* and shear stress (τ) for 6 flows ranging from 0.64-3.4 m^3/s ($0.19Q_{bf}$ - $1.0Q_{bf}$) using the Flow and Sediment Transport with Morphological Evolution of Channels (FaSTMECH) analytical solver. FaSTMECH is embedded within the International River Interface Cooperative (iRIC) software and developed by the United States Geological Survey (USGS). FaSTMECH uses finite differencing numerical methods to simulate flow by calculating solutions to the mass and momentum equations (also known as the Navier-Stokes equations) making the following assumptions: 1) The fluid is incompressible and hydrostatic, 2) Reynold's averaging can be used to account for turbulence within the flow structure (the Reynold's equations), 3)

An isotropic eddy viscosity can provide closure to the Reynold's stresses and can be estimated assuming a logarithmic velocity (i.e. the "law of the wall") and 4) Boundary layer stresses (i.e. τ) can be accounted for using a drag coefficient (C_d) closure and the cross-stream (v) and downstream (u) components of velocity following Equation 2-3 [*Lisle et al.*, 2000; *Nelson*, 2015; *Nelson et al.*, 2015a]. The calculations are performed within an orthogonal curvilinear grid that follows the surveyed planform topography of the channel and divides local velocities into cross-stream and downstream components (v and u). The model inputs include bed topography, Q, roughness (estimated as a constant or variable C_d), a measure of lateral eddy viscosity (LEV), and the downstream stage. The model calibration procedure involves adjusting the C_d and LEV, the two free, unmeasured input parameters, in order to minimize the root mean square error (RMSE) between modeled and observed WSE.

$$\tau = \rho C_d (u^2 + v^2) \tag{2-3}$$

where τ is the bed shear stress (N/m^2), ρ is the density of water (1000 kg/m^3), and C_d is the drag coefficient.

The input data to our FaSTMECH model included an interpolation of the surveyed topography, the measured downstream stage, and Q. Calculations were conducted within a 110 m long, 16m wide curvilinear grid with a spacing of 0.2 m x 0.2 m. The number of grid nodes varied from 10593-15094 depending on flow level (Table 2.2). A constant C_d was used for each model run. The model was calibrated using field observations of streamwise WSE from 13 locations throughout the study reach (Figure – Site Map, Table – Model calibration). Streamwise WSE for bankfull flow (Q_{bf}) were estimated based on time-lapse photography, field observations of bankfull stage, and the analysis of cross-section topography because WSE observations were not made during an actual bankfull event. Two separate researchers performed the field bankfull stage observations and agreed upon the location of bankfull elevations. The value of 3.4 m^3/s was selected as Q_{bf} by comparing photographs of the flow overtopping the banks with

discharge estimated using the rating curve (Figure 2.6). This value agrees with the previously published value for Oak Creek [*Milhous*, 1973].

Figure 2.6 - Photograph of Bankfull Discharge: Time-lapse photograph showing bankfull flow (Q_{bf}) conditions at Oak Creek, OR. Measurements of water surface elevation from the rebar staff gauges visible in the photograph were used to calibrate the Q_{bf} flow model.

Streamwise plots of measured versus modeled WSE for each flow yield RMSE values between 0.025-0.031 m and R^2 >0.96 (Figure 2.7, Table 2.2). Calibrated C_d and LEV ranged from 0.017-0.038 and 0.0010-0.0032, respectively. Calibration plots for three of the flows (0.64, 1.46, and 3.4 m^3/s) demonstrate that the WSE slopes decrease slightly with increasing discharge between 0.0142-0.0153 (Figure 2.8, Table 2.2). This is consistent with results presented elsewhere for gravel bed rivers [*Segura and Pitlick*, 2015]. The RMSE of the adjusted flows were well within acceptable ranges found in other studies using FaSTMECH [*May et al.*, 2009; *McDonald et al.*, 2010; *Legleiter et al.*, 2011; *Segura et al.*, 2011; *Harrison et al.*, 2015; *Segura and Pitlick*, 2015].We used the linear relation between Q and calibrated C_d and LEV values to estimate these model parameters for a 1.9 m^3/s flow event relevant to the disturbance definition (see below).

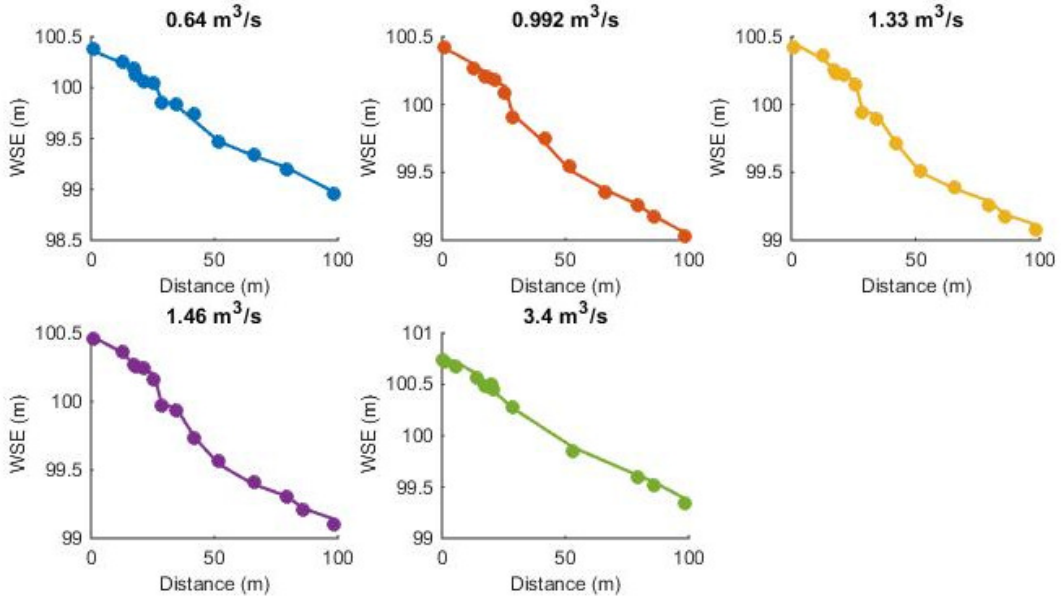

Figure 2.7 - Hydraulic Model Water Surface Calibration Curves: Measured vs. Modeled water surface elevations (WSE) for 5 flows in Oak Creek. The markers are measured values and the lines represent modeled WSE output from FaSTMECH.

Table 2.2 - Hydraulic Model Development and Calibration Summary: FaSTMECH model development and calibration summary: discharge (Q), ratio of Q to bankfull Flow (Q/Q_{bf}), downstream (D.S.) stage, the number of calculation nodes, the Root-Mean-Square Error (RMSE) between measured and modeled water surface elevations (WSE), the coefficient of determination (R^2) of the relation between measured and modeled WSE, the calibrated drag coefficient (C_d), lateral eddy viscosity (LEV), and the WSE slope.

Flow Conditions			***Model Parameters and Evaluation***					
Q	**Q_i/Q_{bf}**	**D.S. Stage[(a)]**	**# wet nodes**	**RMSE**	**R^2**	**C_d**	**LEV**	**WSE Slope (m/m)**
0.64	0.19	98.96	10593	0.028	0.996	0.038	0.0016	0.0153
0.99	0.29	99.03	10593	0.031	0.996	0.025	0.0024	0.0150
1.33	0.39	99.08	10835	0.028	0.997	0.018	0.0032	0.0150
1.46	0.43	99.10	11147	0.025	0.997	0.017	0.0031	0.0150
1.9[(b)]	0.56	99.17	11140	N/A	N/A	0.021	0.0025	0.0143
3.4	1.00	99.34	15094	0.031	0.996	0.035	0.0010	0.0142

(a)- From an arbitrary datum
(b) - This flow was not calibrated directly based on WSE.
N/A – Not available

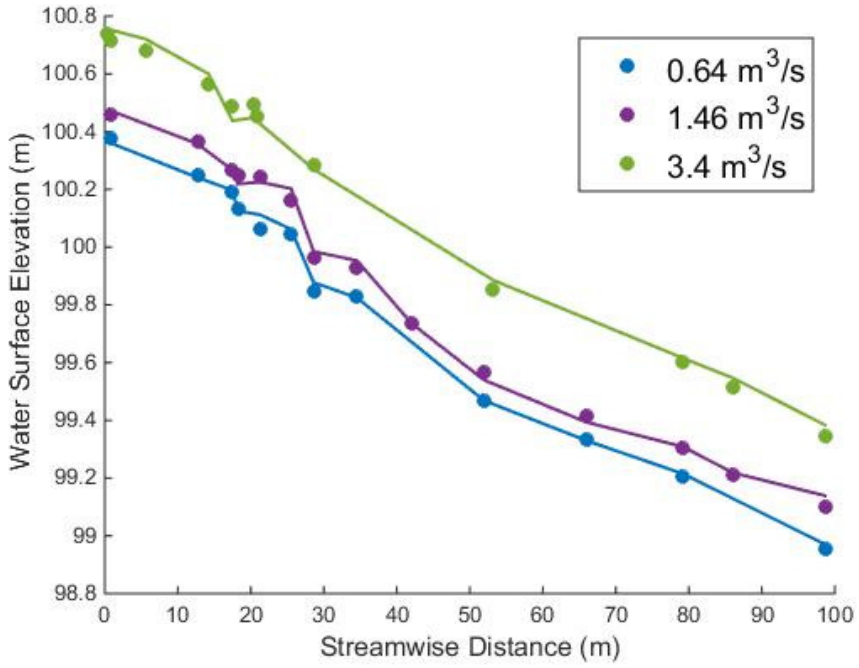

Figure 2.8 - Modeled Water Surface Slopes: Measured vs. Modeled water surface elevation (WSE) for 3 flows in Oak Creek. The markers are measured values and the lines represent modeled WSE output from FaSTMECH. RMSE and R^2 are presented in Table 2.2.

2.4.2 Characterization of Benthic Algae growth dynamics

2.4.2.1 Field Data Collection

Benthic Chlorophyll-*a* (Chl-*a*) was measured using a BBE Moldaenke BenthoTorch (http://www.bbe-moldaenke.de). The Benthotorch is a hand-held, in-situ fluorimeter that measures Chl-*a* directly from the stream substrate [*Kahlert and McKie*, 2014]. Chl-*a* measurements were taken on 18 separate occasions before and after high flow events between 10/23/15 and 4/11/16 (Figure 2.5). Chl-*a* measurements were made within a 20 m section of the reach using a gridded sampling scheme. The grid had a spacing of 0.5 m x 0.5 m and a total of 352 cells. Five replicates were randomly selected within each ($0.25m^2$) grid cell, however we avoided sampling the same area twice within a sampling period. Grid cells were only sampled when the entire grid cell was submerged and the stream substrate within the cell was visible. Thus the total number of grid cells sampled during each sampling period varied with flow level between 63 and 90. In order

to minimize disturbance of the stream substrate in sampled cells, measurements were taken across alternating rows leaving rows available for access. Sampling was conducted by a single person in order to ensure consistency both across sampling locations and between sampling dates.

The sampling grid encompassed a riffle-run sequence directly upstream from a pool (Figure 2.1, Figure 2.9). The area of the grid is surrounded primarily by deciduous vegetation and was selected in a section with relatively similar light availability (i.e. similar shading from the riparian area). Measurements of nutrients, light, and temperature were taken during the study period in order to quantify the availability of abiotic resources for benthic algae (See Sections 2.4.2.3-2.4.2.5)

Figure 2.9 - Chlorophyll-a Sampling Grid: Chlorophyll-*a* sampling grid. Each line indicates a grid row.

2.4.2.2 Comparison of Chlorophyll-a Measurement Methods

Benthic Chl-a measurements made with the BenthoTorch were compared against the standard brush sampling/ethanol extraction/spectrophotometric analysis method in

order to assess the ability to compare the in-situ data collected in this study against the standard methods used by others. Comparisons were made against both 40 measurements on individual substrate particles [e.g. *Biggs et al.*, 1999] and 27 composite samples consisting of three particles [e.g. *Segura et al.*, 2011]. Sediment particles were removed from a riffle upstream from the sampling grid and analyzed using the BenthoTorch. Care was taken not to disturb the algal community during this measurement. The same location on the sediment particle was then sampled using the brush sampling method. The location was covered with a cap of similar diameter to the measurement surface of the BenthoTorch (3 cm vs 1 cm for the cap and BenthoTorch respectively) and the remainder of the rock was scrubbed with a nylon brush and rinsed. Following the rinsing procedure, the cap was removed and the area below it was scrubbed vigorously with a nylon brush. This procedure was repeated two additional times for the composite samples. The removed material was placed into a 250 mL bottle and topped off to 250 mL with stream water. The samples were kept cold prior to transport to the laboratory. In the laboratory, the samples were filtered in the dark and collected onto 0.7 μm glass fiber filters. The filters were stored in centrifuge tubes at -20°C for 18 days prior to extraction using sonication and hot 95% ethanol. Chl-a concentrations of the extractant were measured using a spectrophotometer and not corrected for phaeophytin as the BenthoTorch cannot distinguish between photoactive pigments.

The compassion between Chl-*a* measurements using both the BenthoTorch and the brush method demonstrates that the same relative result to characterize contrasting Chl-*a* concentrations can be achieved using either method. Furthermore, the comparison also highlightsthe utility of replicating Chl-*a* measurements when using either method (Figure 2.10). The slopes and R^2 values of both regression lines (0.81 vs 1.34 and 0.61 vs 0.64 for the composite and individual respectively) demonstrate strong linear relationship between measurements made by both analytical methods.. Variability in the measurements can be reduced through replication as indicated by the slope of the linear regression of the composite samples being closer to 1 than the individual samples. The individual samples were consistently greater than the 1:1 line while there was a random

dispersion of the composite samples around the 1:1 relationship. This comparison underscores the replication that we employed in our sampling scheme.

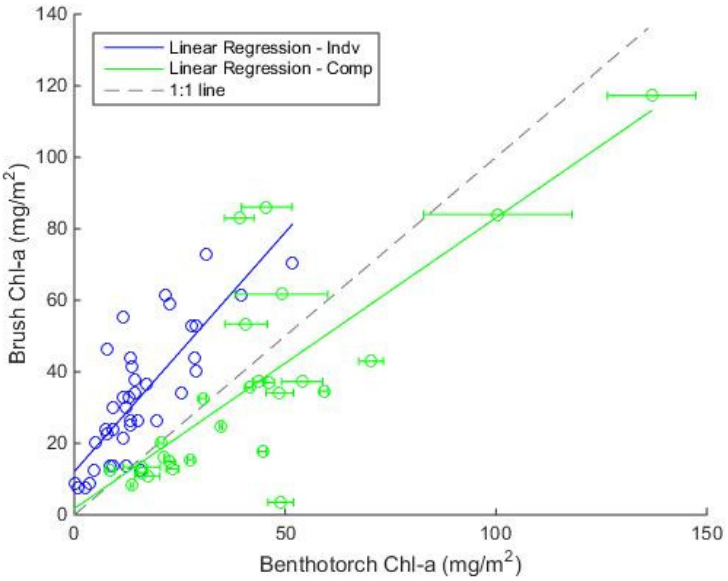

Figure 2.10 - Chlorophyll-a Measurement Method Comparison: Relationship between Chlorophyll-*a* concentrations measured using both the BenthoTorch and a standard brush method followed by ethanol extraction and spectrophotometry. Results are shown for both individual (indv) and composite (comp) brush samples. The individual linear regression corresponds to the equation $[\text{Chl-}a]_{\text{Brush-indv}}=1.33*[\text{Chl-}a]_{\text{BenthoTorch}} + 12.12$ ($R^2=0.64$). The composite linear regression corresponds to the equation $[\text{Chl-}a]_{\text{brush-comp}}=0.81*[\text{Chl-}a]_{\text{BenthoTorch}} + 1.76$ ($R^2=0.61$). Error bars on the composite samples correspond to the standard deviation of the three BenthoTorch replicates. The data is also plotted against the 1:1 agreement line.

2.4.2.3 Nutrients

Water samples were collected monthly during the study period (October-April) for analysis of nitrate (NO_3^- -N), ammonia (NH_4^+-N), and phosphate (PO_4^{3-} -P) (Table 2.3). Samples were collected in acid-washed bottles that were conditioned three times in stream water immediately prior to collection. Samples were immediately frozen (-20°C) upon collection. Prior to analysis, the samples were thawed at room temperature, filtered using 0.7 µm glass filters and the filtrate was collected in clean acid-washed bottles. The samples were analyzed for nitrate and phosphate using a Dionex ICS-1500 ion chromatograph. The ammonia analysis was performed by the Cooperative Chemical

Analytical Laboratory (CCAL) at Oregon State University using a Technicon Auto-Analyzer II.

Table 2.3 - Nutrient Concentrations: Dissolved concentrations of nitrate (NO_3^--N), ammonia (NH_4^+-N), and phosphate (PO_4^{3-} -P) at the study site between 10/23/15-4/11/2016. The nitrogen to phosphorus (N:P) ratio is calculated by summing the nitrate and ammonia concentrations and dividing by the phosphate concentration.

Date	NO_3^- -N (µg/L)	NH_4^+ -N (µg/L)	PO_4^{3-} -P (µg/L)	N:P
10/23/2015	4.8	39	38.6	1.1
11/2/2015	102.4	6	36.0	3.0
11/13/2015	30.6	6	24.9	1.5
12/23/2015	63.2	16	13.0	6.1
1/11/2016	60.5	9	17.6	3.9
2/8/2016	47.6	27	9.0	8.3
3/19/2016	36.6	7	6.4	6.8
4/11/2016	20.2	4	11.3	2.1

There was no clear trend in nutrient concentrations during the study period. Nutrient concentrations ranged from 4.8-102.4 µg/L, 4-39 µg/L, and 6.4-38.6 µg/L for nitrate, ammonia and phosphate respectively. The only visual outlier in the data is the nitrate concentration measured for 11/2/2015. This sample was taken immediately following high flow event A which flushed significant amounts of fallen leaf material through the study reach. The elevated nitrate concentrations in this sample could be due to the high flow event dissolving nitrate bound within the fallen leaves, particularly those of alder trees surrounding the site. The nitrogen to phosphorus ratio (N:P) indicates that there was consistently a nitrogen deficiency in the stream water during the study period (i.e. <16:1) [*Redfield*, 1934]. The low variability in the nutrient concentrations, especially the constant nitrogen limitation, indicate that the influence of nutrients as a growth factor on benthic algal remained constant throughout the study period.

2.4.2.4 Light

Light was measured using a HOBO pendant light meter which measures light intensity in LUX and an Odyssey photosynthetically active radiation (PAR) logger. The

sensors were suspended above the stream bed within the middle of the sampling grid at the edge of the bank (Figure 2.1). The light intensity meter was deployed between 10/23/15-11/16/15 and again from 1/8/16-3/19/16. It was removed between those dates in order to prevent it from being lost or damaged during the large winter high flow events of the period. Another logger was lost during that period as well. The PAR sensor was deployed between 2/8/16-4/11/16. Because only the PAR portion of sunlight is used by benthic algae for photosynthesis, a relationship was developed between LUX and PAR in order to convert the light intensity data to PAR for the entire study period (Figure 2.11). The PAR sensor reported integrated measurements over 10 minute intervals while the LUX sensor reported instantaneous measurements made every 30 minutes. To develop a LUX-PAR relationship the PAR data was averaged over the 30 minute LUX measurement interval into a rate per second. The LUX data was then compared to the time-averaged PAR data. The power function presented in Figure 2.11 was used to convert LUX to PAR for measurements taken between 10/23/16-11/16/15 by calculating instantaneous "per-second" PAR data using the LUX measurements. A daily total PAR ($mol/m^2/day$) was then calculated by interpolating the converted LUX data and summing the values for each day of the study period (Figure 2.12).

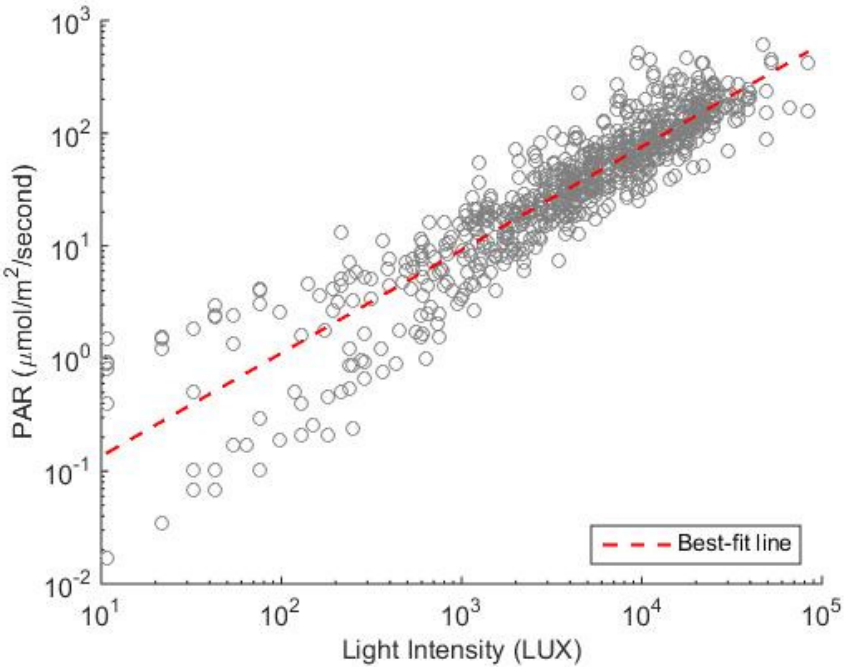

Figure 2.11 - LUX to PAR Conversion: Relationship between light intensity (LUX) and photosynthetically active radiation (PAR) measured in Oak Creek, OR between 2/8/16-3/19/16. The data corresponds to time-averaged PAR measurements that correspond to the interval between when instantaneous LUX measurements were made. The best-fit line represents the power-function regression ($y=0.0165*x^{0.9154}$, $R^2=0.84$) used to convert measured light intensity data into PAR.

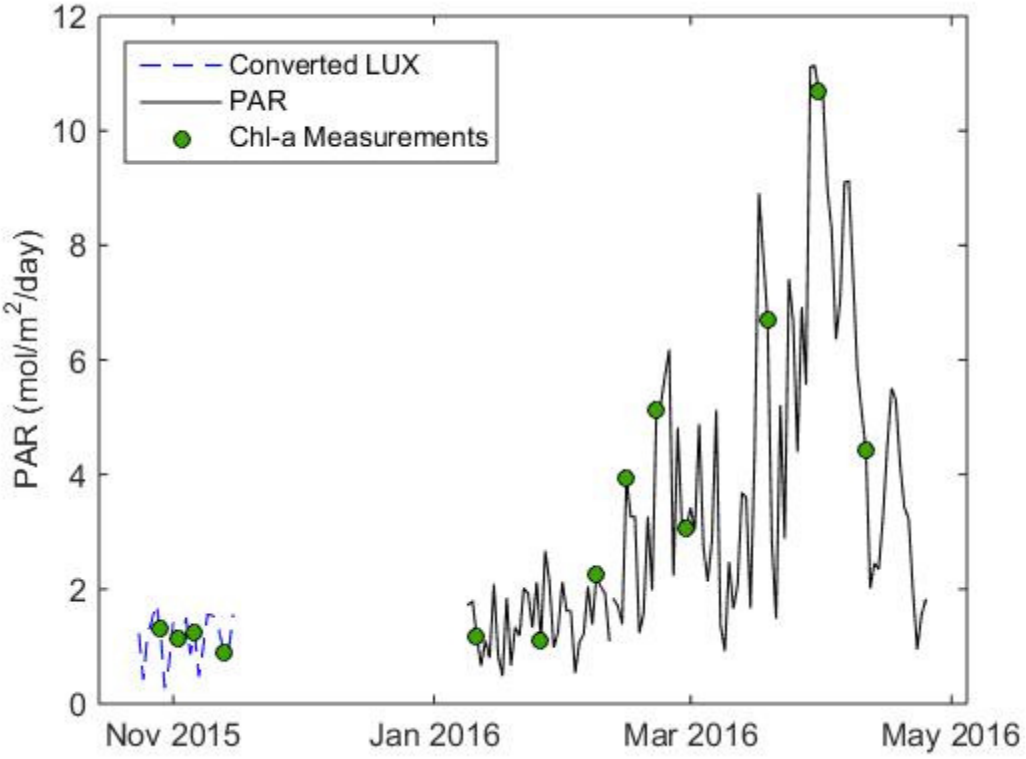

Figure 2.12 - Light Measurements: Daily average photosynthetically average radiation (PAR) for Oak Creek, OR during the study period. Light intensity data between 10/23/15 and 11/13/15 was converted into PAR using the relationship presented in Figure 2.11. Measurements were taken within the Chl-*a* sampling grid. The green points represent the PAR values when Chl-*a* measurements were taken.

2.4.2.5 Temperature

Stream temperature at 10-minute increments was measured at two locations. The Hobo U20 water level logger used to record stage at the downstream end of the reach (Section 1.2.1.2) also provided temperature with a precision of +/- 0.44°C. A second temperature time series was recorded ~50m upstream from the upper end of the study reach using a Solinst Edge water level logger with a precisions of +/- 0.05°C. The time-series of temporal fluctuations in stream temperature are very similar and presented in Figure 2.13.

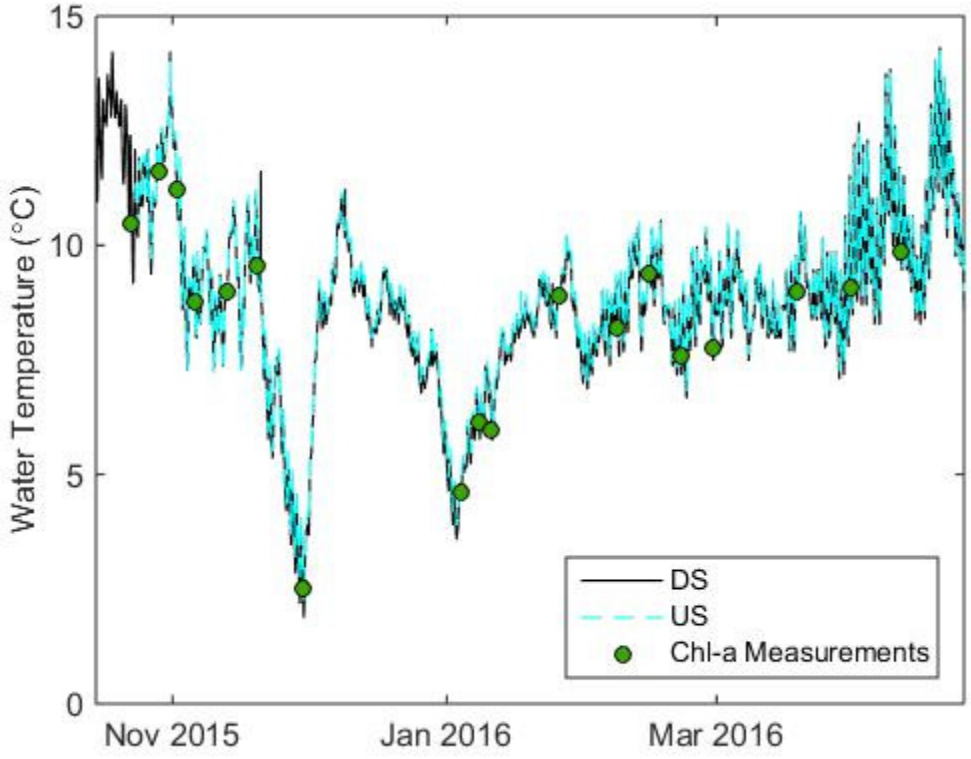

Figure 2.13 - Water Temperature Measurements: Fluctuations in stream temperature measured during the study period in Oak Creek, OR. Measurements were made at 10- minute time intervals at the downstream (DS) and upstream (US) end of the study reach. The green points represent the measured temperature during Chl-*a* sampling events.

2.4.2.6 Disturbance Level Characterization

In order to investigate the influence of physical disturbance on benthic Chl-*a* concentrations, sediment transport disturbance categories were developed for grid cells within the Chl-*a* sampling grid. The study period was divided into periods (fall and winter) based on the hydrograph, which were separated by a large high flow event in December 2015 (Figure 2.5, Table 2.4). Estimated values of τ from peak flows that occurred during each of these periods were then used to calculate a value of τ for each Chl-*a* grid cell. Because the FaSTMECH model grid and the Chl-*a* sampling grid had different resolutions (0.2x0.2m vs 0.5x0.5m respectively), a computer algorithm was developed to combine the datasets. The algorithm calculated the distance between the

center of each Chl-a grid cell and each node of the FaSTMECH model grid. The distances were then sorted and an average of non-zero τ values from the four closest FaSTMECH grid cells was assigned to the Chl-*a* sampling grid cell.

Table 2.4 - High Flow Event Summary: Summary of high flow events used to classify disturbance categories during the study period. The dates and duration of each high flow event were determined visually from the hydrograph. The peak discharge was calculated using the site rating curve.

Storm Designation	Sampling Period	Dates	Duration (days)	Peak Discharge (m^3/s)	Fraction of Qbf	Modeled flow used to characterize shear stress and disturbance
A	Fall	10/30/15-10/31/15	2	0.34	0.10	N/A
B	Fall	11/16/15-11/20/15	5	0.69	0.20	0.64
C	---	12/3/15-12/29/15	27	>6.7	>1.97	3.4
D	Winter	1/12/16-1/22/16	11	1.91	0.56	1.9
E	Winter	1/29/16-1/31/16	3	1.29	0.38	1.33
F	Winter	2/14/16-2/15/16	2	0.49	0.14	N/A
G	Winter	2/19/16-2/20/16	2	0.56	0.16	N/A
H	Winter	3/6/16-3/17/16	12	1.46	0.43	1.46

N/A = Not available because flow not modeled due to peak discharge being outside of the calibrated discharge range.

High flow events were first grouped into Fall and Winter study periods and then estimated τ for the peak Q of the high flow events of each study period within the calibrated model range (0.64-3.4 m^3/s) were used to define τ values to the Chl-*a* grid (Table 2.4). Calibrated model flows were used as surrogates for these events in instances where the Q of the high flow events was within 0.05 m^3/s of the calibrated flow and WSE observations were not made for the specific high flow event itself. The fall period disturbance (events A and B) was characterized based on flow event B (Q = 0.69 m^3/s). Disturbance during the winter period (events D-H, Table 2.4), was calculated based on the average τ among 3 events (D, E, and H) for which similar calibrated modeled flows were available (1.91 m^3/s, 1.29 m^3/s, and 1.46 m^3/s, respectively, Table 2.2). Disturbance for the largest high flow event (C), which was outside of the range of the stage-Q rating curve (Figure 2.4, Figure 2.5), was characterized based on the modeled Q_{bf} (Q=3.4 m^3/s). Q_{bf} is a conservative estimate of the disturbance caused by this event as τ values are likely to have been greater during the peak than those estimated by this flow level. This

high flow event is not used to calculate disturbance categories (fall or winter) for the Chl-*a* grid cells and is only used for comparison purposes below.

Once τ values were assigned to the cells of the Chl-*a* sampling grid, they were categorized into regions of high and low disturbance. Disturbance categories were assigned based on a metric of incipient motion calculated using the Shield's equation (2-4). Shield's stress (τ*) was calculated for each grid cell using the measured surface D_{50} (45.1 ± 2.5 mm, Table 2.1) and the assigned τ value. The applied τ* was then compared to a reference (τ^*_r) with a value of 0.0386 [*Parker*, 1990]. Grid cells were assigned to the high disturbance category when $\tau^*/\tau^*_r \geq 1$ and to the low disturbance category when $\tau^*/\tau^*_r < 1$. These values correspond to regions where mobilization of the D_{50} are expected to either occur (high) or not occur (low).

$$\tau^* = \frac{\tau}{(\rho_s - \rho) g D_{50}} \qquad (2\text{-}4)$$

where τ* is the Shield's stress, ρ is the density of water (1000 kg/m^3) and ρ_s is the density of the sediment (2850 kg/m^3 for basalt).

2.4.2.7 Statistical Analysis

Raw Chl-*a* concentrations were grouped by disturbance category for statistical analysis. The average and variance of the Chl- *a* concentrations per sampling date and per grid cell were calculated based on the 5 replicates collected. Grid cells were then grouped by disturbance category and summarized in terms of variance-weighted mean Chl-*a* concentrations (2-5). Comparisons were made between mean Chl-*a* concentrations per disturbance level using a two sample t-test. Normality of each sample population (i.e. mean Chl-*a* concentrations per grid cell grouped by disturbance category) was tested using a Kolmogorov-Smirnov test prior to performing the t-test. Percent change in Chl-*a* concentrations were calculated for each disturbance category using weighted mean concentrations between sampling periods.

$$\bar{x} = \frac{\sum_{i=1}^{n}(x_i \sigma_i^{-2})}{\sum_{i=1}^{n} \sigma^{-2}} \quad (2\text{-}5)$$

where $\bar{x}$ is the variance-weighted mean, n is the total number of grid cells per disturbance category, x_i is the mean of a grid cell and σ_i is the standard deviation of a grid cell.

2.4.2.8 Quantile Regression Analysis

We used quantile regression analysis to test whether the influence of τ on Chl-a was consistent with the Intermediate Disturbance Hypothesis (IDF). Quantile regression analysis is a statistical method used for estimating the conditional quantile of a distribution instead of only the mean as in linear least squares regression [*Koenker and Bassett Jr*, 1978; *Koenker and Hallock*, 2001]. Any quantile of the distribution (i.e. 50%, the median) can be chosen and the method estimates a regression relationship in which the predicted data will fall below the chosen quantile. Quantile regression analysis has been used successfully in ecological studies to identify the influence of limiting factors, such as disturbance, on a biotic response [*Cade et al.*, 1999; *Dunham et al.*, 2002; *Cade and Noon*, 2003; *Drevnick and Sandheinrich*, 2003; *Warren et al.*, 2014; *Fornaroli et al.*, 2016]. The method is particularly useful when other potential limiting factors, such as grazing pressure in this case, were not measured because while other factors may cause scatter in a dataset around the mean, the maximum influence of the test variable (i.e. τ) can still be evaluated [*Cade and Noon*, 2003]. Thus, in a complex stream ecosystem where multiple factors may influence the growth of benthic algae, the influence of τ can be isolated and tested.

Quantile regression analysis was performed on the 95th quantile of Chl-*a* concentrations from each sample date using the matlab function *quantreg* (www.mathworks.com), which is based on Koenker and Hallock [2001]. Values of τ were consistent with the disturbance classification scheme presented above. In order to understand whether our data exhibited the bell shaped curve of the IDF, we performed a 3rd-order polynomial regression so that generation of a bell shaped curve would be possible in the regression model.

2.4.2.9 Analysis of recovery rates

The recovery of benthic algal communities following high flow events was investigated by calculating the doubling times (T_D) of mean Chl-*a* concentrations grouped by disturbance category. Doubling times were calculated for two recovery periods ($T_{recovery}$) during the study period: one during the fall sampling period (10/29/2015-11/13/2015) and one during the winter sampling period (1/4/2016-2/29/2016). Changes in Chl-*a* concentrations during both periods were treated as exponential growth curves as is typically done for studies of primary production [*Roberts et al.*, 2007]. The T_D was then calculated using the slope of the exponential regression equation (b) and the e-folding time ($T_{efolding}$) using Equations 2-6, 2-7, and 2-8.

$$[Chl-a] = a * e^{b*T_{recovery}} \quad (2\text{-}6)$$

$$T_{efolding} = 1/b \quad (2\text{-}7)$$

$$T_D = ln(2) * T_{efolding} \quad (2\text{-}8)$$

where [Chl-*a*] is the Chl-*a* concentrations, *a* and *b* are the intercept and the slope of the exponential best-fit line respectively, and ln is the natural log.

2.5 Results:

2.5.1 Sediment Transport Disturbance

2.5.1.1 Temporal patterns of discharge

The flow regime during the study period was characterized by a series of 8 high flow events followed by dry periods where the stream returned to base flow (Figure 2.5, Table 2.4). The peak discharge for the 8 high flow events ranged from 0.34->6.7 m^3/s and the duration from 1-26 days. The events ranged in peak flow magnitude and duration from small, minor events lasting for a period of a day to larger, major events that lasted for several weeks and were comprised of several discrete events. The dynamism of the flow regime and the subsequent sediment transport characteristics can be grouped into

three distinct periods to investigate the influence on benthic Chl a: Minor fall events (High flow events A and B), a channel-forming flow (High flow event C), and moderate winter flow events (High flow events D-H).

There were two minor high flow events that occurred during the fall sampling period (events A and B, Table 2.4). Event A was the first precipitation event of the rainy season and had a peak Q of 0.34 m^3/s (0.1 Q_{bf}). Field observations prior to, during and following high flow event A indicated that the event flushed significant allocthonous leaf material from the stream bed. High flow event B occurred ~2 weeks after event A and had a peak Q of 0.69 m^3/s (0.2 Q_{bf}). Event B was followed by a large, long duration event that occurred between 12/3/15-12/29/15 (Storm C, Table 2.4). This high flow event was comprised of several individual events over the 26 day period. The maximum peak Q was outside the range of the rating curve (Figure 2.4). Field observations of high water marks following high flow event C indicated significant out of bank flow and sediment transport and deposition (Figure 2.14).

Figure 2.14 - High Flow Event C Field Observations: Field observation photograph following high flow event C. The photograph was taken on 12/22/16. The stream overtopped its banks during high flow event C as evidenced by the alluvial sediment deposition and wood accumulation piling up on a former bridge pylon along the right bank of Oak Creek. The top of the pylon is roughly 0.8 m above the active stream channel. Note the weir in the background of the photograph.

A total of five individual high flow events occurred during the winter period. Peak Q ranged from 0.49-1.91 m^3/s and event durations ranged from 1-11 days (Table 2.4). The beginning of the winter period was characterized by several large high flow events occurring during January and immediately following the large channel-forming flow in December. The peak Q of the January events were 1.91 and 1.29 m^3/s for high flow events D and E respectively. There was a dry period during February where only two minor high flow events occurred (High flow event F and G) with peak Q ranging from 0.49-0.56 m^3/s. A long, low intensity event occurred during a 11-day period in March where several smaller precipitation events yielded a peak Q of 1.46 m^3/s (High flow event H).

Table 2.5 - High Flow Event Disturbance Summary: Summary of disturbance parameters for the three study periods. N refers to the number of Chlorophyll-*a* sampling grid cells in each disturbance category. Mean, median, and maximum shear stress (τ) values are presented for each flow. The percentage of the bed capable of mobilizing the median grain size particle (D_{50}) ($\tau^*/\tau_r^* \geq 1$) is also presented.

Study Period (High Flow Event)[(a)]	n (High)	n (Low)	τ_{mean} (N/m^2)	τ_{median} (N/m^2)	τ_{max} (N/m^2)	$\tau^*/\tau_r^* \geq 1$ (% of bed)
Fall (B)	120	232	23.10	22.62	75.80	20%
High Flow Event C	352	0	51.12	51.46	163.06	79%
Winter (D,E and H)	182	170	27.48	27.04	88.69	35%

(a) These are the flow events used to characterize each period.

The magnitude and variability of τ for the high flow events was investigated using a calibrated 2-D hydraulic model of the study site. Only peak Q of high flow events that fell within the calibrated range of the model (0.64-3.4 m^3/s) were used to estimate τ. The fall period was characterized by high flow event B and the winter period was

characterized using an average of τ values for high flow events D, E and H. The maximum Q of the calibrated model range (3.4 m^3/s) was used to characterize high flow event C. As expected, the magnitudes of estimated τ increased with increasing discharge between the three flows (Table 2.5). Mean τ ranged from 23.1 - 51.46 N/m^2, median τ ranged from 22.62-51.46 N/m^2 and maximum τ ranged from 75.8-163.06 N/m^2. τ is highly variable throughout the reach for each of the modeled flows (Figure 2.15). There is a strong influence of bed topography on τ where the bank boundaries exhibit low τ (0-13 N/m2) for all of the modeled flows. The highest τ values for all flows are found within the bend and immediately downstream of it. This location corresponds to a pool formed against cohesive clay banks that constrain the flow into a small and stable portion of the stream. This section is located at the upstream end of the Chl-*a* sampling grid. τ values decrease along the straight portion of the stream and are highest in riffle areas. The spatial τ estimates were used to calculate the sediment transport capacity of the reach in terms of the Shields parameter.

2.5.1.2 Sediment Transport Capacity– Shields stress

The sediment transport capacity increased with Q for the three study periods with the % of the bed capable of mobilizing the D_{50} (i.e. $\tau^*/\tau^*_r > 1$) ranging from 20-79% (Table 2.5). For the fall flow, areas of the bed with $\tau^*/\tau^*_r > 1$ (denoted as orange and red locations on Figure 2.15) were concentrated within the thalweg and along riffle crests, and comprised 20% of the stream bed (Figure 2.15, Table 2.5). These areas increased in size for the larger winter flow to encompass a greater portion of the stream bed (35%). In the large, channel forming flow (High flow event C), the entire central portion of the study reach (79% of the total reach) has $\tau^*/\tau^*_r > 1$ with lower values only along the bank boundaries. The spatial distribution of τ^*/τ^*_r values was used to designate disturbance categories for nodes of the Chl-*a* grid.

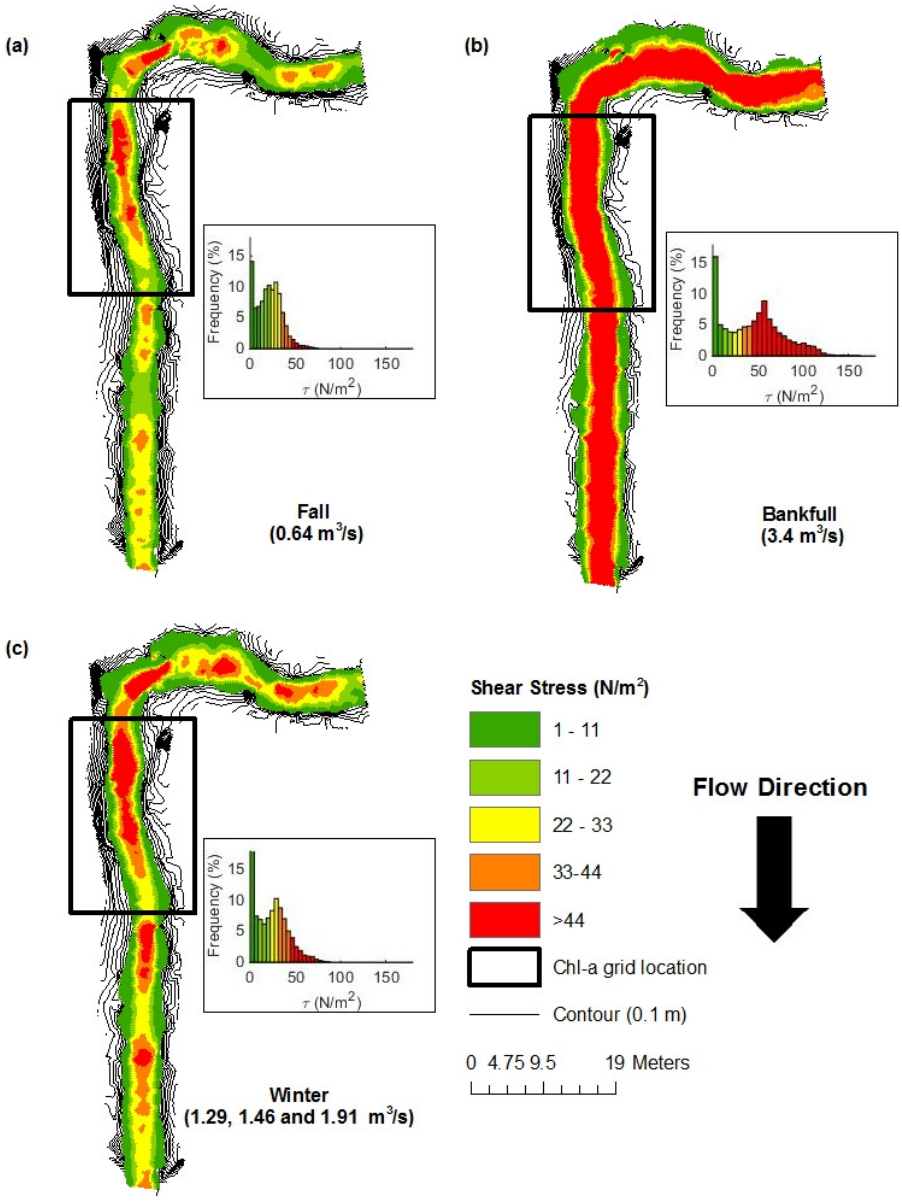

Figure 2.15 - Shear Stress Distributions of Disturbance Categories: Shear stress (τ) distributions for flows of the three study periods used to designate disturbance categories. A) The fall study period – High flow event B (Q =0.64 m^3/s). B) A bankfull flow event representing high flow event C (Q=3.4 m^3/s). C) The winter study period –An average of τ for high flow events D, E and H (Q=1.29 m^3/s, 1.46 m^3/s, and 1.9 m^3/s respectively). Colors in the histograms correspond to the legend of the spatial distributions. Orange and red colored locations and bins correspond to τ values capable of mobilizing the median grain size particle (D_{50}) based on the relationship between the applied and reference Shield's stress ($\tau^*/\tau^*_r > 1$)

2.5.1.3 Disturbance classification and implications

The results of the disturbance classification within the Chl-*a* sampling grid varied between the three periods (Figure 2.16). In general, there was a region of high disturbance along the center of the sampling grid which grew in size with increasing Q. This area corresponds to the stream thalweg along the pool-riffle transition sequence. Areas of low disturbance are found along the edges and within the lower portion of the Chl-*a* grid, which corresponds to the banks and the head of a pool at the downstream end of the grid. During the fall period, 66% and 34% of the grid cells were classified as having low and high disturbance respectively (Table 2.5). During the bankfull flow, 100% of the grid cells experienced high sediment disturbance (i.e. all grid cells had $\tau^*/\tau^*_r>1$). The classification of low and high disturbance were roughly equal (48 and 52) for the winter period. The disturbance classification scheme for each sampling period was used to investigate benthic algal growth dynamics both temporally and spatially. These results will be discussed below.

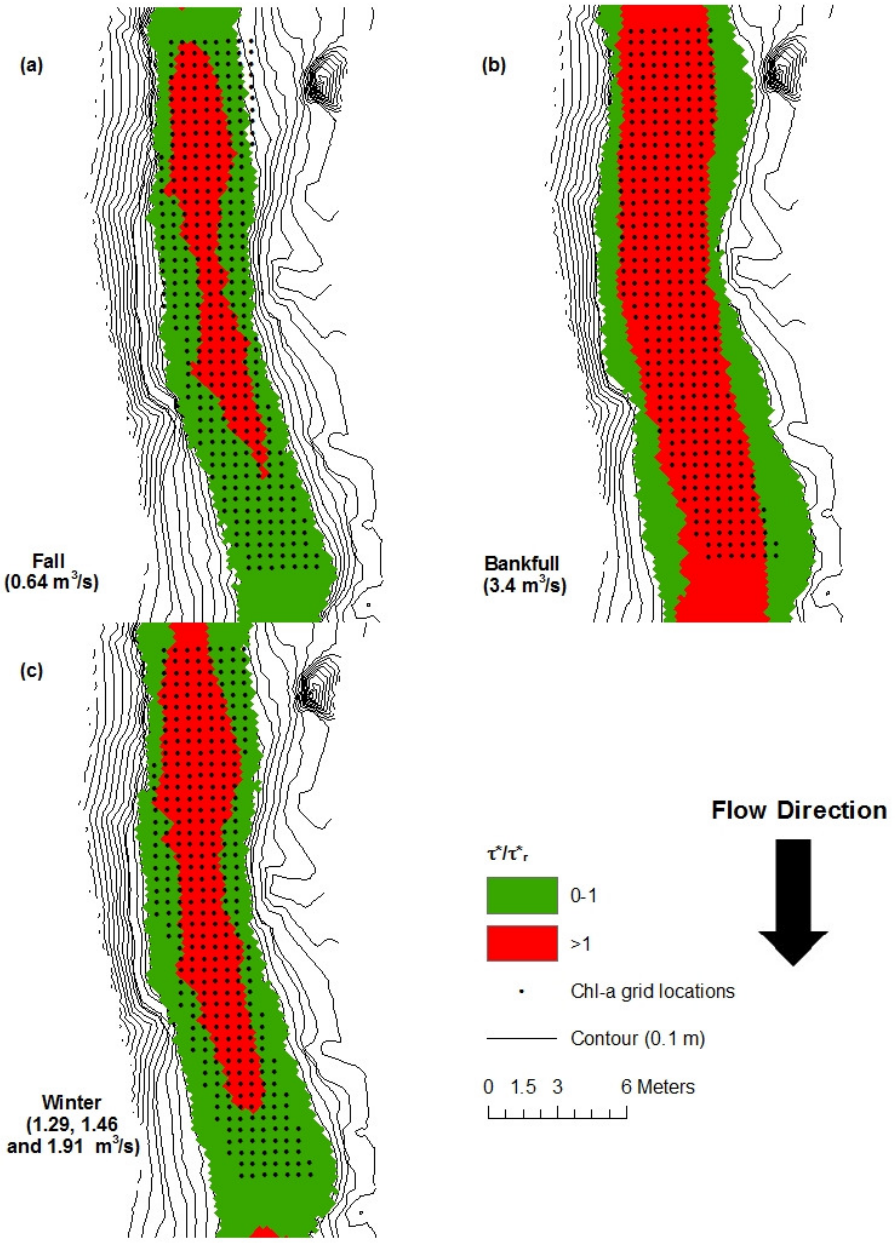

Figure 2.16 - Disturbance Map: Distributions of disturbance categories for the Chl-*a* sampling grid for flows of the three study periods. Disturbance categories are based on the ratio of applied to reference Shield's stress (τ^*/τ^*_r). Grid nodes with $\tau^*/\tau^*_r>1$ are classified as having high disturbance and $\tau^*/\tau^*_r<1$ as having low disturbance. High and low disturbance are designated in red and green colors respectively. A) The fall study period – High flow event B (Q =0.64 m^3/s). B) A bankfull flow event representing high flow event C (Q=3.4 m^3/s). C) The winter study period –An average of τ for high flow events D, E and H (Q=1.29 m^3/s, 1.46 m^3/s, and 1.9 m^3/s respectively).

2.5.2 Chlorophyll-a

2.5.2.1 The influence of Shear Stress on Chl-a

The relationship between τ and Chl-*a* is highly variable. There are a wide range of Chl-*a* concentrations for the same level of τ for all of the sampling dates in the study. However, the highest values of Chl-*a* seem to occur at intermediate values of τ in most sampling dates (Figure 2.17). This is further highlighted by the 95th quantile regression equation which shows a bell curve type shape for 10 out of 18 sampling dates (10/23/15-11/20/15, 1/11/16, 1/26/16, 2/15/16, 2/22/16, and 3/31/16). On these sampling dates, the highest Chl-*a* concentrations are found in grid cells with intermediate values of τ (i.e. 25-50 N/m^2) and the lowest concentrations at both high (i.e. >55 N/m^2) and low (i.e. <20 N/m^2) values of τ. The bell-curve shape of the 95th quantile regression is consistent with the intermediate disturbance hypothesis [*Connell*, 1978] which states that the highest levels of biodiversity and productivity will be found in areas with intermediate levels of disturbance. There were not clear relationships between τ and Chl-*a* for the remaining 7 sampling dates in the study as there was considerable scatter in the data and often elevated Chl-*a* values in either the high or low range of τ that changed the shape of the quantile regression (See 3/19/16 as an example).

The influence of τ on Chl-*a* can also be investigated by grouping the concentrations into disturbance categories. There were statistically significant differences ($p<0.1$) in mean Chl-*a* concentrations between high and low disturbance categories (Table 2.6) on 11 of 18 (61%) of the sampling dates (9 of 18 [50%] with $p<0.05$). The mean Chl-*a* concentration was significantly greater in the low disturbance category on 7 (39%) of the sampling dates with 4 of those instances occurring during the winter sampling period and 3 during the fall. Mean Chl-*a* concentrations were significantly greater in the high disturbance category on 4 (22%) of the sampling dates with 1 instance occurring during the winter sampling period and 3 during the fall.

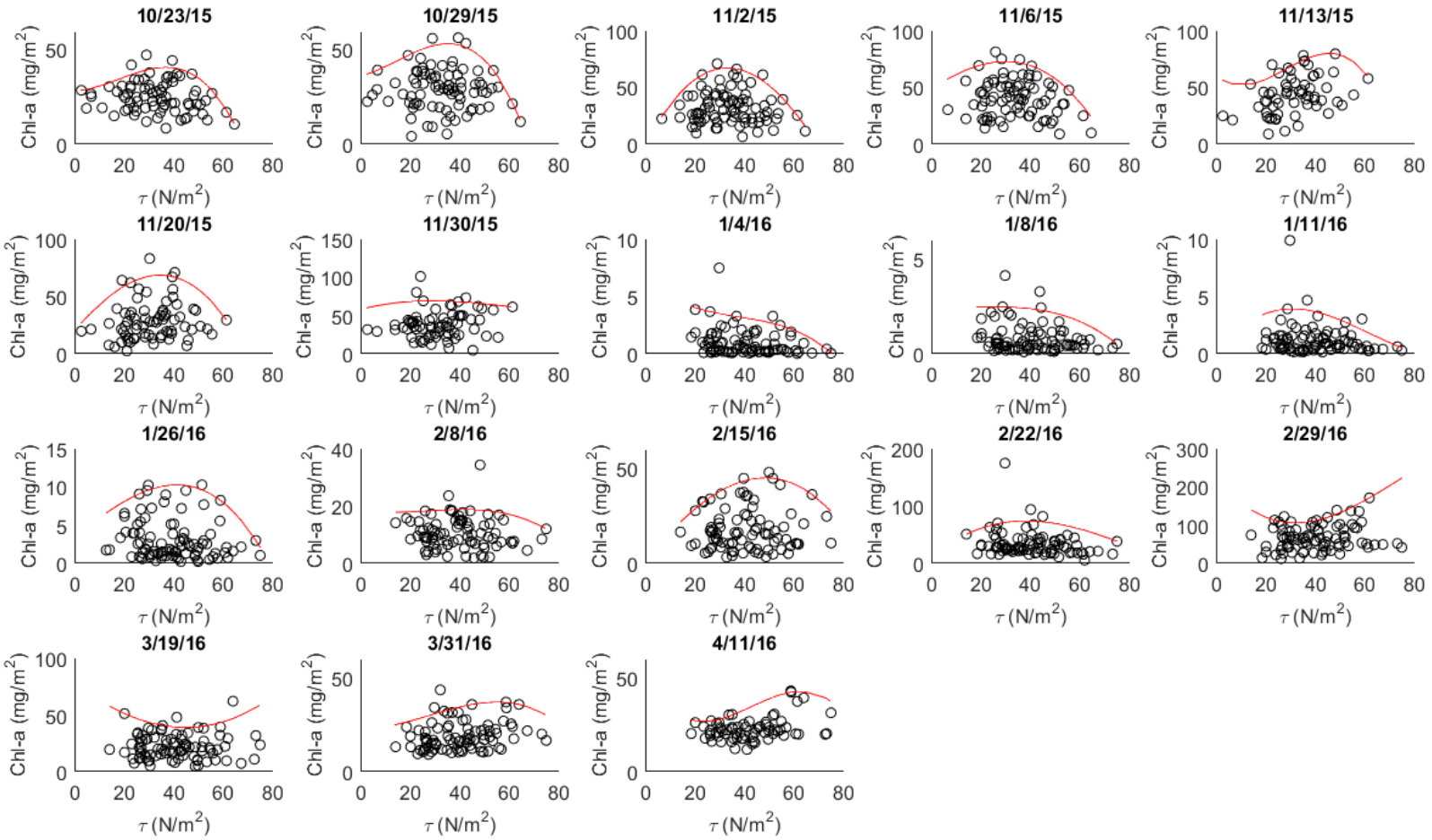

Figure 2.17 - Relationship between Chlorophyll-a and Shear Stress: Distributions of Chlorophyll-*a* (Chl-*a*) concentrations for a range of shear stress (τ) values during each sampling date of the study period. The red line represents the 95th quantile 3rd order polynomial regression of each dataset. The bell-shaped curves of several of the sampling dates indicate that those datasets are consistent with the Intermediate Disturbance Hypothesis.

2.5.2.2 Temporal Changes

The temporal variation of Chl-*a* concentrations during the study period can be characterized by periods of biomass loss immediately following high flow events and periods of biomass accrual in between high flow events (Figure 2.18). Overall, mean Chl-*a* values ranged from 0.12-52.30 mg/m^2 for the high disturbance areas and from 0.21-36.56 mg/m^2 for the low disturbance areas during the study duration (Table 2.6). The lowest measured mean concentrations occurred following high flow event C (0.12 and 0.21 mg/m^2 for low and high disturbance, respectively). The highest measured mean concentrations occurred in the high disturbance areas during the recovery periods after high flow events (11/13/15 – 52.30 mg/m^2, after high flow event A and 2/29/16 – 40.84 mg/m^2 after high flow event G). Chl-*a* concentrations were similar during both the beginning (10/23/15 – 20.59-25.63 mg/m^2) and end (4/11/16 – 19.06-19.41 mg/m^2) of the study period where algal biomass appears to reach a plateau preceding and following the rainy season. Changes in biomass loss and accrual is contextualized with each high flow event below.

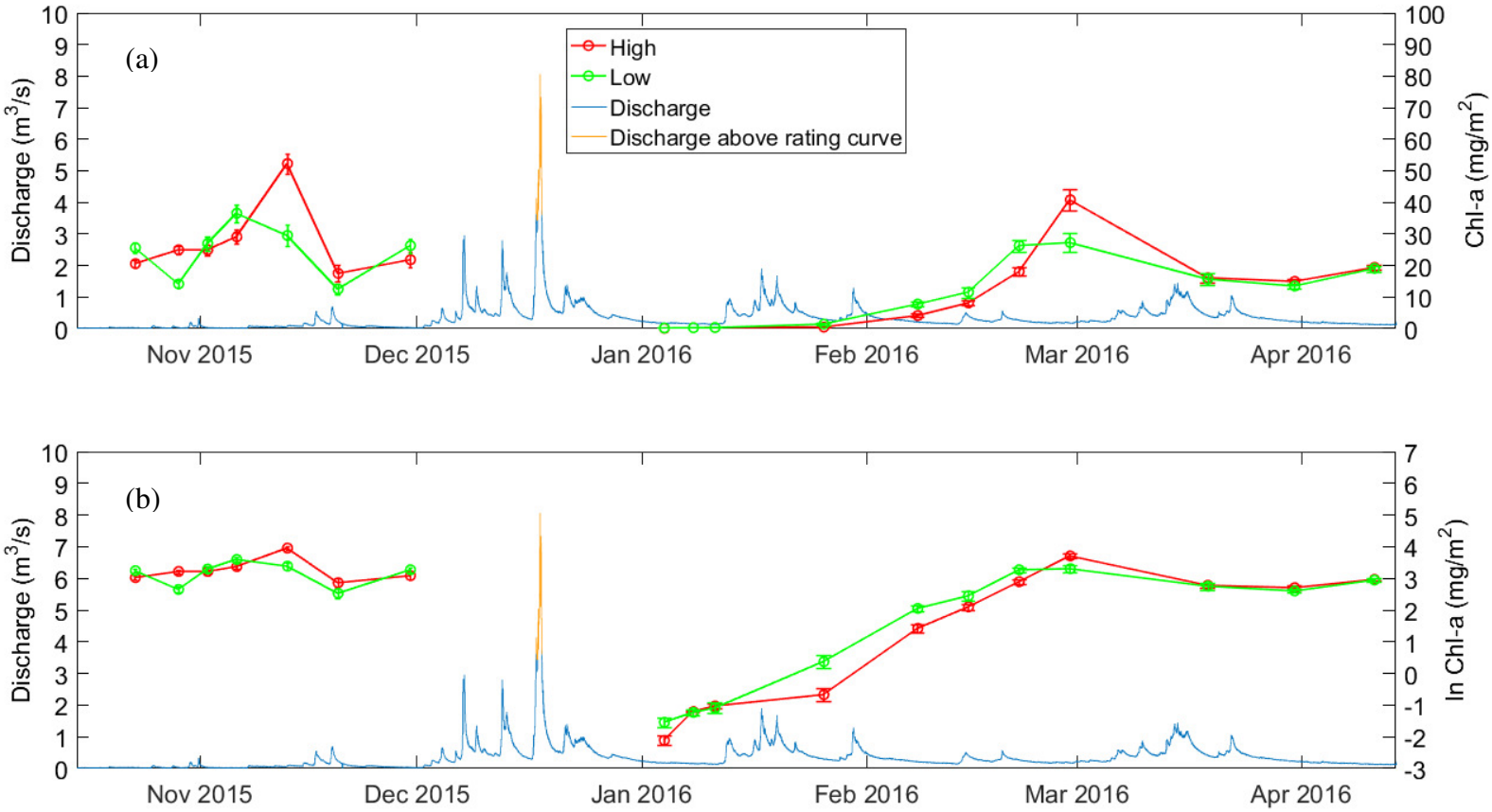

Figure 2.18 - Temporal Variability of Chlorophyll-a: Mean Chlorophyll-*a* (Chl-*a*) measurements for both low and high areas of disturbance in Oak Creek, OR between 10/16/15 and 4/11/16 in both (A) linear and (B) log space. The hydrograph is shown to contextualize the disturbance regime. The specific occurrence of high flow events can be found above in Figure 2.5.

Table 2.6 - Summary of Chlorophyll-a Measurements: Summary of benthic Chlorophyll-*a* (Chl-*a*) measurements taken on 18 sampling dates between 10/23/15-4/11/2016: The total number of grid cells sampled (n), mean Chl-*a* concentrations (Chl-a_{mean}), the standard deviation of Chl-*a* measurements (Chl-a_{std}), the p-value of the Komolgogorov-Smirnov test (KS p-value) and the percent change between sampling dates are presented for both low and high disturbance categories. The Student's t-test p-value comparing both low and high distributions during each sampling date are also presented. * denotes significant differences at $p<0.05$. ** denotes significant differences at $p<0.10$

Date	Low					High					T-test	
	n	*Chl-a $_{mean}$ (mg/m^2)*	*Chl-a $_{std}$ (mg/m^2)*	*KS p-value*	*% Change*	*n*	*Chl-a $_{mean}$ (mg/m^2)*	*Chl-a $_{std}$ (mg/m^2)*	*KS p-value*	*% Change*	*p value*	*Different?*
10/23/2015	26	25.41	1.48	0.81		51	20.53	1.30	0.70		0.019	*
10/29/2015	28	14.63	1.15	0.96	-42%	54	24.91	1.36	0.61	21%	0.000	*
11/2/2015	29	28.14	2.11	0.30	92%	56	23.96	1.73	0.82	-4%	0.154	
11/6/2015	27	36.81	2.51	0.69	31%	52	28.10	2.33	0.97	17%	0.014	*
11/13/2015	26	29.70	3.24	0.81	-19%	37	52.79	3.27	0.97	88%	1.12E-05	*
11/20/2015	30	12.58	1.84	0.42	-58%	44	17.65	2.59	0.86	-67%	0.065	**
11/30/2015	28	26.45	2.22	0.15	110%	44	21.54	2.57	0.99	22%	0.137	
1/4/2016	30	0.21	0.03	0.08	-99%	56	0.12	0.02	0.00	-99%	0.013	*
1/8/2016	31	0.29	0.03	0.04	36%	56	0.30	0.00	0.01	152%	0.742	
1/11/2016	31	0.35	0.05	0.01	19%	56	0.36	0.03	0.03	18%	0.876	
1/26/2016	33	1.05	0.24	0.53	204%	57	0.52	0.10	0.01	46%	0.074	**
2/8/2016	30	7.76	0.82	0.88	640%	54	4.11	0.56	0.56	691%	0.001	*
2/15/2016	29	9.07	1.38	0.49	17%	57	8.78	0.91	0.21	114%	0.862	
2/22/2016	29	26.22	1.83	0.04	189%	57	18.03	1.31	0.21	105%	3.87E-04	*
2/29/2016	29	27.52	2.88	0.79	5%	57	40.60	3.34	0.33	125%	3.76E-04	*
3/19/2016	29	15.84	1.73	0.77	-42%	58	16.04	1.43	0.59	-60%	0.922	
3/31/2016	29	13.51	0.79	0.63	-15%	57	15.01	0.88	0.45	-6%	0.128	
4/11/2016	17	19.06	0.97	0.97	41%	52	19.41	0.72	0.06	29%	0.749	

2.5.2.3 Biomass loss/gain immediately following high flow events

High flow events significantly influenced Chl-*a* concentrations in both low and high disturbance areas throughout the study duration. The degree to which regions were effected however, varied with disturbance classification and algal standing stocks preceding a given high flow event. Chl-*a* concentrations decreased following high flow events in which Chl-*a* concentrations were >20 mg/m^2 prior to the event in all but one instance (High flow event A). This occurred three times during the study period (High flow events B, C, and H). There was a 99% loss in Chl-*a* concentration following high flow event C, which was the largest event during the study period. High flow events B and H caused similar decreases in both regions of low (58% and 42%) and high (67% and 61%) disturbance, respectively. There was no significant Chl-*a* concentration difference between disturbance categories following events B and H ($p>0.05$, Table 2.6). Although mean Chl a concentrations were low (<0.21 mg/m2) and significantly different between disturbance categories following high flow event C ($p=0.014$). High flow event A caused a 0.1% loss in Chl-*a* concentrations in the high disturbance areas. Conversely there was a 90% increase in Chl-*a* concentrations in the low disturbance. The Chl-*a* concentrations were statistically similar ($p>0.05$) on 11/2/2015 following high flow A.

Chl-*a* concentrations increased for both disturbance categories following high flow events when Chl-*a* concentrations were <20 mg/m^2 prior to the event (Figure 2.18, Table 2.6). This occurred 4 times during the study period (high flow events D, E, F, and G). These events occurred during the winter sampling period immediately following high flow event C. Chl-*a* concentrations increased in low disturbance regions by 204%, 640%, 17% and 189% and by 46%, 691%, 114% and 105% in the high disturbance regions for the 4 events respectively. These increases occurred even though high flow events D and E were the second and fourth largest during the study period. There were significant differences in Chl a between disturbance categories during two sampling events (2/8/16 and 2/22/16, $p<0.05$) which preceded high flow events E and G respectively.

Differences in biomass accrual rates between disturbance categories can be investigated by focusing on two distinct periods of biomass growth during the study

duration: once during the fall sampling period (10/29/15-11/13/15), and during the winter sampling period (1/4/16-2/29/16). In both instances, Chl-*a* concentrations were similar prior to the growth period and areas of low disturbance showed a faster initial growth rate. The growth rates for disturbance categories switched however during the accrual period and Chl-*a* concentrations were higher for areas of high disturbance at the end of the growth phase (Figure 2.18, Table 2.7). In both of these sampling periods (11/13/15 and 2/29/16) there were significant differences between sample populations of both disturbance categories (p=1E-05 and p=3E-4 respectively). During the fall period, the T_D was faster for the high disturbance category (13.2 days, $R^2 = 0.84$) than the low disturbance category (16.4 days, R^2=0.46) (Table 2.7). This is in consistent to the winter period where the T_D was also faster for the high disturbance category (7.0 days, R^2=0.97) than the low disturbance category (7.4 days, R^2=0.98).

Table 2.7 - Chlorophyll-a Doubling Time: Summary of exponential regression parameters used to calculate the doubling time of benthic Chlorophyll-*a* (Chl-*a*) in Oak Creek, OR during periods in the fall and winter. The listed parameters follow the general regression equation [Chl-*a*]=$ae^{b*Trecovery}$ where [Chl-*a*] is the mean Chl-*a* concentration, $T_{recovery}$ is the recovery time, *a* is the intercept, and *b* is the slope. The doubling time (T_D) is calculated using the equation T_d=ln(2)*(1/b). The coefficient of determination (R^2) of the regression is also presented.

Date Range	Low Disturbance				High Disturbance			
	a	***b***	***T_d (days)***	***R^2***	***a***	***b***	***T_d (days)***	***R^2***
10/29/15-11/13/15	20.31	0.04	16.4	0.46	0.18	0.09	7.4	0.98
1/4/16-2/29/16	22.67	0.05	13.2	0.83	0.12	0.10	7.0	0.97

2.6 Discussion

The goal of our study was to quantify how spatial and temporal variability in fluvial disturbance and sediment transport processes influence benthic algal communities. We conducted this study in a rainfall dominated system characterized by a temporally dynamic flow regime. The spatial variability of sediment transport processes was assessed using a 2-D hydrodynamic model at high spatial resolution (<0.5 m^2). We coupled this detailed physical description with high resolution measurements of Chl-*a* in order to capture the growth dynamics of benthic algal communities through both space

and time. Our results indicate that fluvial disturbance processes significantly influence benthic algal Chl-*a* concentrations, however the strength of this influence varied throughout the study period. In order to understand this variability, we will first discuss how our definition of disturbance was able to characterize sediment transport processes. Next, we will contextualize temporal variability in Chl-*a* concentrations using ecological concepts (resistance and resilience) about how algal communities respond to disturbance. Lastly, we will investigate how spatial variability of τ directly structures benthic algal communities. Our findings highlight the need to incorporate spatial and temporal heterogeneity of the disturbance regime to understand how fluvial processes influence benthic algal communities.

2.6.1 Defining disturbance – Incorporating the variability of flow into metrics of disturbance

Our results indicate that 2-D estimates of bed mobility are better predictors of benthic algal response to fluvial disturbances than 1-D estimates alone. Utilizing 2-D τ estimates to quantify the sediment transport dynamics within a river reach is a common strategy in the fields of river engineering and geomorphology [e.g. *Lisle et al.*, 2000; *Pasternack et al.*, 2004; *Legleiter et al.*, 2011]. However, these methods have only been rarely applied [e.g. *Segura et al.*, 2011] to study the influence of sediment transport processes on benthic algal communities even though the importance of using cross-discipline methods to study stream ecosystems has been recognized [see review by *Stanley et al.*, 2010]. Typically, studies rely on metrics of discharge [e.g. *Fisher et al.*, 1982; *Biggs and Close*, 1989; *Townsend and Douglas*, 2014], 1-D estimates of substrate mobility [e.g. *Uehlinger et al.*, 1996a; *Biggs et al.*, 1999], or spatial patterns of scour and fill [e.g. *Matthaei et al.*, 2003; *Luce et al.*, 2013] to quantify fluvial disturbance. Because these metrics do not account explicitly for the spatial variability of τ and over-simplify sediment transport processes within a reach, they are not able to identify the underlying disturbance processes. Our 2-D hydrodynamic modeling results were able to capture the spatial and temporal variability of τ within our study site (see Figure 2.15) and identify the relative location of patches of potential substrate mobility for each fluvial disturbance event that occurred. Indeed, the location of stable and mobile areas within our study reach

varied with each high flow event. This characterization allowed us to mechanistically categorize our Chl-*a* measurements within a bed mobility framework and quantify spatial and temporal trends. Our work goes beyond previous efforts by linking the growth dynamics of benthic algae to 2-D estimates of bed mobility at high spatial and temporal scales.

The difference between utilizing 2-D and 1-D metrics of bed mobility (such as discharge) is best illustrated by examining the changes we observed in Chl-*a* concentrations following two high flow events of different magnitudes – high flow events B ($Q=0.69\ m^3/s$) and H ($Q=1.46\ m^3$). The reductions in Chl-*a* concentrations were similar for both disturbance categories following both events although the peak Q of event B was only 47% that of event H. If the disturbance from these events had been characterized using discharge or 1-D τ, there would have been large (i.e. 47%) differences between the events. However, utilizing 2-D estimates of bed mobility allowed us to characterize similarities between each high flow event. The greater reduction in Chl-*a* concentrations in the high disturbance categories indicates that mobilization of moderate- large grain sizes (i.e. at least the D_{50}) is an important metric of disturbance to benthic algae. However, the reductions in the low disturbance categories show that other processes such as the mobilization of smaller particles, abrasion cause by suspended sand, and sloughing of algal mats due to elevated velocity, could also be responsible for disturbing algal communities. This is confirmed by a number of studies where a myriad of disturbance processes have been highlighted [e.g. *Biggs et al.*, 1999; *Francoeur and Biggs*, 2006; *Segura et al.*, 2011; *Luce et al.*, 2013]. Although the results from these two high flow events indicate the influence of sediment transport processes on benthic algae from flood disturbances, they are contrasted with observations after four other events after which Chl-*a* concentrations increased.

2.6.2 The influence of disturbance history on algal resistance

The Chl-*a* concentration (and thus algal abundance) prior to a disturbance event is an important factor in determining the response of the algal community to the event. There were increases in Chl-*a* concentrations following high flow events D, E, F, and G

which occurred in succession during the winter study period and had magnitudes and bed mobility that were similar to B and H (which reduced Chl-*a* concentrations). What is different about these events however, is that Chl-*a* concentrations prior to the events was much lower than for B and H. High flow events D-G occurred following a complete reset of both the channel bed and the benthic algal community following high flow event C, while B and H occurred after periods of growth and minimal disturbance. Furthermore, the increases found following events D-G occurred during the cold winter months where growth conditions were sub-optimal compared to the other group. The results of other studies focusing on the resistance and succession of individual taxa that comprise algal communities can help explain the observed differences that resulted between these groups of high flow events.

There are differences in the resistance to flood disturbance amongst benthic algal species and thus the stage of community succession present during a high flow event can influence the community's response. Previous studies [e.g. *Stevenson*, 1990; *Peterson and Stevenson*, 1992; *Biggs and Thomsen*, 1995; *Davie and Mitrovic*, 2014] have shown that in temperate climates, early successional species such as diatoms show greater resistance to flood disturbance than late successional species such as filamentous algae because of differences in their growing habit (i.e compact single cell diatoms vs. lengthy multicellular filamentous algae). Although we did not monitor species composition data, the contrasting results found for the two groups of storms mentioned above are consistent with there being different species present right before the disturbance event. High flow events B and H, where decreases in Chl-*a* were detected, occurred after periods of minimal disturbance (a dry Mediterranean-*esque* summer for B and a dry winter period for G). During these periods, succession in the benthic algal communities was allowed to proceed un-interrupted by high flow events for 3 months-whole summer. Communities in the later stages of succession have shown to be less resistant to flood disturbance [i.e. *Peterson and Stevenson*, 1992], which explains the similar responses exhibited after each of these high flow events. High flow events D-G, where Chl-*a* did not decrease, occurred both during and after periods of frequent disturbance events and thus succession may have been interrupted several times. The benthic algal community was essentially reset

following high flow event C and only the most resistant taxa likely remained. These taxa grew slowly during the period that followed where high flow events D-H frequently disturbed the system and prevented less-resistant species from establishing. Stevenson [1990] documented similar responses of temperate diatom growth during frequent flood disturbances. These differences in the response of benthic algal communities to flood disturbance highlight the need to consider the disturbance history of a community when establishing disturbance thresholds.

2.6.3 Resilience of algal communities from areas of contrasting disturbance

The results of our study also show that the resilience of algal communities during the recovery period following a high flow event is dependent on the spatial variability of bed mobility of the disturbing event. During the initial recovery period, regions of the bed that did not experience mobilization of the D_{50} (i.e. low disturbance) were associated to faster Chl-*a* recovery rates than areas in which the D_{50} was likely mobile (i.e. high disturbance). However, higher Chl-*a* concentrations were measured in areas of high disturbance at the end of the recovery periods and the overall doubling time was faster. Possible mechanisms for these findings include increased nutrient flux and light availability (due to removal of dead biomass) in areas of elevated velocity. These results are consistent with several studies [*Stevenson*, 1990; *Peterson et al.*, 1994; *Matthaei et al.*, 2003; *Murdock et al.*, 2004; *Townsend and Douglas*, 2014] yet in contrast to many others [*Biggs and Close*, 1989; *Peterson and Stevenson*, 1992; *Uehlinger et al.*, 1996; *Biggs et al.*, 1999; *Bergey and Resh*, 2006; *Segura et al.*, 2011] which showed inverse relationships between resilience and disturbance. The inconsistency in the resiliency/disturbance relationship highlights the complexity of process identification in stream ecology.

The resilience of an algal community is dependent not only on the disturbance history but on the availability of abiotic resources such as light, temperature, and nutrients, as well as biotic interactions such as grazing pressure and community composition [*Larned*, 2010; *Townsend and Douglas*, 2014]. Our study was able to control for the availability of these abiotic resources because we compared communities

within the same stream reach and thus disturbance was the only spatially variable abiotic factor. Typically, studies investigating the influence of disturbance on the resilience of benthic algae compare streams with different disturbance histories [e.g. *Lyford and Gregory*, 1975; *Biggs et al.*, 1999; *Stanish et al.*, 2011], through flume experiments [*Peterson and Stevenson*, 1992; *Peterson et al.*, 1994; *Biggs et al.*, 1998; *Coundoul et al.*, 2015] or most commonly by studying temporal changes in one stream with multiple disturbance events [*Fisher et al.*, 1982; *Power and Stewart*, 1987; *Biggs and Close*, 1989; *Stevenson*, 1990; *Uehlinger et al.*, 1996; *Gustina and Hoffmann*, 2000; *Murdock et al.*, 2004; *Davie et al.*, 2012; *Snell et al.*, 2014; *Townsend and Douglas*, 2014]. Differences in abiotic growth resources either between sites or within the same site at different times of the year may affect the growth rates of benthic algae which complicates isolating the influence of disturbance processes. Our study design however, allowed us to isolate the influence of disturbance on algal resilience. It should be noted however, that we did not control for grazing pressure which may have influence growth rates.

2.6.4 The relationship between shear stress and Chl-a – support for the Intermediate Disturbance Hypothesis

The relationship between τ and the 95th percentile quantile regression of Chl-*a* exhibit a bell-shaped pattern consistent with the Intermediate Disturbance Hypothesis (IDH) for most sampling dates throughout the study period. The IDH is a fundamental theory in ecology proposed by Connell [1978] in regards to patterns of biodiversity exhibited in coral reefs and tropical rainforests. The theory proposed that species diversity would be greatest in systems that undergo an intermediate level of disturbance, with diversity decreasing for both infrequent and very frequent levels of disturbance (hence the bell-shaped curve). This hypothesis has been well supported in respect to community composition of invertebrates and bryophytes in streams, with taxa richness tending to be maximized at some intermediate level of disturbance [*Townsend et al.*, 1997; *Suren and Duncan*, 1999; *Lake*, 2000]. Although there have been fewer studies, the relationships also hold for benthic algae [*Ács and Kiss*, 1993; *Fayolle et al.*, 1998; *Ryder*, 2004]. While we measured productivity (as proxied by Chl-*a* concentrations) and not biodiversity, the diversity-productivity relationship of benthic algae has been shown to be

positive for streams with highly variable disturbance regimes like our study site [*Cardinale et al.*, 2005].

The bell-shaped relationship between τ and Chl-*a* was surprising compared with the documented negative relationship exhibited elsewhere [*Biggs and Thomsen*, 1995; *Biggs et al.*, 1999; *Biggs and Smith*, 2002; *Segura et al.*, 2011]. However, these negative relations were found either by comparing different streams [e.g. *Biggs et al.*, 1999] or patches within a stream [e.g. *Segura et al.*, 2011]. In fact, our study is the only we are aware of that considered fine spatial scale variability in Chl-*a* associated to flow hydraulics. It should be noted however, that not all of these studies (i.e. Segura 2011) were conducted in streams with "highly variable" disturbance regimes in which the IDH relationship with productivity (in addition to biodiversity) would be expected. We hypothesize that the patterns we find in our data may have been caused by species differences in resistance/resilience (discussed in detail above), differences in nutrient fluxes and biomass removal due to flow variability, and heterogeneity in grazing pressure due to fluvial variations [e.g. *Townsend et al.*, 1997; *Matthaei and Townsend*, 2000; *Jowett*, 2003; *Blettler et al.*, 2012]. While the specific process cannot be identified by this study, all of those suggested above are influenced by fluvial forces. These results demonstrate that heterogeneity of flow forces within natural systems can have profound influences on the productivity (and diversity) of benthic primary producers and thus on structuring stream ecosystems as a whole because biodiverse ecosystems are more efficient at capturing resources, producing biomass, cycling nutrients and are in general more resistant to change [*Cardinale et al.*, 2012]. The majority of τ values in our study site fell within the "intermediate" range (see the histograms within Figure 2.15) responsible for the maximum productivity during the sampling dates that are consistent with the IDH. These findings imply that the benthic algal communities present in our study site have adapted to the highly variable flow regime so that production (and thus biodiversity) are maximized even during (or because of) the presence of fluvial disturbance.

2.6.5 Broader implications

The results of our study show that fluvial disturbance processes influence benthic algal communities through scales of space and time. Our findings support previous studies but demonstrate that the influence occurs within the spatial scales of a stream reach as well as over temporal scales or larger (i.e. between streams) spatial scales. We were able to make these conclusions by characterizing both fluvial and ecological processes within the same scale and at resolutions not measured elsewhere. The conclusions of our study demonstrate that fluvial processes are fundamental to structuring stream ecosystems and that spatiotemporal heterogeneity in the flow regime translates into heterogeneous ecological processes such as differences in resistance, resilience, and productivity. This indicates that streams with variable disturbance regimes may be most susceptible to human alteration as decreased heterogeneity may cause reductions in biodiversity/productivity and have a negative effect on the ecosystem. These findings will be informative to the broader community as efforts increase to re-establish natural flow regimes and to incorporate concepts of ecological heterogeneity into river restoration projects and the management of water resources in general.

2.7 Conclusion

The results of this study indicate that spatial and temporal variability in sediment transport processes significantly influence the growth dynamics of benthic algal communities. By defining fluvial disturbance based on metrics of sediment mobility and evaluating areas of contrasting disturbance, we were able to isolate these effects for high flow events of different magnitudes and demonstrate that 2-D metrics of disturbance are better indicators of benthic algal response than 1-D metrics such as discharge. Temporal variability in the response and recovery of benthic algae to high flow events demonstrate that the pre-disturbance productivity of the algal community can determine the amount of influence a fluvial disturbance event will exert. This was most likely due to variations in the resistance of different algal species present at the time of the each high flow event. The consistency of the relationship between τ and the 95^{th} quantile regression of Chl-*a* with the intermediate disturbance hypothesis demonstrate that spatial variability in τ acts

as a limiting factor on benthic algae to fundamentally structure the productivity (and biodiversity) at the base of stream ecosystems. The data presented in this study highlight the importance of quantifying the spatial and temporal variability of sediment transport processes in future studies of how fluvial disturbance influences stream ecosystems.

3. CAN FLUVIAL-HYDRAULIC MODELS ACCURATELY PREDICT BED LOAD TRANSPORT RATES IN GRAVEL BED STREAMS?

3.1 Abstract

This study investigates whether incorporating spatially variable shear stress (τ) estimates into bed load transport functions for gravel bed streams can be used to accurately predict bed load transport rates. Sediment transport is the result of complex interactions between the flow and sediment supply regimes which produce spatio-temporal variability in both the distribution of the flow forces causing transport as well as the sizes of the particles being transported. This variability is not however, incorporated into commonly used transport equations which use reach-averaged values of τ to estimate bed load. Because of this, uncertainty can result in bed load transport calculations due to the non-linear dependence on τ in the transport equations. Our study was conducted in a 96 m reach of Oak Creek, OR – a small gravel bed stream in the Oregon Coast range. The study site is located in the same reach that was used to collect the historic Oak Creek bed load dataset of Milhous [1973] which was used to develop many common transport equations. Contemporary bed load measurements were taken during 5 flow events ranging from 0.24 bankfull (Q_{bf}) to 0.52 Q_{bf} using a Helly-Smith bed load sampler in order to confirm the stability of sediment transport dynamics in Oak Creek. The contemporary measurements were consistent with the historical dataset for total load however, they had a finer grain size distribution (GSD). A 2-dimensional (2-D) hydrodynamic model (FaSTMECH) was used to calculate spatial distributions of τ for 5 flow levels ranging from 0.2 Q_{bf} to Q_{bf} (0.64-3.4 m^3/s). Results indicate that τ is highly variable within the study reach and that mean normalized τ distributions are remarkably similar between flow levels. The τ distributions were then discretized and used to calculate bed load transport rates using the transport equations of Parker and Klingeman [1982] (PK) and Wilcock and Crowe [2003] (WC) and the discretization methods of Segura and Pitlick [2015], and compared against the historical dataset for accuracy. Modeled bed load transport was consistently larger and coarser than the historical samples. Areas of τ greater than 2 times the mean comprised <2.5% of the bed and were responsible for transporting 48.1-95.8% and 31.9-37.3% using the PK and WC equations

respectively. We hypothesize that the inconsistency in our estimates may be due to using 2-D τ with a reach averaged reference shields stress (τ_r*) value which may have caused such high transport rates from a small portion of the bed. Scaling τ_r* with τ throughout a reach may provide the basis for future work to incorporate spatially variable τ into commonly used bed load transport functions.

3.2 Introduction

The transport of sediment along a river's flow path is a defining feature of natural alluvial river systems. Sediment transport is the result of complex interactions between the flow and sediment regimes which create spatially and temporally heterogeneous patterns of transport within a river system [*Pitlick*, 1988; *Lisle et al.*, 2000; *Clayton and Pitlick*, 2007; *McDonald et al.*, 2010; *Segura et al.*, 2011; *Recking*, 2013a; *Segura and Pitlick*, 2015]. The variability of these processes result in adjustments of channel form through the creation of bed-forms such as riffles, pools, bars, and steps, which in turn create variability in the flow hydraulics responsible for moving sediment. The feedback between these processes (sediment transport, channel form, and flow hydraulics) is complicated by additional interactions with the changing flow regime [*Leopold and Maddock Jr.*, 1953; *Ferguson*, 1986; *Knighton*, 1998], supply of sediment available for transport [*Schumm*, 1960; *Beechie and Bolton*, 1999; *Buffington et al.*, 2003], channel geometry [*Leopold and Maddock Jr.*, 1953; *Parker*, 1979; *Mueller et al.*, 2005], and surrounding hillslope and riparian influences such as vegetation and watershed lithology [*Grant et al.*, 1990; *Faustini and Jones*, 2003; *Yager and Schmeeckle*, 2013; *Mueller and Pitlick*, 2014; *O'Connor et al.*, 2014; *Bywater-Reyes et al.*, 2015]. Changes to any (or all) of these processes that result from both natural and anthropogenic perturbations are in turn expressed in a river's sediment transport regime. Thus, being able to quantify sediment transport rates (Q_b) for a particular river system is important to understand changes in fundamental river processes and for guiding efforts to restore these natural processes in altered river systems.

While the importance of understanding the sediment transport dynamics of a river system is well known, measuring Q_b brings forth many challenges for researchers and practitioners alike. Quantifying Q_b is both expensive and practically challenging, as data from a wide range of flows is required to develop robust relationships and many of those flows can be too dangerous to wade [*Bunte et al.*, 2008]. Samples collected using hand-held sediment samplers have been shown to be widely variable due to factors such as orifice size and sampling time [*Emmett*, 1980; *Beschta*, 1981; *Pitlick*, 1988; *Vericat et al.*, 2006]. While advances in safe, accurate sediment sampling technology such as bed load

traps [e.g. *Bunte et al.*, 2008], radio tracers [*Schmidt and Ergenzinger*, 1992; *Bradley and Tucker*, 2012; *May and Pryor*, 2014; *Olinde and Johnson*, 2015], and acoustic impact methods [*Rickenmann and McArdell*, 2007; *Yager et al.*, 2007; *Wyss et al.*, 2016] provide possible alternatives to hand-held samplers, field efforts remain expensive and out of reach for many practical applications.

Due to the challenges of collecting robust field measurements, modeling Q_b can be a convenient strategy. The development of empirical Q_b relationships has progressed significantly over the past three decades and allows for the estimation of Q_b based on input data such as hydraulic conditions and the grain size distribution (GSD) of a site [*Parker and Klingeman*, 1982; *Parker et al.*, 1982; *Parker*, 1990; *Wilcock and Crowe*, 2003; *Barry et al.*, 2004; *Recking*, 2013b]. Much of this work, and in particular the work of Parker and others, utilized Q_b data from Oak Creek, a steep, coarse gravel bed stream in the Oregon Coast Range [*Milhous*, 1973]. The Oak Creek dataset was collected using a vortex sampler between 1969-1990; data from 1971 was published in the thesis work of Milhous [1973]. The dataset is unique in that the vortex sampling method was able to capture the entire Q_b flux of gravels and cobbles for a wide range of flows over long time periods, reducing the error associated with hand-held samplers [*Parker et al.*, 1982]. Although it has been reported that the efficiency of the vortex sampler decreased for smaller grain sizes [*Milhous*, 1973; *O'Leary and Beschta*, 1981], the Oak Creek dataset remains one of the most comprehensive to date.

The transport relations of Parker and others were developed based on Oak Creek data by collapsing the relations between reference conditions for the motion of different grain sizes into a single function (i.e. a similarity collapse) [*Einstein*, 1950; *Parker and Klingeman*, 1982; *Parker et al.*, 1982; *Parker*, 1990]. The original two studies, Parker et al. [1982] (PKM) and Parker and Klingeman [1982] (PK), introduced the concept of equal mobility which was based on the observation that the GSD of Q_b corresponded more closely with the subsurface GSD than that of the coarser surface layer evident at low flows [see explanation in *Parker and Toro-Escobar*, 2002]. They hypothesized that although coarser grains are more difficult to move because they are heavier, grains

actually move in accordance with their abundance in the bed. They related this to the formation of a coarse "pavement" (surface material) which overlies a finer "sub pavement" (subsurface material) in a stream bed. The coarser surface material effectively over-exposes the larger grain sizes in comparison to finer grains resulting in movement of all grain sizes in direct proportion to their abundance. Both PKM and PK limited their analysis to flows during which the "pavement" was broken to develop their transport functions. PKM computes total Q_b based on a single grain size (the median - D_{50}) whereas PK expands that relationship to the entire GSD. This is accomplished through a hiding function to account for differences in the exposure of particles to the flow in mixed-sized beds. Additionally, PK incorporated a low flow transport relation to estimate the GSD of Q_b at a full range of flows.

Although the two transport relations of PKM and PK have been successfully applied to many types of river systems, recent work by Recking [2013a] highlights the variability that can be incorporated into Q_b estimates due to uncertainty in input shear stress (τ) values. The high spatial variability in τ varies throughout a river reach has been well documented [*Lisle et al.*, 2000; *Clayton and Pitlick*, 2007; *May et al.*, 2009; *McDonald et al.*, 2010; *Segura et al.*, 2011; *Recking*, 2013a; *Segura and Pitlick*, 2015; *Monsalve et al.*, 2016]. Most transport functions however (including PKM and PK) utilize width and reach averaged estimates of τ in their calculations and are highly sensitive to uncertainties in these values due to the non-linear exponents on each function [*Recking*, 2013a]. Significant differences in Q_b estimates computed using both 1-D and 2-D approximations of τ have been found to be caused because of the spatial variability of τ [*Gomez and Church*, 1989; *Ferguson*, 2003; *Recking*, 2013a]. Thus, the oversimplification of τ to a 1-D variable may not capture spatial changes in Q_b associated with localized values of high τ [*Segura and Pitlick*, 2015].

The advancement and wide applicability of 2-D hydrodynamic modeling provides an opportunity to incorporate the spatial variability of τ within a river reach into transport functions [*Nelson et al.*, 2015b; *Segura and Pitlick*, 2015]. In this study we will utilize the historic Oak Creek dataset coupled with a 2-D hydrodynamic model of Oak Creek to

test the applicability of using spatially variable estimates of τ and commonly used transport equations to make accurate estimates of Q_b. Our study site is the same one used by Milhous [1973]. First we will compare decadal trends in Q_b in Oak Creek through historic and contemporary Q_b measurements to determine the suitability of comparing contemporary modeling results to the historic Oak Creek dataset. We will use a 2-D hydrodynamic model and employ the discretization methods of Segura and Pitlick [2015] to incorporate spatially variable estimates of τ into PK and the transport equation of Wilcock and Crowe [2003] (WC) a surface based relation developed using flume data. We will compare the results between PK and WC in order to assess how the discretization methods perform using both surface and subsurface equations and for a function that was developed with data other than Oak Creek.

3.3 Study Site

This study was conducted in a 110 m reach of Oak Creek, Corvallis, OR. Oak Creek drains 7 km^2 of steep forested terrain, underlain by basaltic lithology [*Milhous*, 1973; *O'Connor et al.*, 2014] (Table 3.1). Our study reach in Oak Creek is a steep (slope = 0.014), gravel bed section with pool-riffle / plain bed morphology [*Montgomery and Buffington*, 1997] (Table 3.1). The stream bed is armored with coarse surface substrate overlying finer subsurface material. The reach is located directly upstream from a historic sediment transport sampling facility where bed load samples were collected between 1969-1971 [*Milhous*, 1973]. Further details regarding the study site including a site map can be found in Section 2.3.

Table 3.1 - Study Site Characteristics : Characteristics of the study reach in Oak Creek, OR (± are standard errors)

Slope (m/m)	0.014
Bankfull width (m)	6
Bankfull depth (m)	0.46
Bankfull hydraulic radius (m)	0.44
Bankfull discharge (m^3/s)	3.4
D_{16} ± standard error (mm)	19.0 ± 1.1
D_{50} ± standard error (mm)	45.1 ± 2.5
D_{84} ± standard error (mm)	83.2 ± 3.5
D_{16s} (mm)	2.8
D_{50s} (mm)	21.26
D_{84s} (mm)	67.32

3.3.1 Field Data Collection

Five composite bed load samples were collected during flows ranging from 0.77-1.54 m^3/s using a 3" Helley-Smith sampler [*Helley and Smith*, 1971]. Samples were taken along a cross section within the downstream hardened broadside weir. This was done to minimize disturbance of the stream bed by the sampler and prevent erroneous (i.e. overestimation) collection of bed material instead of bed load [*Bunte et al.*, 2008]. A composite sample was collected from a total of 9 locations evenly spaced across the 3.65 m cross section. Each location was sampled for 1 minute. Two passes along the traverse were used to collect each composite sample [*Emmett*, 1980; *Sandra E. Ryan*, 1999]. Samples were dried at 100°C for at least 24 hours, all organic material was removed and the GSD was measured using standard sieves between 0.063-360 mm.

Detailed topography of the study site was surveyed using a Nikon total station during the summer of 2015. The topographic data collected during this event was used as an input into the hydraulic model (discussed below). For more detail regarding the topographic data collection please see Section 2.4.1.1.

The bed surface grain size distribution (GSD) was characterized based on point pebble counts along 23 cross sections totaling 2347 particles [*Wolman*, 1954]. Individual point counts were then combined to obtain a reach averaged GSD (Figure 3.1) that was

summarized in terms of the grain sizes representing the 16th, 50th, and 84th percentiles of the distribution (D_{16}, D_{50}, D_{84}, Table 3.1). The calculated D_{50} was 45.1 ± 2.5 mm which is finer than the previously reported value for Oak Creek of 54 mm [*Milhous*, 1973].

The bed subsurface GSD was characterized based on two bulk samples of the subsurface material. Samples were taken at two locations in exposed bars after removing the surface material. The samples ranged from 5.54-5.64 kg which were large enough to ensure that the largest sampled grain did not account for greater than 5% of the total sample weight [*Church et al.*, 1987]. Particle sizes greater than 32 mm were sorted and weighed in the field. The remaining sample was homogenized and sub-samples were taken for laboratory analysis. The sub-samples were dried at 100°C for at least 24 hours, weighed, and measured using standard sieves between 0.063-32mm. The calculated subsurface D_{50s} was 21.26 mm which is slightly coarser than the previously reported value for Oak Creek of 20 mm [*Milhous*, 1973].

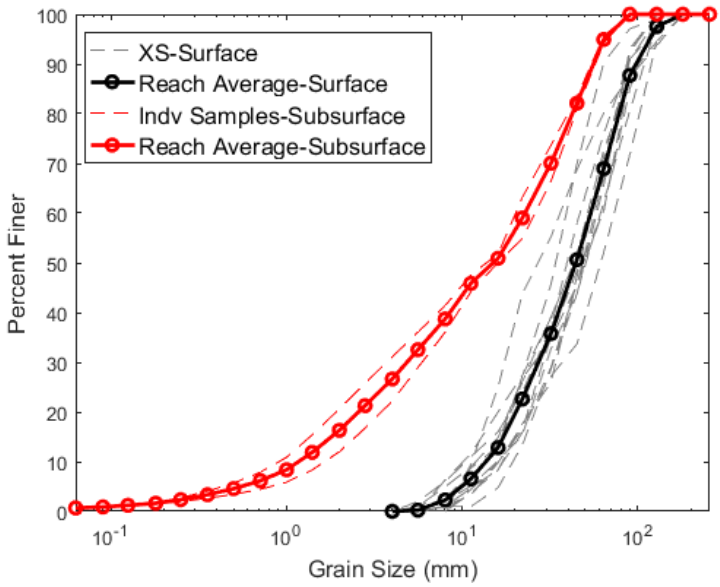

Figure 3.1 - Surface and Subsurface Grain Size Distribution: Surface and subsurface grain size distributions (GSD) for the study site. The average surface GSD is comprised of 23 cross sections (XS). The average subsurface GSD is comprised of 2 samples of the substrate collected from exposed bars.

A stage-discharge relationship (rating curve) was developed in order to estimate discharge from logger-recorded stage at the downstream end of the reach. A total of 12 discharge (Q) measurements were taken between 0.043-1.94 m^3/s. Additionally, the flow resistance equation of Ferguson [2007] was used along with measured depth to estimate Q outside of this range within the concrete weir. The final rating curve was for Q ranging 0.043-3.4 m^3/s. A detailed explanation of the rating curve development can be found in Section 2.4.1.2.

3.3.2 2-D Hydrodynamic Model Development

We made 2-D estimates of velocity (*u)* and shear stress (τ) for 6 flows ranging from 0.64-3.4 m^3/s ($0.19Q_{bf}$ - $1.0Q_{bf}$) using the Flow and Sediment Transport with Morphological Evolution of Channels (FaSTMECH) analytical solver. FaSTMECH is embedded within the International River Interface Cooperative (iRIC) software and developed by the United States Geological Survey (USGS). The input data to the model included an interpolation of the surveyed topography, the measured downstream stage, and Q. Calculations were conducted within a 110 m long, 16m wide curvilinear grid with a spacing of 0.2 m x 0.2 m. The number of grid nodes varied from 10,593-15,094 depending on flow level (Table 3.2). A constant C_d was used for each model run. The model was calibrated using field observations of streamwise WSE from 13 locations throughout the study reach. Streamwise WSE for bankfull flow (Q_{bf}) were estimated based on time-lapse photography, field observations of bankfull stage, and the analysis of cross-section topography because WSE observations were not made during an actual bankfull event. Streamwise plots of measured versus modeled WSE for each flow yield RMSE values between 0.025-0.031 m (Table 3.2) and R^2 >0.96. Calibrated C_d and LEV ranged from 0.017-0.038 and 0.0010-0.0032, respectively. Further detail pertaining to the 2-D hydrodynamic model development can be found in Section 2.4.1.3.

Table 3.2 - Hydraulic Model Development and Calibration Summary: FaSTMECH model development and calibration summary: discharge (Q), ratio of Q to bankfull Flow (Q/Q_{bf}), downstream (D.S.) stage, the number of calculation nodes, Root-Mean-Square Error (RMSE) between measured and modeled water surface elevations (WSE), the coefficient of determination (R^2) of the relation between measured and modeled WSE, the calibrated drag coefficient (C_d), lateral eddy viscosity (LEV), and the WSE slope.

Flow Conditions			***Model Parameters and Evaluation***					
Q	**Q_i/Q_{bf}**	**D.S. Stage**	**# wet nodes**	**RMSE**	**R^2**	**C_d**	**LEV**	**WSE Slope (m/m)**
0.64	0.19	98.96	10593	0.028	0.996	0.038	0.0016	0.0153
0.99	0.29	99.03	10593	0.031	0.996	0.025	0.0024	0.0150
1.33	0.39	99.08	10835	0.028	0.997	0.018	0.0032	0.0150
1.46	0.43	99.10	11147	0.025	0.997	0.017	0.0031	0.0150
1.9	0.56	99.17	11140	N/A	N/A	0.021	0.0025	0.0143
3.4	1.00	99.34	15094	0.031	0.996	0.035	0.0010	0.0142

(a)- From an arbitrary datum

(b) - This flow was not calibrated directly based on WSE.

3.3.3 Bed load estimation methods

3.3.3.1 General Methodology

Values of τ calculated for each flow level were used to estimate Q_b along the study reach. Q_b were estimated for individual grain size fractions (D_i) of the surface and subsurface ($D_{i,s}$) sediment using the discretization methods outlined in Segura and Pitlick [2015]. Their approach incorporates the discretized spatial distribution of τ, as estimated by FaSTMECH, into sediment transport calculations rather than using only a single value of shear stress per flow level as has been done by previous researchers [e.g. *Parker and Klingeman*, 1982; *Parker et al.*, 1982; *Parker*, 1990; *Wilcock and Crowe*, 2003]. Transport rates are calculated for each D_i using the range of discretized τ values (τ_j) and then weighted by the proportion of each size fraction within the bed material. These fractional transport rates are then weighted by the frequency of occurrence of each τ value throughout the model domain.

We compared Q_b estimates from two commonly used bed load transport relations; those of Parker and Klingemann [1982] (PK) and Wilcock and Crowe [2003] (WC). Each transport relation was modified based on the methods of Segura and Pitlick [2015] to incorporate 2-D τ distributions into the calculations. Each transport function is described in detail below.

3.3.3.2 Parker and Klingeman 1982

The transport function presented by Parker and Klingeman [1982] was modified in the following manner to estimate Q_b. The transport function presented by Parker and Klingemann [1982] is a subsurface equation based on Parker 1979's power function approximation of the Einstein 1950 transport relation as follows:

$$G = 5.6 \times 10^3 (1 - \frac{0.853}{\varphi})^{4.5} \quad (3\text{-}1)$$

where:

$$G = \frac{W_j^*}{W_r^*} \quad (3\text{-}2)$$

and

$$\varphi = \frac{\tau_j^*}{\tau_r^*} \quad (3\text{-}3)$$

and W* is defined as a dimensionless transport rate, τ_j* is the dimensionless shear stress for each τ value (also known as Shield's stress) and the subscript *r* refers to reference values of both W* and τ_r* where a "small but measurable" amount of transport is known to occur. W* and τ* are defined as:

$$W_j^* = \frac{(s-1) g q_b}{(\frac{\tau_j}{\rho})^{1.5}} \quad (3\text{-}4)$$

and

$$\tau_{i,j}^{*} = \frac{\tau_j}{(\rho_s - \rho) g D_{i,s}} \tag{3-5}$$

where q_b is the volumetric transport rate per unit width, s is the specific gravity of the sediment (1.85 for basalt), ρ_s is the density of the sediment (2850 kg/m^3 for basalt), ρ is the density of water, *g* is gravity, and D_i is the grain size of interest.

As is discussed in Parker et al [1982], Parker and Klingeman [1982], and Segura and Pitlick [2015], the above equations can be modified for mixtures of sediment and low transport rates as follows:

First, a reference transport rate is defined as $W_r^* = 0.002$ [*Parker et al.*, 1982] and a function accounting for low transport rates, $\varphi \leq 0.853$, is incorporated into Equation 3-4 above. Additionally, a "hiding function" is utilized so that transport rates for any size fraction, *i,* can be calculated. This results in the following set of equations:

$$W_{i,j}^{*} = \begin{cases} 0.0025\varphi^{14.2} & for\ \varphi < 0.853 \\ 11.2\left(1 - \frac{0.853}{\varphi}\right)^{4.5} & for\ \varphi \geq 0.853 \end{cases} \tag{3-6}$$

The hiding function is taken from Parker et al. [1982] where:

$$\varphi = \frac{\tau_{r,is}^{*}}{\tau_{r,50s}^{*}} = \frac{D_{i,s}}{D_{50,s}}^{-b} \tag{3-7}$$

where the subscripts *i,s* refer to an individual grain size of the subsurface bed material, *50,s* refer to the median grain size of the subsurface bed material and *b* is an empirically derived exponent relating to the degree of equal mobility demonstrated by the bed material and accounts for processes such as grain hiding, protrusion angle, and grain size distribution amongst others [*Parker and Klingeman*, 1982]. In this study we use values of b=0.982 and $\tau_{r,50s}^{*}$=0.0875 which were calculated for our study reach of Oak Creek by Parker et al [1982] and Parker and Klingeman [1982].

Subsurface grain size distributions were truncated to include only particle sizes that are likely to move as bed load and not be transported in suspension [*Dietrich*, 1982].

This was determined by comparing the settling velocity of individual sized particles (W_s) against the near-bed shear velocity (u^*, Equation 3-8) and removing size fractions where u^* is greater than W_s (and thus suspension is predicted).

$$u^* = \sqrt{gHS} \tag{3-8}$$

where H is the average flow depth as calculated in the flow model and S is the channel slope.

W_s was calculated using the following empirical relationship proposed by Dietrich [1982] which includes calculations of the dimensionless grain size (D_*, Equation 3-9), the dimensionless settling velocity (W_*, Equation 3-11) and an empirical relationship combining the two dimensionless relationships (Equation 3-10)

$$D_* = \frac{(\rho_s - \rho) g D_i^3}{\rho \nu^2} \tag{3-9}$$

Where ν is the kinematic viscosity of water (1.52 E-06 for water @ 5°C.

$$\log W_* = -3.76715 + 1.92944\ (\log D_*) - 0.04815\ \ (\log D_*)^{2.0} - 0.0575\ \ (\log D_*)^{3.0} + 0.00056\ \ (\log D_*)^{4.0} \tag{3-10}$$

And Ws is calculated using Equations 3-10, 3-11, and the following relationship for W_*:

$$W_* = \frac{\rho W_s^3}{(\rho_s - \rho) g \nu} \tag{3-11}$$

3.3.3.3 Wilcock and Crowe 2003

The transport relation of Wilcock and Crowe [2003] is a flume based, surface grain size function. Much like Parker and Klingeman [1982] it is also based on a similarity collapse of the 1950 Einstein bed load transport function. Because of this, the generalized form of the dimensionless transport rate (W*) is similar to PK through

Equation 3-4. The generalized hiding function also takes the same form as PK through equation 3.7. In WC, the value of b was calculated by fitting a function to the relationship of D_i/D_{50} vs. $\tau^*_{r,i}/\tau^*_{r,50}$ for data from the flume experiment. The resulting equation is as follows:

$$b = \frac{0.67}{1 + exp(1.5 - \frac{D_i}{D_{50}})} \tag{3-12}$$

W* is also calculated using a two part function accounting for two separate stages of transport:

$$W^*_{i,j} = \begin{cases} 0.002\varphi^{7.5} & for\ \varphi < 1.35 \\ 14(1 - \frac{0.894}{\varphi^{0.5}})^{4.5} & for\ \varphi \geq 1.35 \end{cases} \tag{3-13}$$

3.3.3.4 Calculation of Bed load Transport Rates

Q_b was calculated using each of the transport functions presented above using the same method. Q_b was calculated for each size fraction (D_i) and each discretized value of shear stress (τ_j) using:

$$W^*_{ij} = \frac{(s-1)gq_{b,ij}}{f_{D,i}(\frac{\tau_j}{\rho})^{1.5}} \tag{3-14}$$

where the subscripts *i* and *j* indicate each grain size fraction and shear stress increment respectively. The shear stress distribution was discretized by dividing the range of modeled shear stress values into equal increments of 0.5 N/m^2. Total q_b for each grain size fraction are calculated by weighting the values by the shear stress frequency distribution. The weighted q_b were then summed for all instances of τ and D_i using the following equation from Segura and Pitlick [2015]:

$$q_b = \rho_s \sum_i \sum_j q_{b,ij} f_{i,j} \tag{3-15}$$

Estimates of total q_b, the q_b for each grain size (q_{bi}) and the grain size distribution (GSD) of the bed load using both PK and WC equations will be compared to the historical measurements from Milhous [1973] for a range of similar flows.

3.4 Results

3.4.1 Shear Stress Variability

A summary of the model results for flows varying between 0.64-3.4 m^3/s is shown in Table 3.3. The predicted values ranged between 0.22-0.47 m, 23.10-51.12 N/m^2, and 22.62-51.46 N/m^2 for mean depth and τ and median τ, respectively. All three parameters show an increasing trend with increasing Q which is consistent with the findings of other studies using FaSTMECH in gravel bed rivers [e.g. *Clayton and Pitlick*, 2007; *May et al.*, 2009; *Segura et al.*, 2011; *Segura and Pitlick*, 2015]. The maximum 2-D τ varied from 75.8 to 163.06 N/m^2 and did not increase consistently with increasing Q for all of the modeled flows. The three flows ranging from 0.99 m^3/s – 1.46 m^3/s had virtually the same maximum τ value (80.87-83.29 N/m^2) which were found in the same location of the stream at the inside of a bend (Figure 3.2). The similarity in maximum τ values for these different flows is most likely due to discrepancies caused by the interaction of high velocity areas with the edge of a point bar at the inside of the bend. The WSE was similar in this location for the three flows (99.87-99.89 m) and at the level of the surface of the point bar. The flow is complex in this location and because of the power dependence on τ due to velocity (see Equation 2-3), any irregular flow interactions with the boundary of the point bar may cause τ estimates to differ irregularly between model runs even though the WSE was similar. We suspsect that this is what occurred during the modeling of these flows and resulted in the similarity in maximum τ estimates for the middle range of flows.

Table 3.3 - Hydraulic Model Result Summary: Summary of flow modeling results for discharge (Q) ranging from 0.64-3.4 m^3/s. Mean depth (H), and mean, median, and maximum values of shear stress (τ) and percentage of the stream bed that is greater than the mean τ value ($<\tau>$) are presented. Statistical calculations are performed on τ distributions truncated at 2 N/m^2. One dimensional (1-D) estimates of mean τ calculated based on water surface slopes and cross-sectional geometry are shown for comparison.

	2-D Model Results					*1-D Results*
Q (m^3/s)	**H_{mean} (m)**	**τ_{mean} (N/m^2)**	**τ_{median} (N/m^2)**	**τ_{max} (N/m^2)**	**$\tau > <\tau>$ (% of bed)**	**τ_{mean} (N/m^2)**
0.64	0.222	23.10	22.62	75.80	45.94	30.37
0.99	0.254	24.62	23.88	83.29	42.88	35.51
1.33	0.280	25.60	24.87	81.72	46.40	37.04
1.46	0.290	26.16	25.47	80.87	49.40	39.61
3.4	0.470	51.12	51.46	163.06	51.76	64.46

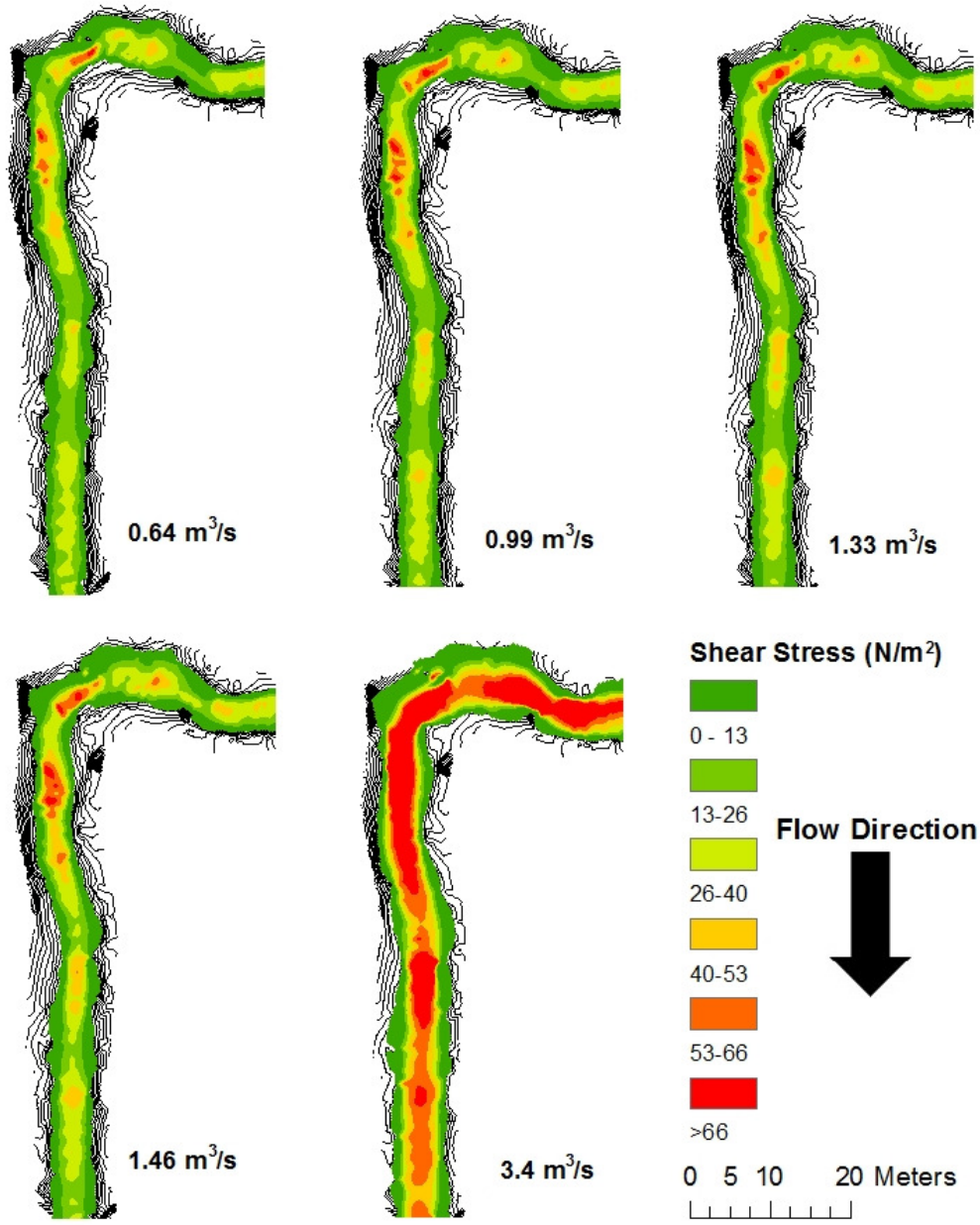

Figure 3.2 - Spatial Shear Stress Distributions: Spatial distribution of shear stress (τ) estimates for 5 flows ranging from 0.64-3.4 m^3/s for a 96 m reach of Oak Creek, OR.

One dimensional τ estimates were larger than the mean 2-D τ for all flow levels and ranged from 30.7-64.5 N/m^2 (Table 3.3). This is consistent with the findings of other studies [e.g. *Segura and Pitlick*, 2015] and is likely due to bed-stress partitioning with grid topography within the 2-D model [*McDonald*, 2016]. Total boundary τ estimates made using Equation 3-16 do not account for friction losses due to interaction of the flow with bed-forms and other large roughness elements [*Yager et al.*, 2007, 2012; *Lamb et al.*, 2008; *Scheingross et al.*, 2013]. This leads to the over-estimation of 1-D τ values, especially when compared against the 2-D model outputs.

$$\tau = \rho g R S \tag{3-16}$$

Where R is the reach-averaged hydraulic radius and S is the water surface slope.

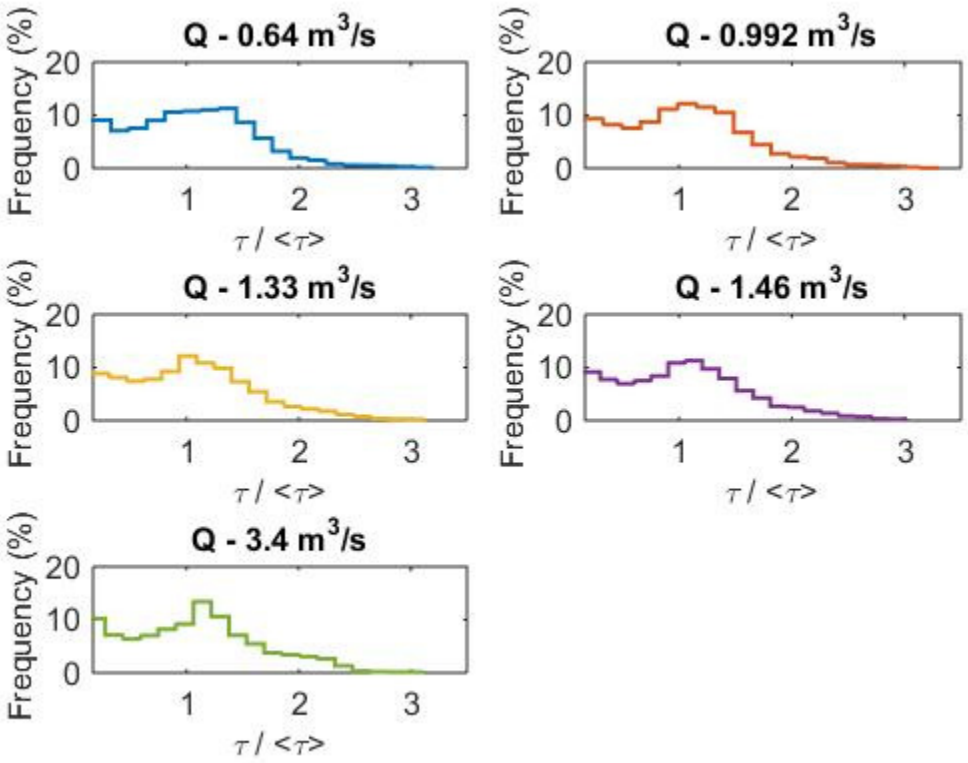

Figure 3.3 - Mean Normalized Shear Stress Distributions: Mean normalized shear stress (τ) distributions estimated using a 2-dimensional hydraulic model for flows ranging from 0.64-3.4 m^3/s. The τ distributions are truncated at 2 N/m^2.

The shape of the probability distributions for mean normalized τ are remarkably similar across flow levels (Figure 3.3, Figure 3.4). The distributions are all bi-modal and right skewed and range from 3.09-3.44 times the mean value ($<\tau>$). They all have a similar shape overlapping each other (Figure 3.4). The percent difference when compared against the average probability distribution among all 5 flows is between -2.04%-0.92%, which re-enforces their similarity. The portion of the bed with τ greater than the mean ($\tau> <\tau>$) varies slightly across distributions between 42.9 and 51.8%. This portion generally increases with Q indicating higher level of symmetry for the higher Q. This is consistent with the findings of other studies [*Lisle et al.*, 2000; *Segura and Pitlick*, 2015]. In general, the distributions for all flows have one population with a high frequency (~10%) of low (i.e. $<0.5 <\tau>$) τ values and a second population that centers around 1-1.5 $<\tau>$ with a frequency between 34.1-35.6%. All distributions have a relatively long tail for τ values between $2<\tau>$-$3.4<\tau>$ indicating a wide range of variability in τ (Figure 3.2).

τ is highly variable throughout the reach for all of the modeled flows (Figure 3.2). There is a strong influence of bed topography on τ where the bank boundaries exhibit low τ (<13 N/m^2) for all of the modeled flows. The highest τ values are consistently found within the bend and immediately downstream of it. These locations corresponds to a pool formed against cohesive clay banks that constrains the flow into a small and stable portion of the stream. τ values decrease along the straight portion of the stream and are highest in riffle areas. The spatial variability of τ and dependences on bed topography show a decreasing trend with increasing flow which is consistent with other studies where FaSTMECH was used to model flow hydraulics[Lisle et al., 2000; Clayton and Pitlick, 2007; May et al., 2009; Nelson et al., 2010; Harrison et al., 2015; Segura and Pitlick, 2015].

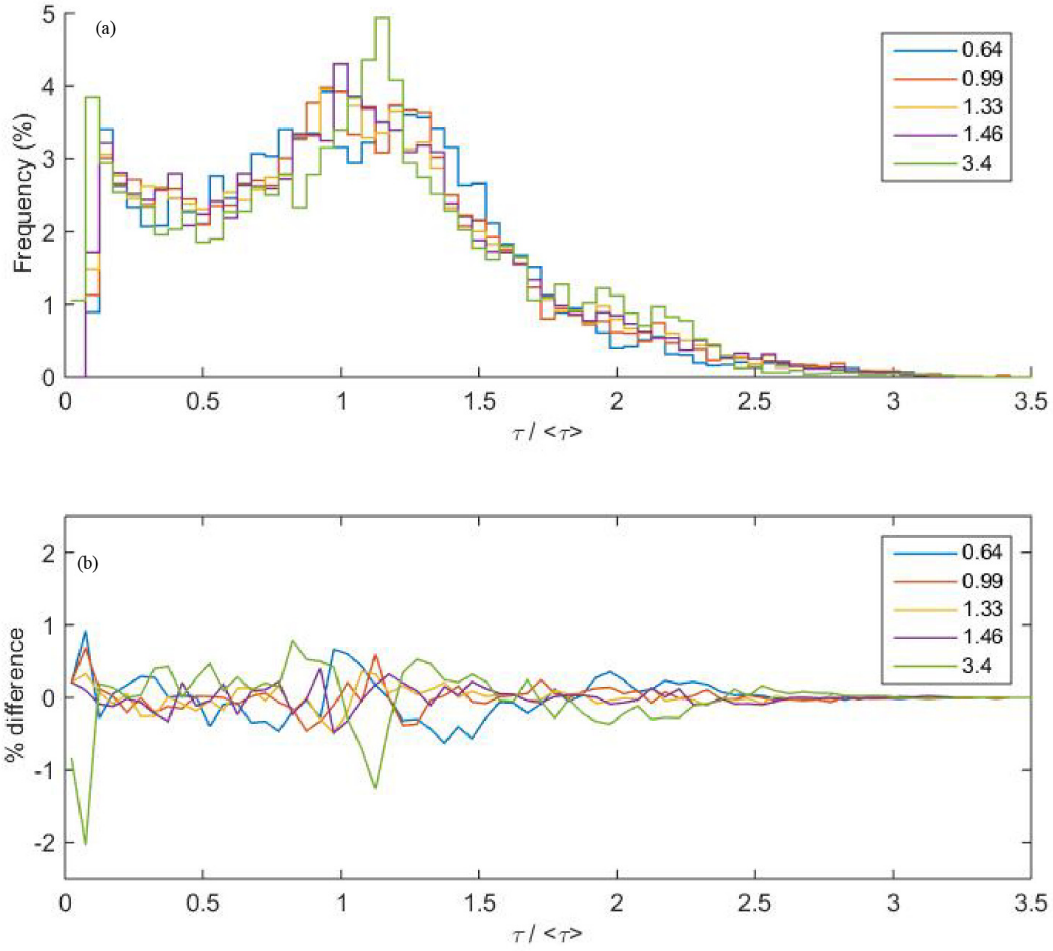

Figure 3.4 - Normalized Shear Stress Distribution Comparison: (A) Mean normalized shear stress (τ) distributions estimated using a 2-dimensional hydraulic model for flows ranging from 0.64-3.4 m^3/s and truncated at 2 N/m^2. (B) Percent difference between mean normalized τ distributions for individual flows and the average mean normalized τ distribution for the full range of 5 flows. Notice that the Y-axis is between -2.5-2.5%.

3.4.2 Bed load transport dynamics in Oak Creek

3.4.2.1 Contemporary Field Samples

Total unit bedload transport rates (q_b) measured in 2014-2015 using a Helley-Smith pressure difference sampler are consistent with those from the Milhous [1973] collected in a vortex sediment trap (Figure 3.5, Table 3.4). Contemporary q_b ranged from 2.64E-04 to 1.43E-02 kg/s for flows ranging from 0.803-1.76 m^3/s and historical q_b from 2.33E-05 to 2.00E-02 for a similar range of flows ranging from 0.796-1-76 m^3/s

[*Milhous*, 1973]. The consistency of measurements from this study indicate that sediment transport, at least in terms of total load, has remained stable since the original work of Milhous [1973]; thus Oak Creek appears to be in equilibrium.

Table 3.4 - Contemporary Bed Load Measurement Summary: Summary of bed load samples collected in Oak Creek using a Helley-Smith sampler in 2015-2016 for flows ranging from 0.803-1.76 m^3/s. Unit width bed load transport rates (q_b) are presented along with a summary of the grain size distribution of the samples in terms of the 16th, 50th, and 84th percentile size (D_{16}, D_{50}, and D_{84}).

Q (m^3/s)	Date	q_b (kg/m/s)	D_{16} (mm)	D_{50} (mm)	D_{84} (mm)
0.803	1/13/2016	2.64E-04	0.20	0.46	1.30
0.871	1/12/2016	8.07E-04	0.22	0.48	1.44
0.906	12/9/2015	1.11E-03	0.35	1.01	4.21
1.567	1/19/2016	4.64E-03	0.27	0.68	2.92
1.76	1/17/2016	1.43E-02	0.27	0.68	3.18

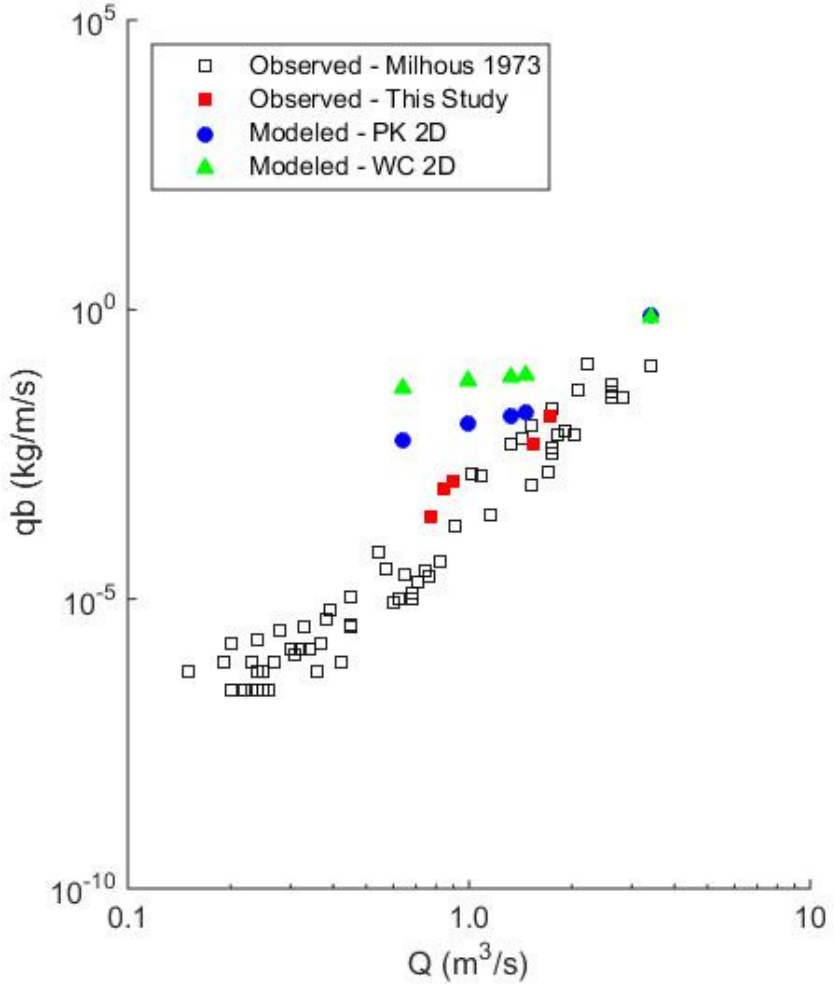

Figure 3.5 - Summary of Measured and Modeled Bed Load: Summary of observed and modeled unit width bed load transport rates (q_b) for Oak Creek, OR for flows ranging from 0.15-3.4 m^3/s. Observations are from measurements made by Milhous [1973] and this study. Modeled values are made using 2-dimensional estimates of shear stress (τ) and the transport equations of Parker and Klingeman [1982] (PK) and Wilcock and Crowe [2003] (WC).

The GSD of contemporary bed load samples are 96-77% finer than those collected by the vortex sampler and plot below the historical distribution in all cases (Figure 3.6, Figure 3.7). The D_{16}, D_{50}, and D_{84} of the contemporary measurements ranged from 0.20-0.35mm, 0.46-1.01mm and 1.30-4.21mm, respectively (Table 3.4). This is compared with ranges of 0.91-4.13mm, 1.95-19.32mm and 6.10-54.52mm for the D_{16}, D_{50}, and D_{84} of the historic dataset respectively [Milhous, 1973] (Figure 3.7). The

contemporary relation between grain size and flow is weak in comparison to the historic. The only recent sample that yields similar grain size values to the historic data was collected at Q=0.91 m^3/s. The scatter evident in the D_i versus Q trend in our bed load samples is consistent with the historical dataset which has a much larger sample size and thus a more robust trend is evident.

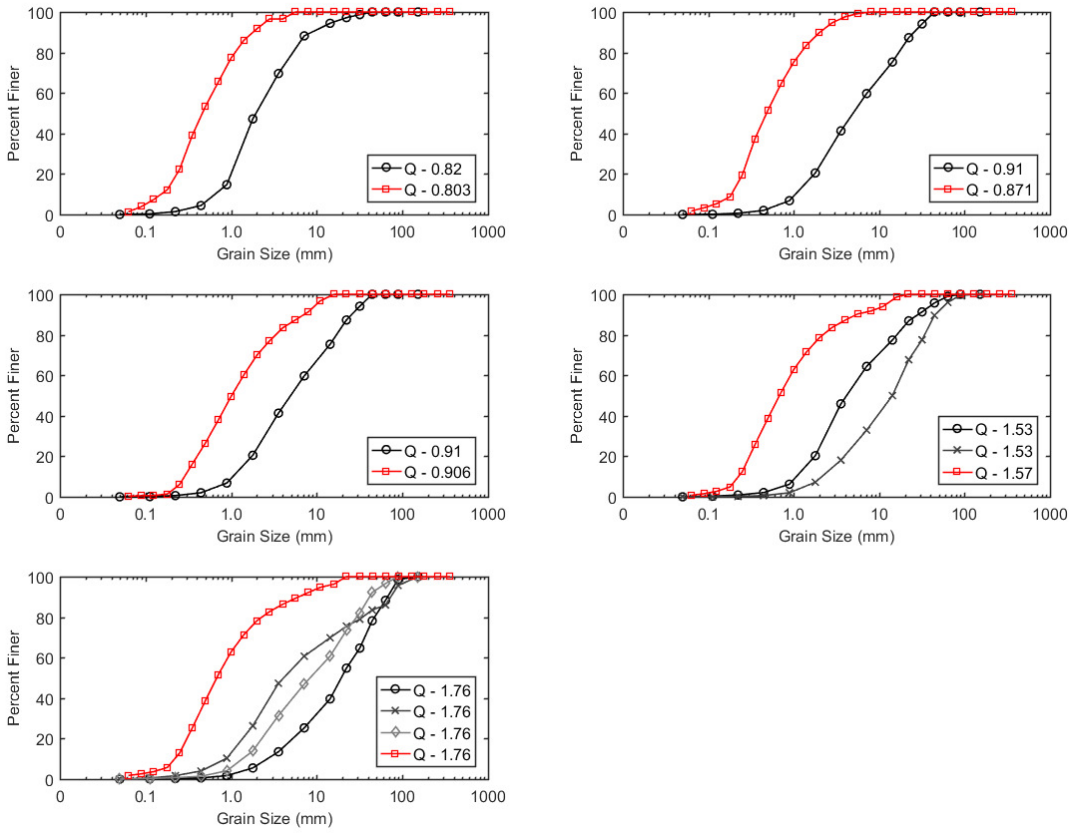

Figure 3.6 - Grain Size Distribution of Bed Load Measurements: Comparison of the grain size distribution (GSD) of bed load samples collected by Milhous [1973] and this study. Measurements taken by Milhous [1973] are presented in black and measurements made in this study are presented in red. In instances when multiple samples were collected at the same discharge, values from all measurements are presented.

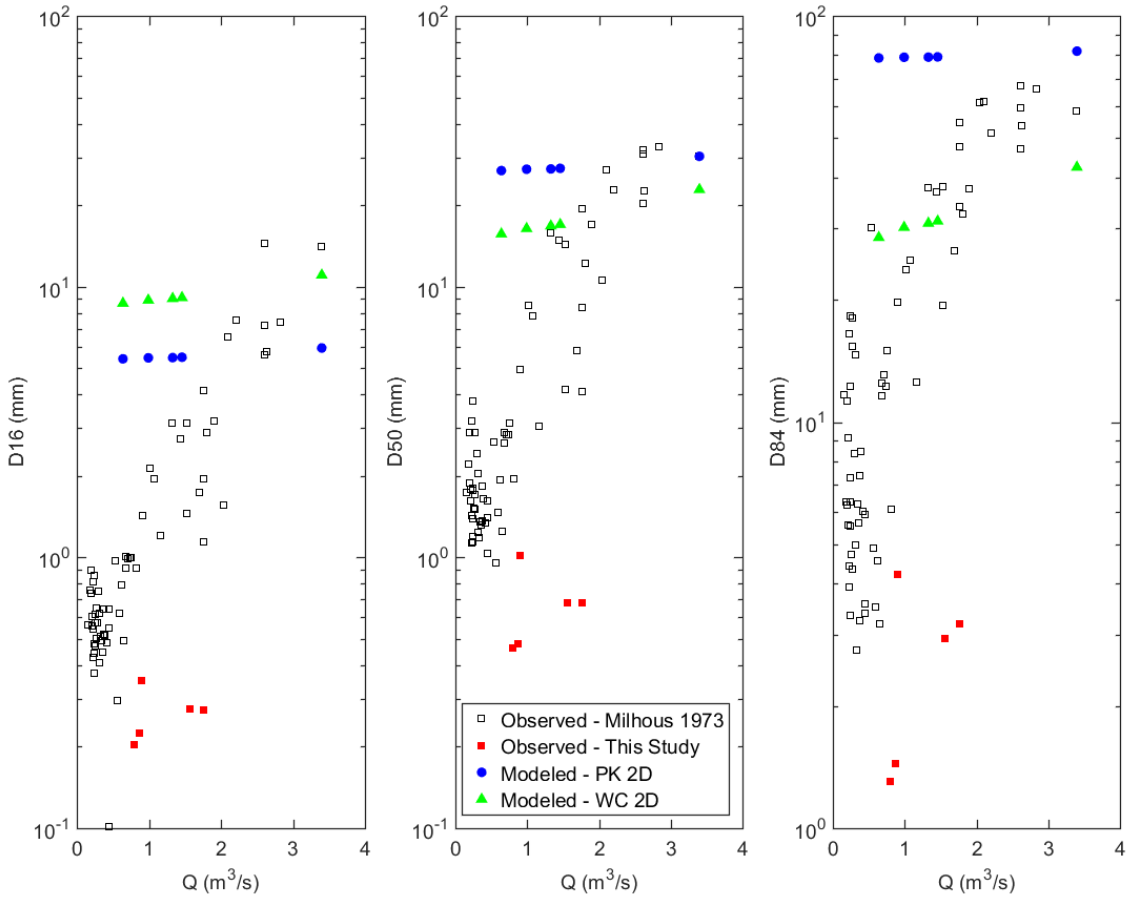

Figure 3.7 - Grain Size Statistics for Measured and Modeled Bed Load: Comparison of grain size distribution statistics for observations and modeled values of bed load in Oak Creek, OR for flows ranging from 0.15-3.4 m^3/s. Particle sizes pertaining to the 16th, 50th, and 84th percentile (D_{16}, D_{50}, and D_{84}) for the bed load samples are presented. Observations were made by Milhous [1973] and in this study. Modeled values are made using 2-dimensional estimates of shear stress (τ) and the transport equations of Parker and Klingeman [1982] (PK) and Wilcock and Crowe [2003] (WC).

3.4.2.2 Estimated Bed load Transport Rates

Estimated unit width bed load transport rates calculated using both the PK (qb_{PK}) and WC (qb_{WC}) equations were consistently higher than measured values for a similar range of flows (Figure 3.5, Table 3.4, and Table 3.5). Estimates of qb_{PK} and qb_{WC} using the range of modeled flows (Q=0.64-3.4 m^3/s) were between 5.59E-03-8.00E-01 kg/m/s and 4.44E-02-7.36E-01 kg/m/s respectively (Table 3.5). These values are roughly an order of magnitude greater than those measured using the vortex sampler ($qb_{Milhous}$) which were between 2.40E-05-1.05E-01 kg/m/s for Q=0.65-3.40 m^3/s. The closest agreement between estimated and historical values were for Q_{bf} (Q=3.4 m^3/s) where the modeled values were within the same order of magnitude (qb_{pk}=8.00E-01, qb_{WC}=7.36E-01 vs $qb_{Milhous}$=1.05E-01 kg/m/s). Values of qb_{WC} were higher than qb_{PK} for all flows except for Q_{bf}.

Table 3.5 - Modeled Bed Load Summary: Summary of modeled unit width bed load transport rates (q_b) for Oak Creek, OR for flows ranging from 0.64-3.4 m^3/s. Modeled values are made using 2-dimensional estimates of shear stress (τ) and the transport equations of Parker and Klingeman [1982] (PK) and Wilcock and Crowe [2003] (WC). Particle sizes pertaining to the 16th, 50th and 84th percentile (D_{16}, D_{50} and D_{84}) for the bed load samples are also presented. The mean (+/- standard deviation) q_b, D_{16}, D_{50}, and D_{84} presented in Milhous [1973] for a similar range of flows is shown for comparison.

Q (m^3/s)	*PK*				WC				Milhous, 1973				
	q_b (kg/m/s)	D_{16} (mm)	D_{50} (mm)	D_{84} (mm)	q_b (kg/m/s)	D_{16} (mm)	D_{50} (mm)	D_{84} (mm)	Q (m^3/s)	q_b (kg/m/s)	D_{16} (mm)	D_{50} (mm)	D_{84} (mm)
0.64	5.59E-03	5.41	26.83	78.77	4.44E-02	8.68	15.65	28.47	0.54-0.74	2.40E-05 ± 1.84E-05	0.79 ± 0.26	2.16 ± 0.77	10.62 ± 8.42
0.99	1.06E-02	5.46	27.14	79.07	5.82E-02	8.91	16.39	30.14	0.91-1.08	0.0010 ± 0.0007	1.83 ± 0.37	7.09 ± 1.89	22.76 ± 2.75
1.33	1.40E-02	5.47	27.22	79.14	6.79E-02	9.04	16.75	30.85	1.16-1.44	0.0037 ± 0.003	2.35 ± 1.02	11.27 ± 7.12	29.04 ± 14.33
1.46	1.67E-02	5.49	27.34	79.26	7.43E-02	9.11	16.95	31.23	1.33-1.53	0.0055 ± 0.004	2.60 ± 0.80	12.29 ± 5.46	30.02 ± 9.08
3.4	8.00E-01	5.94	30.29	81.89	7.36E-01	11.03	22.83	42.39	3.40	0.105	14.09	30.23	58.35

According to our modelling results using both the PK and WC equations, most bed load moves over a very small (<2.5%) portion of the bed characterized with high τ (Figure 3.8, Figure 3.9, and Table 3.6). The area of the bed with τ greater than 2 times the mean (τ> 2*<τ) ranged from 1.16-2.49% proportionally increasing with Q. This region of the bed, although small in terms of area, is predicted to transport 48.11-95.84% and 31.93-31.36% of the total q_b using the PK and WC equations respectively. There was a positive relationship between the percentage of total q_b transported within these regions and Q for the PK model, however that relationship did not exist for WC. While the percentage of total q_b was smaller for WC, the absolute values of q_b for that portion of the bed were greater for all flows besides $Q_{bf.}$ This is not surprising as WC predicted higher q_b overall in all instances but $Q_{bf.}$ These results are consistent with the findings of others [e.g. *Lisle et al.*, 2000; *Nelson et al.*, 2010; *Segura and Pitlick*, 2015; *Monsalve et al.*, 2016] who found that a large portion of bed load transport occurs through a small portion of the stream bed with high τ.

Table 3.6 - Regions of High Shear Stress Bed Load Summary: Summary of shear stress (τ) and unit bed load transport rates (q_b) for areas of the bed with τ greater than 2 times the mean (τ>2*<τ>) for flows with discharge (Q) ranging from 0.64-3.4 m^3/s. The percentages (%) of the total q_b are calculated using total q_b presented in Table 3.5.

Q (m^3/s)	*2D model results*	*PK*		*WC*	
	τ > 2*<τ> (% of bed)	**$q_{b,\ \tau > 2*<\tau>}$ (kg/m/s)**	**% of total q_b**	**$q_{b,\ \tau > 2*<\tau>}$ (kg/m/s)**	**% of total q_b**
0.64	1.16	5.36E-03	95.84	1.42E-02	31.93
0.99	1.52	9.84E-03	93.12	2.17E-02	37.25
1.33	1.64	1.26E-02	89.96	2.54E-02	37.36
1.46	1.64	1.47E-02	87.95	2.73E-02	36.72
3.4	2.49	3.85E-01	48.11	2.35E-01	31.91

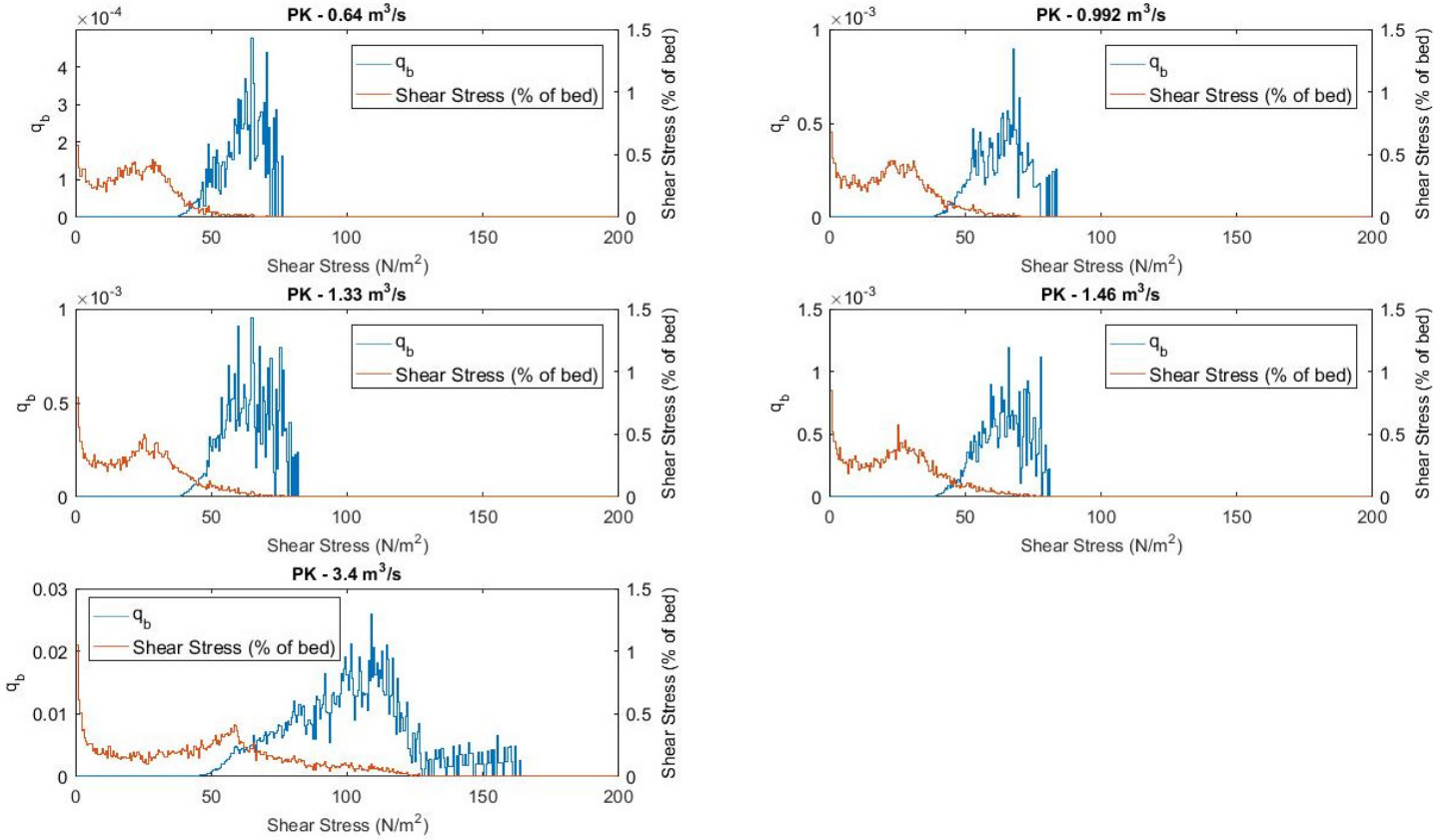

Figure 3.8 - Discretized Shear Stress and Bed Load Transport Rates (PK): Unit bed load transport rate (q_b) discretized by shear stress (τ) interval [left y-axis] and τ frequency distribution [right y-axis] calculated using the Parker and Klingeman [1982] (PK) bed load transport equation for modeled flows ranging from 0.64-3.4 m^3/s. Total q_b is calculated by integrating the discretized q_b. Note the different scales for q_b [left y-axis].

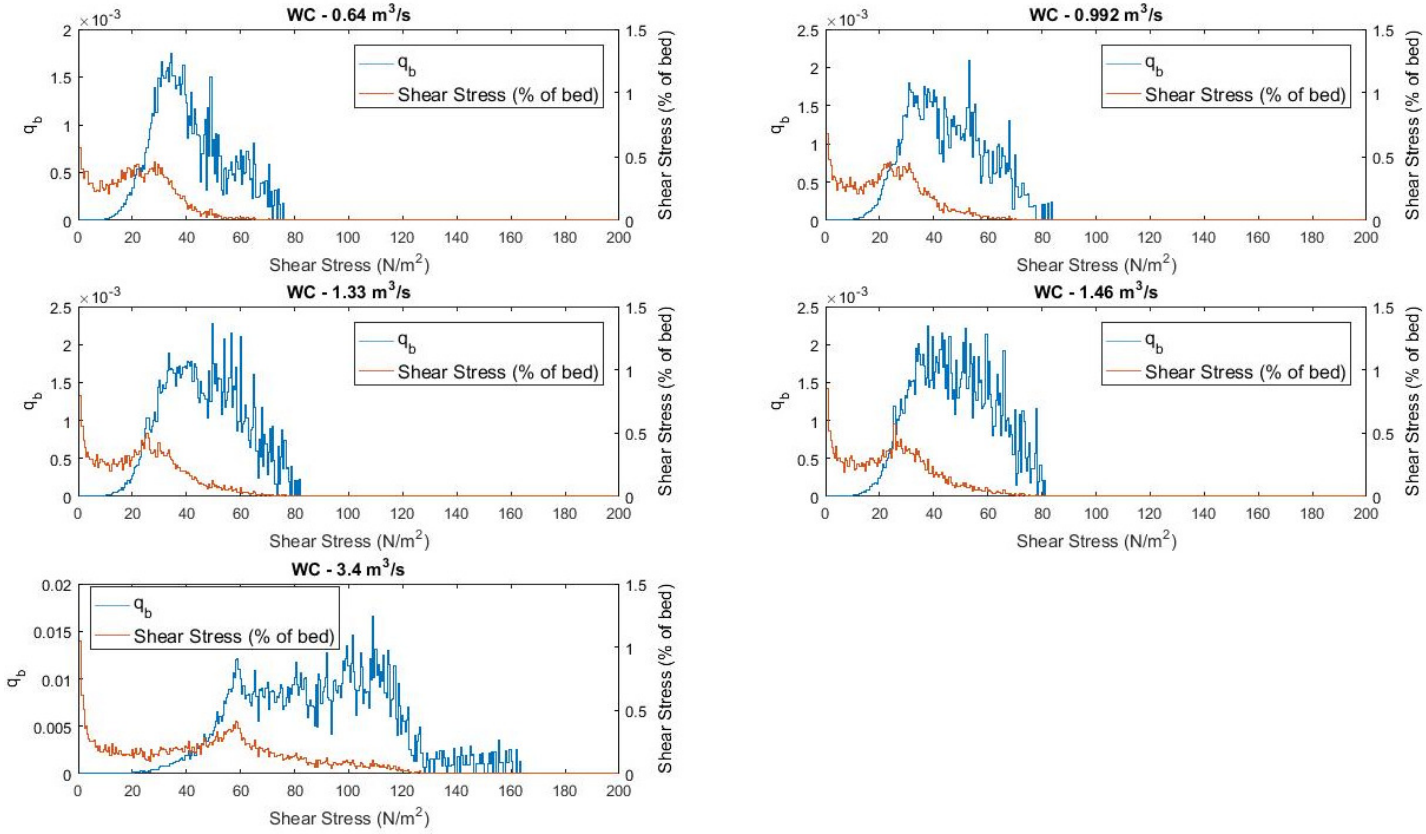

Figure 3.9 - Discretized Shear Stress and Bed Load Transport Rates (WC): Unit bed load transport rate (q_b) discretized by shear stress (τ) interval [left y-axis] and τ frequency distribution [right y-axis] calculated using the Wilcock and Crowe [2003] (WC) bed load transport equation for modeled flows ranging from 0.64-3.4 m^3/s. Total q_b is calculated by integrating the discretized q_b. Note the different scales for q_b [left y-axis].

The GSD of the modeled q_b did not agree with either the contemporary or historical measurements (Figure 3.7). The GSD of the historical measurements ($GSD_{Milhous}$) coarsened with increasing flow although there was considerable scatter in measurements taken at higher values of Q. The overall coarsening trend however, did not occur in the modeled q_b (Figure 3.10, Figure 3.11, and Table 3.5). The D_{16} ranged from 5.41-5.94 mm and 8.68-11.03 mm, the D_{50} ranged from 26.82-30.29 mm and 15.65-22.83 mm, and the D_{84} ranged from 78.77-81.89 mm and 28.46-42.42.39 mm for qb_{PK} and qb_{WC} respectively (Table 3.5). While there was a slight increase in the grain size with increasing Q for the model estimates, the range was significantly smaller than the historical estimates where the $D_{16,}$ $D_{50,}$ and D_{84} were between 0.49-14.08mm, 1.25-30.23 mm and 3.19-58.35 mm respectively [*Milhous*, 1973]. The GSD of qb_{PK} for all flow levels consistently resembled the subsurface GSD which was used as an input into the equation. The GSD of qb_{WC} was consistently finer than the surface GSD which was used as an input for that calculation. The D_{16} of qb_{WC} was coarser than qb_{PK} for all flow levels while the D_{50} and D_{84} was finer. This is most likely due to there being a greater proportion of fines in the sub-surface GSD than the surface GSD due to truncation of the datasets at 2mm and 4mm respectively.

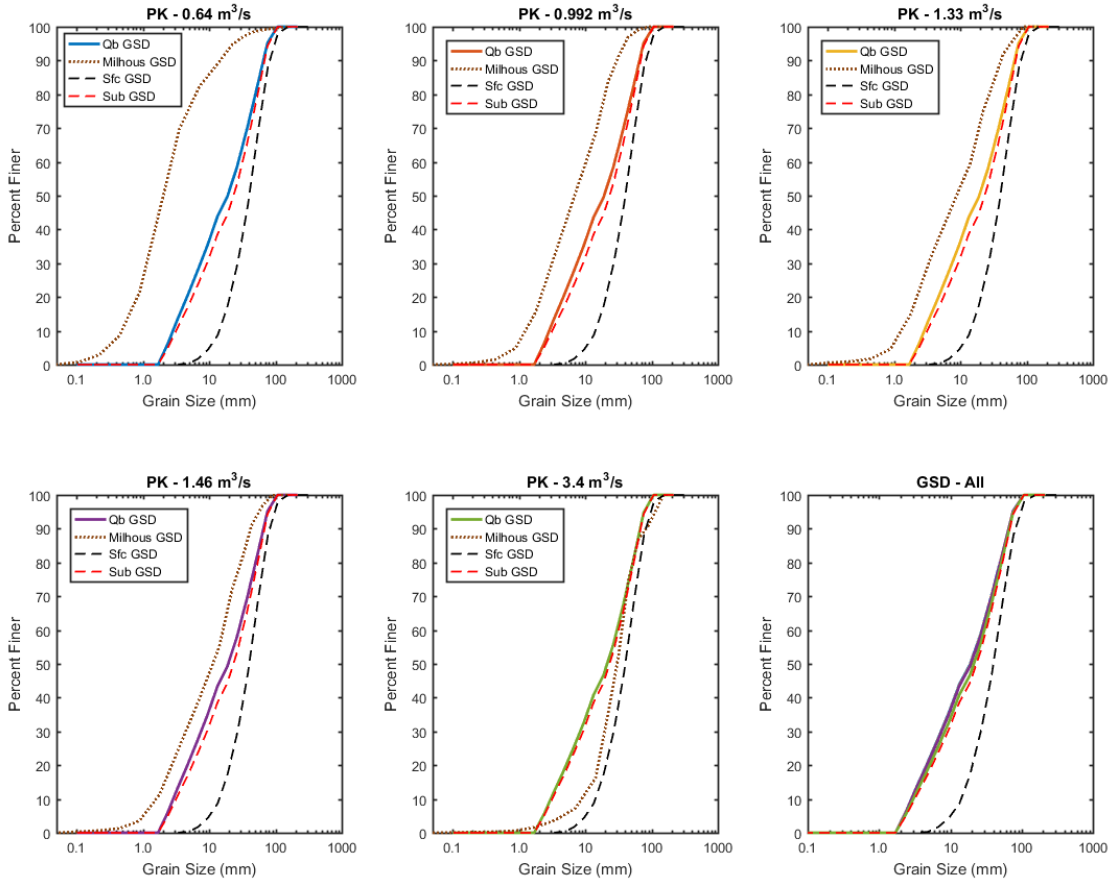

Figure 3.10 - Grain Size Distributions of Modeled Bed Load (PK): Grain size distributions of modeled bed load in Oak Creek, OR for flows ranging from 0.64-3.4 m^3/s using the Parker and Klingemann [1982] bed load transport formula. The average GSD presented in Milhous [1973] for the range of flows presented in Table 3.5 as well as the surface (Sfc) and sub-surface (Sub) GSD measured in this study are presented for comparison. The GSD – All plot shows the GSD for all modeled flows using colors presented in their respective legends.

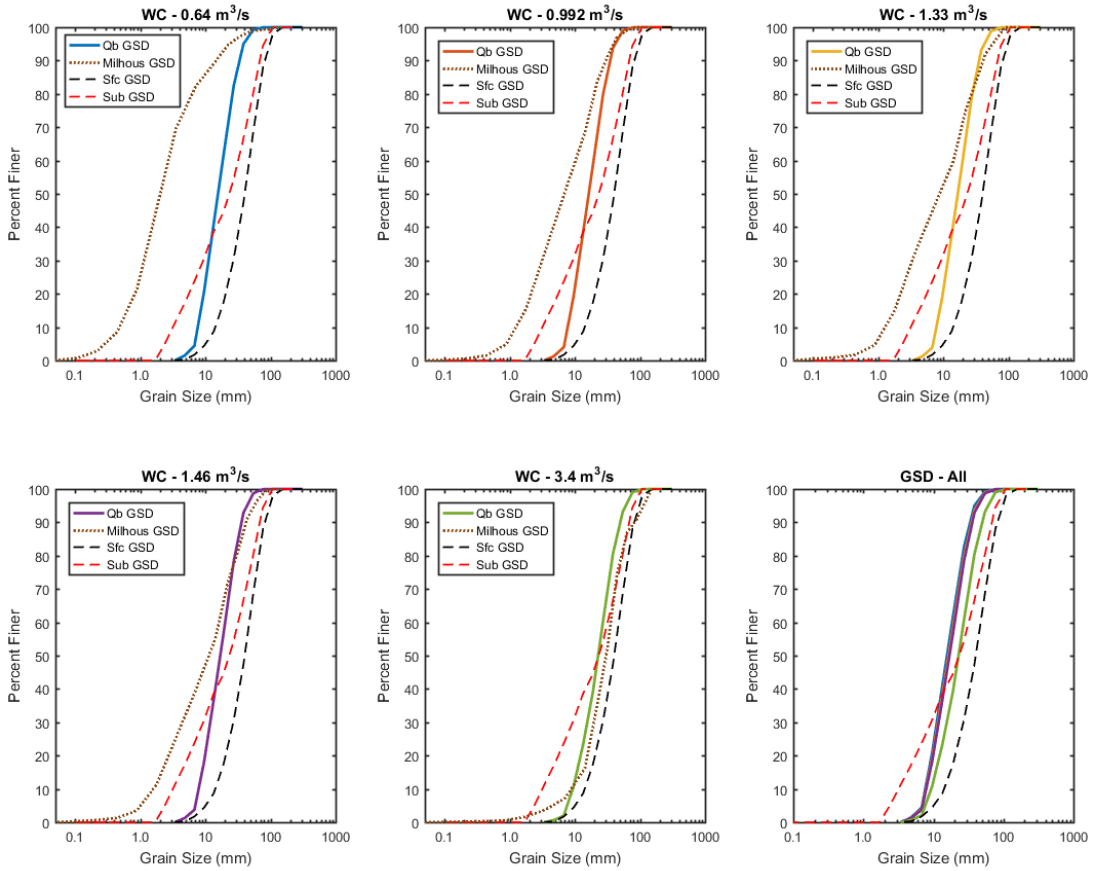

Figure 3.11 - Grain Size Distributions of Modeled Bed Load (WC): Grain size distributions of modeled bed load in Oak Creek, OR for flows ranging from 0.64-3.4 m^3/s using the Wilcock and Crowe [2003] bed load transport formula. The average GSD presented in Milhous [1973] for the range of flows presented in Table 3.5 as well as the surface and sub-surface GSD measured in this study are presented for comparison. The GSD – All plot shows the GSD for all modeled flows using colors presented in their respective legends.

3.5 Discussion

3.5.1 Shear stress variability in Oak Creek

A 2-D hydraulic model (FaSTMECH) was used to estimate shear stress (τ) distributions in Oak Creek across a range of flows from 0.64-3.4m^3/s (0.2-1.0 Q_{bf}). Even though the range of modeled discharges (Q) was quite large, the shapes of the mean normalized τ frequency distributions were remarkably similar between all flows. The distributions were all bi-modal, with high frequencies found in the low (<0.2 $\tau/<\tau>$) and intermediate (1-1.2 $\tau/<\tau>$) ranges of τ. Additionally, the distributions were all right skewed with tails extending to ~3-3.5 $\tau/<\tau>$). The similarity we found among distributions is different to the previous observation of consistent change in the τ distribution shape with increasing Q. The study of Lisle et al. [2000] calculated bankfull τ distributions in 6 gravel bed rivers in California and Colorado with Q_{bf} ranging from 11-430 m^3/s and while they found that the distributions had a similar shape to ours (i.e. bi-modal and right skewed), they saw a decrease in τ variability with increasing stream size. A similar shape was also observed by Segura and Pitlick [2015] in a study of 3 gravel bed reaches in Colorado with Q_{bf} ranging from 7.0-20.1 m^3/s, however their results found a shift in the distributions towards higher values of τ with increasing Q in addition to decreased τ variability with increasing Q, which is analogous to the decrease in τ variability with stream size as found in Lisle et al [2000]. The authors of both studies concluded that the observed decrease in τ variability at higher flows was due to the decreased influence of roughness elements on the flow field. This same rationale can be used here to explain the observed similarity found in our results. The rivers investigated by both Lisle et al [2000] and Segura and Pitlick [2015] are considerably larger (bankfull width 10.5-101 m in Lisle et al. [2000] vs 5.5 m in this study) than Oak Creek. In those systems, the influence of flow resistance exerted by grains, bed-forms, vegetation, and the banks decreases with flow depth. In addition, the influence of the boundary roughness is likely small in the middle of the channel. The similarity in the mean normalized τ frequency distributions in our study indicate however, that the systematic decrease in roughness with flow and stream size may be absent in the case in Oak Creek even at Q_{bf}.

The presence of relatively large bed-forms and dense riparian vegetation in Oak Creek create a consistence influence of roughness elements on the flow field even at high levels of Q. In many instances, these roughness elements only exert an influence at high flows so that while resistance due to grains and smaller bed forms may be reduced as Q increases, the flow field remains altered by other roughness features. An example of this is caused by several large trees that grow directly over the stream bed and only interact with the stream at high flows. Furthermore, the presence of complex bed forms such as a point bar on the inside of a bend in the study site complicates the flow field in this location and potentially creates the non-linear relationship in maximum values of τ with Q for the mid-range flows that we observed. We hypothesize that these features in the channel maintain the variability in τ compared with the larger rivers studied by Lisle et al. [2000] and Segura and Pitlick [2015] by creating low τ locations even at high flows. There are portions of the channel however, where these effects are not felt, which allow for the creation of high τ locations and cause the peak τ in the frequency distribution to be $>1\ \tau/\langle\tau\rangle$ as well as the large right tail. This is reinforced by what was observed by Cienciala and Hassan [2016] for a stream smaller than Oak Creek (i.e. bankfull width 2.5 m). The peak of the τ distribution in their study was shifted below the mean and was unimodal. In their study, the roughness of the bank had a greater influence on the hydraulics than in ours due to the smaller size of the stream. This may have caused the shift in peak τ below the mean and caused the differences between our distributions. These results indicate that spatial variability in τ is inherently different in small streams where roughness is always an influence on the flow field compared with larger systems.

3.5.2 A comparison of bed load sampling methods

The contemporary bed load measurements taken during this study using a Helly-Smith pressure differential sampler were consistent in terms of total load with the historical dataset of Milhous [1973] collected using a vortex sampler. However, the grain size distribution (GSD) of the contemporary samples were considerably finer. The difference between the GSD of samples collected using different sampling methods is not surprising when considering the sampling mechanism employed by each of the samplers and the subsequent sampling efficiencies. The vortex sampler works by creating turbulent

flow which traps sediment passing over it. Milhous [1973] reported that the sampling efficiency of the Oak Creek vortex sampler to collect individual grain sizes decreases over the range of 10-0.6 mm to values around 70% whereas it was around 100% for particles greater than 10mm. The author hypothesized that the turbulence associated with the vortex sampling method could remove some of the fine material from the sampler altogether. In contrast, the Helley-Smith sampler was originally designed to sample small gravels within the range of 2-10mm [*Helley and Smith*, 1971]. The sampler captures sediment directly from the flow field through a square orifice and collects it in a mesh bag [see *Emmett*, 1980 for a complete description of the sampler]. Although these samplers have since been used in high-energy, coarse gravel bed streams for sampling bed load [e.g. *Emmett*, 1980; *Burrows et al.*, 1981; *Ryan et al.*, 2002, 2005], studies have shown a wide range of sampling efficiencies due to experimental factors such as bag size, sampler wall thickness, mesh size, orifice size, and sampling duration [*Beschta*, 1981; *O'Leary and Beschta*, 1981; *Pitlick*, 1988; *Vericat et al.*, 2006; *Bunte et al.*, 2008]. Short sampling times to measure q_b using a Helley-Smith sampler may not capture particles that are at the threshold for entrainment (i.e. $\tau^*/\tau_r^* \sim 1$) as those particles move infrequently and thus may not be captured within the relatively small sampling orifice of the sampler [*Bunte et al.*, 2008]. The work of Emmett [1980] tested this hypothesis and demonstrated that the Helley-Smith sampler when deployed for a sampling duration of 30 seconds has a sampling efficiency of ~50% for particles greater than 16.0 mm [*Emmett*, 1980]. The differences in sampling efficiency and sampling duration may have caused the discrepancy in our data.

The difference in sampling efficiency between both sampling methods was compared by O'leary and Beschta [1981] in Flynn Creek, OR, a steep gravel bed stream in the Oregon Coast range. Although not a perfect comparison, Flynn Creek is generally similar to Oak Creek in terms of climate and watershed land use (forested), however it is smaller (drainage area 2.2 km^2 vs. 7 km^2) and the lithology is primarily sandstone compared with basalt in Oak Creek [*O'Leary and Beschta*, 1981]. Their sampling methods are comparable to those employed in our study in that they also used the Helley-Smith sampler from a concrete structure within the stream bed to minimize disturbance of

the stream substrate and any subsequent sampling errors. They found that the efficiency of the vortex sampler decreased for smaller size particles (<10 mm) which is consistent with Milhous [1973]. Because of this, the samples collected using the vortex sampler were 42-47% those collected using the Helley-Smith sampler. The influence of sampling method on total q_b was probably larger in their study than in Oak Creek because of the greater proportion of fine particles in the GSD of their study site compared to ours due to the sandstone lithology [*O'Leary and Beschta*, 1981; *O'Connor et al.*, 2014].

The finer GSD for contemporary q_b measured in this study compared to the historic Oak Creek dataset can be explained by the difference in sampling efficiencies for coarse and fine particles between the two sampling methods. The greater efficiency of the Helley-Smith sampler to collect fine particles would greatly reduce D_{16}, $D_{50,}$ and D_{84} due to the larger proportion of small (i.e. <10 mm) particles in the bulk sampler. Additionally, the long sampling periods employed by the vortex sampler in Oak Creek which ranged from 0.38-94 hours allowed the capture of coarser particles which were at the threshold for incipient motion during a particular sampling period. Because the total loads between the two sampling methods are consistent, the capture of coarse particles by the vortex sampler may have balanced the lack of fines compared to samples collected with the Helley-Smith. Future work is needed to address the difference in GSD in contemporary samples of q_b when compared with the historical dataset.

3.5.3 Discrepancies between estimated bed load and measured data

Two dimensional estimates of τ were used to estimate q_b in Oak Creek for 5 flows ranging from 0.64-3.4 m3/s. Distributions of τ were discretized and input into the transport functions of Parker and Klingeman [1982] (PK) and Wilcock and Crowe [2003] (WC) to calculate q_b using the methods employed by Segura and Pitlick [2015]. The results produced by our 2-D estimation methods did not generate values that were consistent with the historical Oak Creek data set of Milhous [1973]. The total q_b was consistently higher and there was minimal difference between the estimated bed load GSD across flow levels which did not match the increasing size trend in the GSD of the historical samples. In order to determine the cause of these discrepancies, we must first

consider the main difference between our methods and those used to develop the original equations, namely the manner in which τ was calculated. The original equations used reach averaged 1-D estimates of τ calculated using Equation 3-16 (depth-slope product) which did not partition the bed-stress between that absorbed by topography and excess stress available to mobilize sediment. Our methodology however, utilized 2-D estimates of τ which did account for topographic partitioning and resulted in lower values than 1-D estimates for the same flow. The reach averaged input values of τ in the original equations were used to fit the empirical parameters and to calculate the reference Shield's stress (τ_r^*), which we also employed in our methods. We hypothesize that it is the discrepancy between 1-D and 2-D τ in fitting the transport function and defining τ_r^* that may have caused the inconsistency between our calculations and the historical dataset. Re-fitting the empirical parameters is a likely solution to the first discrepancy and is consistent with the methodology of other studies such as Yager et al. [2012] who fitted the hiding function of Parker [1990] to site specific data. To address solutions to the issue of using 2-D τ estimates with a reach averaged τ_r^* however, an investigation into the topographic variability of sediment transport processes is necessary.

Spatial averaging of τ_r^* does not account for the variability of sediment transport processes. The patchiness of the GSD throughout gravel bed rivers has been well documented [*Lisle and Madej*, 1992; *Buffington and Montgomery*, 1999; *Lisle et al.*, 2000; *Nelson et al.*, 2010; *Monsalve et al.*, 2016] and has been demonstrated to arise due to spatial variability in τ within the flow field [*Lisle and Madej*, 1992; *Paola and Seal*, 1995; *Nelson et al.*, 2010]. Although it has been found that there is not a systematic relationship between grain size and τ at the local grain scale [e.g. *Lisle et al.*, 2000; *Nelson et al.*, 2010; *Segura and Pitlick*, 2015], Monsalve et al. [2016] found that the median grain size (D_{50}) of textural patches correlated with the patch average τ from a 2-D model with higher τ resulting in larger D_{50}. In terms of sediment transport, the increase in the D_{50} in patches of higher τ suggested by their relationship causes the τ_r^* to increase proportionally as the Shield's stress is directly related to both τ and the grain size. Thus, the patch τ_r^* should be greater in regions with high τ and likely higher than the spatially averaged τ_r^* we used in our calculations. This would explain the overestimated transport

rates we reported here. This is demonstrated in our data where a small proportion (<2.5%) of the bed with high τ transported a majority of the sediment. These findings are supported by those of others [e.g. *Nelson et al.*, 2010; *Segura and Pitlick*, 2015; *Monsalve et al.*, 2016] and highlight the necessity to incorporate a spatial variable τ^* or $\tau_r^*$for the D_{50} into the calculation. Based on the Shield's equation, this can be accomplished by adjusting τ_r^* with spatially variable surface grain sizes and τ as has been done in other studies [e.g. *Lisle et al.*, 2000; *Monsalve et al.*, 2016]. However, it is unknown how the surface GSD changes during a transport event, and thus there will be uncertainty in scaled estimates of τ_r^* using spatially variable grain sizes. To address this, we suggest that τ_r^* be scaled solely based on τ while relying on the relationship between τ and patch D_{50} found by Monsalve et al. [2016] to account for spatially variable grain sizes. To reduce uncertainty in the input GSD, we recommend the use of a subsurface transport function (such as PK) as it has been shown that the subsurface material is relatively homogenous throughout a reach even during high transport stages [e.g. *Parker and Klingeman*, 1982]. This will dramatically reduce field efforts compared with adequately characterizing the spatial variability of the surface GSD. The utility of these adjustments is demonstrated through a thought experiment in conjunction with field observations of stream bed armoring in the high τ regions of the bed identified in this study.

High τ areas (i.e. $\tau = 2^*<\tau>$) were estimated to transport the majority of sediment using the PK equation for all flows besides Q_{bf} where transport was more evenly distributed due to consistently higher τ throughout the reach. These regions are heavily armored with coarse particles (greater than the reach averaged surface D_{50}) as identified through field observations at low flow. Thus, it should take higher τ values to expose the subsurface in these locations than the reach average. Using the reach average τ_r^* however, implies that the armor layer would be pierced in these locations at low-moderate flows exposing the subsurface even when this may not actually occur, thus yielding the overestimation of sediment flux. The high transport rates for all grain size fractions in these areas cause our predicted bed load GSD to resemble that of the subsurface (i.e. the supply) for all flows, even though in actuality the transport would

eventually become supply limited in these high τ locations during a transport event as the surrounding armor may not be pierced as dramatically due to lower τ. By scaling τ_r^* with τ (i.e. increasing τ_r^* with τ), the transport rates would be reduced equally for all grain size fractions and the GSD of the load would show better consistency with the measured values. This would provide a quantitative solution, rather than a field approach, for correcting the discrepancy shown in our Q_b estimation methods.

3.5.4 Future work

The conclusions reached by this study bring forth many questions regarding flow hydraulics and sediment transport processes in small, headwater streams. A few specific future lines of inquiry are suggested below:

- The similarity in mean normalized τ frequency distributions over the range of flows was unique compared with the results of other studies. Future work regarding these results could include fitting gamma functions to the frequency distributions (per Segura and Pitlick [2015]) to better compare them between each other and with the work of others. Additionally, τ distributions could be generated in other small streams with a varying degree of roughness in order to understand the influence of roughness and stream size on τ variability.

- The discrepancy between bed load measurements taken using a Helly-Smith pressure differential sampler and the historical dataset do not allow for the definitive conclusion that sediment transport dynamics have remained stable since the original work of Milhous [1973]. Further work is needed to measure contemporary bed load using a variety of methods so that a complete dataset can be generated. Measurements using the Helley-Smith sampler should be made over longer time frames to enhance better representation of the movement of larger particles. Additionally, the use of a hand held sampler with a larger orifice (i.e. an Elwha sampler) should be employed to investigate the influence of orifice size on our measurements. Other methods such as radio transmitters and instream bed load traps could also be employed and compared to the original dataset.

- Further work is needed to address the inconsistencies between the Q_b estimates made using our 2-D models and the historical dataset of Milhous [1973]. As discussed above, we hypothesize that using 1-D reach averaged τ to fit both the empirical constants and the τ_r^* used in the original equations are not suitable for use with 2-D estimates of τ. We suggest scaling τ_r^* with τ as well as re-fiting the empirical constants using 2-D τ estimates coupled with historic and contemporary bed load measurements may resolve these discrepancies.

3.6 Conclusion

The results of this study indicate that τ is highly variable but that the shapes of mean normalized τ distributions were similar for flows ranging from 0.2 Q_{bf} to Q_{bf}. We hypothesize that the similarity across flow levels is caused by the influence of roughness elements which are still present even at Q_{bf}. The τ distributions were coupled with measured GSD to generate estimates of q_b that were not consistent with the historical measurements of Milhous [1973], although contemporary q_b measurements did match. The q_b estimates were greater and coarser than the historic data and the GSD did not change substantially between flow levels. A large portion of the estimates were transported from high τ ($>2*<\tau>$) portions of the bed which comprised <2.5% of the area. We hypothesize that utilizing a reach averaged τ_r^* with our 2-D τ estimates may have caused this phenomenon where an infinite supply of sediment was allowed to transport from these high τ areas. Scaling τ_r^* with τ throughout the reach may reduce the dramatic importance of these high τ areas and provides the foundation for future work to incorporate spatially variable τ into bed load transport equations.

4. CONCLUSION

This study incorporated the spatial and temporal variability of sediment transport processes to answer two research questions: 1) How do sediment transport processes influence benthic algal communities?, and 2) Can fluvial-hydraulic models make accurate predictions of bed load transport rates?.

The results of study 1 indicate that spatial and temporal variability in sediment transport processes significantly influence the growth dynamics of benthic algal communities. By defining fluvial disturbance based on metrics of sediment mobility and evaluating areas of contrasting disturbance, we were able to isolate these effects for high flow events of different magnitudes and demonstrate that 2-D metrics of disturbance are better indicators of benthic algal response than 1-D metrics such as discharge. Temporal variability in the response and recovery of benthic algae to high flow events demonstrate that the pre-disturbance productivity of the algal community can determine the amount of influence a fluvial disturbance event will exert. This was most likely due to variations in the resistance of different algal species present at the time of the each high flow event. The consistency of the relationship between τ and the 95^{th} quantile regression of Chl-*a* with the intermediate disturbance hypothesis demonstrate that spatial variability in τ acts as a limiting factor on benthic algae to fundamentally structure the productivity (and biodiversity) at the base of stream ecosystems. The data presented in this study highlight the importance of quantifying the spatial and temporal variability of sediment transport processes in future studies of how fluvial disturbance influences stream ecosystems.

The results of study 2 indicate that τ is highly variable in our study reach of Oak Creek but that the shapes of mean normalized τ distributions were similar for flows ranging from 0.2 Q_{bf} to Q_{bf}. We hypothesize that the similarity across flow levels is caused by the influence of roughness elements which are still present even at Q_{bf}. The τ distributions were coupled with measured GSD to generate estimates of Q_b that were not consistent with the historical measurements of Milhous [1973], although contemporary Q_b measurements did match. The Q_b estimates were greater and coarser than the historic data and the GSD did not change substantially between flow levels. A large portion of the

estimates were transported from high τ ($>2*<\tau>$) portions of the bed which comprised <2.5% of the area. We hypothesize that utilizing a reach averaged τ_r* with our 2-D τ estimates may have caused this phenomenon where an infinite supply of sediment was allowed to transport from these high τ areas. Scaling τ_r* with τ throughout the reach may reduce the dramatic importance of these high τ areas and provides the foundation for future work to incorporate spatially variable τ into bed load transport equations.

5. BIBLIOGRAPHY

Ács, É., and K. T. Kiss (1993), Effects of the water discharge on periphyton abundance and diversity in a large river (River Danube, Hungary), *Hydrobiologia*, *249*(1–3), 125–133, doi:10.1007/BF00008849.

Allan, J. D., and M. M. Castillo (2007), *Stream Ecology*, Springer Netherlands, Dordrecht.

Barry, J. J., J. M. Buffington, and J. G. King (2004), A general power equation for predicting bed load transport rates in gravel bed rivers, *Water Resour. Res.*, *40*(10), W10401, doi:10.1029/2004WR003190.

Beechie, T., and S. Bolton (1999), An Approach to Restoring Salmonid Habitat-forming Processes in Pacific Northwest Watersheds, *Fisheries*, *24*(4), 6–15, doi:10.1577/1548-8446(1999)024<0006:AATRSH>2.0.CO;2.

Bergey, E. A., and V. H. Resh (2006), Differential Response of Algae on Small Streambed Substrates to Floods, *Am. Midl. Nat.*, *155*(2), 270–277, doi:10.1674/0003-0031(2006)155[270:DROAOS]2.0.CO;2.

Beschta, R. L. (1981), *Increased bag size improves Helley-Smith bed load sampler for use in streams with high sand and organic matter transport*, Erosion and Sediment Transport Measurements.

Biggs, B., and H. Thomsen (1995), Disturbance of Stream Periphyton by Perturbations in Shear-Stress - Time, *J. Phycol.*, *31*(2), 233–241, doi:10.1111/j.0022-3646.1995.00233.x.

Biggs, B. J. F. (2000), Eutrophication of streams and rivers: dissolved nutrient-chlorophyll relationships for benthic algae, *J. North Am. Benthol. Soc.*, *19*(1), 17–31, doi:10.2307/1468279.

Biggs, B. J. F., and M. E. Close (1989), Periphyton biomass dynamics in gravel bed rivers: the relative effects of flows and nutrients, *Freshw. Biol.*, *22*(2), 209–231, doi:10.1111/j.1365-2427.1989.tb01096.x.

Biggs, B. J. F., and P. Gerbeaux (1993), Periphyton development in relation to macro-scale (geology) and micro-scale (velocity) limiters in two gravel-bed rivers, New Zealand, *N. Z. J. Mar. Freshw. Res.*, *27*(1), 39–53, doi:10.1080/00288330.1993.9516544.

Biggs, B. J. F., and R. A. Smith (2002), Taxonomic richness of stream benthic algae: Effects of flood disturbance and nutrients, *Limnol. Oceanogr.*, *47*(4), 1175–1186, doi:10.4319/lo.2002.47.4.1175.

Biggs, B. J. F., D. G. Goring, and V. I. Nikora (1998), Subsidy and Stress Responses of Stream Periphyton to Gradients in Water Velocity as a Function of Community Growth Form, *J. Phycol.*, *34*(4), 598–607, doi:10.1046/j.1529-8817.1998.340598.x.

Biggs, B. J. F., R. A. Smith, and M. J. Duncan (1999), Velocity and Sediment Disturbance of Periphyton in Headwater Streams: Biomass and Metabolism, *J. North Am. Benthol. Soc.*, *18*(2), 222–241, doi:10.2307/1468462.

Blettler, M. C. M., M. L. Amsler, I. Ezcurra De Drago, E. C. Drago, A. R. Paira, and L. A. Espinola (2012), Hydrodynamic and morphologic effects on the benthic invertebrate ecology along a meander bend of a large river (Paraguay River, Argentina–Paraguay), *Ecol. Eng.*, *44*, 233–243, doi:10.1016/j.ecoleng.2012.04.023.

Bradley, D. N., and G. E. Tucker (2012), Measuring gravel transport and dispersion in a mountain river using passive radio tracers, *Earth Surf. Process. Landf.*, *37*(10), 1034–1045, doi:10.1002/esp.3223.

Buffington, J. M., and D. R. ; Montgomery (1999), A procedure for classifying textural facies in gravel-bed rivers, *Water Resour. Res.*, *35*(6), 1903–1914.

Buffington, J. M., R. D. Woodsmith, D. B. Booth, and D. R. Montgomery (2003), Fluvial processes in Puget Sound rivers and the Pacific Northwest, *Restor. Puget Sound Rivers Univ. Wash. Press Seattle WA*, 46–78.

Bunte, K., S. R. Abt, J. P. Potyondy, and K. W. Swingle (2008), A Comparison of Coarse Bedload Transport Measured with Bedload Traps and Helley-Smith Samplers, *Geodin. Acta*, *21*(1–2), 53–66, doi:10.3166/ga.21.53-66.

Burrows, R. L., W. W. Emmett, and B. Parks (1981), *Sediment transport in the Tanana River near Fairbanks, Alaska, 1977-79*, Water-Resources Investigations Report, USGS Numbered Series, U.S. Geological Survey,.

Bywater-Reyes, S., A. C. Wilcox, J. C. Stella, and A. F. Lightbody (2015), Flow and scour constraints on uprooting of pioneer woody seedlings, *Water Resour. Res.*, *51*(11), 9190–9206, doi:10.1002/2014WR016641.

Cade, B. S., and B. R. Noon (2003), A gentle introduction to quantile regression for ecologists, *Front. Ecol. Environ.*, *1*(8), 412–420.

Cade, B. S., J. W. Terrell, and R. L. Schroeder (1999), Estimating Effects of Limiting Factors with Regression Quantiles, *Ecology*, *80*(1), 311–323, doi:10.1890/0012-9658(1999)080[0311:EEOLFW]2.0.CO;2.

Cardinale, B. J., M. A. Palmer, C. M. Swan, S. Brooks, and N. L. Poff (2002), The Influence of Substrate Heterogeneity on Biofilm Metabolism in a Stream

Ecosystem, *Ecology*, *83*(2), 412–422, doi:10.1890/0012-9658(2002)083[0412:TIOSHO]2.0.CO;2.

Cardinale, B. J., M. A. Palmer, A. R. Ives, and S. S. Brooks (2005), Diversity–Productivity Relationships in Streams Vary as a Function of the Natural Disturbance Regime, *Ecology*, *86*(3), 716–726, doi:10.1890/03-0727.

Cardinale, B. J. et al. (2012), Biodiversity loss and its impact on humanity, *Nature*, *486*(7401), 59–67, doi:10.1038/nature11148.

Cattaneo, A., T. Kerimian, M. Roberge, and J. Marty (1997), Periphyton distribution and abundance on substrata of different size along a gradient of stream trophy de Montréal, *Hydrobiologia*, *354*(1–3), 101–110, doi:10.1023/A:1003027927600.

Church, M. A., D. G. McLean, and J. F. Wolcott (1987), River bed gravels: sampling and analysis, *Sediment Transp. Gravel-Bed Rivers John Wiley Sons N. Y. 1987 P 43-88 17 Fig 3 Tab 50 Ref.*

Clayton, J. A., and J. Pitlick (2007), Spatial and temporal variations in bed load transport intensity in a gravel bed river bend, *Water Resour. Res.*, *43*(2), W02426, doi:10.1029/2006WR005253.

Connell, J. H. (1978), Diversity in tropical rain forests and coral reefs, *Science*, *199*(4335), 1302–1310.

Coundoul, F., T. Bonometti, M. Graba, S. Sauvage, J.-M. Sanchez Pérez, and F. Y. Moulin (2015), Role of Local Flow Conditions in River Biofilm Colonization and Early Growth, *River Res. Appl.*, *31*(3), 350–367, doi:10.1002/rra.2746.

Davie, A. W., and S. M. Mitrovic (2014), Benthic algal biomass and assemblage changes following environmental flow releases and unregulated tributary flows downstream of a major storage, *Mar. Freshw. Res.*, *65*(12), 1059–1071.

Davie, A. W., S. M. Mitrovic, and R. Lim (2012), Succession and accrual of benthic algae on cobbles of an upland river following scouring, *Inland Waters*, *2*(2), 89–100.

Dietrich, W. E. (1982), Settling velocity of natural particles, *Water Resour. Res.*, *18*(6), 1615–1626, doi:10.1029/WR018i006p01615.

Drevnick, P. E., and M. B. Sandheinrich (2003), Effects of Dietary Methylmercury on Reproductive Endocrinology of Fathead Minnows, *Environ. Sci. Technol.*, *37*(19), 4390–4396, doi:10.1021/es034252m.

Dunham, J. B., B. S. Cade, and J. W. Terrell (2002), Influences of Spatial and Temporal Variation on Fish-Habitat Relationships Defined by Regression Quantiles, *Trans.*

Am. Fish. Soc., *131*(1), 86–98, doi:10.1577/1548-8659(2002)131<0086:IOSATV>2.0.CO;2.

Einstein, H. A. (1950), *The Bed-load Function for Sediment Transportation in Open Channel Flows*, U.S. Department of Agriculture.

Emmett, W. W. (1980), *A field calibration of the sediment-trapping characteristics of the Helley-Smith bed-load sampler*, Professional Paper, USGS Numbered Series, U.S. Govt. Print. Off.,.

Faustini, J. M., and J. A. Jones (2003), Influence of large woody debris on channel morphology and dynamics in steep, boulder-rich mountain streams, western Cascades, Oregon, *Geomorphology*, *51*(1–3), 187–205, doi:10.1016/S0169-555X(02)00336-7.

Fayolle, S., A. Cazaubon, K. Comte, and E. Franquet (1998), The Intermediate Disturbance Hypothesis : application of this concept to the response of epilithon in a regulated Mediterranean river (Lower-Durance, southeastern France), *Arch. Für Hydrobiol.*, *143*(1), 57–77.

Ferguson, R. (2007), Flow resistance equations for gravel- and boulder-bed streams, *Water Resour. Res.*, *43*(5), W05427, doi:10.1029/2006WR005422.

Ferguson, R. I. (1986), Hydraulics and hydraulic geometry, *Prog. Phys. Geogr.*, *10*(1), 1–31, doi:10.1177/030913338601000101.

Ferguson, R. I. (2003), The missing dimension: effects of lateral variation on 1-D calculations of fluvial bedload transport, *Geomorphology*, *56*(1–2), 1–14, doi:10.1016/S0169-555X(03)00042-4.

Fisher, S. G., L. J. Gray, N. B. Grimm, and D. E. Busch (1982), Temporal Succession in a Desert Stream Ecosystem Following Flash Flooding, *Ecol. Monogr.*, *52*(1), 93–110, doi:10.2307/2937346.

Fornaroli, R., R. Cabrini, S. Zaupa, R. Bettinetti, M. Ciampittiello, and A. Boggero (2016), Quantile regression analysis as a predictive tool for lake macroinvertebrate biodiversity, *Ecol. Indic.*, *61*, *Part 2*, 728–738, doi:10.1016/j.ecolind.2015.10.024.

Francoeur, S. N., and B. J. F. Biggs (2006), Short-term Effects of Elevated Velocity and Sediment Abrasion on Benthic Algal Communities, *Hydrobiologia*, *561*(1), 59–69, doi:10.1007/s10750-005-1604-4.

Gomez, B., and M. Church (1989), An assessment of bed load sediment transport formulae for gravel bed rivers, *Water Resour. Res.*, *25*(6), 1161–1186, doi:10.1029/WR025i006p01161.

Grant, G. E., F. J. Swanson, and M. G. Wolman (1990), Pattern and origin of stepped-bed morphology in high-gradient streams, Western Cascades, Oregon, *Geol. Soc. Am. Bull.*, *102*(3), 340–352, doi:10.1130/0016-7606(1990)102<0340:PAOOSB>2.3.CO;2.

Gustina, G. W., and J. P. Hoffmann (2000), Periphyton Dynamics in a Subalpine Mountain Stream during Winter, *Arct. Antarct. Alp. Res.*, *32*(2), 127–134, doi:10.2307/1552444.

Harrison, L. R., T. Dunne, and G. B. Fisher (2015), Hydraulic and geomorphic processes in an overbank flood along a meandering, gravel-bed river: implications for chute formation, *Earth Surf. Process. Landf.*, *40*(9), 1239–1253, doi:10.1002/esp.3717.

Hart, D. D., B. J. F. Biggs, V. I. Nikora, and C. A. Flinders (2013), Flow effects on periphyton patches and their ecological consequences in a New Zealand river, *Freshw. Biol.*, *58*(8), 1588–1602, doi:10.1111/fwb.12147.

Helley, E. J., and W. Smith (1971), *Development and calibration of a pressure-difference bedload sampler*, Open-File Report, USGS Numbered Series.

IPCC (2014), *Climate Change 2014: Synthesis Report. Contributions of Working Groups I, II and III to the Firth Assessment Report of the Intergovernmental Panel on Climate Change*, IPCC, Geneva, Switzerland.

Johnson, R. E., N. C. Tuchman, and C. G. Peterson (1997), Changes in the Vertical Microdistribution of Diatoms within a Developing Periphyton Mat, *J. North Am. Benthol. Soc.*, *16*(3), 503–519, doi:10.2307/1468140.

Jowett, I. G. (2003), Hydraulic constraints on habitat suitability for benthic invertebrates in gravel-bed rivers, *River Res. Appl.*, *19*(5–6), 495–507, doi:10.1002/rra.734.

Jowett, I. G., and B. J. F. Biggs (1997), Flood and velocity effects on periphyton and silt accumulation in two New Zealand rivers, *N. Z. J. Mar. Freshw. Res.*, *31*(3), 287–300, doi:10.1080/00288330.1997.9516767.

Kahlert, M., and B. G. McKie (2014), Comparing new and conventional methods to estimate benthic algal biomass and composition in freshwaters, *Env. Sci Process. Impacts*, *16*(11), 2627–2634, doi:10.1039/C4EM00326H.

Kanavillil, N., D. Balika, and S. Kurissery (2014), Edge effect: a catalyst of spatial heterogeneity in natural biofilms, *Hydrobiologia*, *744*(1), 77–90, doi:10.1007/s10750-014-2058-3.

Knighton, D. (1998), *Fluvial Forms and Processes: A New Perspective*, Hodder Headline Group.

Lake, P. S. (2000), Disturbance, patchiness, and diversity in streams, *J. North Am. Benthol. Soc.*, *19*(4), 573–592.

Lake, P. S., N. Bond, and P. Reich (2007), Linking ecological theory with stream restoration, *Freshw. Biol.*, *52*(4), 597–615, doi:10.1111/j.1365-2427.2006.01709.x.

Larned, S. T. (2010), A prospectus for periphyton: recent and future ecological research, *J. North Am. Benthol. Soc.*, *29*(1), 182–206, doi:10.1899/08-063.1.

Legleiter, C. J., L. R. Harrison, and T. Dunne (2011), Effect of point bar development on the local force balance governing flow in a simple, meandering gravel bed river, *J. Geophys. Res. Earth Surf.*, *116*(F1), F01005, doi:10.1029/2010JF001838.

Leopold, L. B., and T. Maddock Jr. (1953), *The hydraulic geometry of stream channels and some physiographic implications*, Professional Paper, USGS Numbered Series.

Lisle, T. E., and M. A. ; Madej (1992), Spatial variation in armouring in a channel with high sediment supply, pp. 277–293.

Lisle, T. E., J. M. Nelson, J. Pitlick, M. A. Madej, and B. L. Barkett (2000), Variability of bed mobility in natural, gravel-bed channels and adjustments to sediment load at local and reach scales, *Water Resour. Res.*, *36*(12), 3743–3755, doi:10.1029/2000WR900238.

Luce, J. J., A. Cattaneo, and M. F. Lapointe (2010), Spatial patterns in periphyton biomass after low-magnitude flow spates: geomorphic factors affecting patchiness across gravel–cobble riffles, *J. North Am. Benthol. Soc.*, *29*(2), 614–626, doi:10.1899/09-059.1.

Luce, J. J., M. F. Lapointe, A. G. Roy, and D. B. Ketterling (2013), The effects of sand abrasion of a predominantly stable stream bed on periphyton biomass losses, *Ecohydrology*, *6*(4), 689–699, doi:10.1002/eco.1332.

Lyford, J. H., and S. V. Gregory (1975), The dynamics and structure of periphyton communities in three Cascade Mountain streams, *Verh Intern. Verin Limnol*, *19*, 1610–1616.

Matthaei, C. D., and C. R. Townsend (2000), Long-term effects of local disturbance history on mobile stream invertebrates, *Oecologia*, *125*(1), 119–126, doi:10.1007/PL00008883.

Matthaei, C. D., C. Guggelberger, and H. Huber (2003), Local disturbance history affects patchiness of benthic river algae, *Freshw. Biol.*, *48*(9), 1514–1526, doi:10.1046/j.1365-2427.2003.01103.x.

May, C. L., and B. S. Pryor (2014), Initial Motion and Bedload Transport Distance Determined by Particle Tracking in a Large Regulated River, *River Res. Appl.*, *30*(4), 508–520, doi:10.1002/rra.2665.

May, C. L., B. Pryor, T. E. Lisle, and M. Lang (2009), Coupling hydrodynamic modeling and empirical measures of bed mobility to predict the risk of scour and fill of salmon redds in a large regulated river, *Water Resour. Res.*, *45*(5), W05402, doi:10.1029/2007WR006498.

McCutchan, J. H. J., and W. M. J. Lewis (2002), Relative importance of carbon sources for macroinvertebrates in a Rocky Mountain stream, *Limnol. Oceanogr.*, *47*(3), 742–752, doi:10.4319/lo.2002.47.3.0742.

McDonald, R. R. (2016), Personal Communication,

McDonald, R. R., J. M. Nelson, V. Paragamian, and G. Barton (2010), Modeling the Effect of Flow and Sediment Transport on White Sturgeon Spawning Habitat in the Kootenai River, Idaho, *J. Hydraul. Eng.*, *136*(12), 1077–1092, doi:10.1061/(ASCE)HY.1943-7900.0000283.

Merwade, V. (2009), Effect of spatial trends on interpolation of river bathymetry, *J. Hydrol.*, *371*(1–4), 169–181, doi:10.1016/j.jhydrol.2009.03.026.

Merwade, V., A. Cook, and J. Coonrod (2008), GIS techniques for creating river terrain models for hydrodynamic modeling and flood inundation mapping, *Environ. Model. Softw.*, *23*(10–11), 1300–1311, doi:10.1016/j.envsoft.2008.03.005.

Merwade, V. M., D. R. Maidment, and J. A. Goff (2006), Anisotropic considerations while interpolating river channel bathymetry, *J. Hydrol.*, *331*(3–4), 731–741, doi:10.1016/j.jhydrol.2006.06.018.

Milhous, R. (1973), Sediment Transport in a Gravel-Bottomed Stream, Oregon State University, 3 May.

Monsalve, A., E. M. Yager, J. M. Turowski, and D. Rickenmann (2016), A probabilistic formulation of bed load transport to include spatial variability of flow and surface grain size distributions, *Water Resour. Res.*, n/a-n/a, doi:10.1002/2015WR017694.

Montgomery, D. R., and J. M. Buffington (1997), Channel-reach morphology in mountain drainage basins, *Geol. Soc. Am. Bull.*, *109*(5), 596–611, doi:10.1130/0016-7606(1997)109<0596:CRMIMD>2.3.CO;2.

Mueller, E. R., and J. Pitlick (2014), Sediment supply and channel morphology in mountain river systems: 2. Single thread to braided transitions, *J. Geophys. Res. Earth Surf.*, *119*(7), 2013JF003045, doi:10.1002/2013JF003045.

Mueller, E. R., J. Pitlick, and J. M. Nelson (2005), Variation in the reference Shields stress for bed load transport in gravel-bed streams and rivers, *Water Resour. Res.*, *41*(4), W04006, doi:10.1029/2004WR003692.

Murdock, J., D. Roelke, and F. Gelwick (2004), Interactions between flow, periphyton, and nutrients in a heavily impacted urban stream: implications for stream restoration effectiveness, *Ecol. Eng.*, *22*(3), 197–207, doi:10.1016/j.ecoleng.2004.05.005.

Nelson, J. M. (2015), *FaSTMECH Solver Manual*, http://i-ric.org/en/downloads.

Nelson, J. M. et al. (2015a), The international river interface cooperative: Public domain flow and morphodynamics software for education and applications, *Adv. Water Resour.*, doi:10.1016/j.advwatres.2015.09.017.

Nelson, P. A., W. E. Dietrich, and J. G. Venditti (2010), Bed topography and the development of forced bed surface patches, *J. Geophys. Res. Earth Surf.*, *115*(F4), F04024, doi:10.1029/2010JF001747.

Nelson, P. A., R. R. McDonald, J. M. Nelson, and W. E. Dietrich (2015b), Coevolution of bed surface patchiness and channel morphology: 1. Mechanisms of forced patch formation, *J. Geophys. Res. Earth Surf.*, *120*(9), 2014JF003428, doi:10.1002/2014JF003428.

O'Connor, J. E., J. F. Mangano, S. W. Anderson, J. R. Wallick, K. L. Jones, and M. K. Keith (2014), Geologic and physiographic controls on bed-material yield, transport, and channel morphology for alluvial and bedrock rivers, western Oregon, *Geol. Soc. Am. Bull.*, B30831.1, doi:10.1130/B30831.1.

O'Leary, S. J., and R. L. Beschta (1981), Bedload Transport in an Oregon Coast Range Stream1, *JAWRA J. Am. Water Resour. Assoc.*, *17*(5), 886–894, doi:10.1111/j.1752-1688.1981.tb01313.x.

Olinde, L., and J. P. L. Johnson (2015), Using RFID and accelerometer-embedded tracers to measure probabilities of bed load transport, step lengths, and rest times in a mountain stream, *Water Resour. Res.*, *51*(9), 7572–7589, doi:10.1002/2014WR016120.

Osmundson, D. B., R. J. Ryel, V. L. Lamarra, and J. Pitlick (2002), Flow-Sediment-Biota Relations: Implications for River Regulation Effects on Native Fish Abundance, *Ecol. Appl.*, *12*(6), 1719–1739, doi:10.2307/3099934.

Paola, C., and R. Seal (1995), Grain Size Patchiness as a Cause of Selective Deposition and Downstream Fining, *Water Resour. Res.*, *31*(5), 1395–1407, doi:10.1029/94WR02975.

Parker, G. (1979), Hydraulic geometry of active gravel rivers, *J. Hydraul. Div.*, *105*(9), 1185–1201.

Parker, G. (1990), Surface-based bedload transport relation for gravel rivers, *J. Hydraul. Res.*, *28*(4), 417–436, doi:10.1080/00221689009499058.

Parker, G., and P. C. Klingeman (1982), On why gravel bed streams are paved, *Water Resour. Res.*, *18*(5), 1409–1423, doi:10.1029/WR018i005p01409.

Parker, G., and C. M. Toro-Escobar (2002), Equal mobility of gravel in streams: The remains of the day, *Water Resour. Res.*, *38*(11), 1264, doi:10.1029/2001WR000669.

Parker, G., P. C. Klingeman, and D. G. McLean (1982), Bedload and size distribution in paved gravel-bed streams, *J. Hydraul. Div.*, *108*(4), 544–571.

Pasternack, G. B., C. L. Wang, and J. E. Merz (2004), Application of a 2D hydrodynamic model to design of reach-scale spawning gravel replenishment on the Mokelumne River, California, *River Res. Appl.*, *20*(2), 205–225, doi:10.1002/rra.748.

Peterson, C. G., and R. J. Stevenson (1992), Resistance and Resilience of Lotic Algal Communities: Importance of Disturbance Timing and Current, *Ecology*, *73*(4), 1445–1461, doi:10.2307/1940689.

Peterson, C. G., A. C. Weibel, N. B. Grimm, and S. G. Fisher (1994), Mechanisms of benthic algal recovery following spates: comparison of simulated and natural events, *Oecologia*, *98*(3–4), 280–290, doi:10.1007/BF00324216.

Pitlick, J. (1988), Variability of bed load measurement, *Water Resour. Res.*, *24*(1), 173–177, doi:10.1029/WR024i001p00173.

Pitlick, J., E. R. Mueller, C. Segura, R. Cress, and M. Torizzo (2008), Relation between flow, surface-layer armoring and sediment transport in gravel-bed rivers, *Earth Surf. Process. Landf.*, *33*(8), 1192–1209, doi:10.1002/esp.1607.

Poff, N. L., J. D. Allan, M. B. Bain, J. R. Karr, K. L. Prestegaard, B. D. Richter, R. E. Sparks, and J. C. Stromberg (1997), The Natural Flow Regime, *BioScience*, *47*(11), 769–784, doi:10.2307/1313099.

Power, M. E., and W. E. Dietrich (2002), Food webs in river networks, *Ecol. Res.*, *17*(4), 451–471, doi:10.1046/j.1440-1703.2002.00503.x.

Power, M. E., and A. J. Stewart (1987), Disturbance and Recovery of an Algal Assemblage Following Flooding in an Oklahoma Stream, *Am. Midl. Nat.*, *117*(2), 333–345, doi:10.2307/2425975.

Recking, A. (2013a), An analysis of nonlinearity effects on bed load transport prediction, *J. Geophys. Res. Earth Surf.*, *118*(3), 1264–1281, doi:10.1002/jgrf.20090.

Recking, A. (2013b), Simple Method for Calculating Reach-Averaged Bed-Load Transport - (ASCE)HY.1943-7900.0000653,

Redfield, A. C. (1934), *On the proportions of organic derivatives in sea water and their relation to the composition of plankton*, university press of liverpool Liverpool, UK.

Resh, V. H., A. V. Brown, A. P. Covich, M. E. Gurtz, H. W. Li, G. W. Minshall, S. R. Reice, A. L. Sheldon, J. B. Wallace, and R. C. Wissmar (1988), The Role of Disturbance in Stream Ecology, *J. North Am. Benthol. Soc.*, *7*(4), 433–455, doi:10.2307/1467300.

Rickenmann, D., and B. W. McArdell (2007), Continuous measurement of sediment transport in the Erlenbach stream using piezoelectric bedload impact sensors, *Earth Surf. Process. Landf.*, *32*(9), 1362–1378, doi:10.1002/esp.1478.

Roberts, B. J., P. J. Mulholland, and W. R. Hill (2007), Multiple Scales of Temporal Variability in Ecosystem Metabolism Rates: Results from 2 Years of Continuous Monitoring in a Forested Headwater Stream, *Ecosystems*, *10*(4), 588–606, doi:10.1007/s10021-007-9059-2.

Rosemond, A. D., P. J. Mulholland, and J. W. Elwood (1993), Top-Down and Bottom-Up Control of Stream Periphyton: Effects of Nutrients and Herbivores, *Ecology*, *74*(4), 1264–1280, doi:10.2307/1940495.

Rounick, J. S., and S. V. Gregory (1981), Temporal changes in periphyton standing crop during an unusually dry winter in streams of the Western Cascades, Oregon, *Hydrobiologia*, *83*(2), 197–205, doi:10.1007/BF00008267.

Ryan, S. E., L. S. Porth, and C. A. Troendle (2002), Defining phases of bedload transport using piecewise regression, *Earth Surf. Process. Landf.*, *27*(9), 971–990, doi:10.1002/esp.387.

Ryan, S. E., L. S. Porth, and C. A. Troendle (2005), Coarse sediment transport in mountain streams in Colorado and Wyoming, USA, *Earth Surf. Process. Landf.*, *30*(3), 269–288, doi:10.1002/esp.1128.

Ryder, D. S. (2004), Response of epixylic biofilm metabolism to water level variability in a regulated floodplain river, *J. North Am. Benthol. Soc.*, *23*(2), 214–223, doi:10.1899/0887-3593(2004)023<0214:ROEBMT>2.0.CO;2.

Sandra E. Ryan, C. A. T. (1999), Measuring Bedload with Handheld Samplers in Coarse-Grained Mountain Channels,

Schmidt, K.-H., and P. Ergenzinger (1992), Bedload entrainment, travel lengths, step lengths, rest periods—studied with passive (iron, magnetic) and active (radio) tracer techniques, *Earth Surf. Process. Landf.*, *17*(2), 147–165, doi:10.1002/esp.3290170204.

Schumm, S. (1960), *The shape of alluvial channels in relation to sediment type*, Professional Paper, USGS Numbered Series.

Segura, C., and J. Pitlick (2015), Coupling fluvial-hydraulic models to predict gravel transport in spatially variable flows, *J. Geophys. Res. Earth Surf.*, *120*(5), 2014JF003302, doi:10.1002/2014JF003302.

Segura, C., J. H. McCutchan, W. M. Lewis, and J. Pitlick (2011), The influence of channel bed disturbance on algal biomass in a Colorado mountain stream, *Ecohydrology*, *4*(3), 411–421, doi:10.1002/eco.142.

Sekar, R., K. Nandakumar, V. P. Venugopalan, K. V. K. Nair, and V. N. R. Rao (1998), Spatial variation in microalgal colonization on hard surfaces in a lentic freshwater environment, *Biofouling*, *13*(3), 177–195, doi:10.1080/08927019809378380.

Snell, M. A. et al. (2014), High frequency variability of environmental drivers determining benthic community dynamics in headwater streams, *Environ. Sci. Process. Impacts*, *16*(7), 1629–1636, doi:10.1039/C3EM00680H.

Stanish, L. F., D. R. Nemergut, and D. M. McKnight (2011), Hydrologic processes influence diatom community composition in Dry Valley streams, *J. North Am. Benthol. Soc.*, *30*(4), 1057–1073, doi:10.1899/11-008.1.

Stanley, E. H., S. M. Powers, and N. R. Lottig (2010), The evolving legacy of disturbance in stream ecology: concepts, contributions, and coming challenges, *J. North Am. Benthol. Soc.*, *29*(1), 67–83, doi:10.1899/08-027.1.

Stevenson, R. J. (1990), Benthic Algal Community Dynamics in a Stream during and after a Spate, *J. North Am. Benthol. Soc.*, *9*(3), 277–288, doi:10.2307/1467591.

Stewart, G., R. Anderson, and E. Wohl (2005), Two-dimensional modelling of habitat suitability as a function of discharge on two Colorado rivers, *River Res. Appl.*, *21*(10), 1061–1074, doi:10.1002/rra.868.

Suren, A. M., and M. J. Duncan (1999), Rolling Stones and Mosses: Effect of Substrate Stability on Bryophyte Communities in Streams, *J. North Am. Benthol. Soc.*, *18*(4), 457–467, doi:10.2307/1468378.

Townsend, C. R., M. R. Scarsbrook, and S. Dolédec (1997), The intermediate disturbance hypothesis, refugia, and biodiversity in streams, *Limnol. Oceanogr.*, *42*(5), 938–949, doi:10.4319/lo.1997.42.5.0938.

Townsend, S. A., and M. M. Douglas (2014), Benthic algal resilience to frequent wet-season storm flows in low-order streams in the Australian tropical savanna, *Freshw. Sci.*, *33*(4), 1030–1042, doi:10.1086/678516.

Townsend, S. A., and A. V. Padovan (2005), The seasonal accrual and loss of benthic algae (Spirogyra) in the Daly River, an oligotrophic river in tropical Australia, *Mar. Freshw. Res.*, *56*(3), 317–327.

Uehlinger, U., H. Bührer, and P. Reichert (1996), Periphyton dynamics in a floodprone prealpine river: evaluation of significant processes by modelling, *Freshw. Biol.*, *36*(2), 249–263, doi:10.1046/j.1365-2427.1996.00082.x.

Vericat, D., M. Church, and R. J. Batalla (2006), Bed load bias: Comparison of measurements obtained using two (76 and 152 mm) Helley-Smith samplers in a gravel bed river, *Water Resour. Res.*, *42*(1), W01402, doi:10.1029/2005WR004025.

Warren, D. R., J. B. Dunham, and D. Hockman-Wert (2014), Geographic Variability in Elevation and Topographic Constraints on the Distribution of Native and Nonnative Trout in the Great Basin, *Trans. Am. Fish. Soc.*, *143*(1), 205–218, doi:10.1080/00028487.2013.833551.

Wilcock, P., and J. Crowe (2003), Surface-based Transport Model for Mixed-Size Sediment, *J. Hydraul. Eng.*, *129*(2), 120–128, doi:10.1061/(ASCE)0733-9429(2003)129:2(120).

Wolman, M. G. (1954), A method of sampling coarse river-bed material, *Eos Trans. Am. Geophys. Union*, *35*(6), 951–956, doi:10.1029/TR035i006p00951.

Woodward, G., and A. G. Hildrew (2002), Food web structure in riverine landscapes, *Freshw. Biol.*, *47*(4), 777–798, doi:10.1046/j.1365-2427.2002.00908.x.

Wyss, C. R., D. Rickenmann, B. Fritschi, J. M. Turowski, V. Weitbrecht, and R. M. Boes (2016), Measuring Bed Load Transport Rates by Grain-Size Fraction Using the Swiss Plate Geophone Signal at the Erlenbach, *J. Hydraul. Eng.*, *142*(5), 4016003, doi:10.1061/(ASCE)HY.1943-7900.0001090.

Yager, E. M., and M. W. Schmeeckle (2013), The influence of vegetation on turbulence and bed load transport, *J. Geophys. Res. Earth Surf.*, *118*(3), 1585–1601, doi:10.1002/jgrf.20085.

Yager, E. M., J. W. Kirchner, and W. E. Dietrich (2007), Calculating bed load transport in steep boulder bed channels, *Water Resour. Res.*, *43*(7), W07418, doi:10.1029/2006WR005432.

6. APPENDICES

6.1 Appendix A - Photo Log

Chlorophyll- a sampling grid during moderate winter flow on 12/4/15

Concrete weir during moderate winter flow on 12/4/15

Riparian vegetation surrounding study site during moderate winter flow on 12/4/15. View from road looking downstream at ~ cross-section 45.

View upstream of plane bed portion of reach during summer low flow on 8/5/16. Picture taken from ~ cross-section 3.

Flow over gravel bar in pool-riffle portion of stream. View upstream from ~ cross-section 17. Marty Katz (my father) on stream bank for scale.

Interaction of riparian vegetation with flow field during high flow. View from left bank at ~ cross-section 22. Note rebar staff gauges along right bank.

Riparian vegetation growing over stream channel. The tree is not interacting with the flow during the summer low flow period, however acts as a roughness element during higher flows. Picture taken looking downstream from ~ cross-section 11 on 8/5/15.

Gravel bar inundated during moderate winter flow. Picture taken looking downstream from ~ cross-section 27 on 12/4/15.

Measuring discharge during a Q = 1.3 m^3/s flow on 2/5/15. Picture taken looking downstream from ~ cross-section 50 of Scott Katz.

Surveying the longitudinal profile. Picture of field assistant Joseph Tinker

Collecting bed load measurements during a Q = 0.91 m^3/s flow on 12/9/15. Photo taken of Scott Katz sampling within concrete weir.

Measuring in-situ Chlorophyll-a with the BenthoTorch. Photo of Scott Katz on 4/11/16.

BenthoTorch taking measurements on stream substrate.

Rebar staff gauge along right bank during moderate winter flow

Subsurface grain size sample taken from exposed bar. Particles >32mm were sorted in the field prior to the sieving.

Original Chlorophyll-a sampling grid following high flow event on 12/4/15. The grid was re-made in the same location following the flow event without cross-strings.

High water marks following the large high flow event on 12/18/15. The flow was outside of the surveyed topography in many instances.

High water marks of high flow event on 12/18/15. Note the freshly exposed bank on the right that is higher in elevation than the concrete weir.

High water marks and piled debris following large high flow event on 12/18/15

6.2 Appendix B - Geomorphic and Hydraulic Data Summary

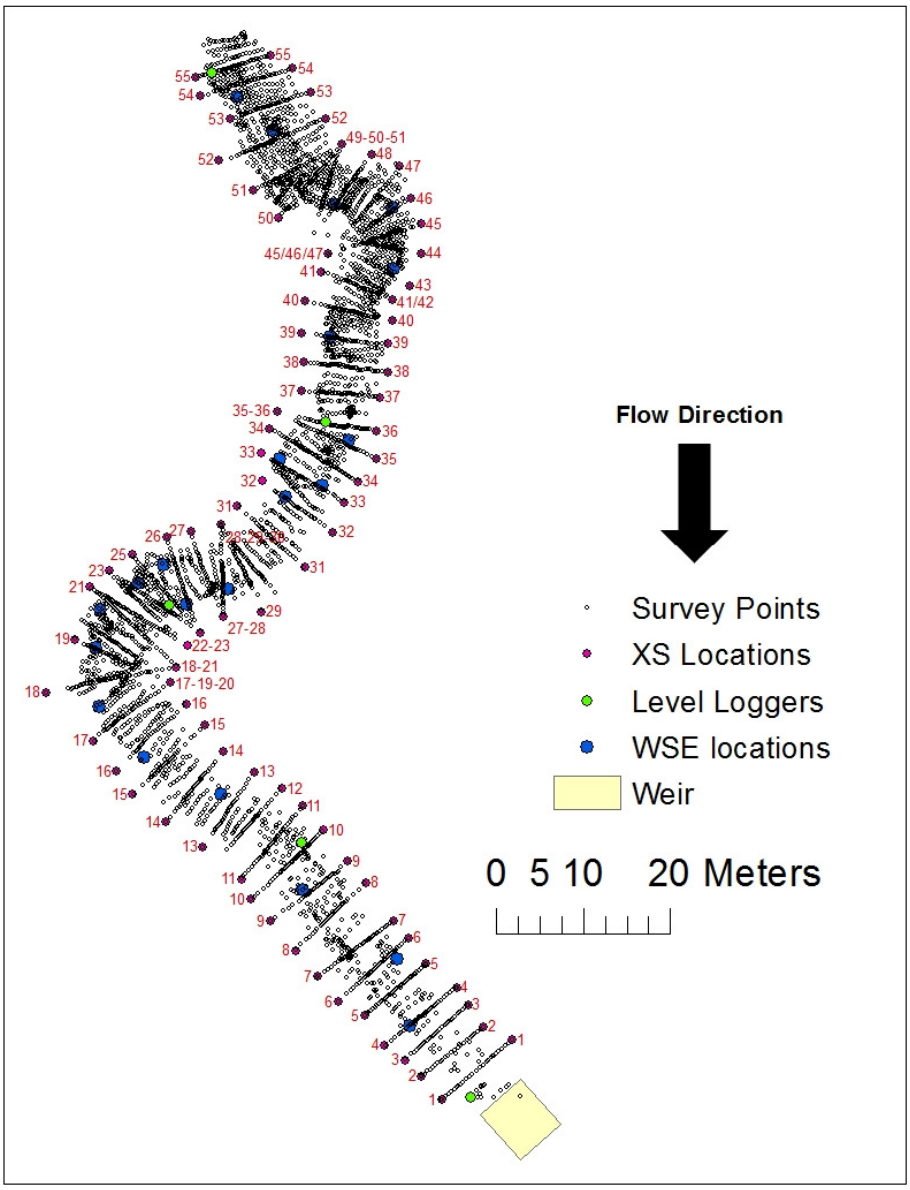

Map of cross-section (XS) locations, level loggers and rebar staff gauges for the full Oak Creek study reach. The reach was shortened to include only XS 1-33 for the analysis presented in the thesis.

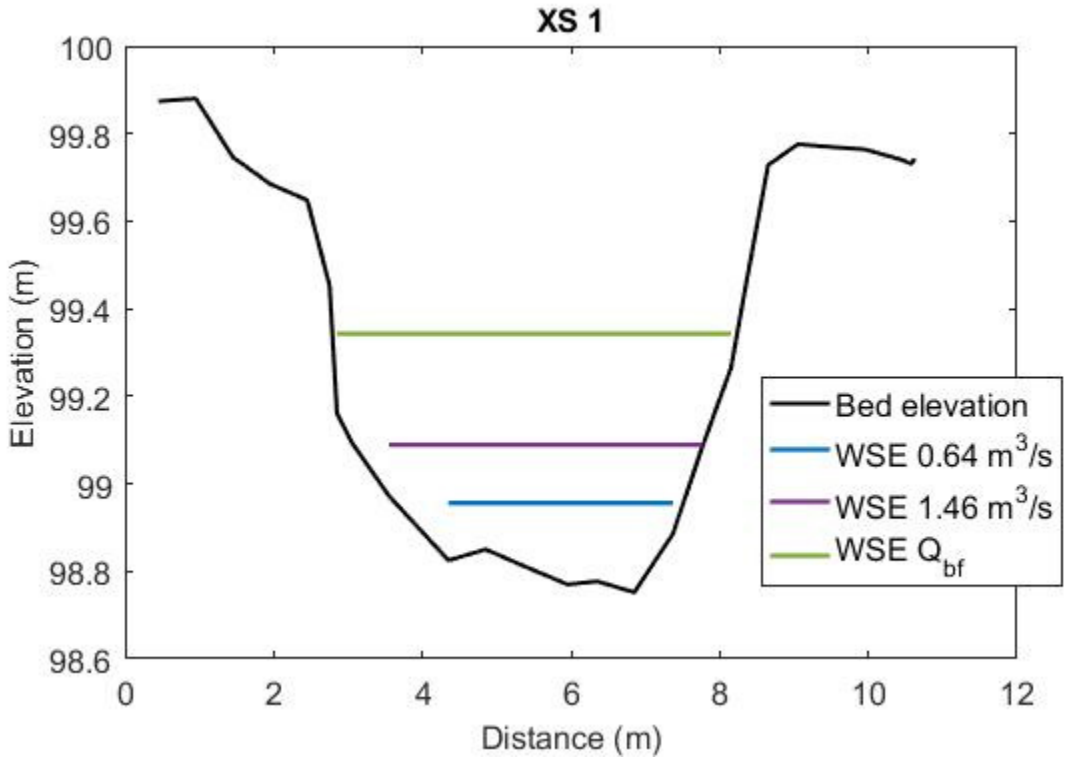

Profile view of cross-section 1 (XS-1) showing distance from the bottom of pin on the left bank and elevation from an arbitrary datum. Water surface elevations (WSE) for 3 model calibration flows ranging from 0.64-bankfull (Q_{bf}) are also shown. WSEs for the 0.64 m^3/s and 1.46 m^3/s flows were observed in the field. The WSE for Q_{bf} was estimated based on time-lapse photography, field observations of bankfull stage and analysis of cross-section topography.

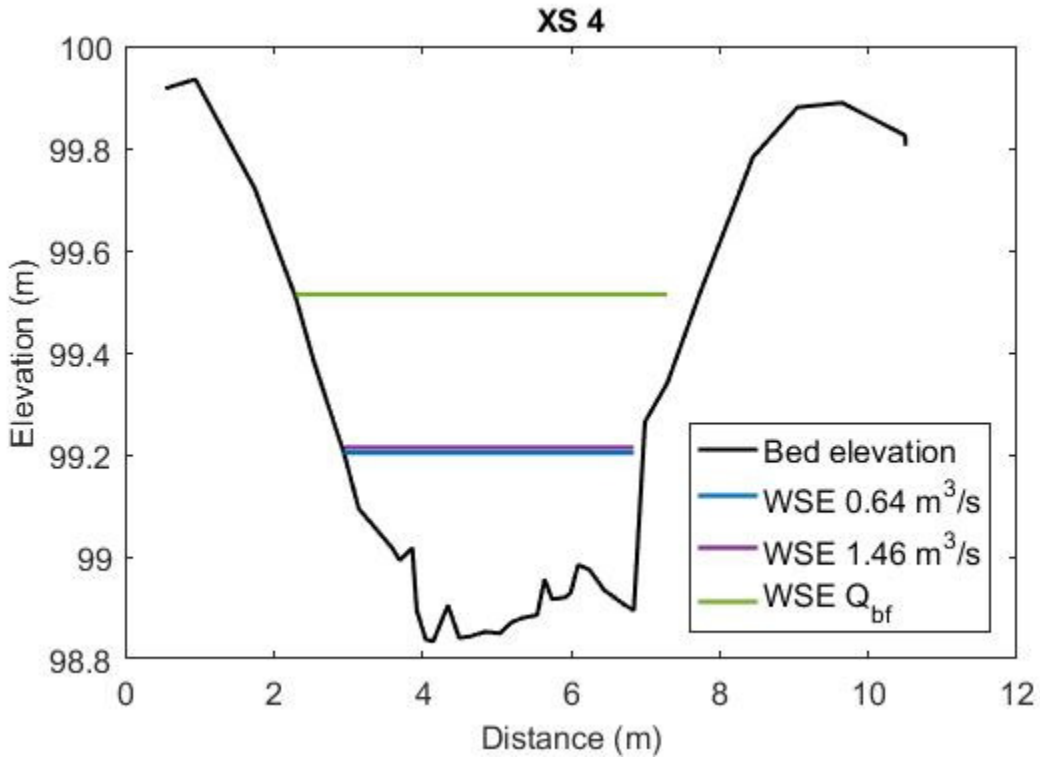

Profile view of cross-section 4 (XS-4) showing distance from the bottom of pin on the left bank and elevation from an arbitrary datum. Water surface elevations (WSE) for 3 model calibration flows ranging from 0.64-bankfull (Q_{bf}) are also shown. WSEs for the 0.64 m^3/s and 1.46 m^3/s flows were observed in the field. The WSE for Q_{bf} was estimated based on time-lapse photography, field observations of bankfull stage and analysis of cross-section topography.

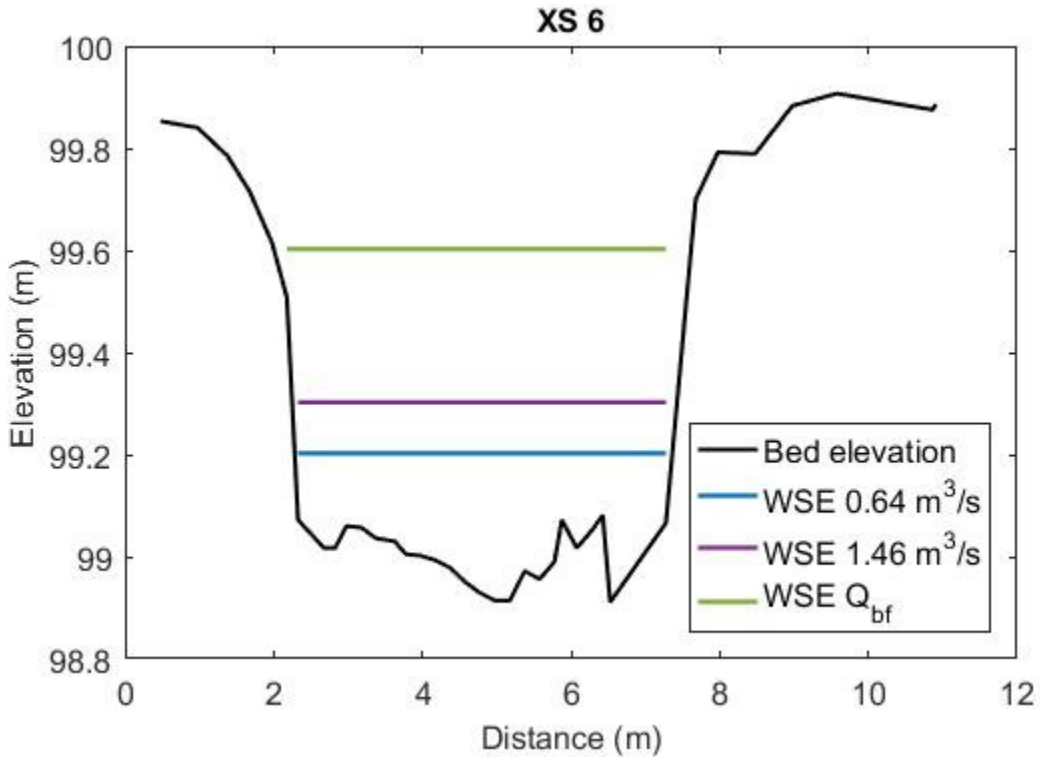

Profile view of cross-section 1 (XS-6) showing distance from the bottom of pin on the left bank and elevation from an arbitrary datum. Water surface elevations (WSE) for 3 model calibration flows ranging from 0.64-bankfull (Q_{bf}) are also shown. WSEs for the 0.64 m^3/s and 1.46 m^3/s flows were observed in the field. The WSE for Q_{bf} was estimated based on time-lapse photography, field observations of bankfull stage and analysis of cross-section topography.

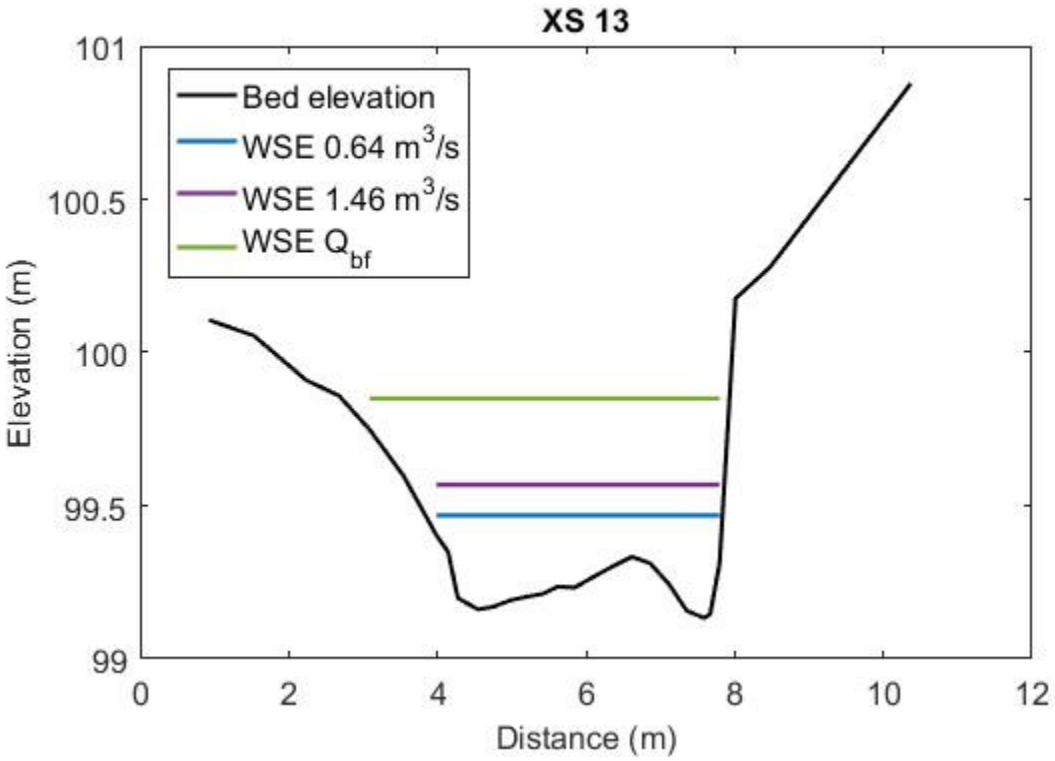

Profile view of cross-section 1 (XS-13) showing distance from the bottom of pin on the left bank and elevation from an arbitrary datum. Water surface elevations (WSE) for 3 model calibration flows ranging from 0.64-bankfull (Q_{bf}) are also shown. WSEs for the 0.64 m^3/s and 1.46 m^3/s flows were observed in the field. The WSE for Q_{bf} was estimated based on time-lapse photography, field observations of bankfull stage and analysis of cross-section topography.

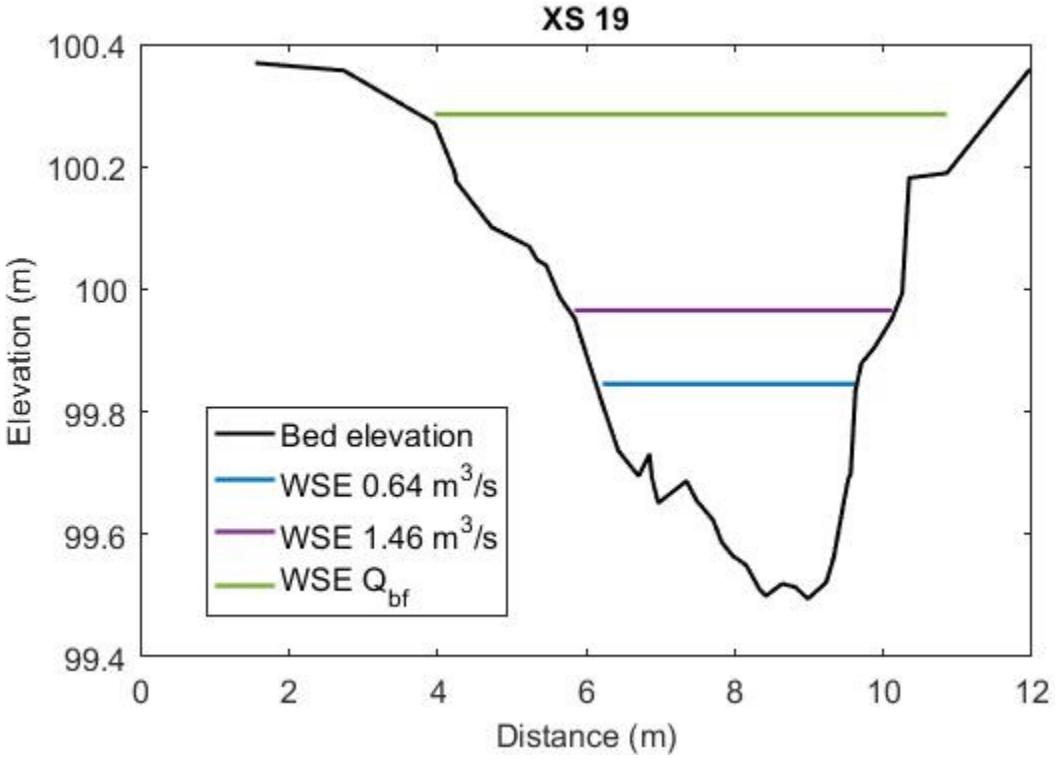

Profile view of cross-section 1 (XS-19) showing distance from the bottom of pin on the left bank and elevation from an arbitrary datum. Water surface elevations (WSE) for 3 model calibration flows ranging from 0.64-bankfull (Q_{bf}) are also shown. WSEs for the 0.64 m^3/s and 1.46 m^3/s flows were observed in the field. The WSE for Q_{bf} was estimated based on time-lapse photography, field observations of bankfull stage and analysis of cross-section topography.

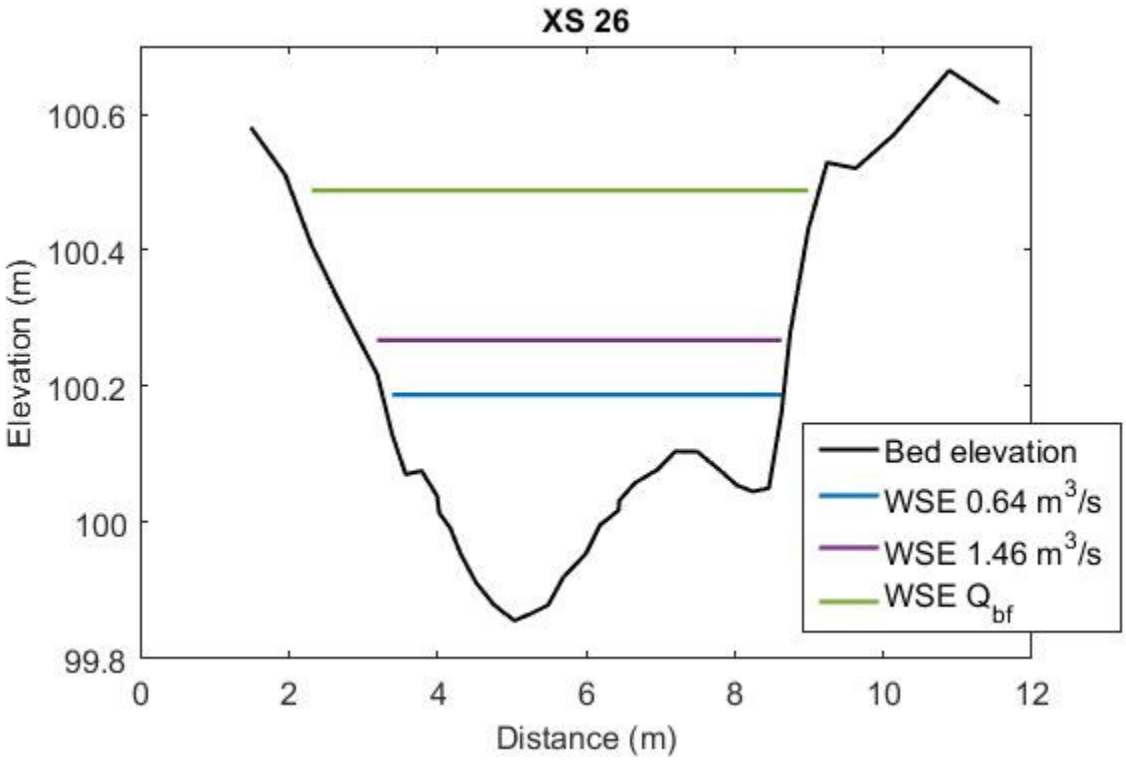

Profile view of cross-section 1 (XS-26) showing distance from the bottom of pin on the left bank and elevation from an arbitrary datum. Water surface elevations (WSE) for 3 model calibration flows ranging from 0.64-bankfull (Q_{bf}) are also shown. WSEs for the 0.64 m^3/s and 1.46 m^3/s flows were observed in the field. The WSE for Q_{bf} was estimated based on time-lapse photography, field observations of bankfull stage and analysis of cross-section topography.

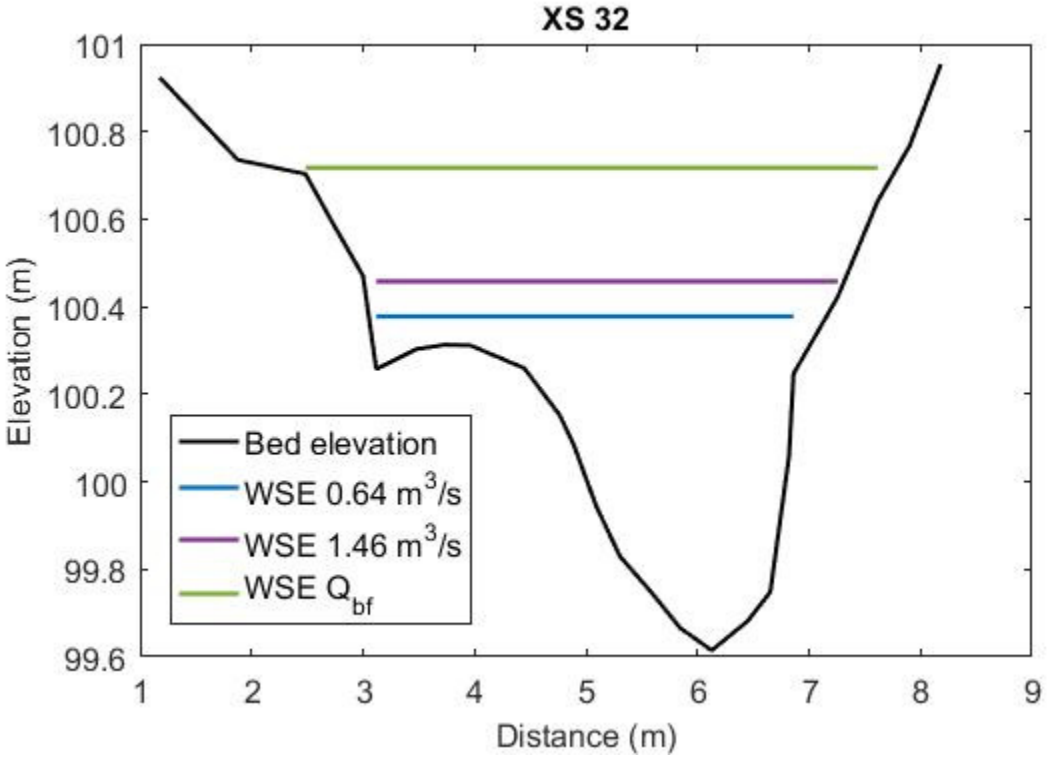

Profile view of cross-section 1 (XS-32) showing distance from the bottom of pin on the left bank and elevation from an arbitrary datum. Water surface elevations (WSE) for 3 model calibration flows ranging from 0.64-bankfull (Q_{bf}) are also shown. WSEs for the 0.64 m^3/s and 1.46 m^3/s flows were observed in the field. The WSE for Q_{bf} was estimated based on time-lapse photography, field observations of bankfull stage and analysis of cross-section topography.

Summary of average cross-sectional hydraulic geometry for flows ranging from 0.64-3.4 m^3/s including the depth, area, wetted perimeter, hydraulic radius and velocity (from continuity). Parameters were calculated using observed water surface elevations from rebar staff gauges near surveyed cross sections. The cross sections used in the analysis include 1, 4, 6, 13, 19, 26, and 32.

Discharge (m^3/s)	Depth (m)	Area (m^2)	Wetted Perimeter (m)	Hydraulic Radius (m)	Velocity (m/s)
0.64	0.23	0.93	4.21	0.22	0.69
0.992	0.27	1.11	4.33	0.26	0.89
1.33	0.28	1.18	4.39	0.27	1.13
1.48	0.30	1.33	4.61	0.29	1.11
3.4	0.51	2.77	5.95	0.47	1.23

Point counts for surface pebble counts conducted along surveyed cross-sections.

XS / Size Range (mm)	**1**	**2**	**3**	**4**	**5**	**6**	**11**	**13**	**22**	**25**	**31**	**33**
256-362	0	0	0	0	0	0	0	0	0	0	0	0
180-256	0	0	0	0	0	0	0	0	0	0	0	0
128-180	5	5	6	2	3	2	3	0	1	1	0	0
90-128	21	6	6	17	8	10	6	7	9	2	16	8
64-90	18	25	14	18	18	7	15	26	21	7	26	28
45-64	17	11	20	18	16	11	18	22	26	21	16	23
32-45	6	12	12	11	11	13	21	11	23	25	18	16
22.6-32	9	17	11	17	12	11	13	8	9	19	14	16
16-22	7	6	7	5	12	18	8	12	10	14	8	9
11-16	6	5	8	5	4	15	5	6	5	7	4	4
8-11.2	2	4	5	3	6	9	5	4	4	4	4	0
5.6-8	1	0	6	2	2	0	4	4	0	3	1	1
4-5.6	0	0	0	0	0	0	2	1	0	0	0	0
2.8-4	0	0	0	0	0	0	0	0	0	0	0	0
Total Counts	92	91	95	98	92	96	100	101	108	103	107	105

Point counts for surface pebble counts conducted along surveyed cross-sections.

XS / Size Range (mm)	**35**	**37**	**39**	**40**	**41**	**44**	**46**	**51**	**52**	**53**	**55**
256-362	0	0	0	0	0	0	0	0	0	0	0
180-256	0	0	0	0	0	0	1	0	0	0	0
128-180	0	0	1	0	0	0	6	1	1	2	3
90-128	7	8	20	4	4	17	14	15	10	8	11
64-90	21	25	31	20	16	19	21	24	20	16	22
45-64	21	32	32	23	28	26	24	23	19	26	31
32-45	19	11	13	24	22	14	23	13	21	25	30
22.6-32	13	10	5	23	21	11	13	10	23	16	12
16-22	13	8	5	6	24	5	7	2	9	4	3
11-16	6	3	1	0	10	2	0	1	2	2	1
8-11.2	1	3	1	0	1	3	0	1	2	1	0
5.6-8	1	0	0	0	0	3	0	0	1	0	1
4-5.6	0	0	0	0	0	0	0	0	0	0	0
2.8-4	0	0	0	0	0	0	0	1	0	0	0
Total Counts	102	100	109	100	126	100	109	91	108	100	114

Percent finer and grain size statistics (D_{16}, D_{50}, D_{84}) for surface pebble counts conducted along surveyed cross sections.

XS / Size Range (mm)	**1**	**2**	**3**	**4**	**5**	**6**	**11**	**13**
256-362	100%	100%	100%	100%	100%	100%	100%	100%
180-256	100%	100%	100%	100%	100%	100%	100%	100%
128-180	100%	100%	100%	100%	100%	100%	100%	100%
90-128	95%	95%	94%	98%	97%	98%	97%	100%
64-90	72%	88%	87%	81%	88%	88%	91%	93%
45-64	52%	60%	73%	62%	68%	80%	76%	67%
32-45	34%	48%	52%	44%	51%	69%	58%	46%
22.6-32	27%	35%	39%	33%	39%	55%	37%	35%
16-22.6	17%	16%	27%	15%	26%	44%	24%	27%
11-16	10%	10%	20%	10%	13%	25%	16%	15%
8-11.2	3%	4%	12%	5%	9%	9%	11%	9%
5.6-8	1%	0%	6%	2%	2%	0%	6%	5%
4-5.6	0%	0%	0%	0%	0%	0%	2%	1%
2.8-4	0%	0%	0%	0%	0%	0%	0%	0%
D_{16} (mm)	21.22	22.03	13.51	22.92	17.30	13.03	16.00	16.54
D_{50} (mm)	61.40	47.21	43.12	50.61	43.63	27.32	39.52	48.36
D_{84} (mm)	108.74	85.74	83.25	96.41	83.88	76.41	76.76	79.81

Percent finer and grain size statistics (D_{16}, D_{50}, D_{84}) for surface pebble counts conducted along surveyed cross sections.

XS / Size Range (mm)	**22**	**25**	**31**	**33**	**35**	**37**	**39**	**40**
256-362	100%	100%	100%	100%	100%	100%	100%	100%
180-256	100%	100%	100%	100%	100%	100%	100%	100%
128-180	100%	100%	100%	100%	100%	100%	100%	100%
90-128	99%	99%	100%	100%	100%	100%	99%	100%
64-90	91%	97%	85%	92%	93%	92%	81%	96%
45-64	71%	90%	61%	66%	73%	67%	52%	76%
32-45	47%	70%	46%	44%	52%	35%	23%	53%
22.6-32	26%	46%	29%	29%	33%	24%	11%	29%
16-22.6	18%	27%	16%	13%	21%	14%	6%	6%
11-16	8%	14%	8%	5%	8%	6%	2%	0%
8-11.2	4%	7%	5%	1%	2%	3%	1%	0%
5.6-8	0%	3%	1%	1%	1%	0%	0%	0%
4-5.6	0%	0%	0%	0%	0%	0%	0%	0%
2.8-4	0%	0%	0%	0%	0%	0%	0%	0%
D_{16} (mm)	21.30	17.01	22.67	24.02	19.96	24.23	36.91	26.29
D_{50} (mm)	46.87	34.03	49.69	49.71	43.41	53.08	62.26	43.12
D_{84} (mm)	79.97	57.41	88.69	80.86	77.36	80.70	95.82	73.35

Percent finer and grain size statistics (D_{16}, D_{50}, D_{84}) for surface pebble counts conducted along surveyed cross sections.

XS / Size Range (mm)	**41**	**44**	**46**	**51**	**52**	**53**	**55**
256-362	100%	100%	100%	100%	100%	100%	100%
180-256	100%	100%	100%	100%	100%	100%	100%
128-180	100%	100%	99%	100%	100%	100%	100%
90-128	100%	100%	94%	99%	99%	98%	97%
64-90	97%	83%	81%	82%	90%	90%	88%
45-64	84%	64%	61%	56%	71%	74%	68%
32-45	62%	38%	39%	31%	54%	48%	41%
22.6-32	44%	24%	18%	16%	34%	23%	15%
16-22.6	28%	13%	6%	5%	13%	7%	4%
11-16	9%	8%	0%	3%	5%	3%	2%
8-11.2	1%	6%	0%	2%	3%	1%	1%
5.6-8	0%	3%	0%	1%	1%	0%	1%
4-5.6	0%	0%	0%	1%	0%	0%	0%
2.8-4	0%	0%	0%	1%	0%	0%	0%
D_{16} (mm)	18.25	24.85	29.88	31.51	23.75	27.48	32.45
D_{50} (mm)	35.67	52.94	53.27	58.83	42.17	46.24	50.41
D_{84} (mm)	63.87	91.88	98.43	93.10	80.86	79.20	84.28

Summary of weights and percent (%) finer of subsurface grain size samples collected from exposed bars.

Size Range (mm)	Sample 1		Sample 2	
	Weight (g)	% finer (%)	Weight (g)	% finer (%)
256-362	0	100.00	0	100.00
180-256	0	100.00	0	100.00
128-180	0	100.00	0	100.00
90-128	3200	100.00	2400	100.00
64-90	7400	94.22	6800	95.67
45-64	8000	80.87	5400	83.39
32-45	6400	66.43	5800	73.65
22.6-32	193.9	54.87	155.6	63.18
16-22	237.6	50.06	208.7	51.76
11-16	325.7	44.15	309.4	47.58
8-11.2	286.1	36.06	265.2	41.39
5.6-8	271.8	28.95	249.3	36.08
4-5.6	219.4	22.19	264	31.09
2.8-4	190.5	16.74	259.4	25.81
2-2.8	147.7	12.01	261.1	20.61
1.4-2	99	8.34	225.7	15.39
1-1.4	58.3	5.88	148.8	10.87
0.71-1	40.6	4.43	108.6	7.89
0.5-0.71	31	3.42	83.1	5.72
0.355-0.5	27.4	2.65	65.7	4.05
0.25-0.355	20.4	1.97	46.5	2.74
0.18-0.25	13.2	1.46	25.2	1.81
0.125-0.18	11.4	1.13	18.9	1.30
0.09-0.125	7.5	0.85	11.3	0.92
0.063-0.09	6.7	0.66	9.4	0.70
0-0.063	20	0.50	25.5	0.51

Summary of discharge (Q) measurements used to develop the site rating curve. Measurements denoted with an "(a)" were made by students of the Water Resources Graduate Program at Oregon State University in conjunction with Dr. Mary Santelmann. Dr. Mary Santelmann is also responsible for installing the stage gauge used in this study.

Date	Time	Q (m^3/s)	Stage (m)
10/26/2012	1:00 PM	0.043[(a)]	98.77
2/16/2013	9:30 AM	0.07[(a)]	98.79
2/13/2013	1:30 PM	0.07[(a)]	98.80
10/31/2015	5:30 PM	0.11	98.80
3/7/2013	3:40 PM	0.15[(a)]	98.84
2/5/2015	4:35 PM	0.15	98.84
10/31/2015	7:00 PM	0.19	98.84
2/25/2013	3:30 PM	0.29[(a)]	98.87
2/23/2013	11:30 AM	0.29[(a)]	98.87
3/24/2015	12:15 PM	0.31	98.88
1/15/2016	8:50 PM	0.74	99.00
12/23/2015	5:20 PM	0.94	99.02
2/6/2015	4:00 PM	1.3	99.09
12/7/2015	4:40 PM	1.3	99.08
12/20/2012	10:15 AM	1.94[(a)]	99.13

Summary of discharge estimates used to develop the site rating curve for flows greater than 1.94 m^3/s. The methods used to calculate the estimates are described in detail in Section 2.4.1.2.

Q (m^3/s)	Stage (m)
1.94	99.18
2.37	99.23
2.83	99.28
3.31	99.33
3.41	99.34
3.82	99.38
4.34	99.43
4.89	99.48
5.46	99.53
6.05	99.58
6.65	99.63

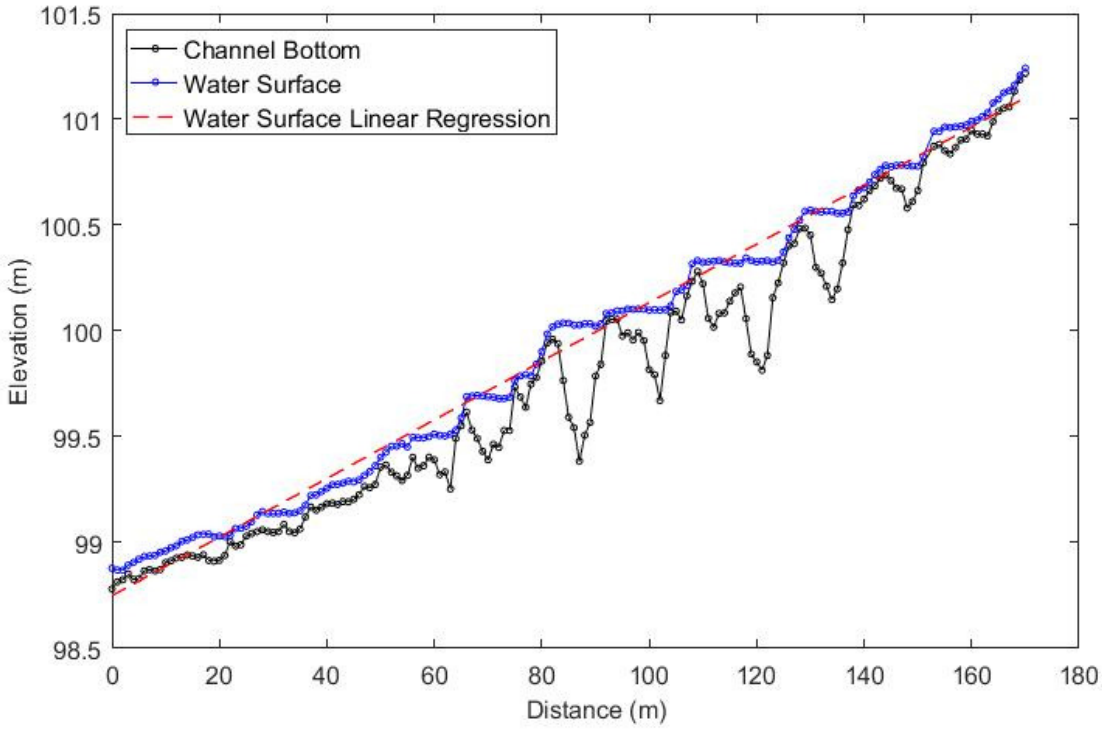

Longitudinal measurements of the channel bottom and the water surface elevation used to develop the channel slope. The red line is the linear regression of the water surface slope with the equation [Water Surface]=0.014[distance]+98.75 with an R^2 *= 0.99.*

6.3 Appendix C - Hydrodynamic Model Calibration

The hydrodynamic FaSTMECH models for the five flows ranging from 0.64-3.4 m^3/s were calibrated in order to provide the most accurate estimates of shear stress (τ). The model calibration procedure involves adjusting the drag coefficient (C_d) and lateral eddy viscosity (LEV), the two free, unmeasured model input parameters, in order to minimize the root mean square error (RMSE) between modeled and observed water surface elevations (WSE). Observations of WSE for flows ranging from 0.64-1.46 m^3/s were made from rebar staff gauge measurements distributed throughout the stream. Observations of WSE for bankfull discharge (Q_{bf}, 3.4 m^3/s) were based on field observations of bank-full stage, time lapse photography and analysis of cross-sectional geometry. The WSE observations were used to calibrate both C_d and the LEV.

Water surface elevation (WSE) measurements for flows ranging from 0.64-1.46 m^3/s. Measurements were taken from rebar staff gauges with the X and Y coordinates listed. All spatial measurements are relative to an arbitrary datum.

X (m)	Y (m)	Q=0.64 m^3/s	Q=0.99 m^3/s	Q=1.33 m^3/s	Q=1.46 m^3/s
		WSE (m)	*WSE (m)*	*WSE (m)*	*WSE (m)*
20004.309	20000.090	98.956	99.025	99.082	99.102
19994.121	20016.813	99.202	99.174	99.262	99.302
19983.279	20024.691	99.334	99.262	99.394	99.414
19973.864	20035.689	99.468	99.354	99.508	99.568
19965.016	20039.889	99.735	99.548	99.715	99.735
19959.869	20045.728	99.830	99.755	99.890	99.930
19959.466	20052.538	99.845	99.905	99.945	99.965
19959.941	20056.887	100.042	100.082	100.142	100.162
19964.386	20059.855	100.063	100.183	100.223	100.243
19967.224	20061.975	100.130	100.210	100.230	100.250
19969.929	20057.546	100.188	100.208	100.248	100.268
19974.617	20059.172	100.247	100.267	100.367	100.367
19981.244	20069.805	100.378	100.418	100.418	100.458
19980.657	20074.181	100.431	100.481	100.491	100.511
19988.490	20076.249	100.534	100.491	100.614	100.654
19986.375	20088.225	100.633	100.554	100.713	100.733
19993.643	20096.033	100.843	100.653	100.943	100.973
19993.525	20102.940	100.927	101.007	101.007	101.007
19987.007	20103.458	100.965	101.025	101.005	101.065

Water surface elevation (WSE) measurements for bankfull discharge (Q_{bf}, 3.4 m^3/s). Measurements were made using field observations of bankfull stage, time-lapse photography and analysis of cross-sectional geometry at locations with the X and Y coordinates listed. All spatial measurements are relative to an arbitrary datum.

X (m)	Y (m)	WSE (m)
20004.309	20000.090	99.343
19995.587	20009.105	99.514
19994.121	20016.813	99.602
19975.034	20035.124	99.850
19959.466	20052.538	100.285
19968.000	20054.600	100.451
19964.400	20062.300	100.496
19969.929	20057.546	100.488
19973.100	20058.500	100.564
19976.800	20067.800	100.682
19981.244	20069.805	100.718
19985.300	20066.900	100.736

A three-step procedure was used to calibrate each model run in order to optimize both the Cd and the LEV. This procedure involved first calibrating C_d with a 1-D approximation of the LEV. The 1-D approximation of LEV was calculated as the depth slope product and the average cross-sectional depth and velocity (from continuity) for each flow level calculated using observed WSE [*Legleiter et al.*, 2011a; *Nelson*, 2015].

Once the C_d was optimized to reduce the RMSE, it was used to then calibrate the model for the LEV. After an optimal LEV was chosen, the model was then re-calibrated for C_d. The re-calibration of C_d was only necessary for Q_{bf} as the initial approximation of the LEV resulted in the minimum RMSE in all other instances.

$$LEV = 0.01 * average\ depth * average\ velocity$$

Values of drag coefficient (Cd) and lateral eddy viscosity (LEV) used to calibrate the FaSTMECH models for flows ranging from 0.64-3.41 m^3/s. The calibration was conducted by iterating values of C_d and LEV to minimize the root mean square error (RMSE) between observed and modeled water surface elevations. Grey highlighted cells indicate selected value.

Q=0.64 m^3/s					
Cd -1 (LEV = 0.0016)		***LEV - 1 (Cd = 0.038)***		***Cd-2***	
Cd	*RMSE*	*LEV*	*RMSE*	*Cd*	*RMSE*
0.015	0.041	0.002	0.026	--	--
0.025	0.032	0.005	0.026	--	--
0.035	0.026	0.050	0.029	--	--
0.045	0.027	0.001	0.026	--	--
0.055	0.032	0.003	0.026	--	--
0.040	0.026	0.002	0.026	--	--
0.038	0.026			--	--
0.039	0.026			--	--
Q=0.99 m^3/s					
Cd -1 (LEV = 0.0024)		***LEV - 1 (Cd = 0.028)***		***Cd-2***	
Cd	*RMSE*	*LEV*	*RMSE*	*Cd*	*RMSE*
0.015	0.043	0.002	0.030	--	--
0.020	0.037	0.005	0.030	--	--
0.030	0.030	0.050	0.036	--	--
0.040	0.036	0.001	0.030	--	--
0.025	0.031	0.003	0.030	--	--
0.035	0.032	0.002	0.030	--	--
0.032	0.031			--	--
0.027	0.030			--	--
0.028	0.030			--	--
0.029	0.030			--	--

Q=1.33 m^3/s					
Cd -1 (LEV = 0.0032)		***LEV - 1 (Cd = 0.015)***		***Cd-2***	
Cd	*RMSE*	*LEV*	*RMSE*	*Cd*	*RMSE*
0.015	0.025	0.003	0.025	--	--
0.025	0.039	0.005	0.028	--	--
0.020	0.029	0.050	0.035	--	--
0.010	0.030	0.001	0.027	--	--
0.018	0.028	0.002	0.026	--	--
0.017	0.027	0.004	0.027	--	--
0.016	0.026			--	--
0.014	0.030			--	--
Q=1.46 m^3/s					
Cd -1 (LEV = 0.0034)		***LEV - 1 (Cd = 0.017)***		***Cd-2***	
Cd	*RMSE*	*LEV*	*RMSE*	*Cd*	*RMSE*
0.025	0.030	0.003	0.022	--	--
0.015	0.027	0.005	0.024	--	--
0.035	0.047	0.050	0.031	--	--
0.020	0.025	0.010	0.025	--	--
0.030	0.037	0.001	0.023	--	--
0.018	0.024	0.001	0.024	--	--
0.016	0.026	0.002	0.025	--	--
0.022		0.004	0.023	--	--
0.017	0.022			--	--
Q=3.4 m^3/s					
Cd -1 (LEV = 0.005)		***LEV - 1 (Cd = 0.035)***		***Cd-2 (LEV = 0.001)***	
Cd	*RMSE*	*LEV*	*RMSE*	*Cd*	*RMSE*
0.018	0.070	0.005	0.034	0.020	0.063
0.020	0.063	0.050	0.043	0.025	0.050
0.025	0.042	0.010	0.035	0.030	0.040
0.030	0.035	0.001	0.033	0.035	0.034
0.035	0.034	0.001	0.034	0.040	0.039
0.040	0.040	0.000	0.035	0.050	0.057

The objective calibration procedure described above resulted in an inconsistent relationship between τ and Q for flows ranging from 0.99-1.46 m^3/s. The C_d for these flows was adjusted in order to establish a linear relationship between Q and τ for all modeled flows. The selected C_d and resulting mean τ can be found above in Sections 2.4.1.3 and 3.3.2

Initial FaSTMECH model calibration results using the objective calibration procedure for flows (Q) ranging from 0.64-3.4 m^3/s. The calibration was conducted by iterating values of drag coefficient (C_d) and lateral eddy viscosity (LEV) to minimize the root mean square error (RMSE) between observed and modeled water surface elevations. Values of mean shear stress (τ) calculated using these model parameters did not result in a consistent relationship with Q.

Q (m^3/s)	C_d	LEV	LEV calc	RMSE (m)	τ mean (N/m^2)
0.64	0.038	0.0016	0.0016	0.026	23.1
0.99	0.028	0.0024	0.0024	0.03	26.02
1.33	0.015	0.0032	0.0032	0.025	23.55
1.46	0.017	0.0034	0.0034	0.025	26.16
3.4	0.035	0.001	0.0062	0.031	51.12

6.4 Appendix D - Spring Algae Sample Methods and Data Summary

Measurements of benthic algal Chlorophyll-*a* (Chl-*a*) were taken between 2/19/2015-5/22/2015 within 9 patches of contrasting disturbance throughout the study site. Three sediment particles were removed from each patch and combined into one sample. To collect the sample, a cap was used to cover a known area on each sediment particle. The area outside of the cap was brushed vigorously with a nylon brush and rinsed with stream water to remove all algae. The cap was then removed and the area under it was brushed to remove all benthic algae and rinsed into a container with stream water. The procedure was repeated for the remaining 2 sediment particles and the composite sample was collected into a 250 mL bottle. The bottle was topped off to 250 mL with stream water. The samples were kept cold prior to transport to the laboratory. In the laboratory, the samples were filtered in the dark and collected onto 0.7 μm glass fiber filters. The filters were stored in centrifuge tubes at -20°C for 18 days prior to extraction using sonication and hot 95% ethanol. Chl-*a* concentrations of the extractant were measured using a spectrophotometer. Chl-*a* concentrations were calculated using the following equation:

$$Chl\ a = 28.78\left((A665_b - A750_b) - (A665_a - A750_a)\right) * (\frac{v}{A} * L)$$

Where A665 is the absorption at 665 nm, A750 is the absorption at 75 nm and the subscripts a and b refer to before and after addition of 0.1mL of 0.1 N HCl respectively. V is the volume of extractant used (in liters), A is the area of benthos sampled in m^2 and L is the path length of the cuvette used in the spectrophotometer.

Results of the Chl-*a* analysis can be found below in addition to the average shear stress (τ) values for each patch. These estimates were made for a Q = 0.87 m^3/s flow which was the peak of a high flow event that occurred on 3/19/15 during the study period.

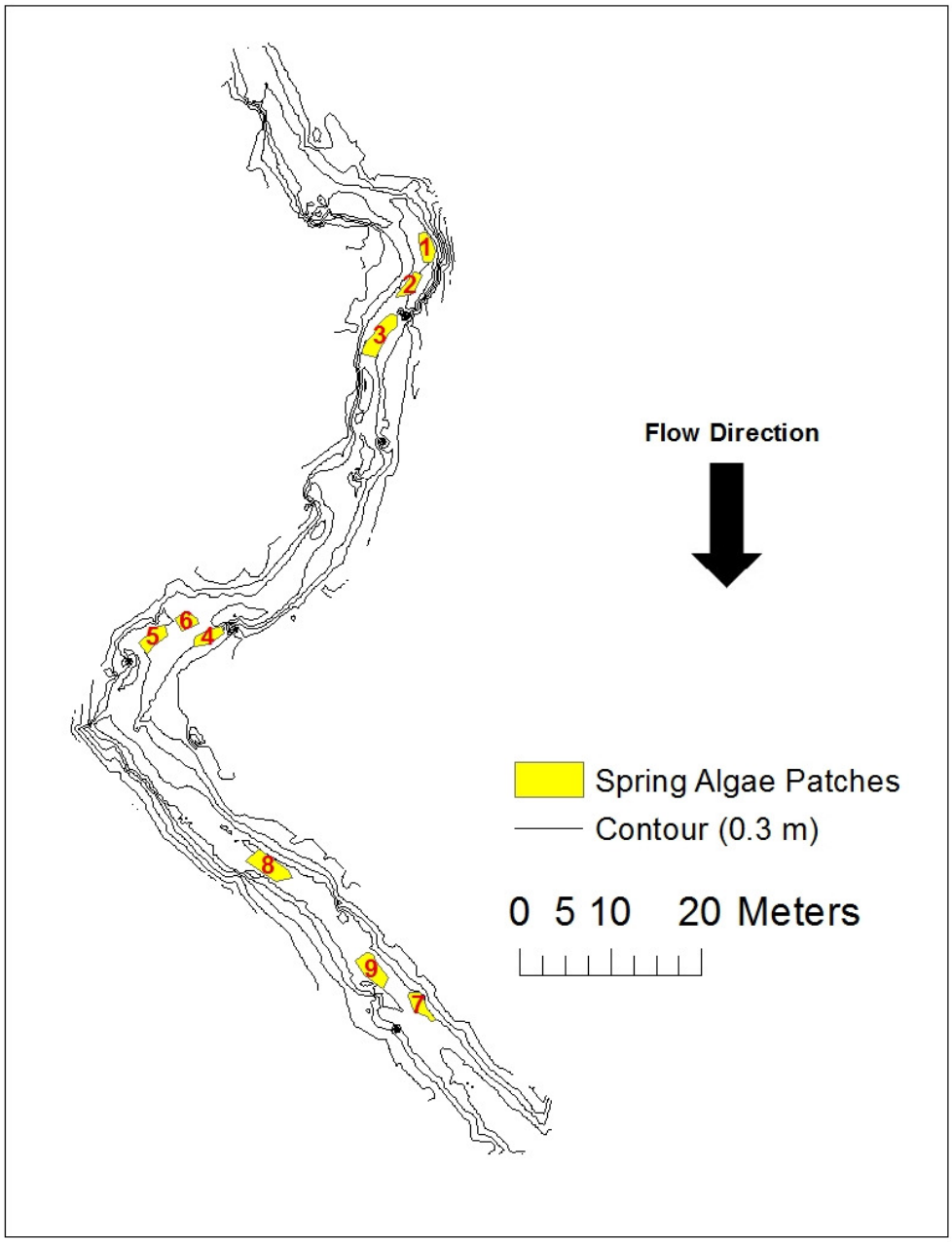

Location of stream bed patches used to sample benthic Chlorophyll-a during the Spring of 2015.

Summary of Chlorophyll-a (Chl-a) samples collected within 9 stream bed patches on 6 sampling dates between 2/19/15-5/22/15. A composite of samples from three sediment particles were analyzed for each patch.

Patch # / Date	**Chl-a (mg/m^2)**								
	1	***2***	***3***	***4***	***5***	***6***	***7***	***8***	***9***
2/19/2015	3.99	8.52	8.01	4.50	6.51	6.51	8.52	5.50	7.01
3/5/2015	29.71	43.31	20.33	47.54	24.55	49.88	14.70	34.87	82.25
3/30/2015	11.11	33.31	107.87	12.37	11.53	29.96	8.18	60.96	20.74
4/17/2015	11.53	21.58	26.19	9.85	19.22	16.14	9.85	27.44	30.80
5/4/2015	16.55	17.39	26.19	24.93	27.44	19.91	30.80	33.73	32.47
5/22/2015	44.26	14.94	18.29	34.20	14.10	18.29	10.75	19.12	12.42

Average shear stress values for each patch estimated for a 0.87 m^3/s flow event.

Patch #	**Shear Stress (N/m^2)**
1	38.20
2	10.70
3	48.24
4	8.64
5	33.94
6	45.04
7	13.10
8	29.59
9	33.65

6.5 Appendix E – Chlorophyll-*a* Maps

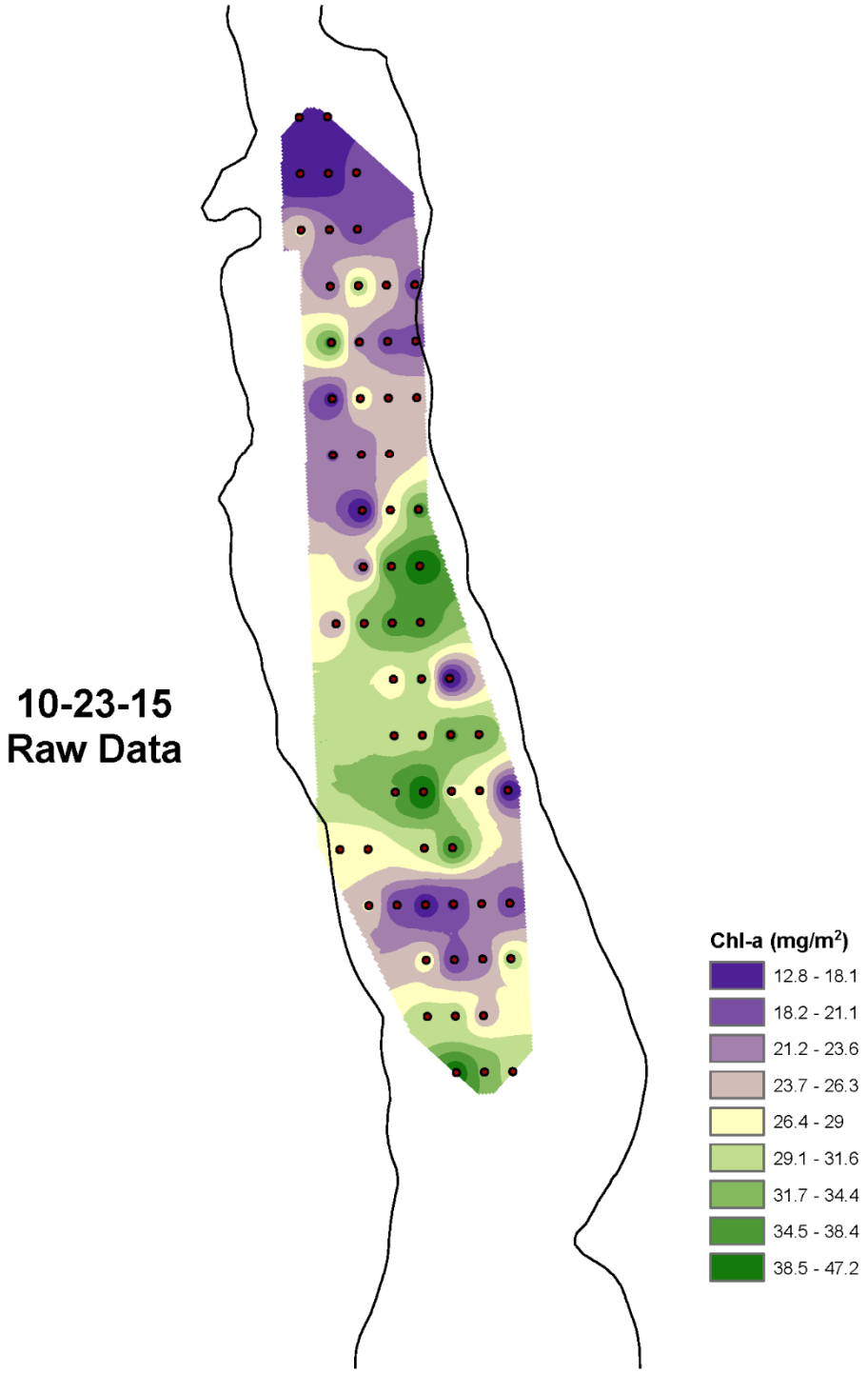

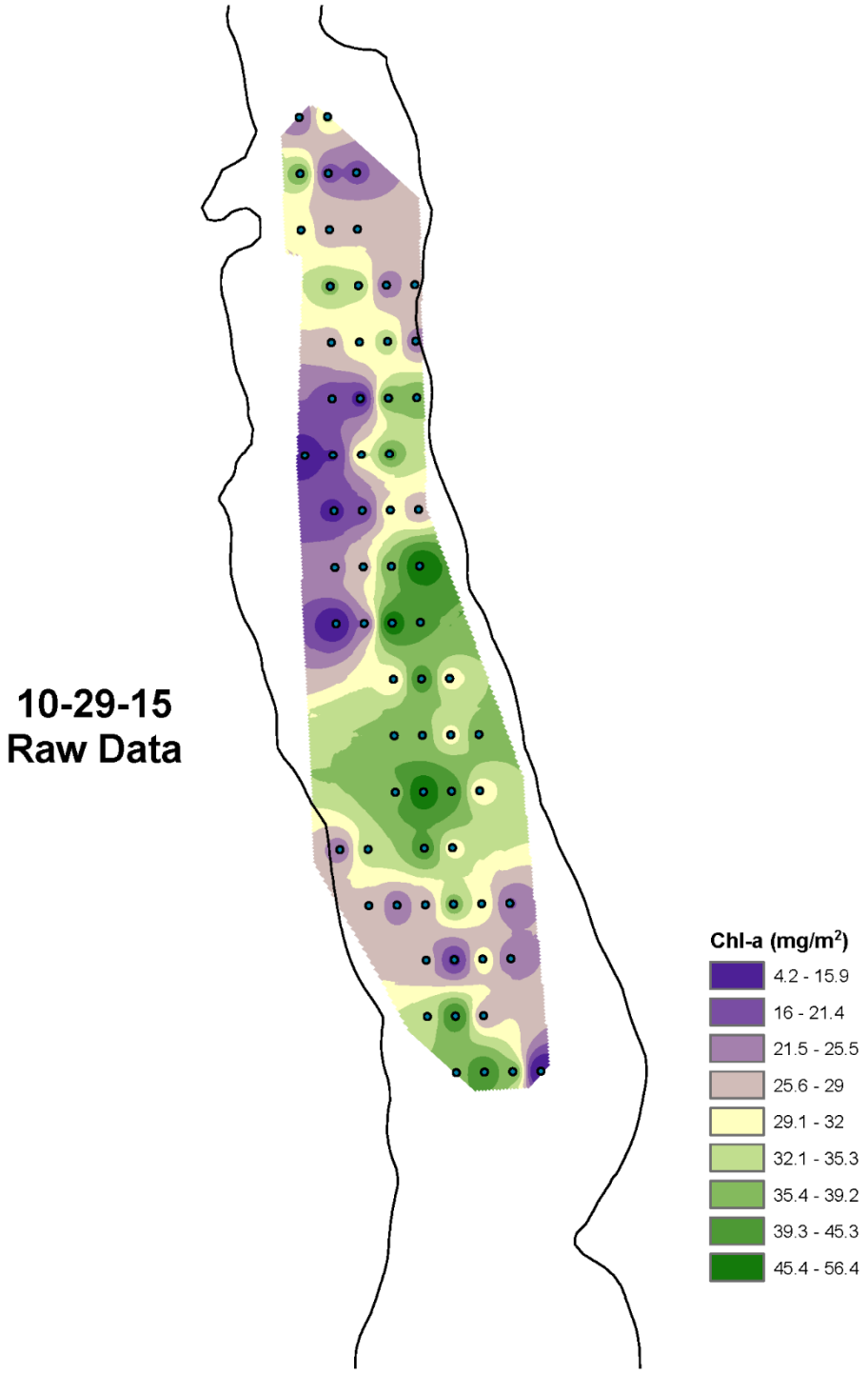
10-29-15
Raw Data
Chl-a (mg/m²)
4.2 - 15.9
16 - 21.4
21.5 - 25.5
25.6 - 29
29.1 - 32
32.1 - 35.3
35.4 - 39.2
39.3 - 45.3
45.4 - 56.4

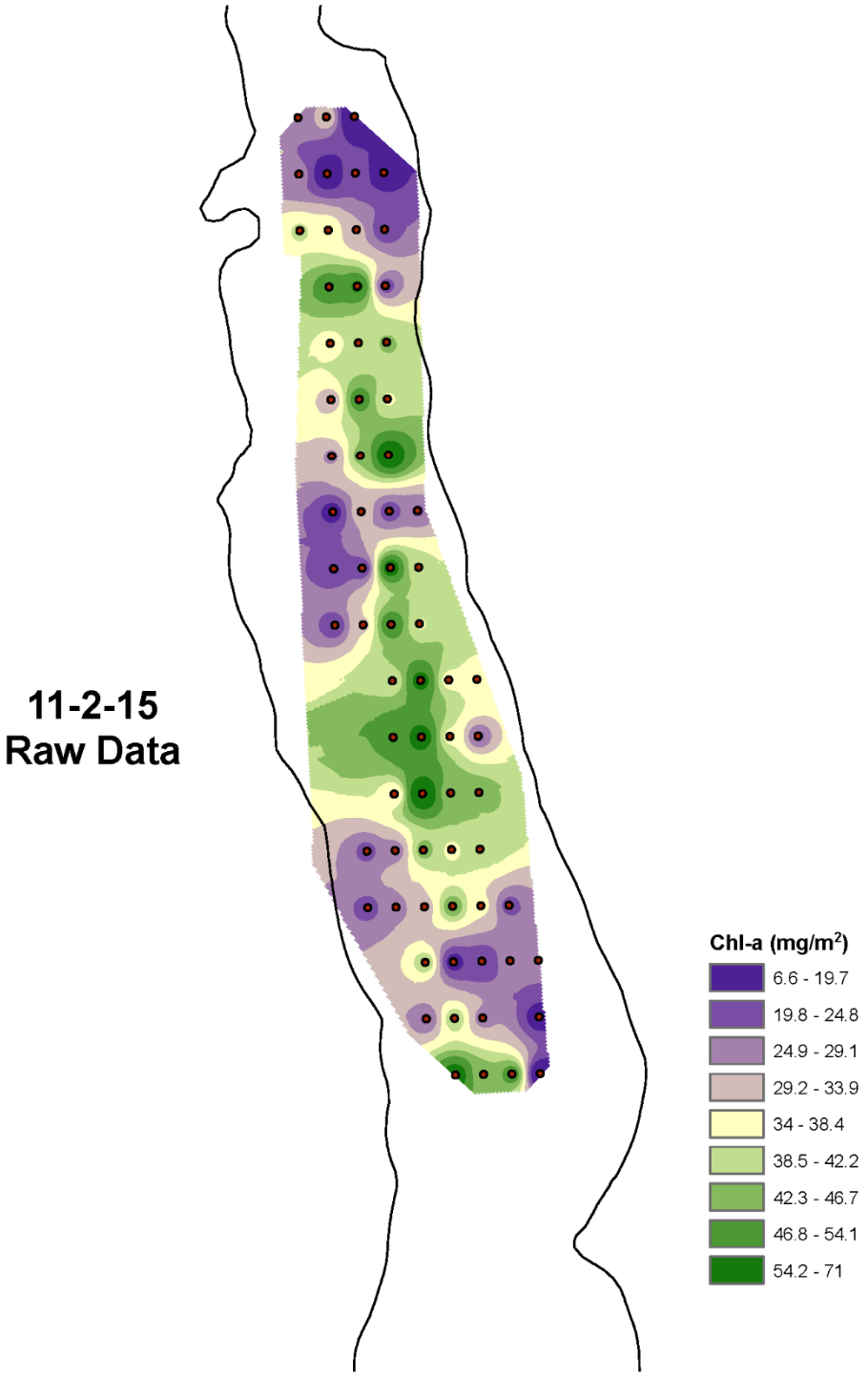
11-2-15
Raw Data
Chl-a (mg/m²)
6.6 - 19.7
19.8 - 24.8
24.9 - 29.1
29.2 - 33.9
34 - 38.4
38.5 - 42.2
42.3 - 46.7
46.8 - 54.1
54.2 - 71

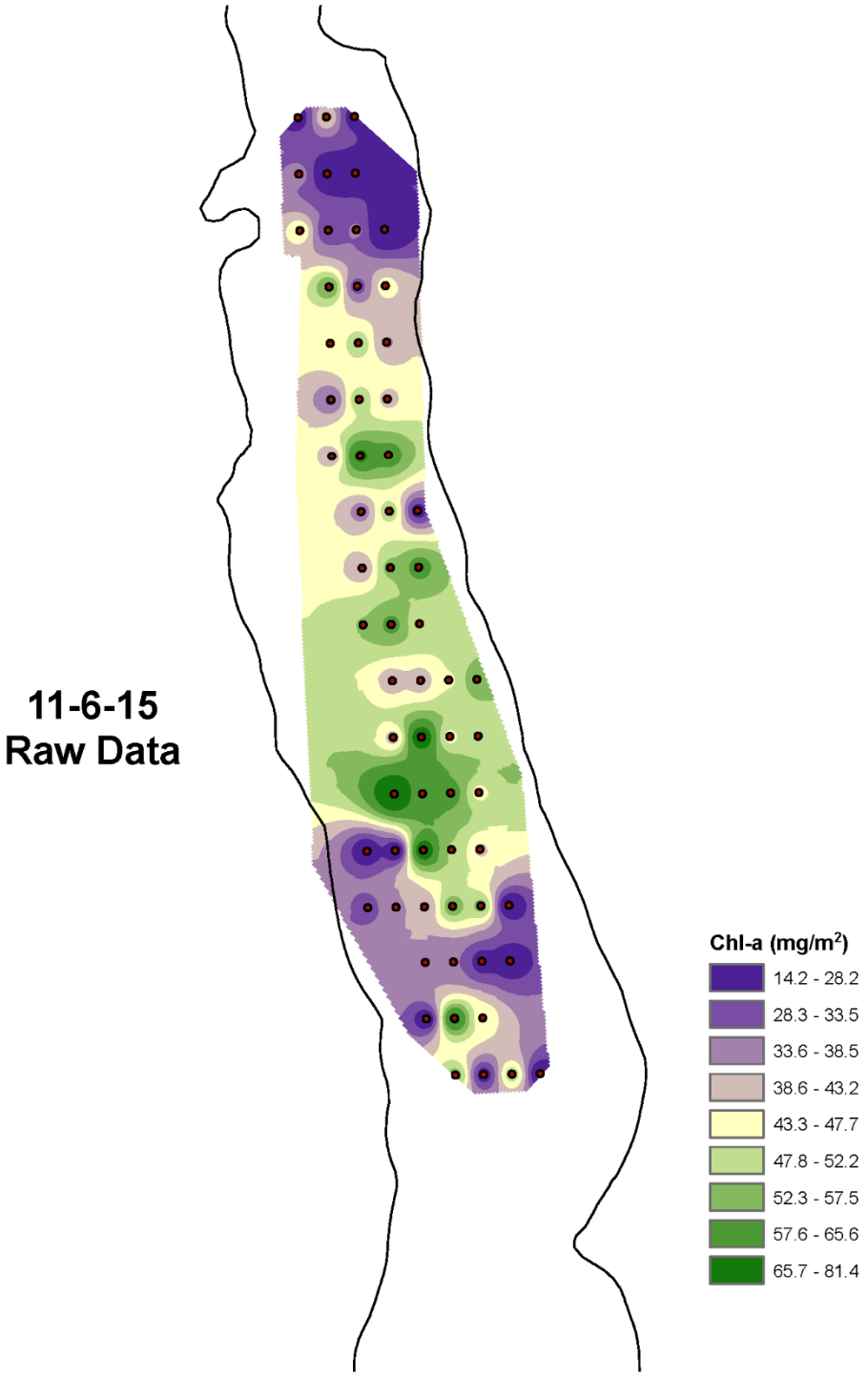
11-6-15
Raw Data
Chl-a (mg/m²)
14.2 - 28.2
28.3 - 33.5
33.6 - 38.5
38.6 - 43.2
43.3 - 47.7
47.8 - 52.2
52.3 - 57.5
57.6 - 65.6
65.7 - 81.4

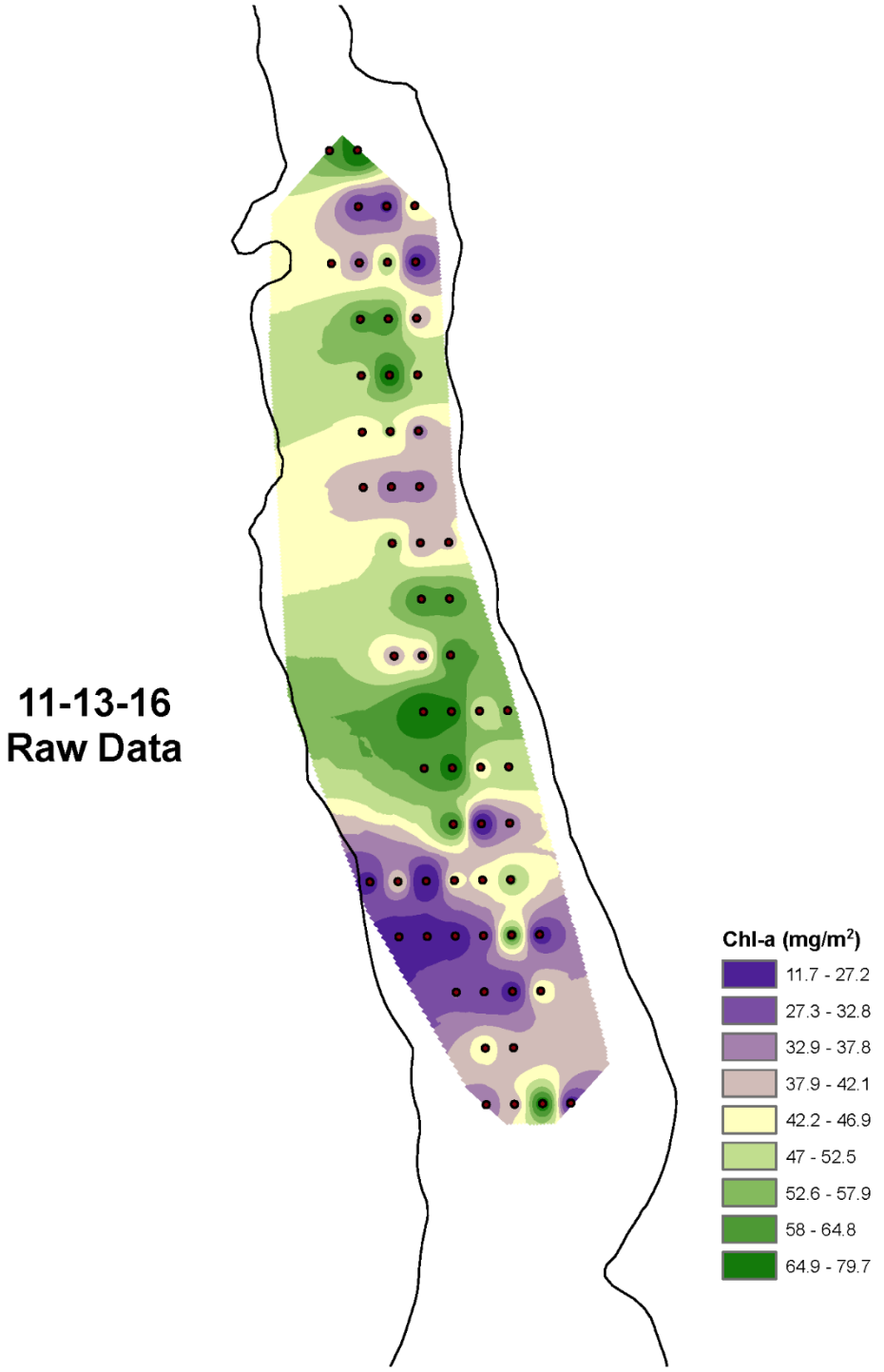
11-13-16
Raw Data
Chl-a (mg/m²)
11.7 - 27.2
27.3 - 32.8
32.9 - 37.8
37.9 - 42.1
42.2 - 46.9
47 - 52.5
52.6 - 57.9
58 - 64.8
64.9 - 79.7

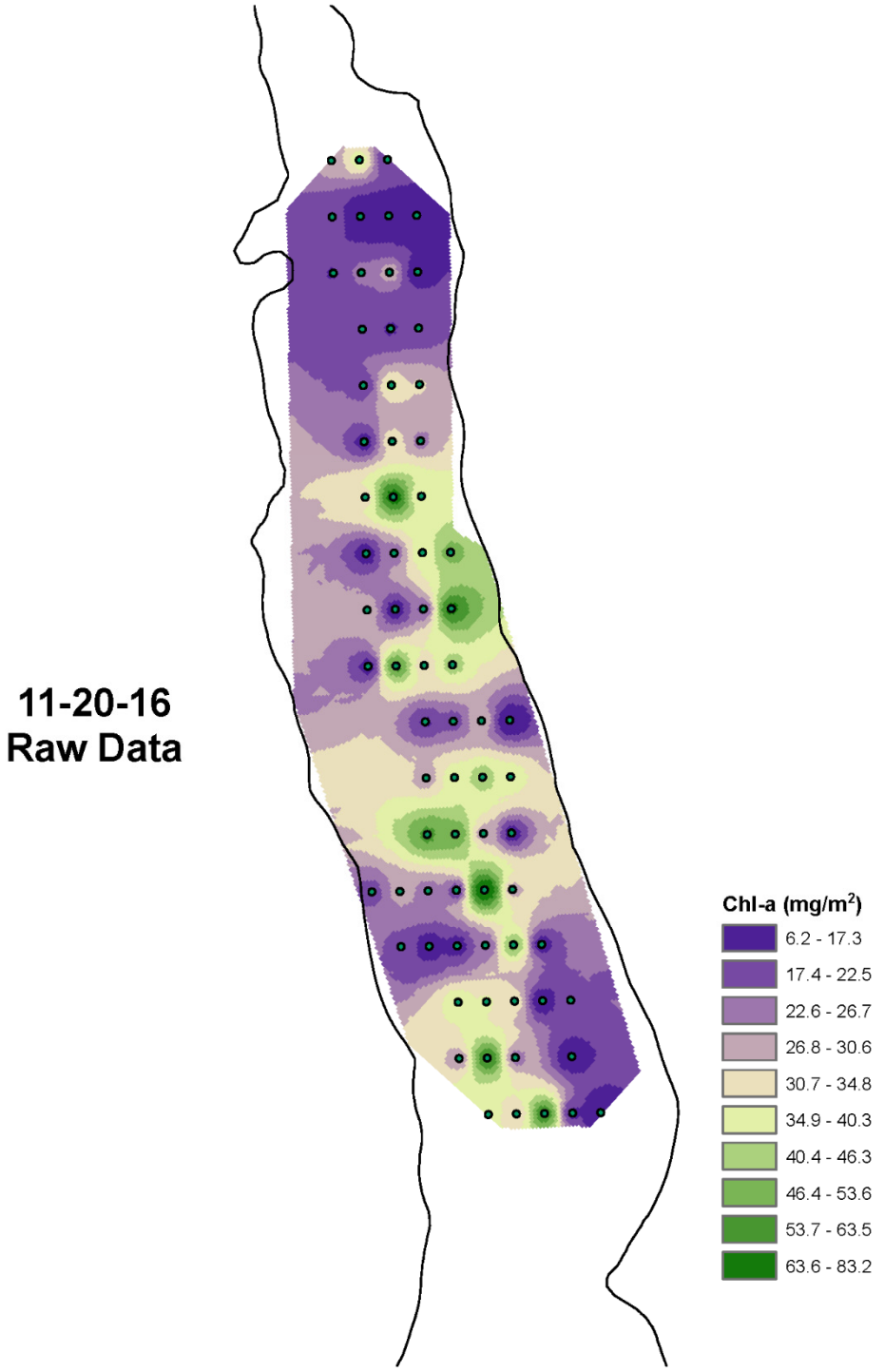
11-20-16
Raw Data
Chl-a (mg/m2)
6.2 - 17.3
17.4 - 22.5
22.6 - 26.7
26.8 - 30.6
30.7 - 34.8
34.9 - 40.3
40.4 - 46.3
46.4 - 53.6
53.7 - 63.5
63.6 - 83.2

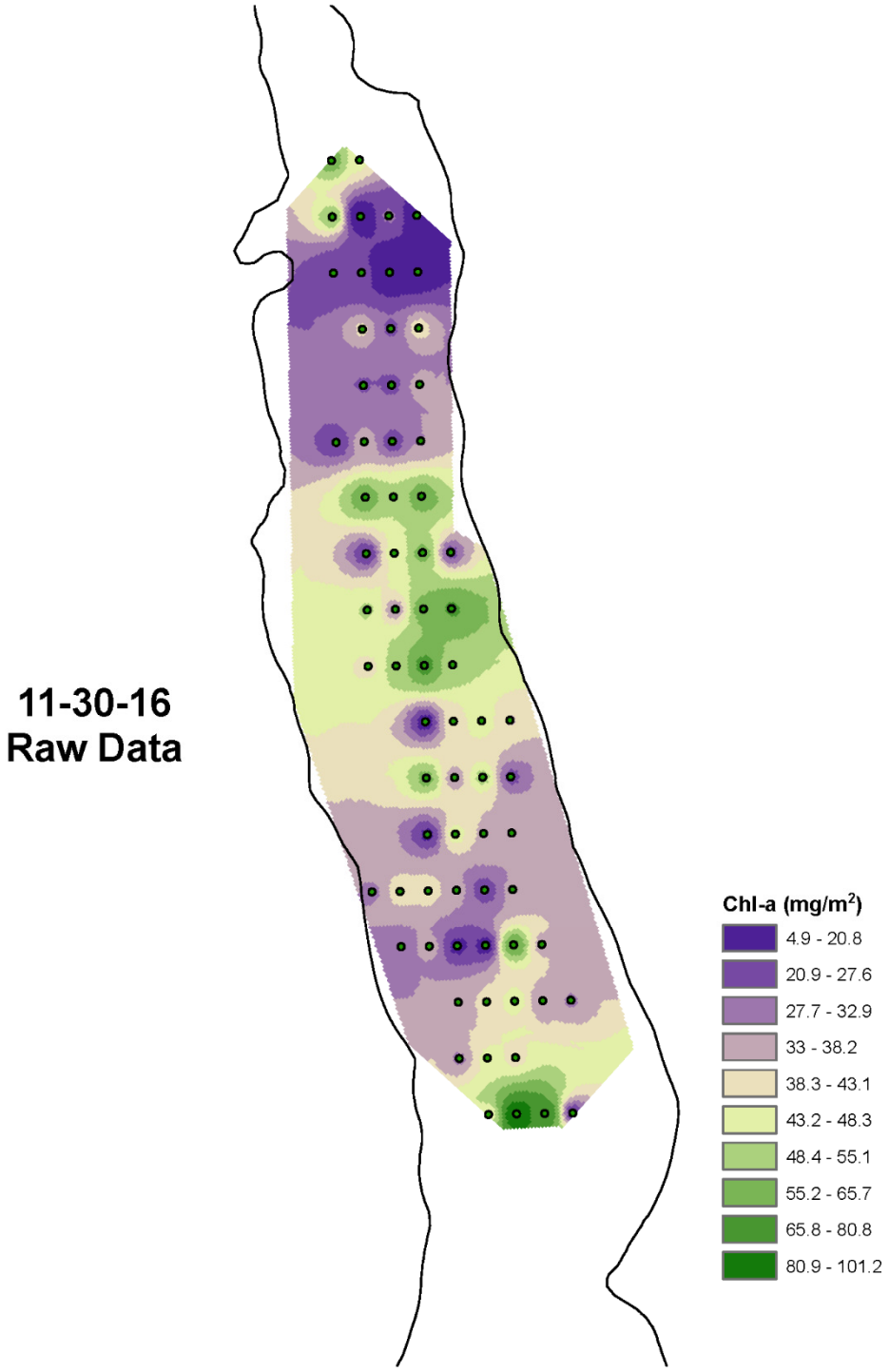
11-30-16
Raw Data
Chl-a (mg/m2)
4.9 - 20.8
20.9 - 27.6
27.7 - 32.9
33 - 38.2
38.3 - 43.1
43.2 - 48.3
48.4 - 55.1
55.2 - 65.7
65.8 - 80.8
80.9 - 101.2

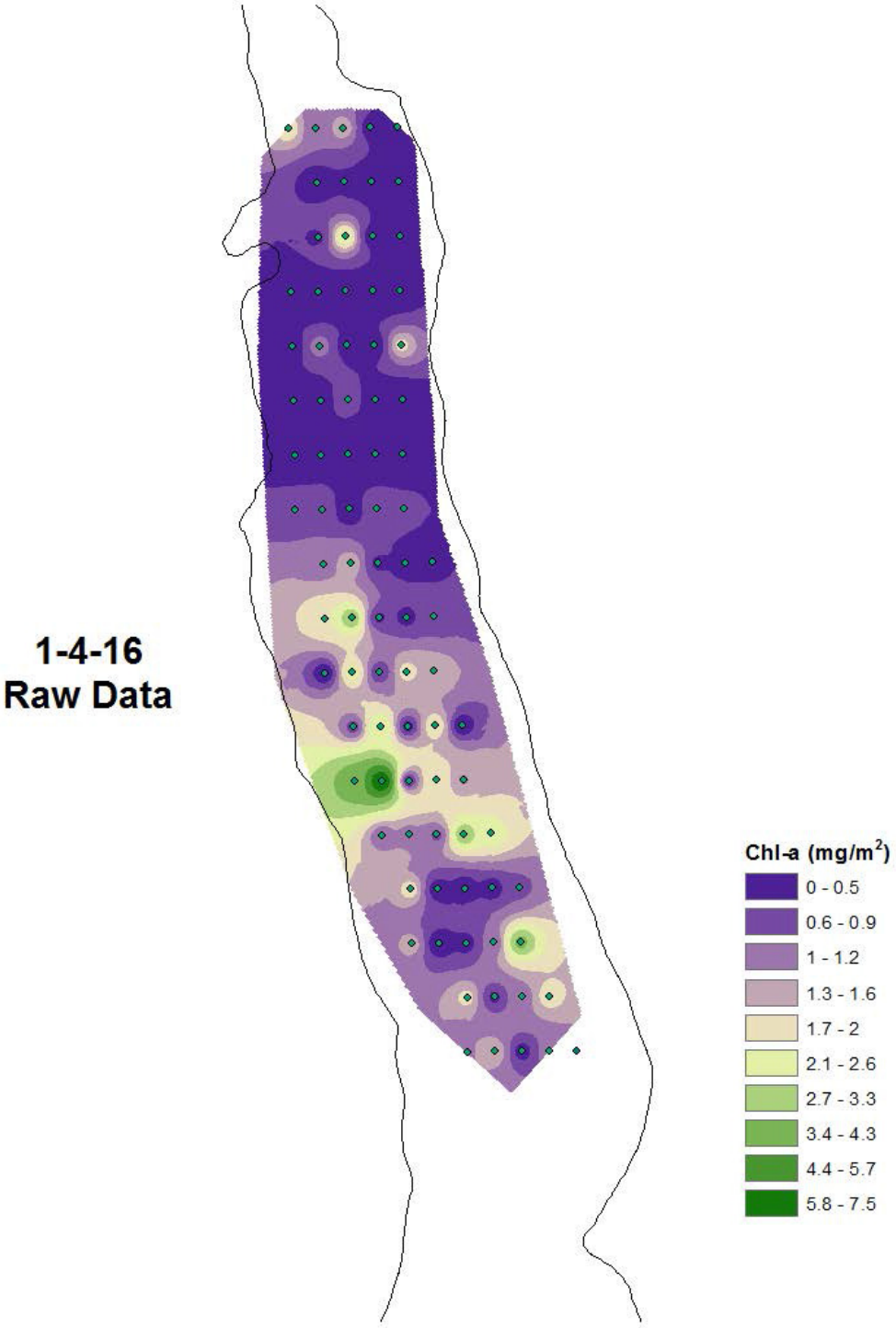
1-4-16
Raw Data
Chl-a (mg/m2)
0 - 0.5
0.6 - 0.9
1 - 1.2
1.3 - 1.6
1.7 - 2
2.1 - 2.6
2.7 - 3.3
3.4 - 4.3
4.4 - 5.7
5.8 - 7.5

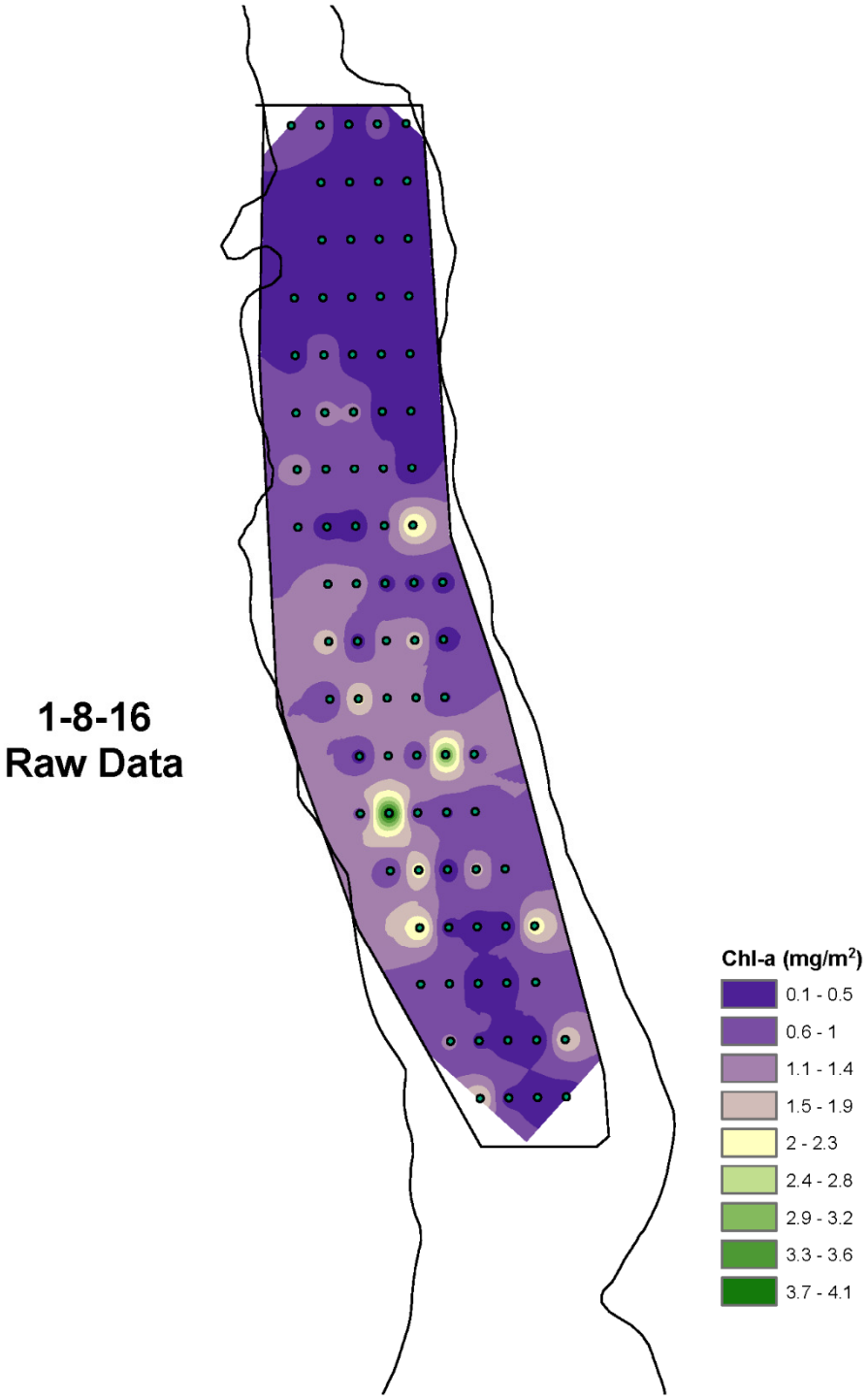
1-8-16
Raw Data
Chl-a (mg/m²)
0.1 - 0.5
0.6 - 1
1.1 - 1.4
1.5 - 1.9
2 - 2.3
2.4 - 2.8
2.9 - 3.2
3.3 - 3.6
3.7 - 4.1

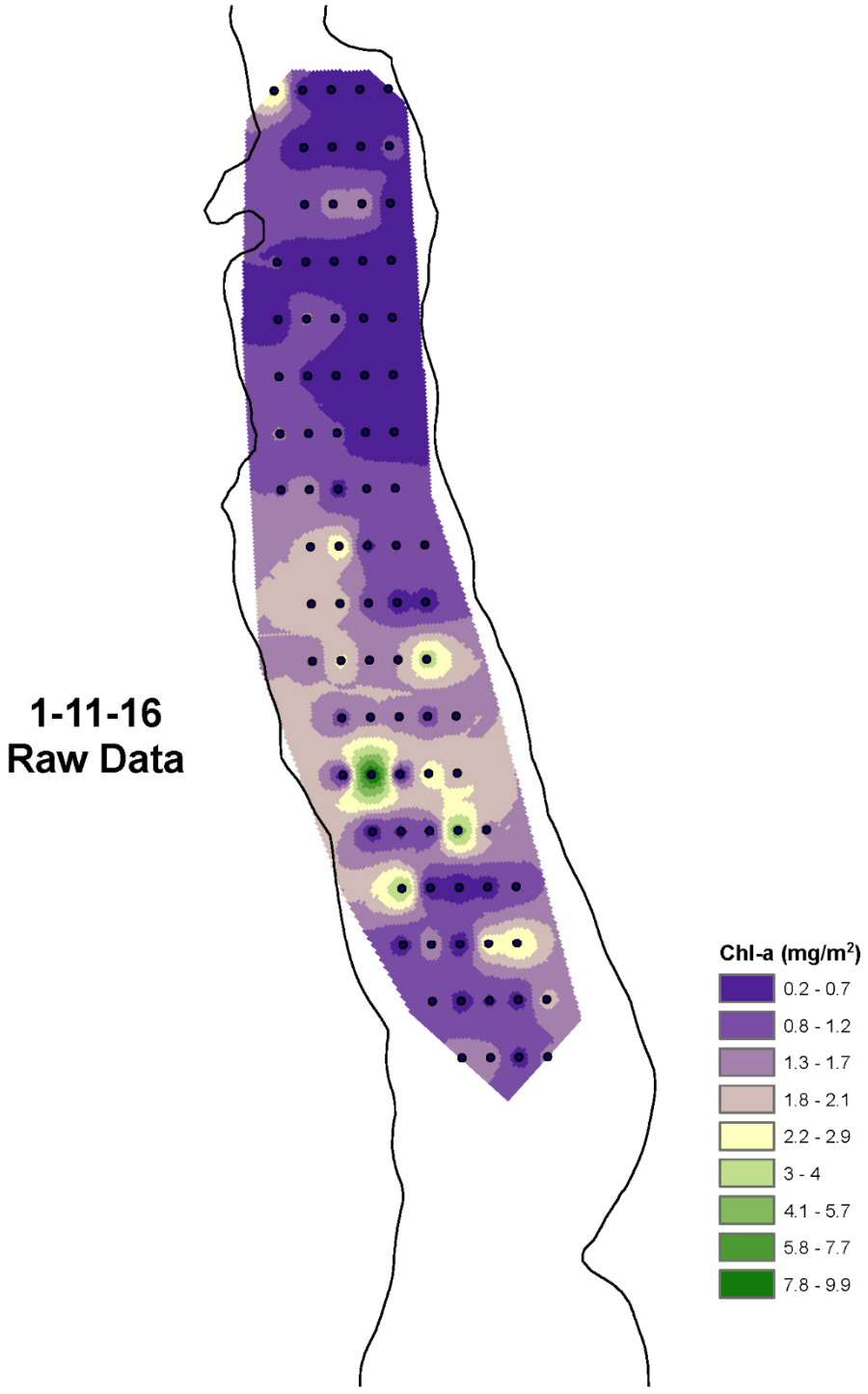
1-11-16
Raw Data
Chl-a (mg/m²)
0.2 - 0.7
0.8 - 1.2
1.3 - 1.7
1.8 - 2.1
2.2 - 2.9
3 - 4
4.1 - 5.7
5.8 - 7.7
7.8 - 9.9

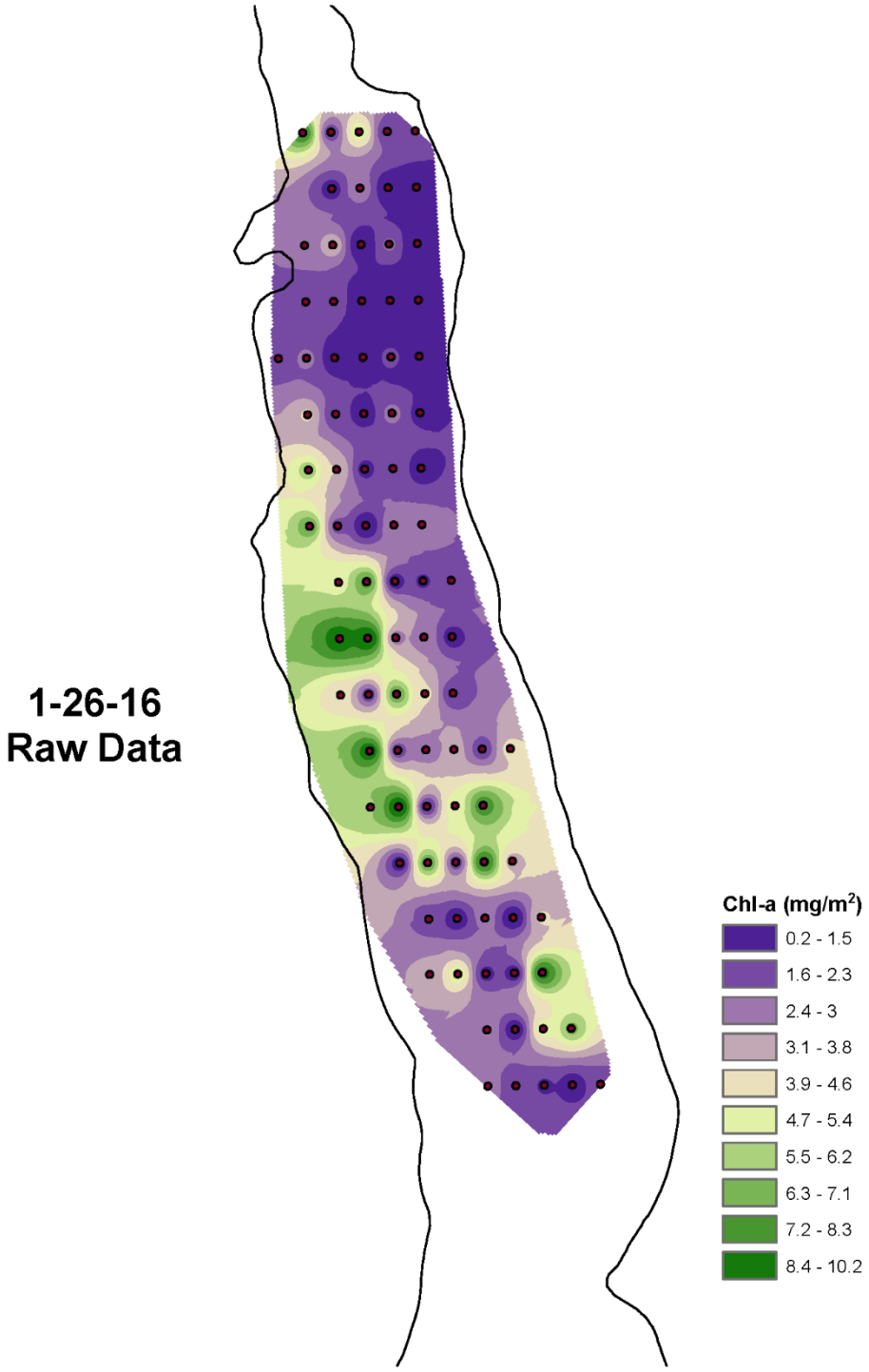
1-26-16
Raw Data
Chl-a (mg/m2)
0.2 - 1.5
1.6 - 2.3
2.4 - 3
3.1 - 3.8
3.9 - 4.6
4.7 - 5.4
5.5 - 6.2
6.3 - 7.1
7.2 - 8.3
8.4 - 10.2

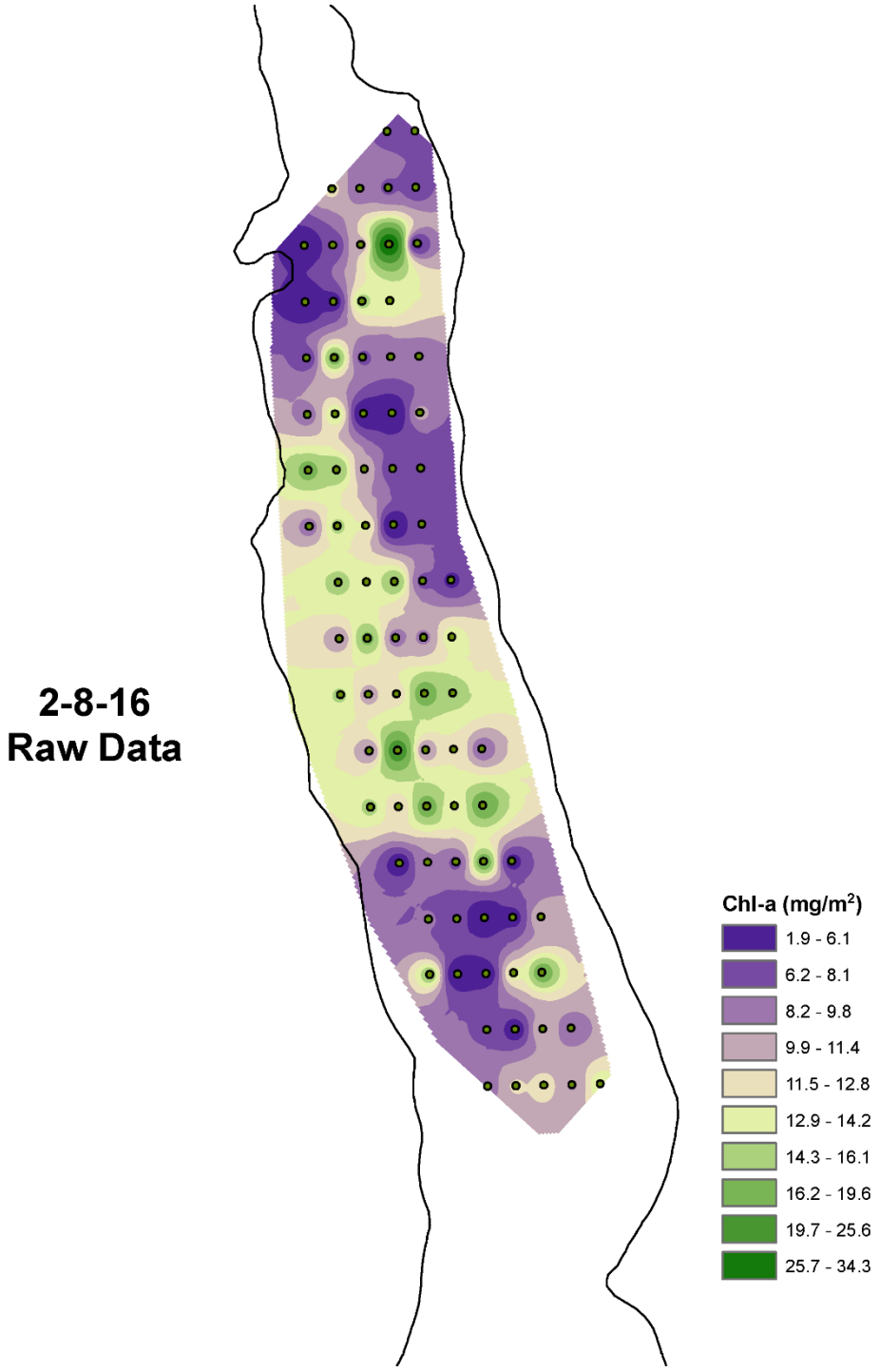
2-8-16
Raw Data
Chl-a (mg/m²)
1.9 - 6.1
6.2 - 8.1
8.2 - 9.8
9.9 - 11.4
11.5 - 12.8
12.9 - 14.2
14.3 - 16.1
16.2 - 19.6
19.7 - 25.6
25.7 - 34.3

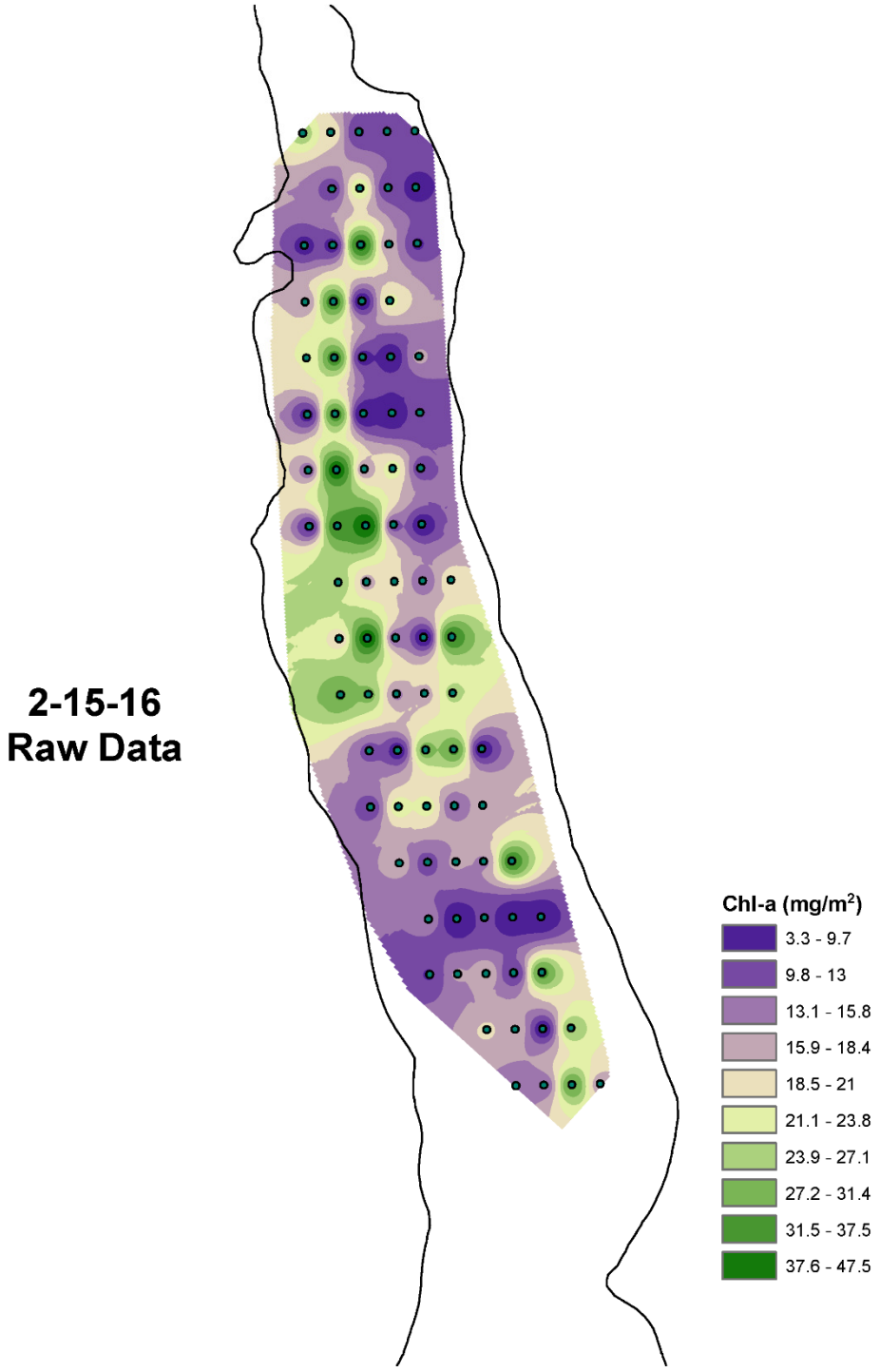
2-15-16
Raw Data
Chl-a (mg/m²)
3.3 - 9.7
9.8 - 13
13.1 - 15.8
15.9 - 18.4
18.5 - 21
21.1 - 23.8
23.9 - 27.1
27.2 - 31.4
31.5 - 37.5
37.6 - 47.5

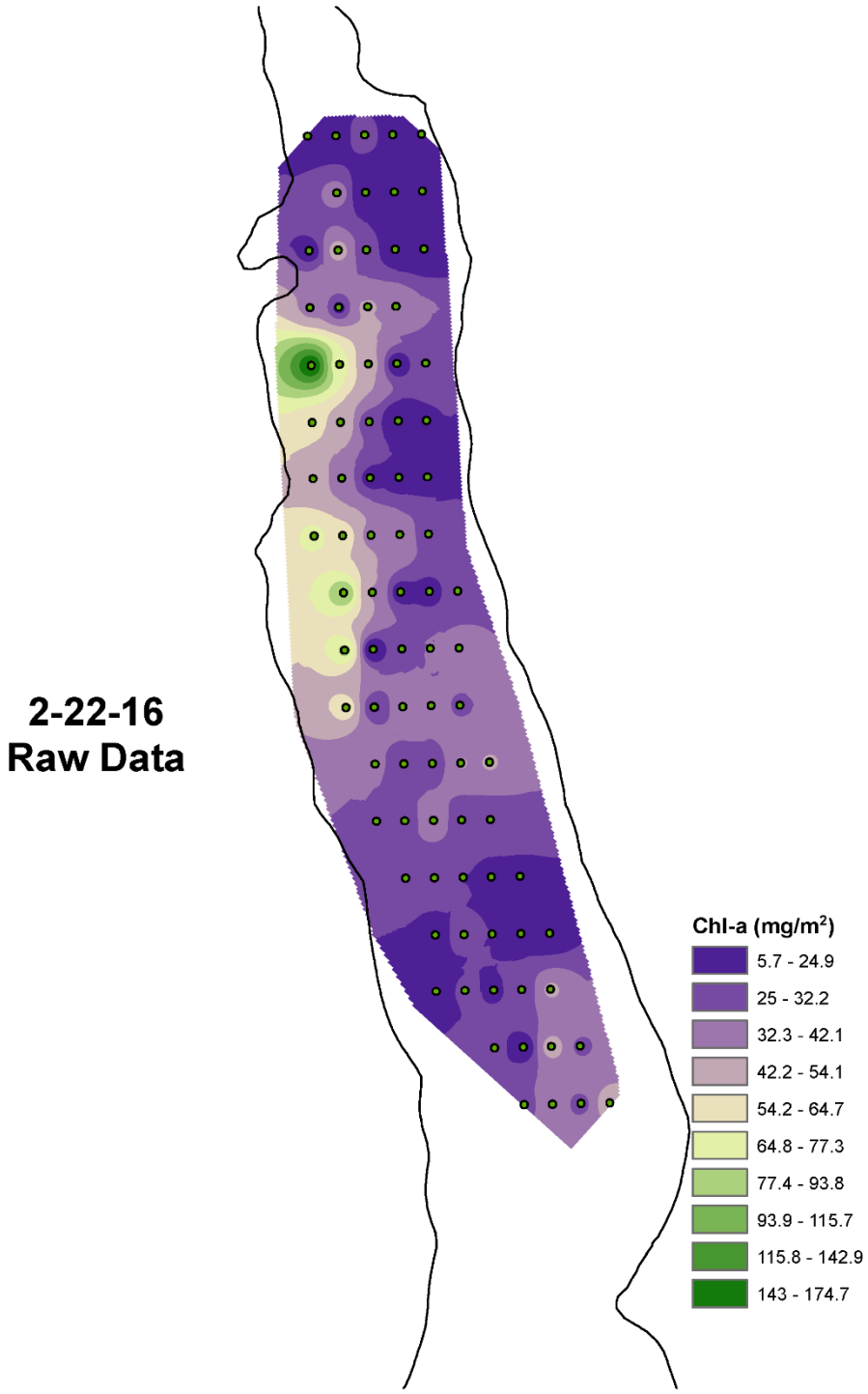
2-22-16
Raw Data
Chl-a (mg/m²)
5.7 - 24.9
25 - 32.2
32.3 - 42.1
42.2 - 54.1
54.2 - 64.7
64.8 - 77.3
77.4 - 93.8
93.9 - 115.7
115.8 - 142.9
143 - 174.7

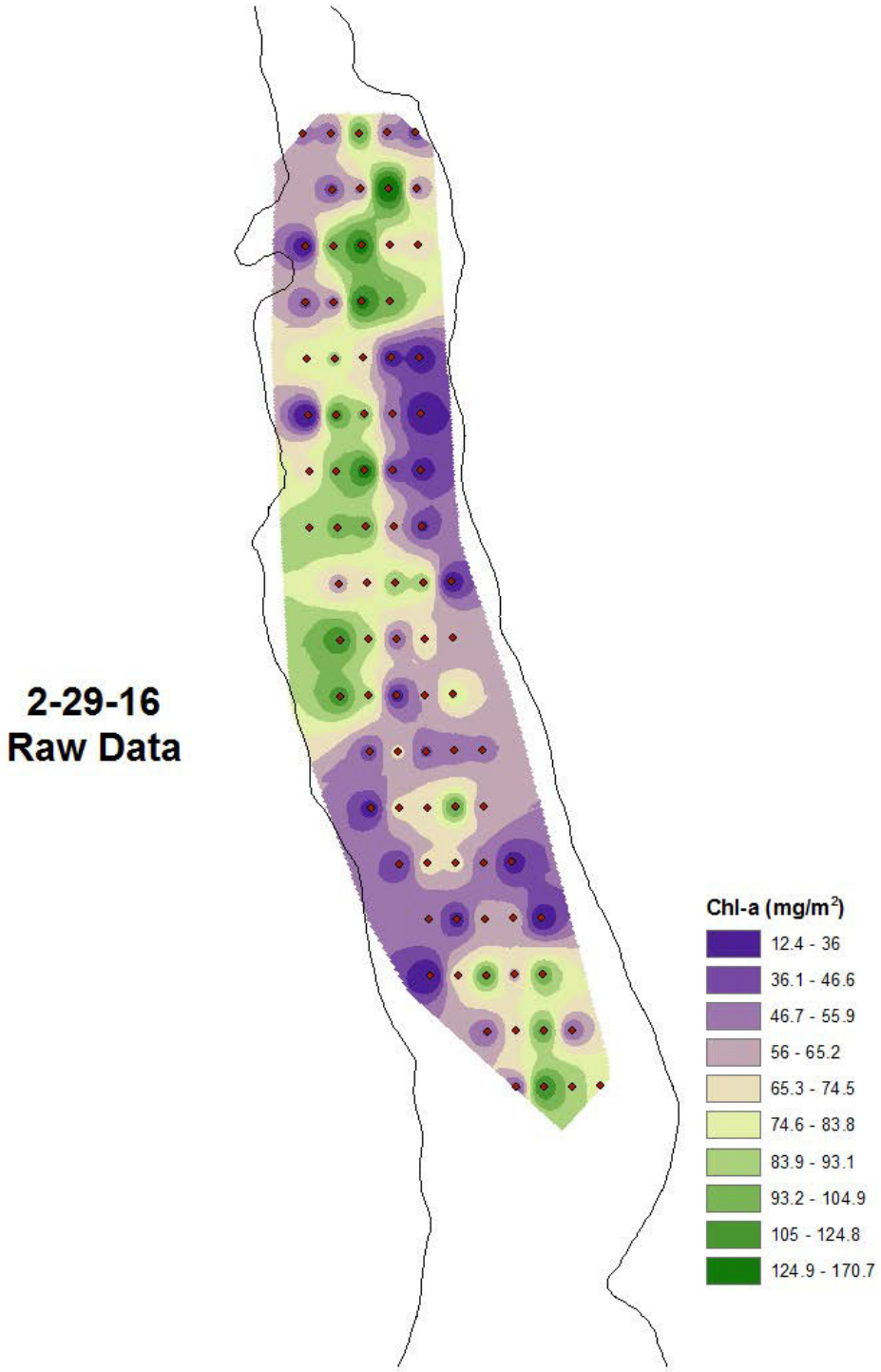
2-29-16
Raw Data
Chl-a (mg/m²)
12.4 - 36
36.1 - 46.6
46.7 - 55.9
56 - 65.2
65.3 - 74.5
74.6 - 83.8
83.9 - 93.1
93.2 - 104.9
105 - 124.8
124.9 - 170.7

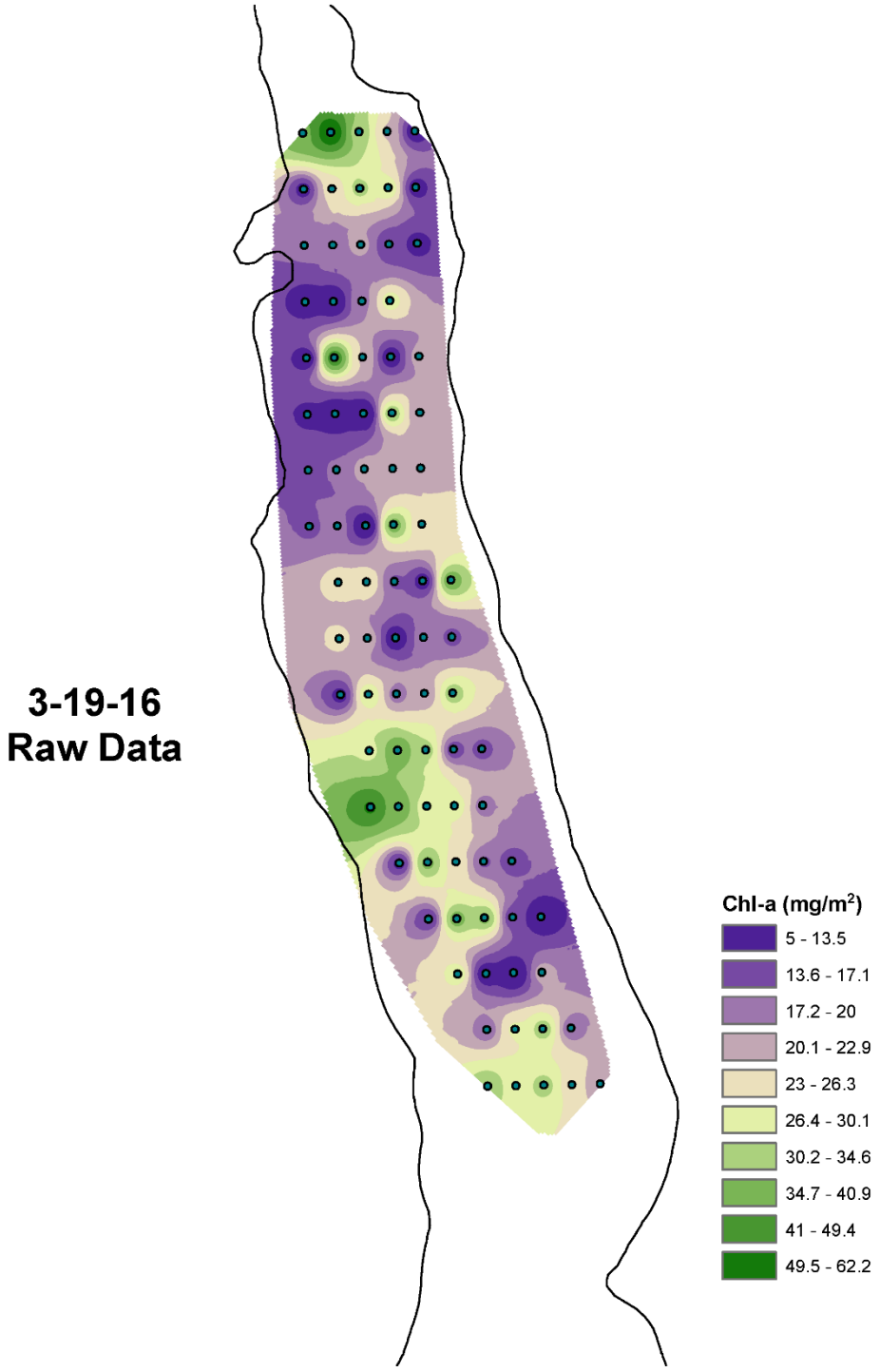
3-19-16
Raw Data
Chl-a (mg/m²)
5 - 13.5
13.6 - 17.1
17.2 - 20
20.1 - 22.9
23 - 26.3
26.4 - 30.1
30.2 - 34.6
34.7 - 40.9
41 - 49.4
49.5 - 62.2

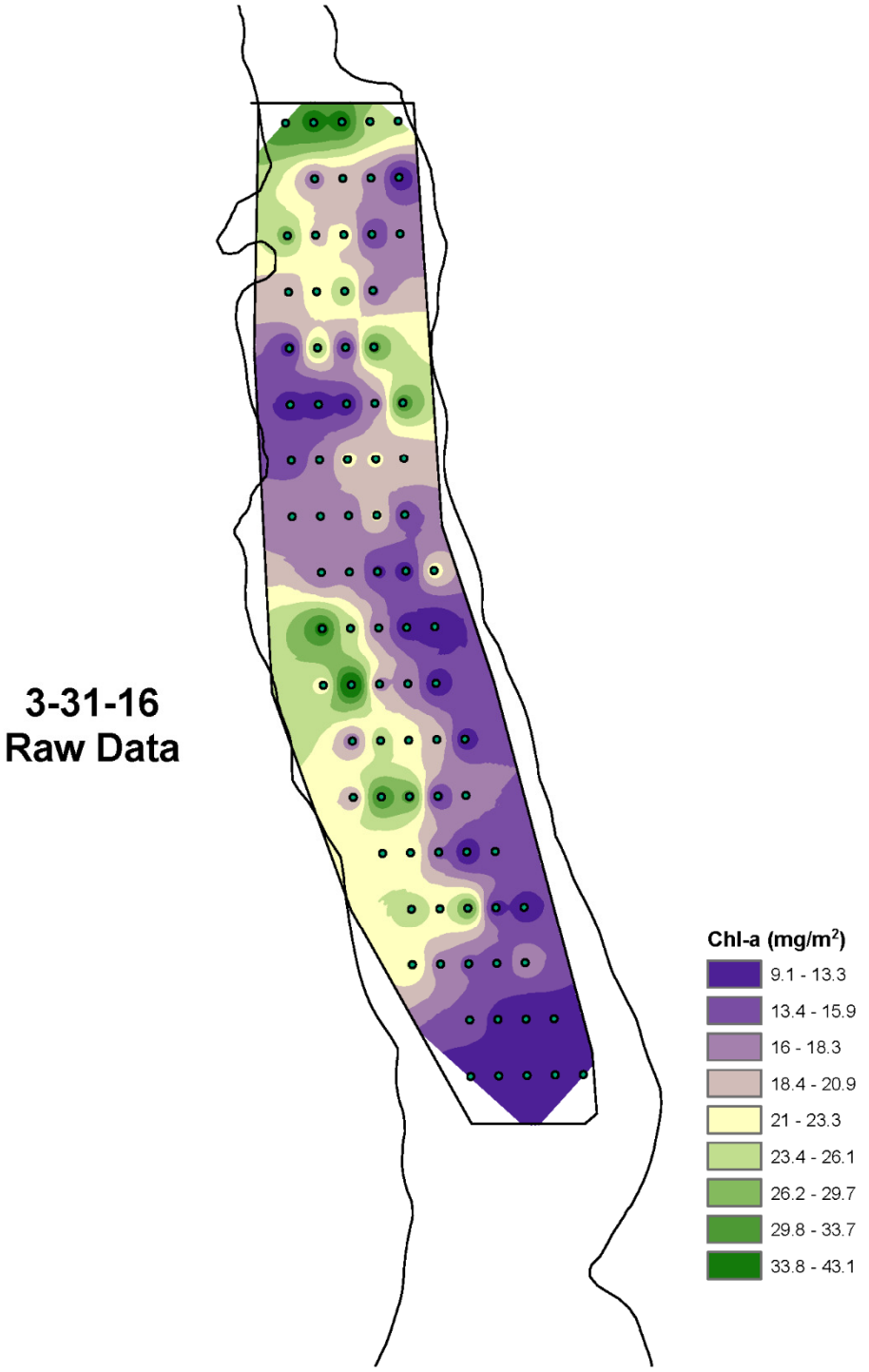
3-31-16
Raw Data
Chl-a (mg/m²)
9.1 - 13.3
13.4 - 15.9
16 - 18.3
18.4 - 20.9
21 - 23.3
23.4 - 26.1
26.2 - 29.7
29.8 - 33.7
33.8 - 43.1

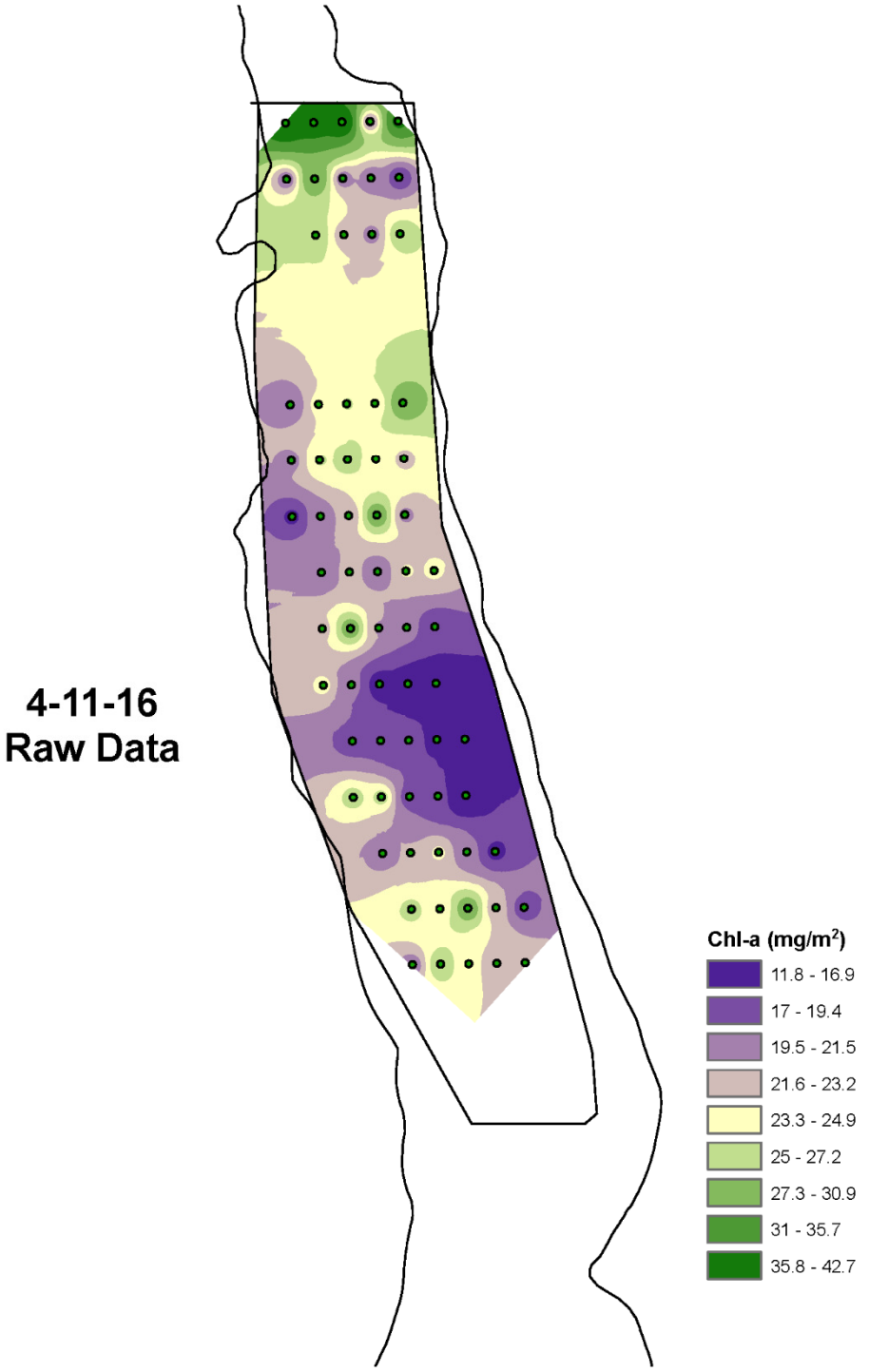
4-11-16
Raw Data
Chl-a (mg/m²)
11.8 - 16.9
17 - 19.4
19.5 - 21.5
21.6 - 23.2
23.3 - 24.9
25 - 27.2
27.3 - 30.9
31 - 35.7
35.8 - 42.7

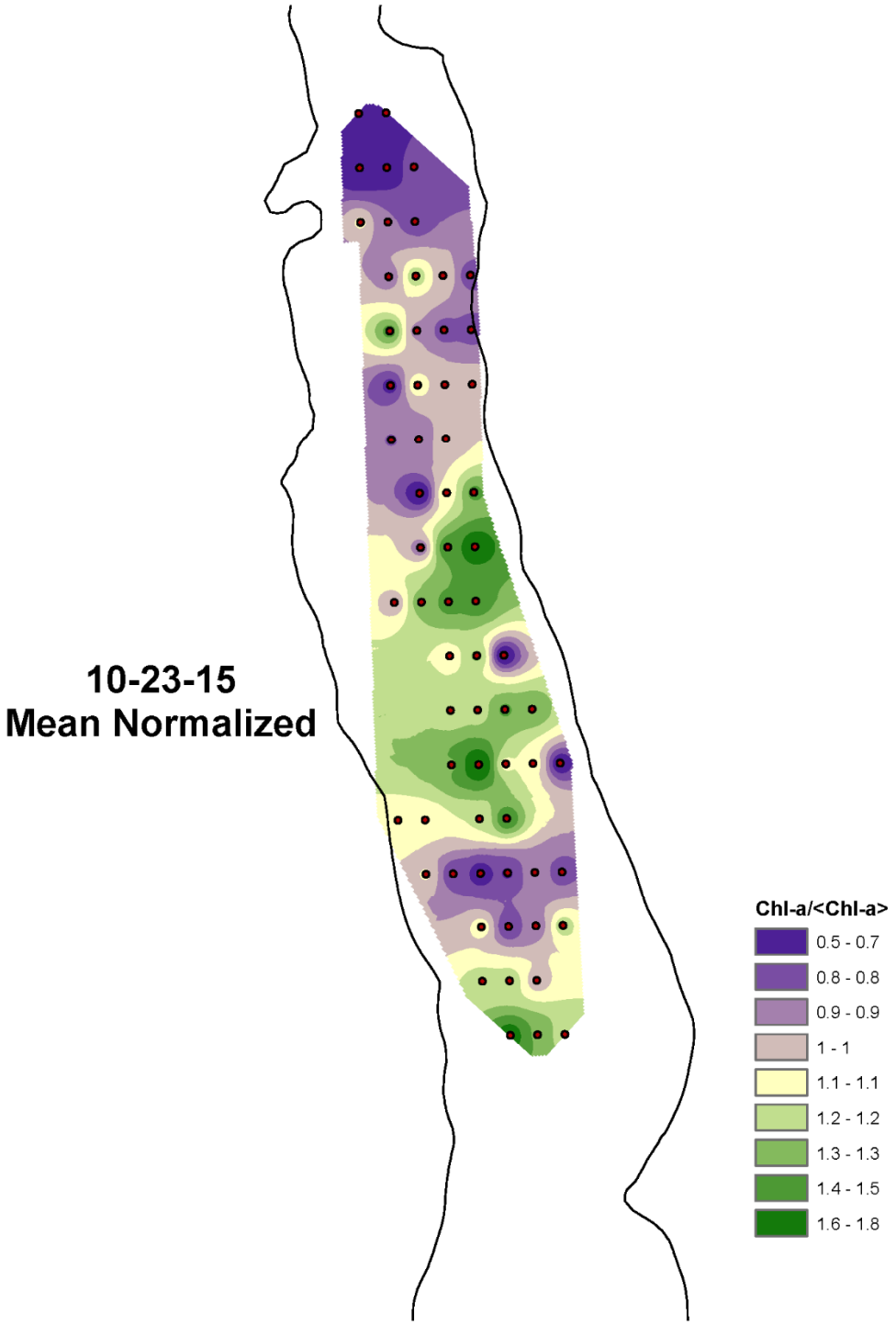
10-23-15
Mean Normalized
Chl-a/<Chl-a>
0.5 - 0.7
0.8 - 0.8
0.9 - 0.9
1 - 1
1.1 - 1.1
1.2 - 1.2
1.3 - 1.3
1.4 - 1.5
1.6 - 1.8

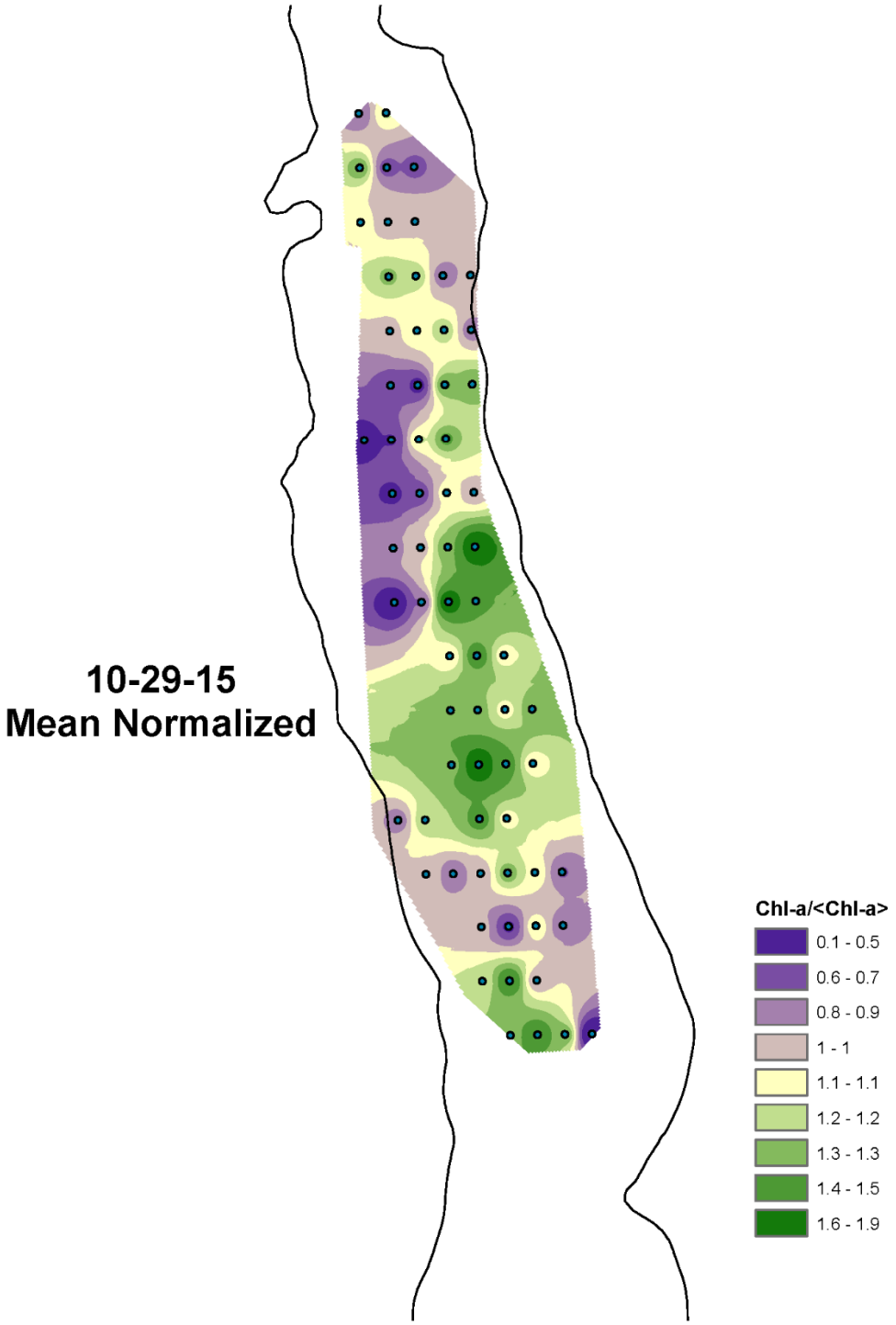
10-29-15
Mean Normalized
Chl-a/<Chl-a>
0.1 - 0.5
0.6 - 0.7
0.8 - 0.9
1 - 1
1.1 - 1.1
1.2 - 1.2
1.3 - 1.3
1.4 - 1.5
1.6 - 1.9

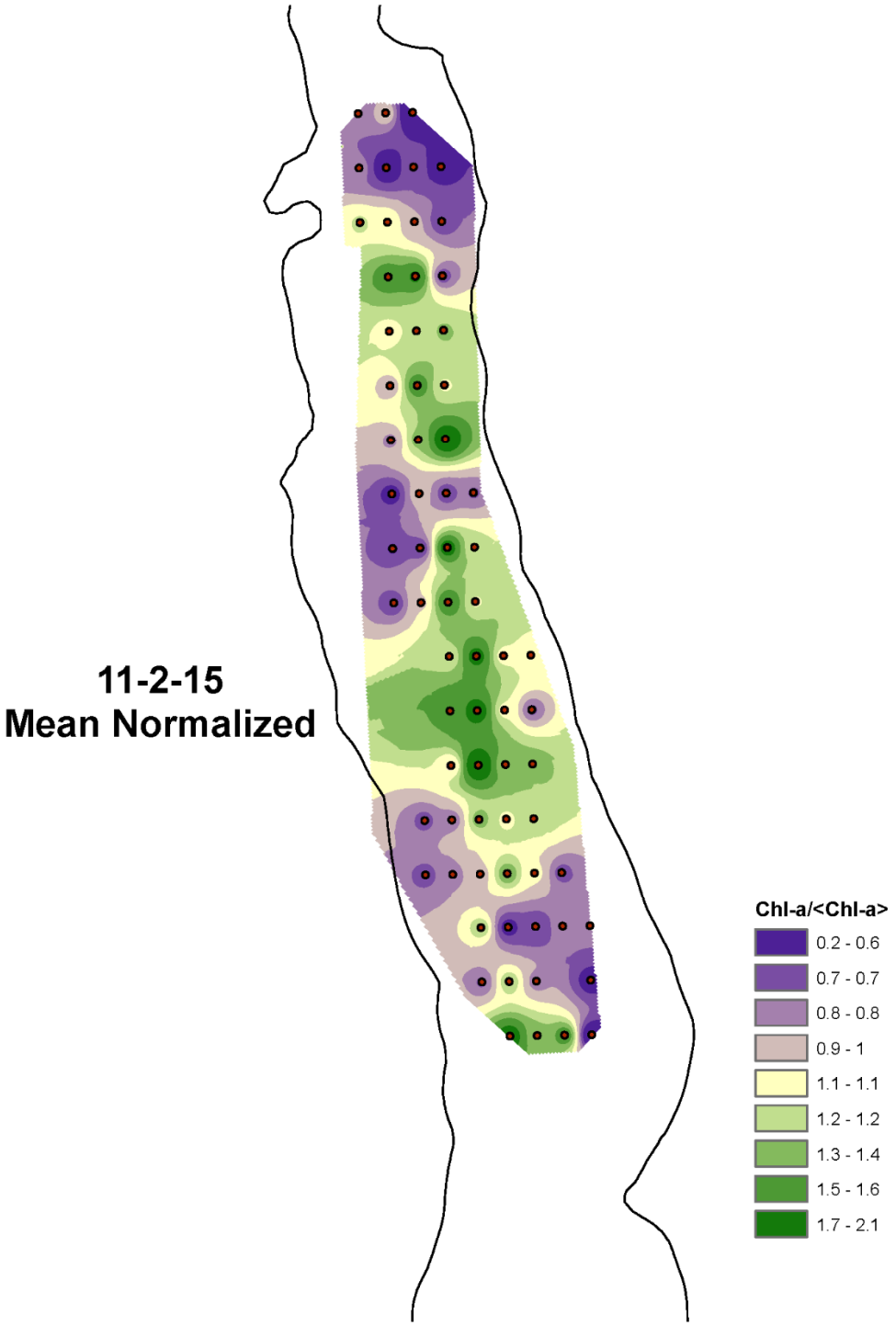
11-2-15
Mean Normalized
Chl-a/<Chl-a>
0.2 - 0.6
0.7 - 0.7
0.8 - 0.8
0.9 - 1
1.1 - 1.1
1.2 - 1.2
1.3 - 1.4
1.5 - 1.6
1.7 - 2.1

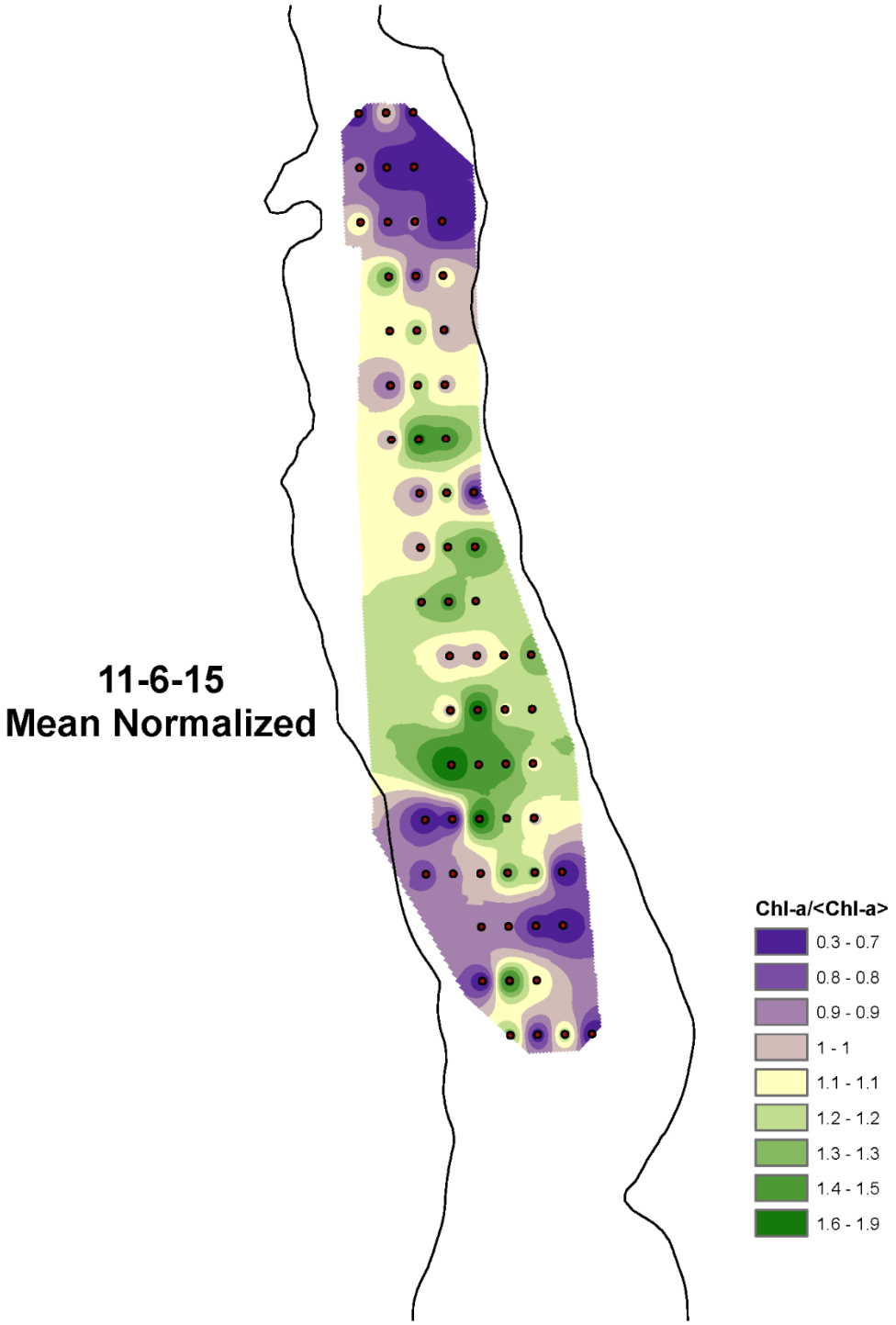
11-6-15
Mean Normalized
Chl-a/<Chl-a>
0.3 - 0.7
0.8 - 0.8
0.9 - 0.9
1 - 1
1.1 - 1.1
1.2 - 1.2
1.3 - 1.3
1.4 - 1.5
1.6 - 1.9

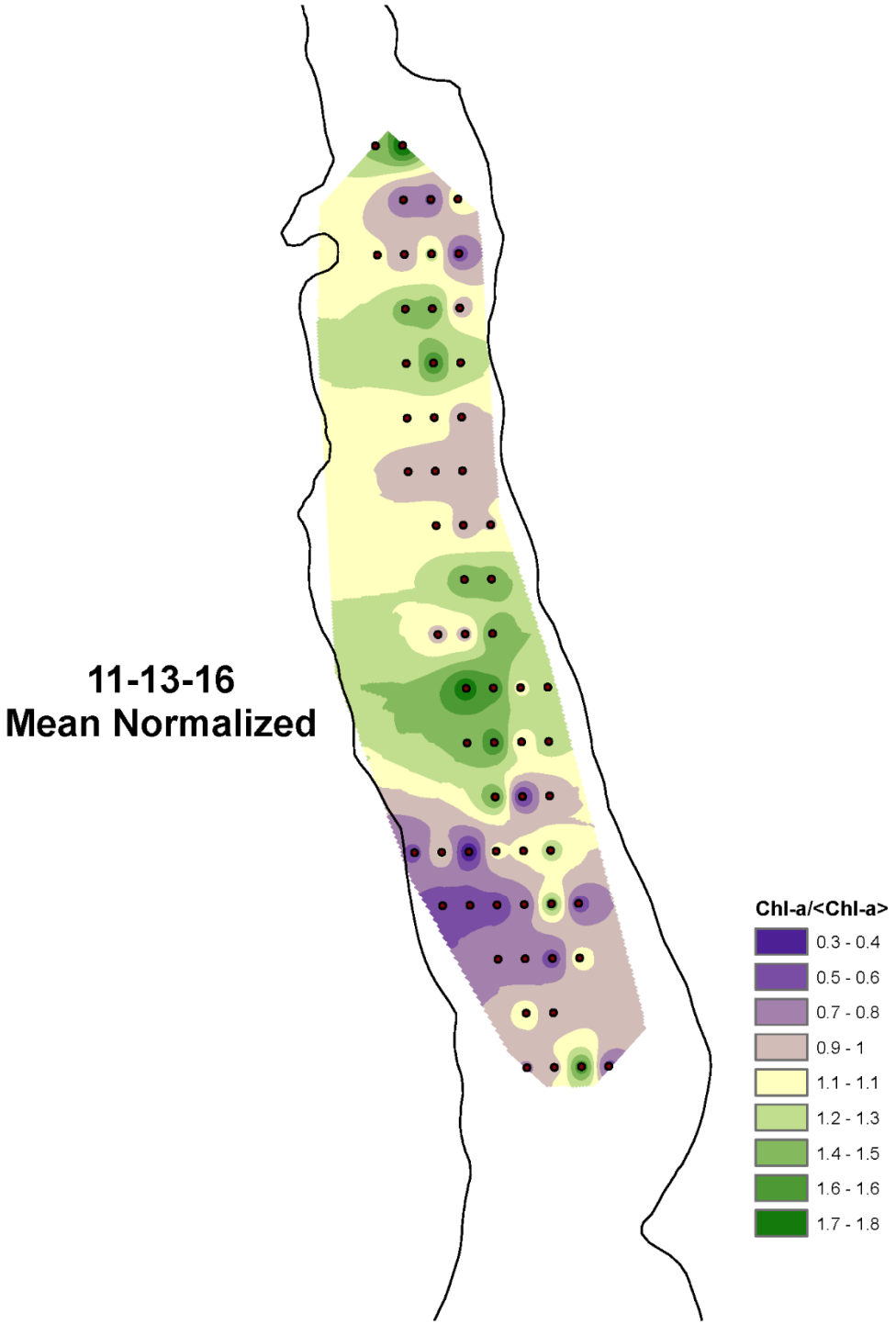
11-13-16
Mean Normalized
Chl-a/<Chl-a>
0.3 - 0.4
0.5 - 0.6
0.7 - 0.8
0.9 - 1
1.1 - 1.1
1.2 - 1.3
1.4 - 1.5
1.6 - 1.6
1.7 - 1.8

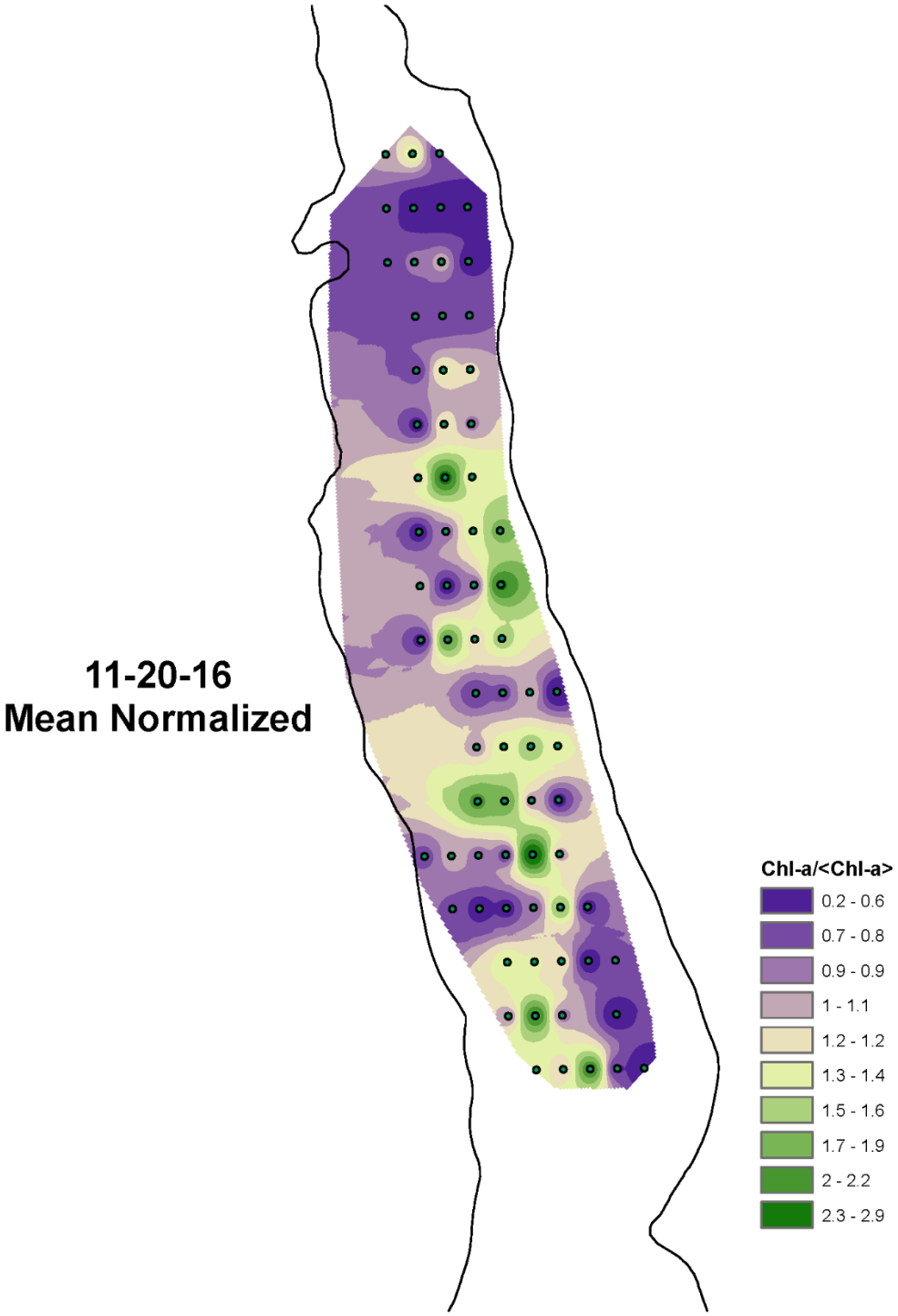
11-20-16
Mean Normalized
Chl-a/<Chl-a>
0.2 - 0.6
0.7 - 0.8
0.9 - 0.9
1 - 1.1
1.2 - 1.2
1.3 - 1.4
1.5 - 1.6
1.7 - 1.9
2 - 2.2
2.3 - 2.9

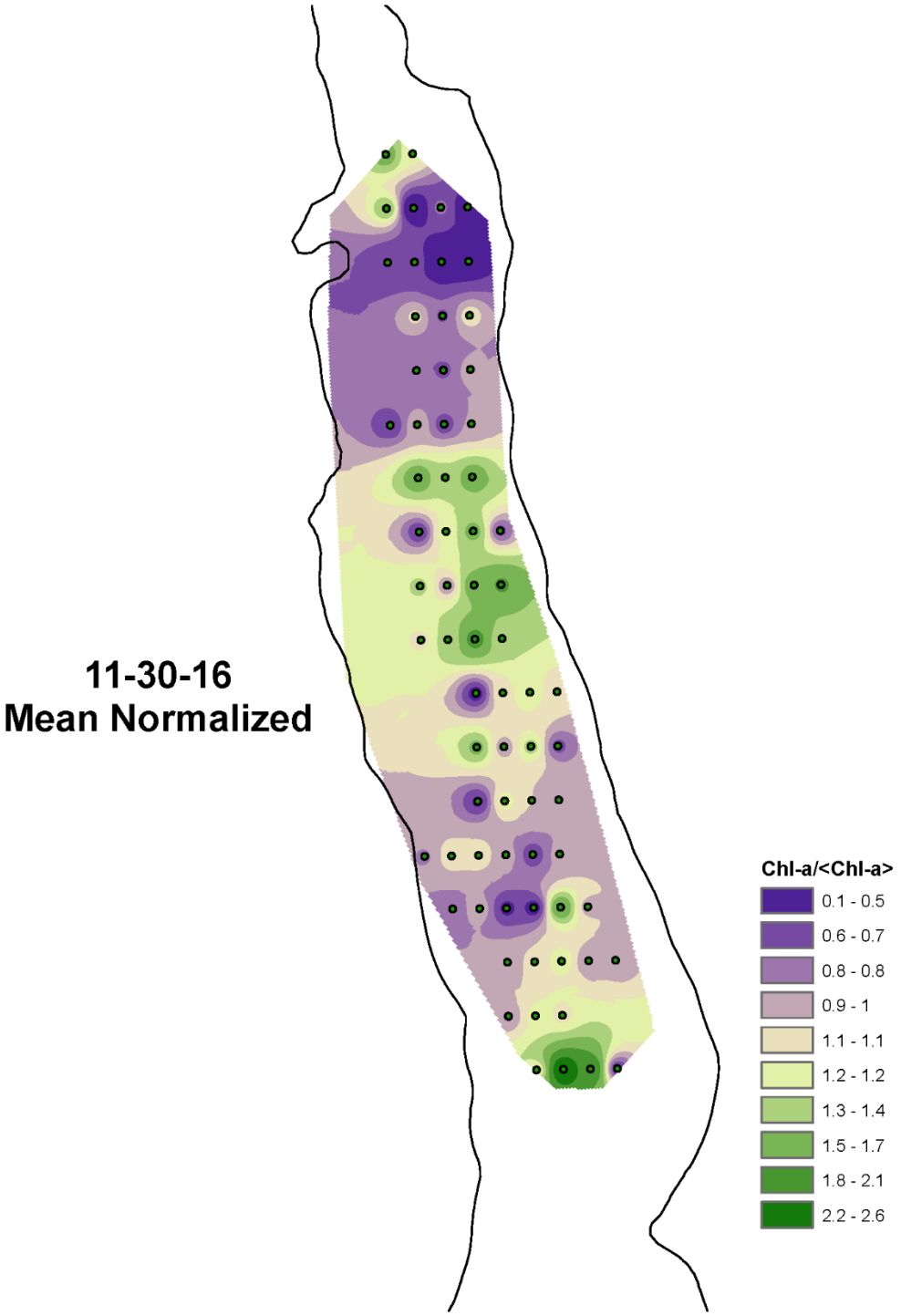
11-30-16
Mean Normalized
Chl-a/<Chl-a>
0.1 - 0.5
0.6 - 0.7
0.8 - 0.8
0.9 - 1
1.1 - 1.1
1.2 - 1.2
1.3 - 1.4
1.5 - 1.7
1.8 - 2.1
2.2 - 2.6

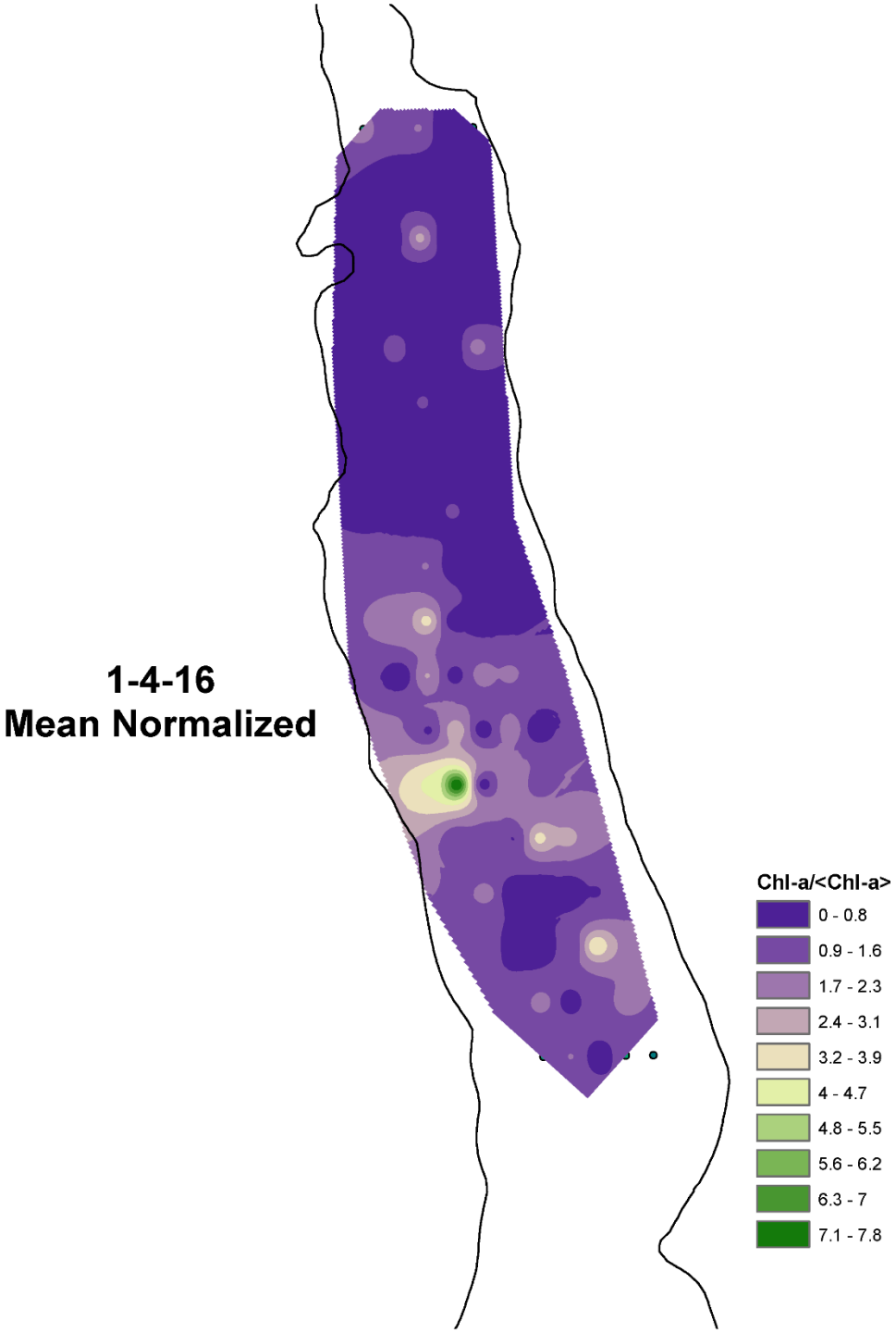
1-4-16
Mean Normalized
Chl-a/<Chl-a>
0 - 0.8
0.9 - 1.6
1.7 - 2.3
2.4 - 3.1
3.2 - 3.9
4 - 4.7
4.8 - 5.5
5.6 - 6.2
6.3 - 7
7.1 - 7.8

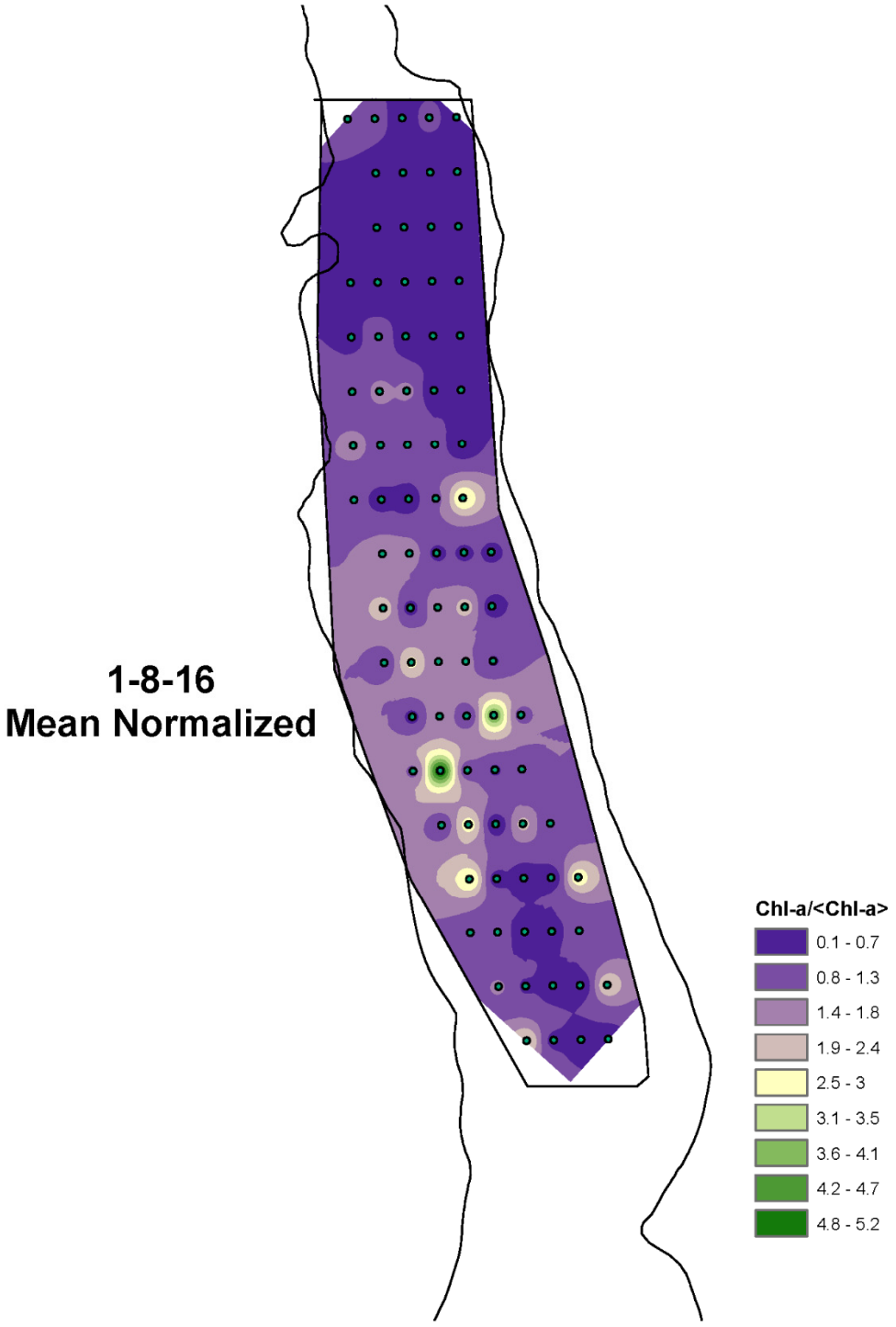
1-8-16
Mean Normalized
Chl-a/<Chl-a>
0.1 - 0.7
0.8 - 1.3
1.4 - 1.8
1.9 - 2.4
2.5 - 3
3.1 - 3.5
3.6 - 4.1
4.2 - 4.7
4.8 - 5.2

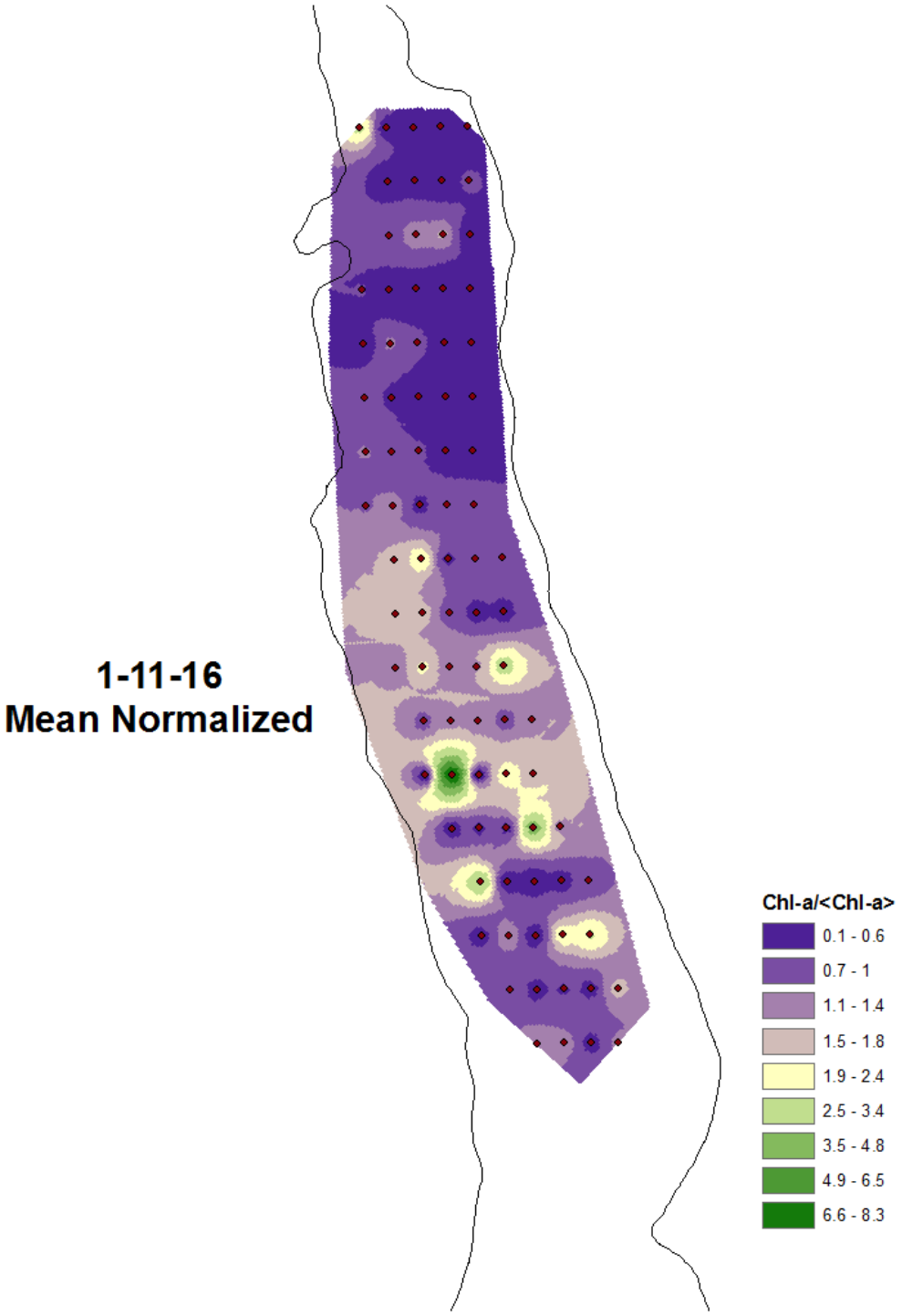
1-11-16
Mean Normalized
Chl-a/<Chl-a>
0.1 - 0.6
0.7 - 1
1.1 - 1.4
1.5 - 1.8
1.9 - 2.4
2.5 - 3.4
3.5 - 4.8
4.9 - 6.5
6.6 - 8.3

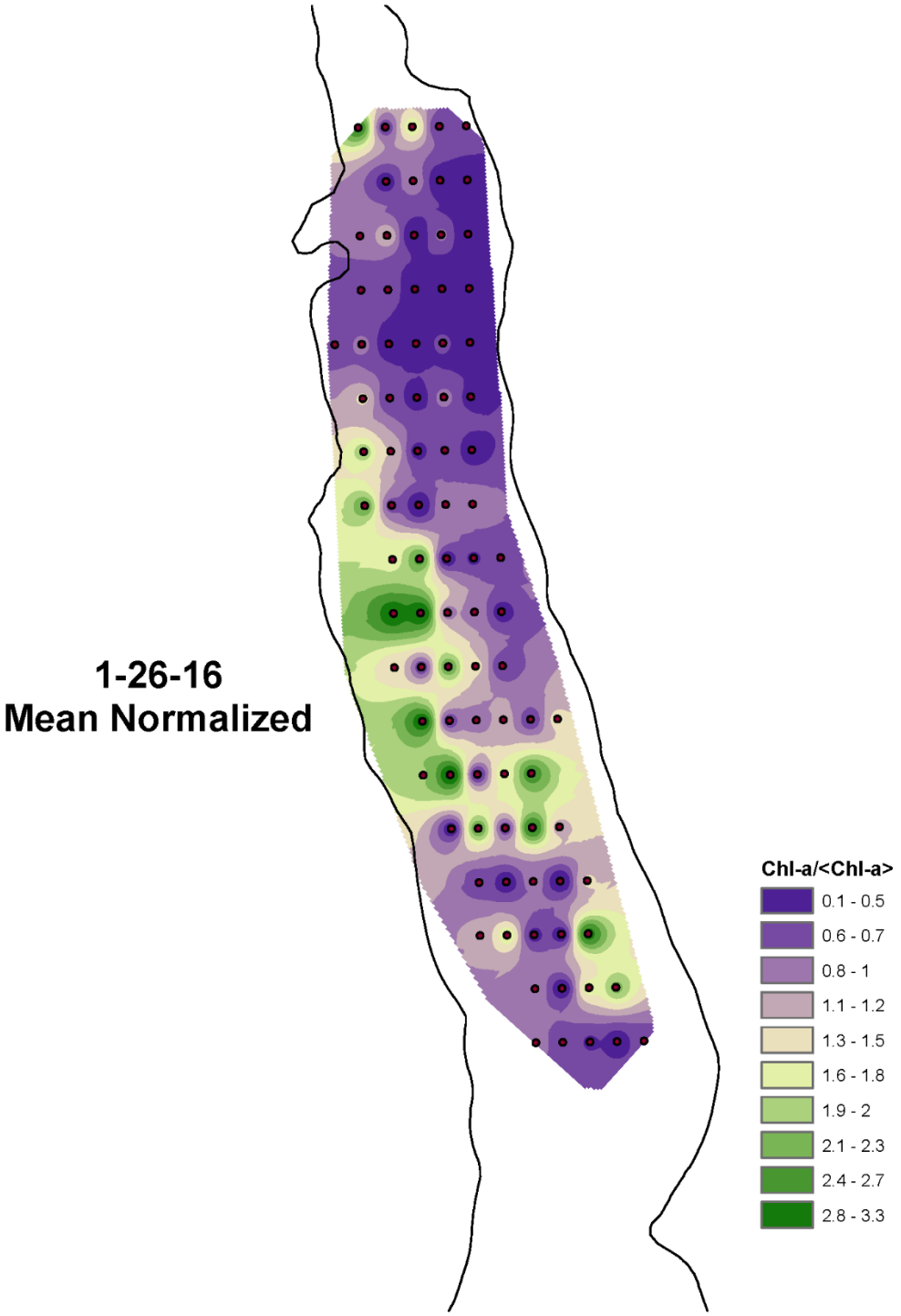
1-26-16
Mean Normalized
Chl-a/<Chl-a>
0.1 - 0.5
0.6 - 0.7
0.8 - 1
1.1 - 1.2
1.3 - 1.5
1.6 - 1.8
1.9 - 2
2.1 - 2.3
2.4 - 2.7
2.8 - 3.3

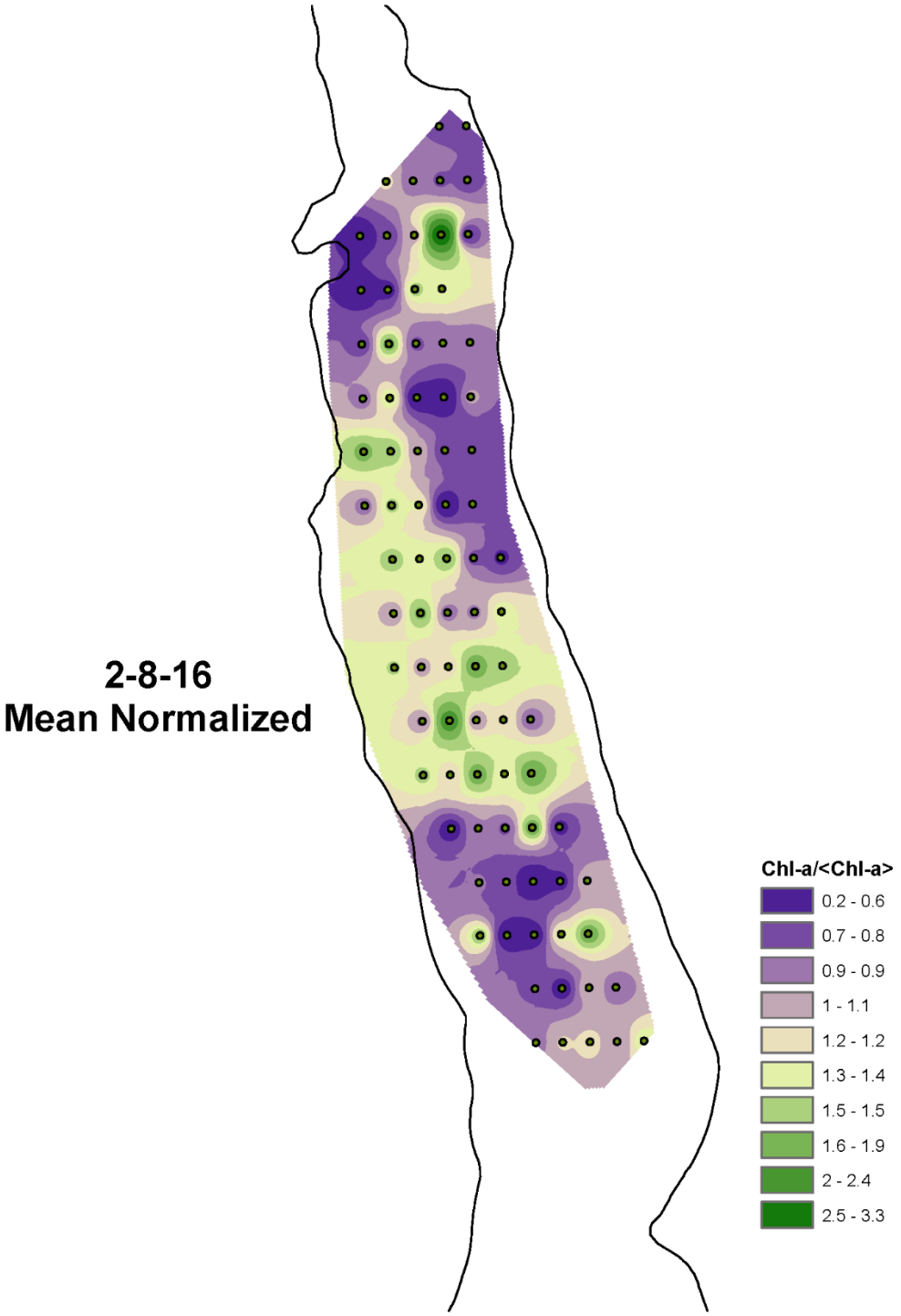
2-8-16
Mean Normalized
Chl-a/<Chl-a>
0.2 - 0.6
0.7 - 0.8
0.9 - 0.9
1 - 1.1
1.2 - 1.2
1.3 - 1.4
1.5 - 1.5
1.6 - 1.9
2 - 2.4
2.5 - 3.3

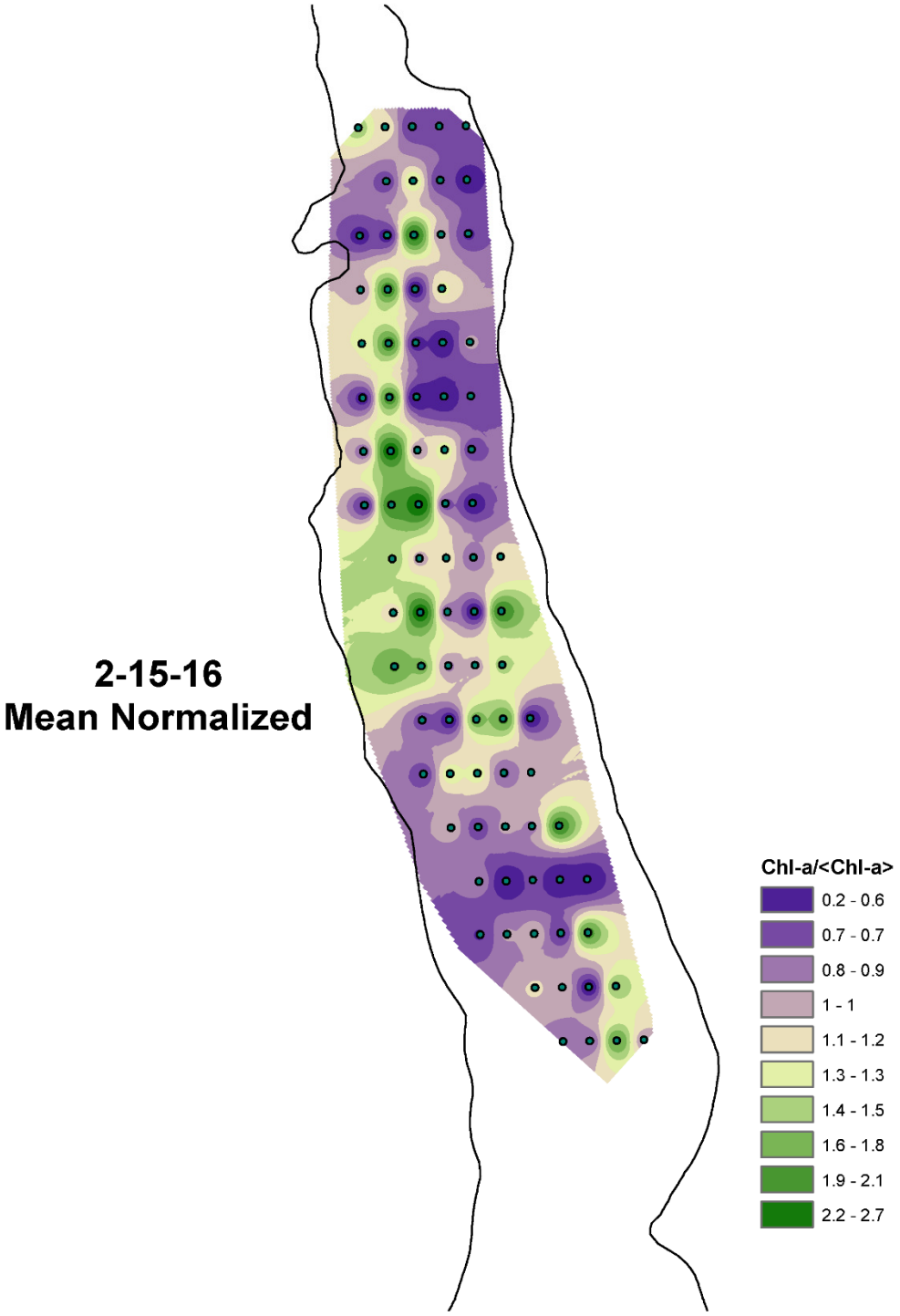
2-15-16
Mean Normalized
Chl-a/<Chl-a>
0.2 - 0.6
0.7 - 0.7
0.8 - 0.9
1 - 1
1.1 - 1.2
1.3 - 1.3
1.4 - 1.5
1.6 - 1.8
1.9 - 2.1
2.2 - 2.7

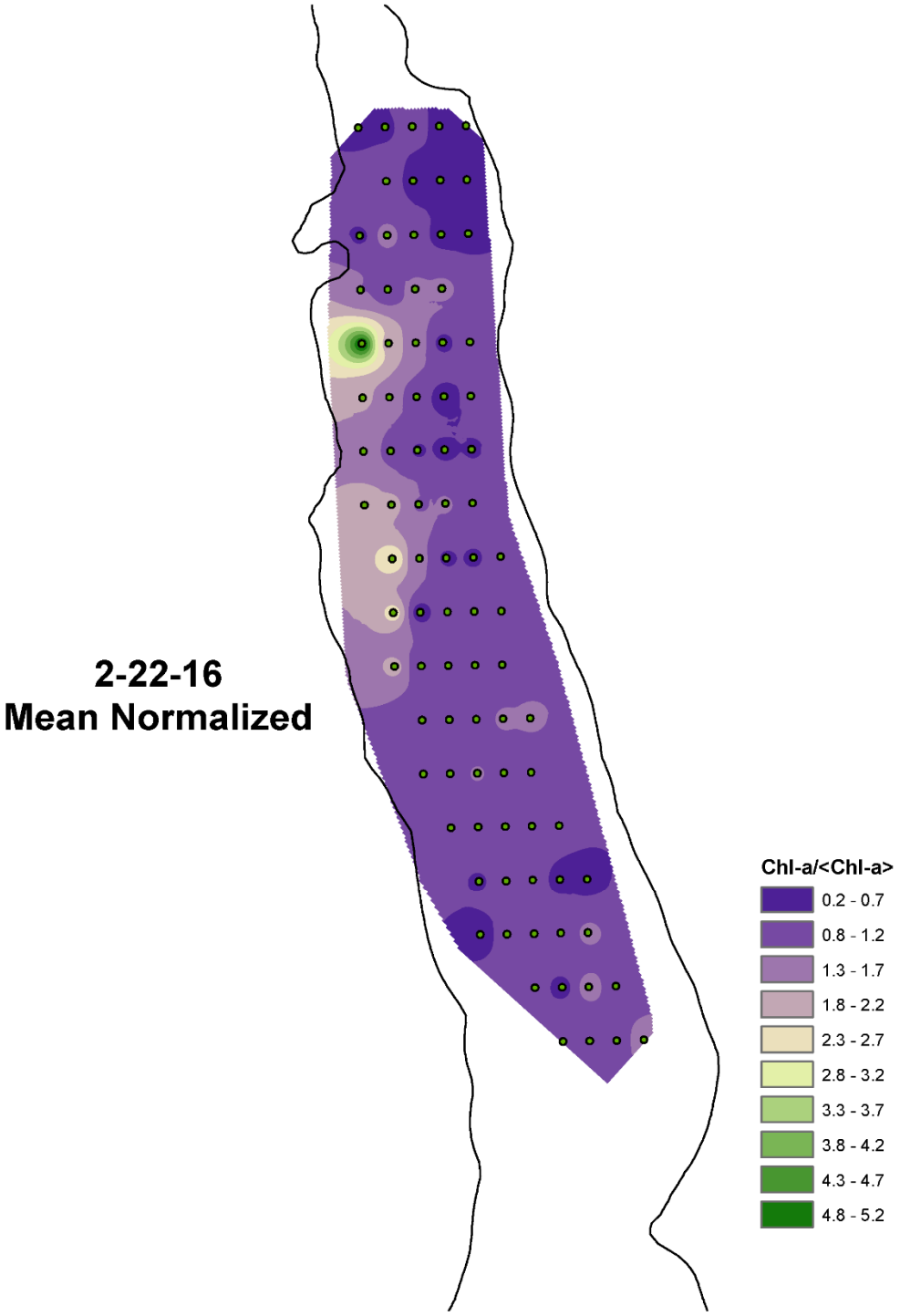
2-22-16
Mean Normalized
Chl-a/<Chl-a>
0.2 - 0.7
0.8 - 1.2
1.3 - 1.7
1.8 - 2.2
2.3 - 2.7
2.8 - 3.2
3.3 - 3.7
3.8 - 4.2
4.3 - 4.7
4.8 - 5.2

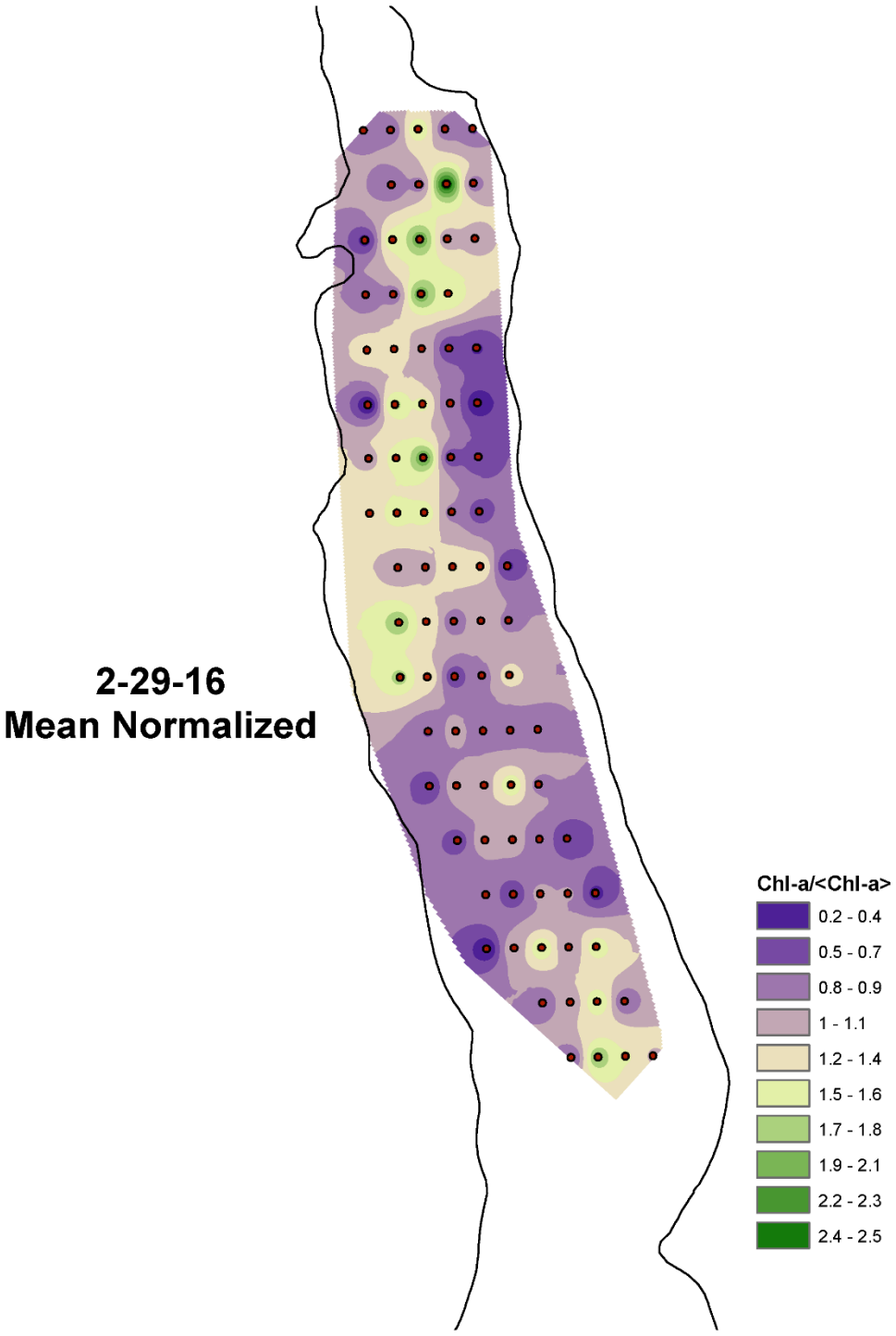
2-29-16
Mean Normalized
Chl-a/<Chl-a>
0.2 - 0.4
0.5 - 0.7
0.8 - 0.9
1 - 1.1
1.2 - 1.4
1.5 - 1.6
1.7 - 1.8
1.9 - 2.1
2.2 - 2.3
2.4 - 2.5

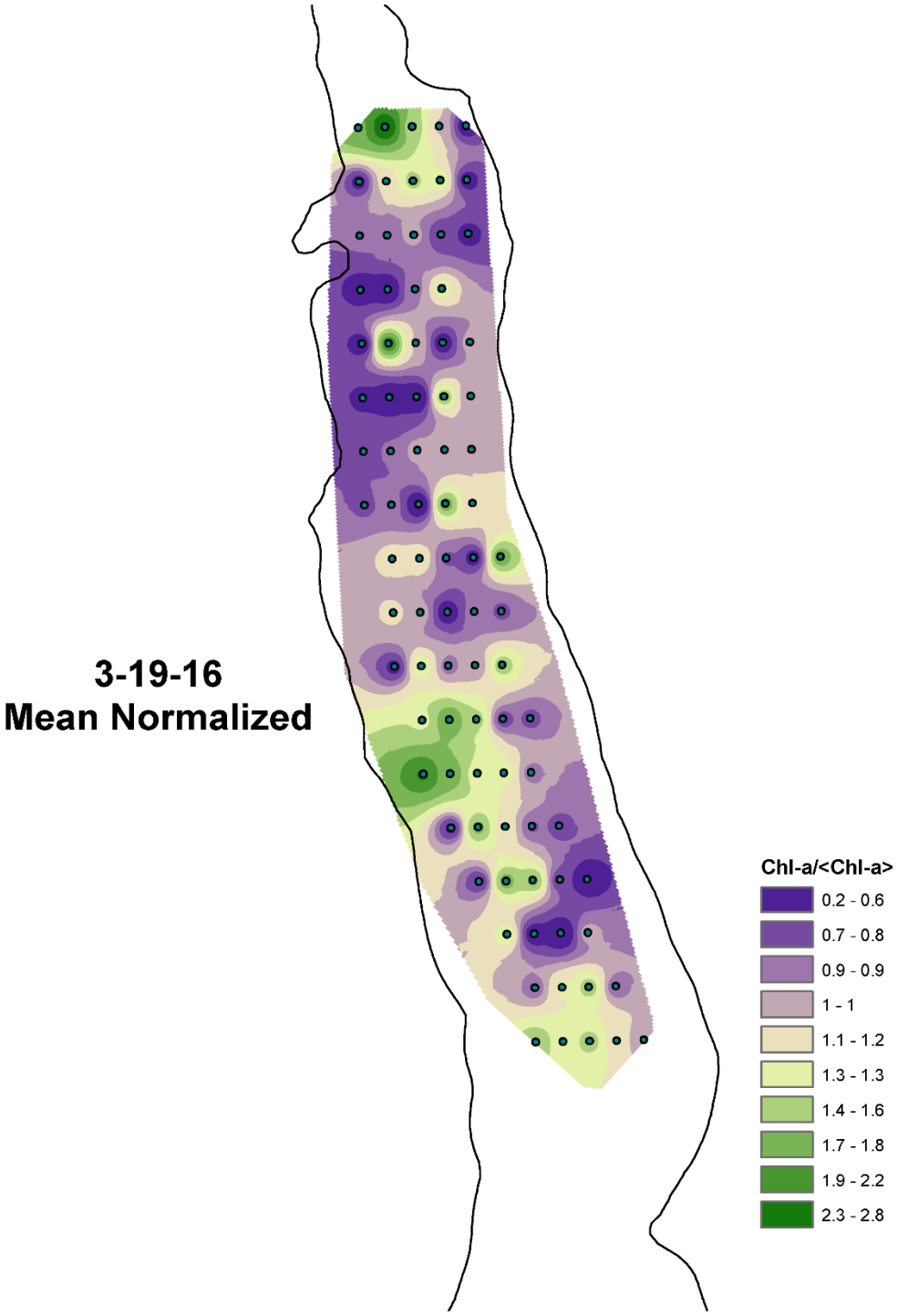
3-19-16
Mean Normalized
Chl-a/<Chl-a>
0.2 - 0.6
0.7 - 0.8
0.9 - 0.9
1 - 1
1.1 - 1.2
1.3 - 1.3
1.4 - 1.6
1.7 - 1.8
1.9 - 2.2
2.3 - 2.8

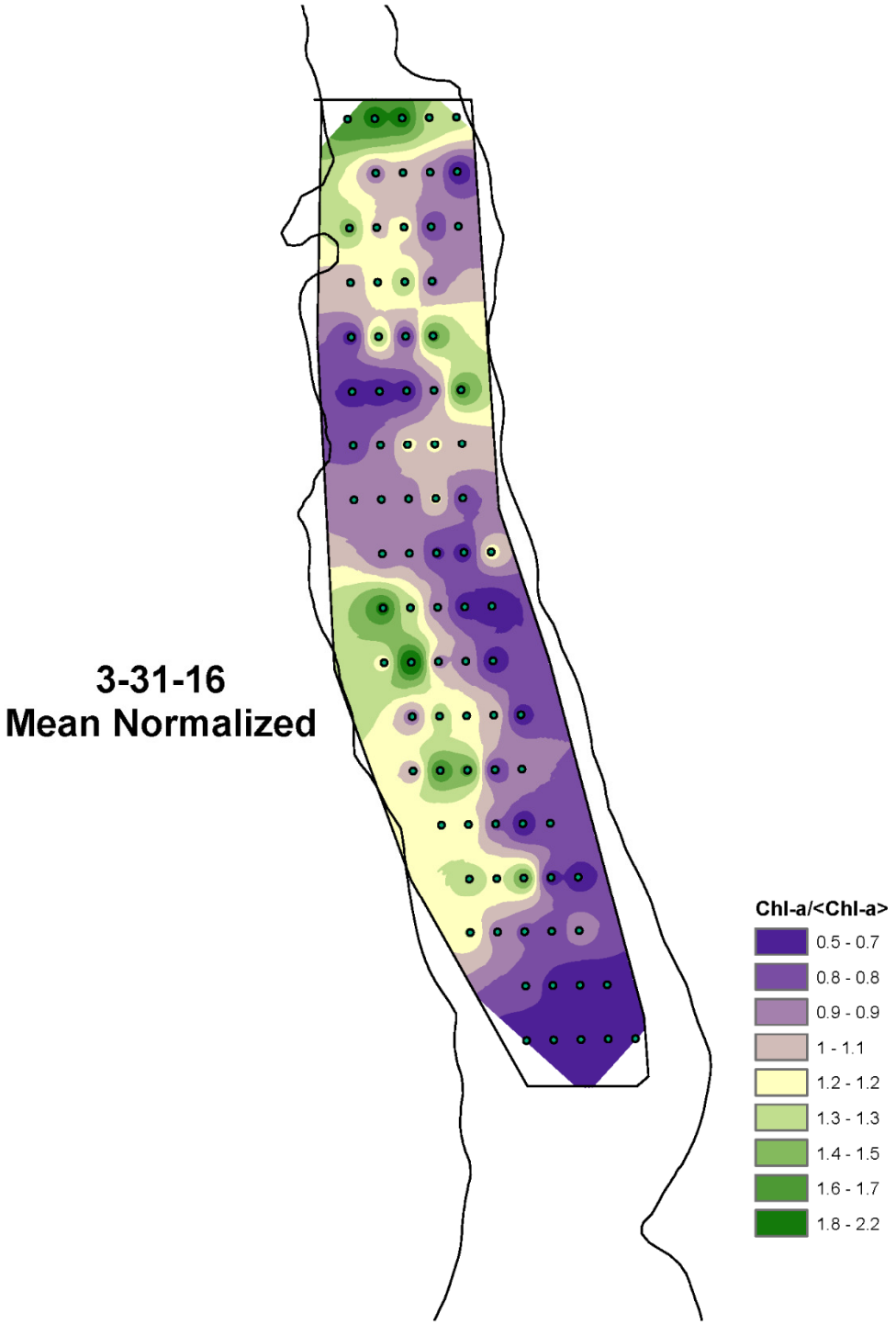
3-31-16
Mean Normalized
Chl-a/<Chl-a>
0.5 - 0.7
0.8 - 0.8
0.9 - 0.9
1 - 1.1
1.2 - 1.2
1.3 - 1.3
1.4 - 1.5
1.6 - 1.7
1.8 - 2.2

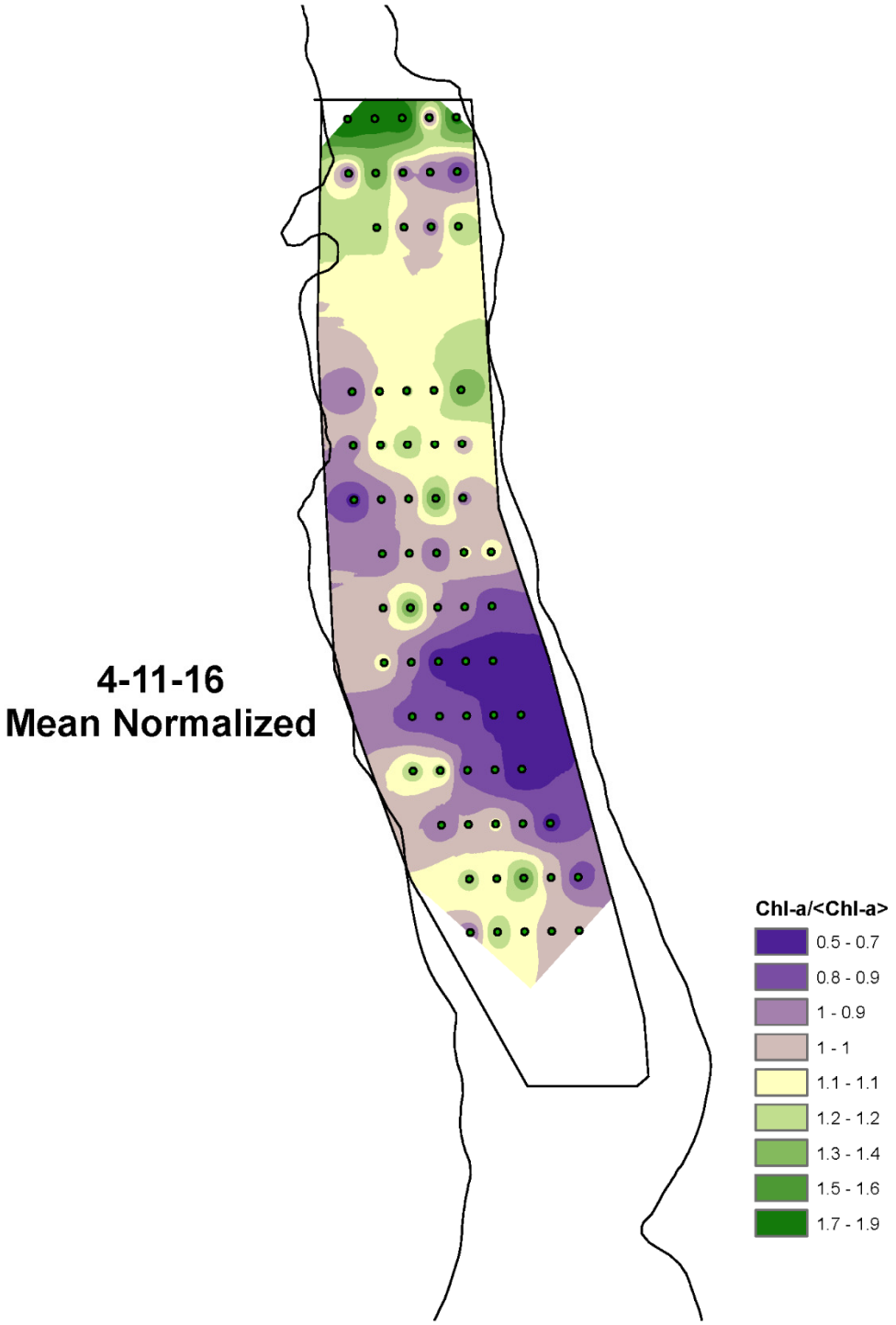
4-11-16
Mean Normalized
Chl-a/<Chl-a>
0.5 - 0.7
0.8 - 0.9
1 - 0.9
1 - 1
1.1 - 1.1
1.2 - 1.2
1.3 - 1.4
1.5 - 1.6
1.7 - 1.9